Advances in Biochemical Engineering/Biotechnology 161
Series Editor: T. Scheper

Bernd Hitzmann *Editor*

Measurement, Modeling and Automation in Advanced Food Processing

Springer

161
Advances in Biochemical Engineering/Biotechnology

Aims and Scope

This book series reviews current trends in modern biotechnology and biochemical engineering. Its aim is to cover all aspects of these interdisciplinary disciplines, where knowledge, methods and expertise are required from chemistry, biochemistry, microbiology, molecular biology, chemical engineering and computer science.

Volumes are organized topically and provide a comprehensive discussion of developments in the field over the past 3–5 years. The series also discusses new discoveries and applications. Special volumes are dedicated to selected topics which focus on new biotechnological products and new processes for their synthesis and purification.

In general, volumes are edited by well-known guest editors. The series editor and publisher will, however, always be pleased to receive suggestions and supplementary information. Manuscripts are accepted in English.

In references, Advances in Biochemical Engineering/Biotechnology is abbreviated as *Adv. Biochem. Engin./Biotechnol.* and cited as a journal.

More information about this series at http://www.springer.com/series/10

Bernd Hitzmann
Editor

Measurement, Modeling and Automation in Advanced Food Processing

With contributions by

M.H. Ahmad · N. Aleixos · A. Barone · J. Blasco · S. Cubero · J. Glassey · B. Hitzmann · K. Kansou · M. Kristiawan · E. Molto · G.A. Montague · S. Munera · M. Özilgen · S. Özilgen · V. Sabou · A. Sahar · G.D. Valle

Springer

Editor
Bernd Hitzmann
Institute of Food Science and Biotechnology
University of Hohenheim
Stuttgart, Baden-Württemberg
Germany

ISSN 0724-6145 ISSN 1616-8542 (electronic)
Advances in Biochemical Engineering/Biotechnology
ISBN 978-3-319-60109-0 ISBN 978-3-319-60111-3 (eBook)
DOI 10.1007/978-3-319-60111-3

Library of Congress Control Number: 2017946472

Printed on acid-free paper

This Springer imprint is published by Springer Nature
The registered company is Springer International Publishing AG
The registered company address is: Gewerbestrasse 11, 6330 Cham, Switzerland

Preface

The automation grade in the food industry differs considerably from that of the (bio) chemical industry, and this observation is mainly caused by the following reasons: (1) For food processing, sensors are not available to provide substantial information about the characteristics of the (raw) material such as microflora, spoilage, and mouth feeling. (2) The composition of the raw material can change, depending on strain, growth (climate and soil), fertilization, and harvesting conditions. (3) The raw material is usually soft, slippery, and fragile and has a variable size, dependent on temperature, pressure, and mechanical stress. (4) The raw material is not always available (harvest period). (5) During processing, the geometry of the material might change and therefore transport coefficients, concentration, and temperature gradients change as well. In food processing, fundamental knowledge is missing on a molecular basis. Consequently, mathematical models are absent, and these are so fundamental for automation as measurements. Furthermore, the demand for hygiene has also to be considered.

Because of the lack of automation in food processing, the section M^3C (Modelling, Monitoring, Measurement and Control) of the European Society of Biochemical Engineering Science has pushed experts in this field to contribute to this book. Here, different contributions are presented to show how to solve the afore-mentioned problems.

Sibel Özilgen and Mustafa Özilgen, after discussing the common steps for the primary processing of the major food groups, present a literature survey of the hazards to be considered during food processing. They focus upon cereals, fruits and vegetables, milk and milk products, meat and meat products, and fats and oils. To demonstrate how Failure Mode Effect Analysis (FMEA) can contribute to assure safe food, an FMEA template is presented in their contribution, using a case study on pasteurized milk production.

Magdalena Kristiawan and coworker present modeling approaches for two cereal food processes—extrusion and bread making—where the expert knowledge of the mechanisms underlying the structural changes of the processed material during the different operations is captured. They demonstrate how scientific

and expert knowledge can be integrated and represented using these modeling approaches for solid/liquid transition and expansion. Based on the models, process simulation can be performed which can contribute to the design of processes and products.

José Blasco and coworkers discuss the significance of machine vision-based measurements for the postharvest processing of fruits and vegetables. They summarize the state of the art in this field and discuss systems based on color images for the inspection of conventional color, shape, or external defects. Furthermore, they consider recent developments in spectral image analysis for internal quality assessment or contaminant detection.

Jarka Glassey and coworkers use different industrial case studies to demonstrate the benefits of advanced measurement, modeling, and control in food processes. First, they show how knowledge elicitation from expert operators and the consequent improvements in process control can be exploited to increase the consistency of the resulting product of a potato chip (French fries) process. The authors discuss the economic benefits of tighter control of the important process parameters of this process. Furthermore, an application of NIR spectroscopy to ensure effective mixing of dry multicomponent mixtures and pastes is presented.

Muhammad Haseeb Ahmad and coworkers present a review of fluorescence application in food processing. They discuss how this spectroscopic technique can be used for classification, authentication, and quantification of various parameters, such as food handling, processing, and storage, of different foods by using examples from dairy, meat, fish, eggs, cereals, and fruits and vegetables. They point out that chemometric modeling is required for the evaluation of the spectra.

Mustafa Özilgen demonstrates how knowledge from thermodynamic, kinetic, heat, and mass transfer analysis can be used to obtain mathematical models. He pointed out that ignoring the conditions of models under which they are valid risks ending up with erroneous conclusions. Therefore, a good balance must be found between a much too complicated or a much too over simplified model when describing the food itself or its processing. Using different case studies, different models are presented, including the Matlab source files, to run simulations.

It is hoped that the different chapters of this book will inspire the reader to apply new measurement systems such as those based on spectroscopy, or apply mathematical models to improve the automation of food processes, to improve product quality and safety and to reduce material and energy consumption. This book will hopefully be a keystone in the overall puzzle to disprove Max Planck, who said that a new scientific truth does not triumph by convincing its opponents and making them see the light, but rather because its opponents eventually die and a new generation grows up that is familiar with it.

Thanks are offered to the people of Springer for their support and patience.

Contents

Adv Biochem Eng Biotechnol (2017) 161: 1–28
DOI: 10.1007/10_2017_10

Published online: 4 April 2017

Integration of Basic Knowledge Models for the Simulation of Cereal Foods Processing and Properties

Magdalena Kristiawan, Kamal Kansou, and Guy Della Valle

Abstract Cereal processing (breadmaking, extrusion, pasting, etc.) covers a range of mechanisms that, despite their diversity, can be often reduced to a succession of two core phenomena: (1) the transition from a divided solid medium (the flour) to a continuous one through hydration, mechanical, biochemical, and thermal actions and (2) the expansion of a continuous matrix toward a porous structure as a result of the growth of bubble nuclei either by yeast fermentation or by water vaporization after a sudden pressure drop. Modeling them is critical for the domain, but can be quite challenging to address with mechanistic approaches relying on partial differential equations. In this chapter we present alternative approaches through basic knowledge models (BKM) that integrate scientific and expert knowledge, and possess operational interest for domain specialists. Using these BKMs, simulations of two cereal foods processes, extrusion and breadmaking, are provided by focusing on the two core phenomena. To support the use by non-specialists, these BKMs are implemented as computer tools, a Knowledge-Based System developed for the modeling of the flour mixing operation or Ludovic®, a simulation software for twin screw extrusion. They can be applied to a wide domain of compositions, provided that the data on product rheological properties are available. Finally, it is stated that the use of such systems can help food engineers to design cereal food products and predict their texture properties.

Keywords Bread, Bubbles, Extrusion, Gluten, Phenomenological model, Starch, Viscosity

M. Kristiawan, K. Kansou, and G.D. Valle (✉)
INRA, UR 1268 Biopolymères Interactions Assemblages (BIA), 44 316 Nantes, France
e-mail: guy.della-valle@inra.fr

Contents

Abbreviations

a, b, c, d, a', b', c'	Parameters of dough porosity and loss of stability
A, B	Coefficients of volume flow rate, depending on extruder screw geometry
AF	Anisotropy factor of extruded products
BKM	Basic knowledge models
Ca^*	Apparent capillary number defined for dough fermentation
C_p	Heat capacity at constant pressure (J/g/K)
DOE	Design of experiment
DSC	Differential scanning calorimetry
E	Activation energy in viscosity equation (J/mol)
E'	Storage modulus (Pa)
E_{cd}, E_f	Specific energy supplied by conduction, by friction, respectively (J/g)
E_v	Specific energy produced by viscous dissipation (J/g)
F	Fineness of the extruded product cellular structure
FEM	Finite element method
H	Dough height (m)
K, K_E	Consistency index in viscosity and elongational viscosity equation, respectively ($Pa.s^m$)
KBS	Knowledge-based system (for dough mixing)
K_s	Characteristic of the mixer when applying Metzner–Otto's principle
LEI, SEI, VEI	Longitudinal, radial (sectional), and volumic expansion indices, respectively
L/D	Length to diameter ratio of die extruder
L_{max}	Dough maximum width (m)
MC	Moisture content
MCS, MWT	Mean values for cell size and cell wall thickness of extruded product cellular structure, respectively (m)

m	Flow (or pseudo plasticity) index in viscosity and elongational viscosity equation
N, Ω	Extruder screw or mixer rotation speed (rpm, rad/s, respectively)
P_s	Specific mixing Power (W)
P_v	Bubble internal gas pressure (Pa)
$P(t)$	Dough porosity during fermentation
Q_v	Volume flow rate in extruder (m^3/s)
r	Bubble radius (m)
R	Gas constant in viscous equation (J/mol/K)
SME	Specific mechanical energy (kJ/kg or kWh/ton)
$S(t)$	Dough shape ratio during fermentation
T, T_a	Absolute temperature of melt (in °C and K, respectively)
T_g, T_m, T_p	Temperature of starch glass transition, melting, product, respectively (°C or K)
V	Volume of screw (m^3)
$\dot{W}$	Power dissipated in extruder (W)
ΔH	Specific enthalpy for the state change (starch melting) (J/g)
ΔP	Pressure variation (Pa) along the angular screw section of extruder $\Delta\theta$
t_m	Mixing time (s)
ΔT	Overall temperature increase up to DSC peak temperature (°C)
$\dot{\gamma}$	Shear rate (s^{-1})
ε_b, $\dot{\varepsilon}$	Elongational strain, strain rate (s^{-1})
η, η_E	Shear, bi-extensional viscosity, respectively (Pa.s)
ρ_m	(Starch) melt density (kg/m^3)
σ	Dough liquor surface tension (N/m)
τ	Elongational stress exerted by gas cell on dough matrix (Pa)

1 Introduction

Whatever the end product, cereal processing covers a range of mechanisms common to breadmaking and extrusion cooking, although they may involve different time scales and physical conditions for these processes [1, 2]. They may be first envisaged as a succession of two phenomena, the modeling of which is still incomplete. First, the transition from a divided solid medium (the flour) to a continuous one that can flow, such as a dough or a melt, either gluten network-entrapping starch granules or a molten phase of starch-encapsulating protein aggregates through hydration, mechanical, biochemical, and thermal actions (mixing, shearing, fermentation, heating). Second, the continuous matrix becomes porous because of the expansion of bubble nuclei either by yeast fermentation or by water vaporization after a sudden pressure drop. For both phenomena, as illustrated in Fig. 1, rheological properties are of pivotal importance as their determination may be tricky and knowledge of them is still incomplete. This chapter focuses on the

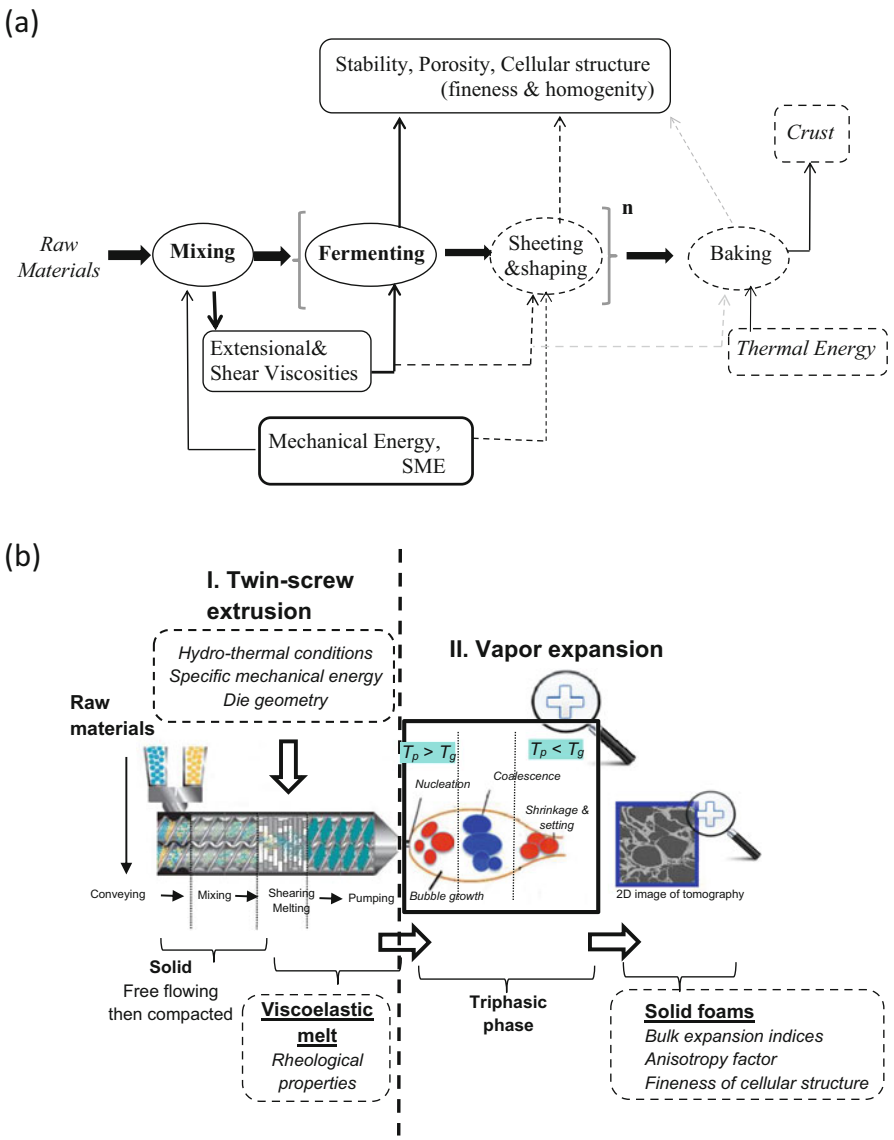

Fig. 1 Schematic representation of cereal-based solid foams processing with main variables and mechanisms. (**a**) Bread making process operations (*ellipses*) with main influencing variables and properties for texture. *Dotted ellipses* and *frames* refer to operations and variables considered to be of lower importance with regards to the properties. Exponent n means that the sequence of operations can be repeated n times ($n \leq 3$ in practice). Adapted from Della Valle et al. [3]. (**b**) Extrusion and vapor expansion as two distinct operations. Expansion involves a succession of dynamic mechanisms: bubble nucleation and growth, coalescence, shrinkage, and finally setting when the melt matrix becomes glassy. The input and output variables are presented in the *rounded boxes* with *dashed border*. T_p and T_g denote the temperature of product and that of glass transition, respectively

modeling of these two phenomena by illustrating the present capacities whilst indicating the need for improving these models.

Solid foam is a valuable model for most processed cereal products (biscuits, bread, breakfast cereals, expanded snacks). The texture, defined by its mechanical properties, depends on (1) density, (2) cellular structure, and (3) the intrinsic properties of the solid matrix [4]. Density, or inversely, specific volume, is a common technological target, and data may be found in the literature. Comparatively, cellular structure has scarcely been studied, in spite of its visual importance for the manufacturer and the consumer. Finally, intrinsic matrix properties refer to the morphology of the blends of biopolymers (starch, gluten, polysaccharides) and internal water distribution. They can be predicted by mechanical modeling using the Finite Element Method (FEM), either for bread or extruded starchy products [5]. However, FEM is too costly to be applied to the succession of operations of the breadmaking and extrusion processes at present. This method is not discussed in detail below but is referred to when relevant.

Despite the large quantity of scientific work dedicated to cereal processing, it is still difficult to foresee how to set the various operating parameters of the process to obtain the desired texture. Indeed, some sophisticated deterministic or physics-based, models based on differential equations have been developed to describe local flow and temperature fields, or the evolution of a chemical species. Regarding cereal processing, bread baking has drawn most attention and such models have been developed considering multiphase transport and evaporation in dough homogenized at macroscale as a deformable porous medium [6–8]. Some attempts have also been made to relate input and output process variables through artificial neural networks, either for extrusion [9] or bread dough mixing [10, 11]. However, at present, there is no deterministic model, based on continuum mechanics, able to describe satisfactorily all physical mechanisms involved at different structural scales. Conversely, at an industrial level, the design of cereal solid foams by extrusion and breadmaking processes is still based on a trial and error approach or, at best, using black box modeling, and it also often relies on experts' know-how. Hence, for various reasons, recently reviewed by Datta [12], physics-based models and their computer implementation are hardly ever used in the industry.

To combine the scientific understanding of material changes during processing and the ability to predict the final properties of the product, *basic knowledge models* (BKMs) can be used. They are defined as elementary models that (1) capture our knowledge of the mechanisms underlying the structural changes of the product during the different operations, (2) provide information on use properties, and (3) are expressed in a mathematical form simple enough to be used by food industry engineers [3]. The purpose of this chapter is twofold: (1) to show how scientific and expert knowledge can be integrated and represented by BKMS for the two phenomena – transition solid/liquid and expansion and (2) to illustrate the use of these BKMs for process simulation. For this purpose, two processes, extrusion and breadmaking, are examined with a focus on the phenomena of divided/continuous medium transition and cellular structure creation in both cases. In each case, the

available modeling approaches – either deterministic or more phenomenological and based on knowledge engineering – are presented.

2 Basic Knowledge Models for the Transition from Divided Solid to Continuous Medium

Both processes, extrusion and breadmaking, include a first step, mixing, the main objective of which is to homogenize ingredients, leading to the distribution of water in the flour components. Because of mechanical input (shear, extension), a macroscopically homogeneous phase is obtained (Fig. 1), either a dough based on gluten network at low energy ($SME < 100$ kJ/kg) and ambient temperature or a starch melt at high temperature ($T \geq T_m$ melting temperature of starch) and for higher *SME* (>100 kJ/kg). Compared to fluid mixing, this operation is complex, because both dough and melt are non-Newtonian, viscoelastic, and strain-history-dependent fluids, which is still challenging for modeling. Moreover, material free surface continuously changes during processing because of the motions of the arm and bowl in the mixer, or screw in the extruder barrel. Therefore, the use of FEM-based models (see for instance [13, 14]) would require extensive numerical developments to take these features into account. However, to achieve a good control of this operation, it is first necessary to determine the specific mechanical energy delivered to the material, *SME*.

Indeed, during *starchy product extrusion*, the essential step of this transition is starch melting. This phenomenon may be achieved at temperatures lower than T_m, the melting temperature, measured by DSC, as shown by Donovan [15]. Various research results reported subsequently have led to the determination of the starchy material melting temperature between 100 and 180°C and the enthalpy of fusion between 3 and 20 kJ/kg for moisture content between 15 and 30% wet basis (see for instance [16–18]). This temperature can be calculated by the Flory–Huggins equation, and its value may be ascertained by DSC experiments for specific recipes [19, 20]. The contribution of *SME* to this transition, indirect by solid friction or viscous dissipation, or direct by granule fragmentation, is still a scientific concern. However, initially, the T_m value may be assumed to be the temperature at the endothermic peak.

Once molten, the flow of the starchy material is controlled by its shear viscosity η, which is generally described by a power law:

$$\eta = K\,\dot{\gamma}^{\,m-1} \tag{1}$$

where K is the consistency in Pa.s^m, m the flow behavior index, and $\dot{\gamma}$ the shear rate (s^{-1}). K and m depend on temperature, moisture content *MC*, and thermomechanical history *(SME)* according to

$$K = K_o \exp\left[\frac{E}{R}\frac{1}{T_a} - \alpha MC - \beta SME\right] \tag{2}$$

$$m = m_o + \alpha_1 T + \alpha_2 MC + \alpha_3 SME + \alpha_{12} T \cdot MC + \alpha_{13} T \cdot SME + \alpha_{23} MC \cdot SME \tag{3}$$

where T and T_a are the absolute temperatures of melt in °C and K respectively, E is the activation energy (in J/mol), R is the gas constant (in J/mol/K). The coefficients $K_0, \ldots \alpha_{23}$ can be determined experimentally using specific rheometers, in-line and off-line, which take into account the effect of the sensitivity of the material on thermomechanical history [21–23]. Various methods allow the determination of the viscous properties of starchy melts in relation to extrusion [24]. Off-line methods, such as Rheoplast, also allow the determination of the elongational viscosity by performing Bagley corrections and Cogswell analysis, but measuring conditions are further from the extrusion conditions than in-line methods. The values of the coefficients can be found in the literature for starches, but they are seldom available for more complex and realistic recipes. For breakfast cereals, Brugger et al. [25] found that the effect of *SME* is not significant. The authors hypothesized that the minor constituents in the cereal flours could play a role as a lubricant and thus protect starch granules against thermal and mechanical stresses.

Once determined, the numerical values of the rheological model coefficients, thermal-physical properties, and melting temperature, can be used in *mechanistic models* and introduced into extrusion simulation software based on such models that allow the determination of the flow profile along the screw. Ludovic®, developed by Vergnes et al. [26] for computing flow conditions along the extruder, is an example of such software for co-rotating twin screw extrusion. It allows the calculation of the main flow variables, melt mean temperature, pressure, shear rate, shear viscosity, specific mechanical energy (*SME*), residence time, etc. along the screws, from the hopper to the die exit. Computation of the various variables is done separately for each type of screw element (partially or totally filled right-handed screw elements, totally filled left-handed screw elements, and blocks of kneading disks) and for the die components. For each screw element, envisioned as a C-shape chamber, pressure/flow rate relationships are computed considering the section of the channel as rectangular, with a constant width taking into account the variations of temperature and viscosity. Under such conditions, axial and tangential velocity components (radial velocity is null) can be determined in each slice and the volume flow rate Qv along a screw channel can be written as

$$Q_V = A\Omega + B\frac{1}{\eta}\frac{\Delta P}{\Delta \theta} \tag{4}$$

where A and B are coefficients depending on the screw geometry, Ω the screw rotation speed (rad/s), and ΔP the pressure variation along the angular screw section $\Delta\theta$. The shear viscosity η is deduced following the power law equation (1), from the shear rate $\dot{\gamma}$ averaged over the screw section. In each type of element,

only a 1D approach is applied and only average values are computed. These element models are linked together to obtain a global description of the flow field along the extruder. Summing up relations (4) along the screws, and knowing viscosity variations, the specific energy produced by viscous dissipation E_v can also be computed according to

$$\dot{W} = \int_V \eta \dot{\gamma}^2 dV \tag{5}$$

and

$$E_v = \frac{\dot{W}}{\rho_m Q_v} \tag{6}$$

where $\dot{W}$ is the power dissipated in the considered volume V of the screw and ρ_m is the melt density. Melting is considered to be instantaneous and takes place before the first restrictive element of the screw profile (kneading disk or left-handed screw element). The region of the melting process is essential for the design of the screw machines and the determination of the operating conditions. It is generally considered to occur in the first restrictive element (kneading disc, left-handed screw for instance), because of the compression and the friction of particles. The overall energy balance on the melting phenomenon within the extruder can be written as

$$\Delta H + C_p \Delta T = E_{cd} + E_f \tag{7}$$

where ΔH is the specific enthalpy for the state change, C_p is the heat capacity at constant pressure, $\Delta \boldsymbol{T}$ is the overall temperature increase up to peak temperature, E_{cd} and E_f are the terms of specific energy supplied by conduction from the barrel and screws by and dissipation by friction, respectively. Several authors found that the energy input for solid/melt transition in starch, cereal, and vegetables extrusion is approximately 500 J/g [27]. When (7) cannot be solved easily, the melting temperature is assumed to be the local temperature at the point before a restrictive element, where the pressure starts to increase. Afterwards, the material is considered to be fully molten and can fill the screw channel according to local geometry and flow conditions. Ludovic® has been applied successfully to various starchy materials and recipes [28–30], in spite of some uncertainties about rheological data. These applications have emphasized the significance of *SME*, suggested early experimentally [31], in defining starch structural modifications such as depolymerization.

Simulation is really useful because it describes the material changes during the complete process and not only in the areas where sensors are located. For thermally sensitive products, such as extruded cereal foods, it is important to consider the temperature distribution along the screw during the process and not only at the die, as shown in Fig. 2 for two breakfast cereal recipes (denoted C and H). Each profile

singularity (pressure peak, steep temperature and energy increases) are caused by the presence of a restrictive screw element downstream. The difference in the behavior between these two recipes is likely because of the viscosity differences. Finally, the similarity between *SME*, T_m, and viscosity profiles underlines the importance of viscous dissipation, which is first governed by the profile of the restrictive screw elements. An additional important feature of simulation is the possibility of the implementation of a virtual design of experiment (DOE). With DOE, the user can vary one or more input variables within a given simulation to determine the process sensitivity of specific results of interest on the changes of these variables. Overall DOE results for extrusion simulation of H recipe are summarized in contour plots shown in Fig. 2b. They show that the moisture content (*MC*) decreases and screw speed (*N*) increases, leading to an increase in *SME*, and thus the product temperature. Conversely, *MC* and *N* increases lead to a decrease in both viscosity and pressure, which is qualitatively explained by (1) and (2). The viscous dissipation is also governed by the screw speed and feed flow rate.

In conclusion, the importance of *SME* for controlling starch modifications and the significance of viscosity for controlling expansion (see the next section) underline the advantage of using such simulation tools for cereal product development by extrusion. Although the model implemented in this software is fully deterministic, it is simple and the software can be easily handled by professionals in the area. Moreover, it captures our knowledge on the mechanisms governing the structural changes of the product during extrusion and it provides information on use properties of extruded products. For these reasons, the model can be considered a BKM for twin-screw extrusion.

In the case of *breadmaking*, such a deterministic model is, for the moment, not available. Despite significant work on the modeling of fluid mixing, modeling of dough mixing has not been developed sufficiently, likely because of the diversity of mixer geometry and of the complexity of dough rheological behavior, which is continuously evolving. Assuming dough is a shear-thinning fluid in a filled vessel, Binding et al. [32] modeled mixing by the finite element method (FEM) and concluded that the outer part of the mixing arm led to the largest shear rates and energy input. The knowledge of *SME* during dough mixing is also important because its evolution reflects the structuration of the gluten network. *SME* can be derived from the torque of the mixing arm or deduced from the measurement of the dough temperature T_d through a simple energy balance [33]. For a given wheat flour, *SME* variations may reflect the degree of cross-linking of the *gluten network*, but the correlation is not so high as in the case of extruded starchy products [34]. The measurement of *SME* is also important because it helps to assess the viscosity of the dough, the determination of which requires extensive experimental effort on standard rotational rheometers. Indeed, *SME* is linked to viscous dissipation and, using Metzner–Otto's principle from the rotation speed of mixer arm *N*, the following can be stated:

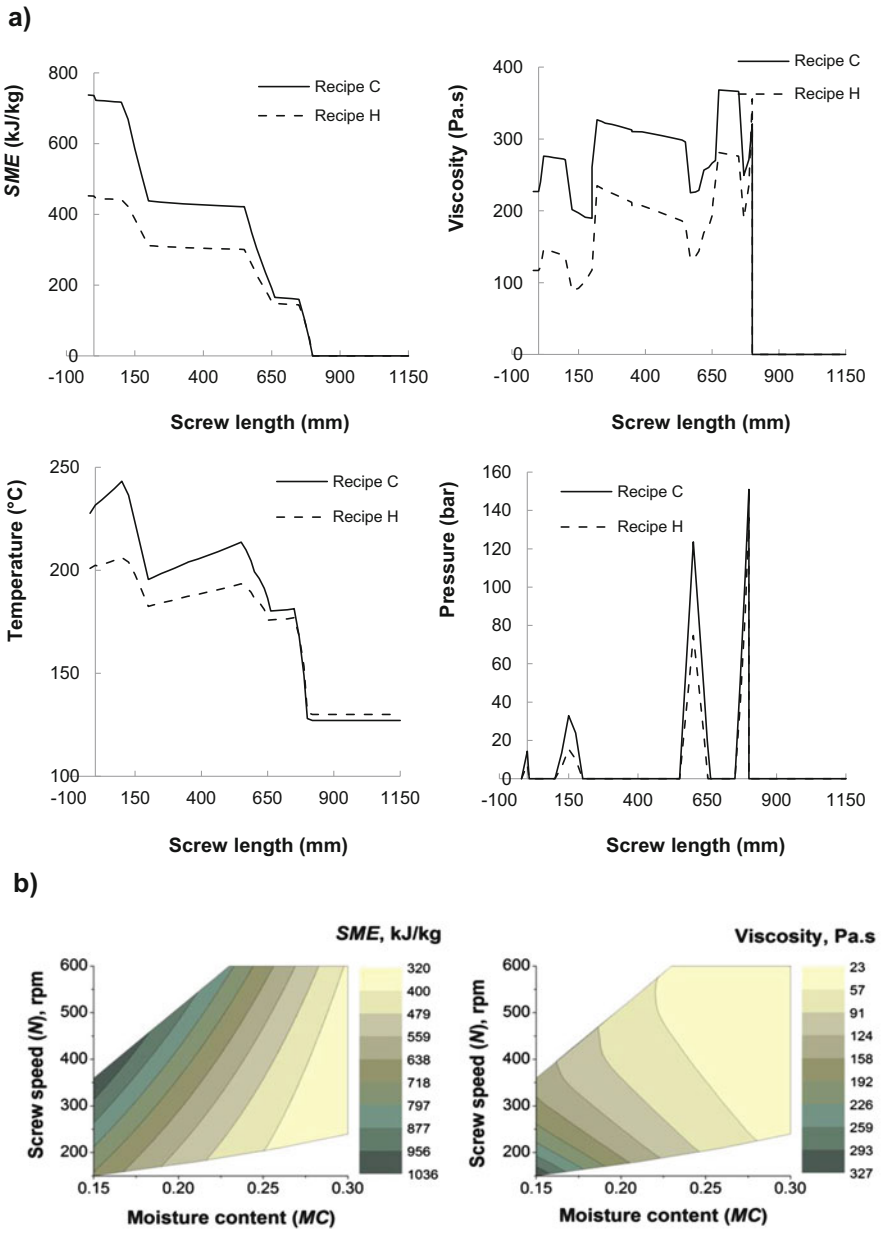

Fig. 2 Examples of results obtained by simulation of cereal twin screw extrusion by Ludovic® software. (**a**) Profile of specific mechanical energy (*SME*), shear viscosity, temperature, and pressure along the screws of the extruder, computed for breakfast cereals (Nusselt number = 12) processed on a Buhler twin screw extruder for the following conditions: flowrate $Q = 40$ kg/h, barrel temperature profile: 30, 80, 80, 100°C, die temperature = 100°C, $MC = 15\%$, and a die ∅ 4 mm. The products both contain 10% of sugar. Adapted from Brugger et al. [25]. (**b**) Application of design of experiment (DOE) in the extrusion simulation of recipe H. Effect of moisture content (*MC*) and screw speed (*N*) on computed variables, specific mechanical energy *SME* (*left*) and shear viscosity (*right*). The delimited areas represent the feasible extrusion domain: product

$$SME/t_m = \eta.\dot{\gamma}^2 \quad \text{and} \quad \dot{\gamma} = K_s.N \tag{8}$$

where η and $\dot{\gamma}$, are the dough shear viscosity and shear rate, respectively, t_m the mixing time, and K_s is a characteristic of the mixer which can be determined by superimposing the specific power consumption curves as a function of N to the flow curve of the dough $\eta(\dot{\gamma})$, provided it has been determined previously. Shear viscosity can be represented by the Cross model (Table 1). This model is more complex than the power law used for starch melts, although it tends to the same at high shear rates. Using same mixer but different flours, the dough shear viscosity can be assessed using (8). Conversely, using the same flour, different mixers can be characterized. Indeed, (8) suggests that the larger K_s the higher the contribution of shear to dough texture formation. Conversely, it is supposed that low K_s values indicate a major contribution of stretching (elongational strain), because stretching is more favorable to gluten network weaving, and intense shearing has been shown to lead to gluten network degradation [38, 39]. Hermannseder et al. [40] developed a model involving kinetics equations to describe the torque evolution in farinograph. This model is a more detailed approach than (8) because it takes into account the different states of the proteins during the measurement.

However, in industry, rheological properties of the dough are rarely measured. Dough state is more often described by a whole set of sensory criteria – stickiness, slackening, consistency, elasticity, for instance. These criteria are not measured instrumentally but evaluated by the baker. Professional experts relate those criteria to recipe and operating conditions, which integrates their practical experience and, sometimes, scientific knowledge. To address such situations, where the lack of rheological data is supplemented by expert knowledge, alternative modeling techniques can be more relevant. In the case of dough state assessment, *qualitative models* were developed to formalize this knowledge and to predict these sensory criteria from the mixing conditions. Algebra (Q-algebra) was developed for modeling in the form of qualitative functions the set of rules used by the experts to assess the sensory characteristics of the wheat flour dough. It has been used to model the states of the dough at the end of first mixing and the end of texturing operations, the two successive steps of mixing [41]. The state of the dough at the end of first mixing is the only output variable of this step. It is influenced by the characteristics of the ingredients (percentage flour, water, protein, and pentosan content, for instance). The state of the dough at the end of texturing (second mixing step) is influenced by the dough consistency at the start of texturing, by the target temperature at the end of mixing, and by the mixer settings: the shear velocity between the arm and bowl, and the specific mechanical energy during texturing. It is defined by the following descriptors: smoothing velocity *SV*, smooth aspect *SA*, extensibility *Ext*, stickiness

Fig. 2 (continued) temperature $\leq$190°C to avoid thermal degradation, pressure $\leq$20 MPa and torque $\leq$100 N.m for extruder support requirement. Other processing parameters were kept constant as in (**a**)

Table 1 Main rheological models and typical numerical values for shear and extensional viscosities of cereal products used in this chapter for computing end properties, with data source in subscripts

Process and material strain mode	Extrusion, starchy melts											Breadmaking, bread dough (gluten network)		
Shear	(1)–(3) [a]											Cross model $\eta = \frac{\eta_0}{1+(\dot{\gamma}/\dot{\gamma}_0)^m}$ [b]		
	K_0 Pa.s	E/R K	α	β g/J	m_0	α_1 C^{-1}	α_2	α_3 g/J	α_{12} C^{-1}	α_{13} C^{-1} g/J	α_{23} g/J	η_0 Pa.s	$\dot{\gamma}_0$ s^{-1}	m
	$1.12.10^{-5}$	10,080	13.5	0	0	0.0037	−2.549	0	0.0095	0	0	7.10^6	$2.2.10^{-5}$	0.88
Extension	Elongational viscosity is replaced by storage modulus E' ($T > Tg + 30°C$) = f(MC) [c] in the expansion model (9)–(11)											$\eta_E = K_E\, \dot{\varepsilon}^{\,m-1}$ (~Eqs. 1, 17) for $\varepsilon_b = 1$ [d]		
	MC	0.12	0.14	0.16	0.18	0.205	0.225	0.245	0.265	0.275	0.305	K_E $Pa.s^m$	m	
	E' (MPa)	42	31	23	17	12	9	7	6	5	4	17,800	0.45	

[a] For cereal blend H [25]
[b] From Shehzad et al. [33] used in (8)
[c] Values taken for recipe from Robin et al. [35] extended by those from Babin et al. [36] for waxy maize starch
[d] For a dough with 62% total water content [37]

Stic, stability *Stab*, consistency *Cons*, elasticity *Ela*s, and creamy color *CC*. The criteria for describing the behavior of the dough and the bread were selected thanks to a glossary of terms defining dough quality and bread baking, developed in French and available on the Web [42]. The terms of language at different levels – empirical, technological, and scientific – are identified by (1) expressing explicitly semantic relationships between terms from different levels of knowledge and (2) accounting for the rheological knowledge that can both describe the behavior of dough and suggest instrumental methods where only sensory assessments exist. Expert rules are written as qualitative functions which allow the computation of the dough state according to the inputs of the operation and the process settings. Radar plots (Fig. 3), show simulations from a qualitative model where a decrease of *SME* has two main effects: (1) decrease of smooth aspect and elasticity and (2) increase of consistency. Besides practical aspects for dough processing, these results clearly infer the dough rheological properties because, for instance, it has been shown that low levels of *SME* induce an increase of dough viscosity [37]. The KBS has been validated by comparing the predictions of dough state after mixing with its assessment by expert bakers and using different mixing equipment [43]. The qualitative functions are rather simple models and are implemented as a KBS with a proper interface that favors use by professionals. As shown before, they capture the experts' knowledge on the main mechanisms governing dough structural changes during mixing. For these reasons, they can be considered a BKM.

As for extrusion, the software (here the KBS) can be used to screen a wide range of inputs and to perform a DOE. For instance, Fig. 4 illustrates the common knowledge that a minimum level of protein is necessary to support more intensive mixing in order to minimize stickiness. Conversely, at greater protein content, a larger level of *SME* is necessary to promote dough elasticity. These trends explain that a lower energy level ($\leq$40 kJ/kg) is used in French breadmaking for mixing dough of wheat flour with medium protein content (10–11%) and why more intense mixing processes (*SME* $>$ 100 kJ/kg), such as the Chorleywood process, are more adapted for wheat flour with higher protein content [44, 45].

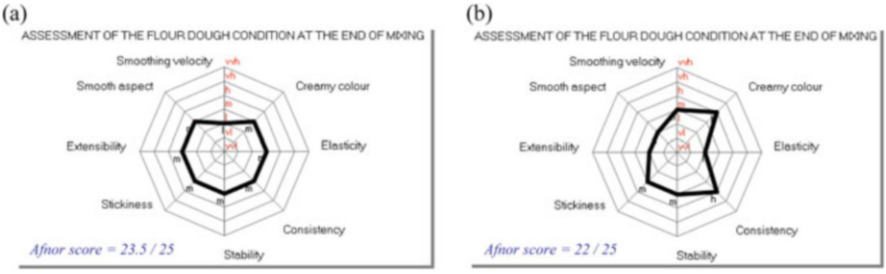

Fig. 3 Examples of the KBS outputs for wheat flour dough mixing: predictions of dough state at the end of mixing, starting from a standard consistency ($350 \leq Cons \leq 450$ UB), a standard dough temperature ($22 \leq T_d \leq 25$°C), an average shear velocity, and a level of specific energy (**a**) medium and (**b**) low. Scale ranges from vvh (very excessive) to vvl (very insufficient)

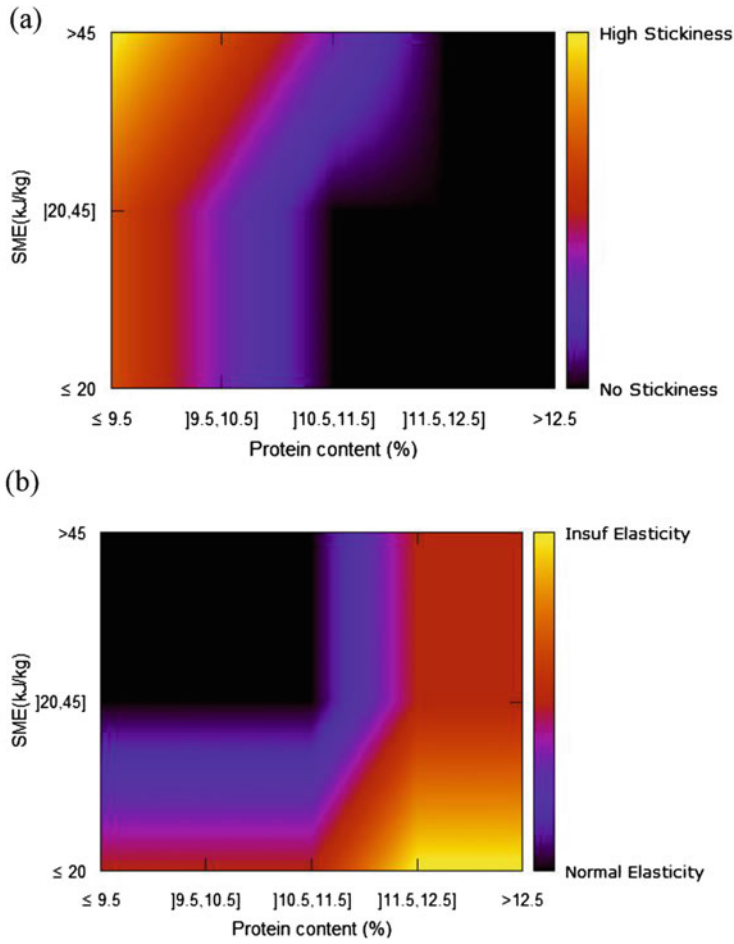

Fig. 4 Two-dimensional contour plots derived from the KBS computation for simulating dough mixing, representing (**a**) dough stickiness and (**b**) elasticity variations with protein content and specific mechanical energy for oblique-axis mixer. Adapted from Kansou et al. [43]

For both processes, extrusion and breadmaking, the presented BKMs, based on rheology and technology, identify SME and average shear rate in the mixer $\dot{\gamma}$, for example, in the extruder, as important variables. These variables account for the transition from solid to continuous medium, and help to predict dough or melt flow.

3 Basic Knowledge Models for Expansion and Cellular Structure Creation

Expansion covers all the steps during which the volume – and the porosity – of the dough/melt increase the most, and the cellular structure is created and largely set (Fig. 1). Imaging methods at different structural scales, especially X-ray micro-tomography (XRT), are very useful to characterize the final structure. When dynamics are not too fast, as is the case in breadmaking, the development of the cellular structure can also be followed. Conversely, the fast kinetics of vapor expansion at the die outlet prohibits the dynamic approach, as is the case in extrusion.

Indeed, in this latter case, *expansion* can be considered as a succession of different mechanisms occurring in a few fractions of a second: bubbles nucleate in the melt and grow before they can possibly coalesce and are set, when the melt becomes glassy, whilst the whole extrudate possibly collapses [46–48]. Given the complexity and fast kinetics of these mechanisms, few attempts at deterministic modeling have been found in the literature [49–52]. These models all refer to uncertainties of the melt rheological properties and bubble number. Clearly, there is a need to derive BKMs that can be used to model this essential phenomenon. More recently, using knowledge reasoning from the literature and expertise, Kristiawan et al. [53] have produced a concept map which provides an overview of texturing mechanism during extrusion process. This map (Fig. 5) depicts the relations between input variables (processing variables and rheological properties), mechanisms of expansion described before, and output variables (foam density ρ^* and anisotropy factor AF). Processing variables are product temperature T_p, moisture content MC, specific mechanical energy SME, and die geometry. Melt rheology involves both shear and elongational viscosities. The relations in the concept map are qualitative: they are expressed by the signs +, positive effect or –, negative effect. The magnitude of the effect is presented and quantified with a number of signs. The net effect of one input variable on one output variable is the sum of all effects between these variables. For instance, it can be seen that shear viscosity largely affects expansion negatively through its major negative influence on bubble growth.

As data about elongational viscosity of starchy melts are scarce in the literature [54–56], it is suggested that the influence of the variable elongational viscosity can be taken into account by the storage modulus (E') in the rubbery domain ($T > T_g$) because it also reflects elastic property and it has also been shown to take into account the effect of amylose content on foam expansion [36]. Thereafter, using the variables presented in the concept map (Fig. 5), given the power law trend for the variations of VEI with shear viscosity [46, 50, 57], and in agreement with the model of bubble growth in a viscous fluid [58], a mathematical expression of a phenomenological expansion model that links the bulk expansion indices to melt shear viscosity can be proposed:

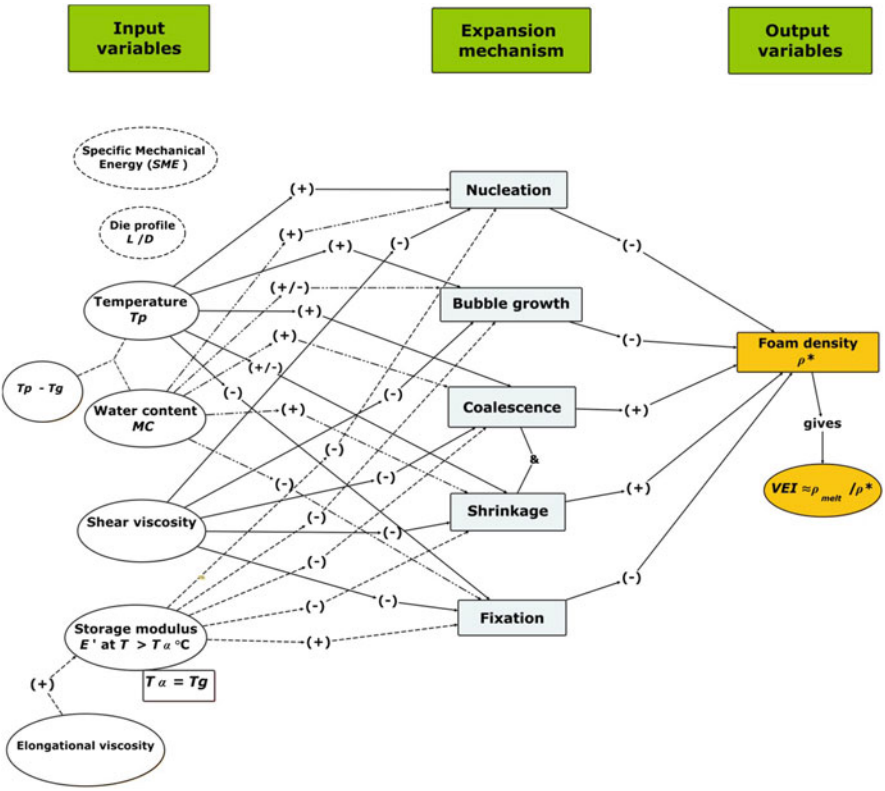

Fig. 5 Concept map of qualitative reasoning of vapor expansion of starchy and cereal products processed by extrusion cooking [53]. For instance, water (*MC*) favors the creation of bubbles by nucleation, which moderately decreases density, leading to a positive influence on expansion

$$VEI = \alpha_v \left(\frac{\eta}{\eta_0}\right)^{n_V} \quad \text{and} \quad SEI = \alpha_s \left(\frac{\eta}{\eta_0}\right)^{n_S} \tag{9}$$

where *VEI* and *SEI* are the volumic and radial (sectional) expansion indices, respectively, which were accurately defined by Alvarez-Martinez et al. [59]. The model parameters (α_i and n_i) take into account the effect of processing variables and melt storage modulus ($E'(T > T_g)$) according to the following equations:

$$\alpha_i = b_{i0}(MC/MC_0)^{b_{i1}} \left(T_p/T_{p0}\right)^{b_{i2}} (SME/SME_0)^{b_{i3}} \left(E'/E'_0\right)^{b_{i4}} (L/D)^{b_{i5}} \tag{10}$$

$$n_i = b_{i6}(MC/MC_0)^{b_{i7}} \left(T_p/T_{p0}\right)^{b_{i8}} (SME/SME_0)^{b_{i9}} \left(E'/E'_0\right)^{b_{i10}} (L/D)^{b_{i11}} \tag{11}$$

The processing variables with subscript 0 aim to obtain dimensionless values. The term L/D represents the deformation history in the die. Because of flow

orientation and melt internal stresses, expansion is often anisotropic, which is important in determining the cellular structure [30, 60]. The anisotropy factor *AF* is then defined by the following relation between longitudinal (*LEI*) and radial expansion (*SEI*):

$$AF = LEI/SEI^{0.5} = VEI/SEI^{3/2} \tag{12}$$

Hence, for isotropic expansion, $LEI = SEI^{0.5}$, $AF = 1$. Using the data of mean cell size and mean cell wall size obtained from granulometry analysis of X-ray tomography images, the fineness of the cellular structure can be defined by

$$F = \sqrt{\frac{\left(\frac{\overline{MCS}}{MCS}\right)^2 + \left(\frac{\overline{MWT}}{MWT}\right)^2}{2}} \tag{13}$$

where *MCS* is the mean cell size, *MWT* the mean cell wall thickness, and $\overline{MCS}$ and $\overline{MWT}$ their respective average values in the experimental data set, chosen equal to 1 mm and 250 μm, according to Babin et al. [36] and Robin et al. [30]. With such a definition, the larger F ($F > 1$), the finer the cellular structure (smaller cells and walls). Conversely, the coarser structures (large cells and walls) are obtained for low F values ($F < 1$). Fineness has been shown to be negatively correlated to anisotropy (*AF*): finer cellular structure is favored by longitudinal expansion [30, 36, 60, 61]. This result allows the prediction of the cellular structure from the knowledge of macroscopic expansion indices (*VEI*, *SEI*). Hence, using (9)–(13), the variations of *SEI* and F with viscosity and temperature, for instance, can be computed. This is illustrated by simulations achieved by using extruder configuration and operating conditions described in Robin et al. [30], results being presented as contour plots (Fig. 6a–d). Clearly, moisture, between 0.2 and 0.24, and viscosity, between 100 and 500 Pa.s, have a negative influence on sectional expansion, which decreases between 2 and 8. A temperature decrease from 170°C to 135°C led to the same result. These trends could be foreseen qualitatively from the concept map (Fig. 5) but they are now evidenced quantitatively. In complement, the computation of the fineness F clearly showed an opposite trend to that of radial expansion. These results are well in line with those found experimentally.

Assuming that product development would target low density (high expansion) and fine cellular structure for optimum texture properties (crispiness among others), these results suggest that a compromise has to be found. For this purpose, simulation can be useful. To address the simultaneous optimization of these two responses, graphical optimization (overlay contour plots) can be performed by superimposing the contour plots of each response, in our case *SEI* and F, as a function of two input variables, the other variables being held constant. By applying the constraints to the responses and input variables, the shared area of the overlaid plots can be obtained as a feasible region of extrusion variables as shown by example with the overlaid contour plot for wheat flour extrusion (Fig. 7). Given

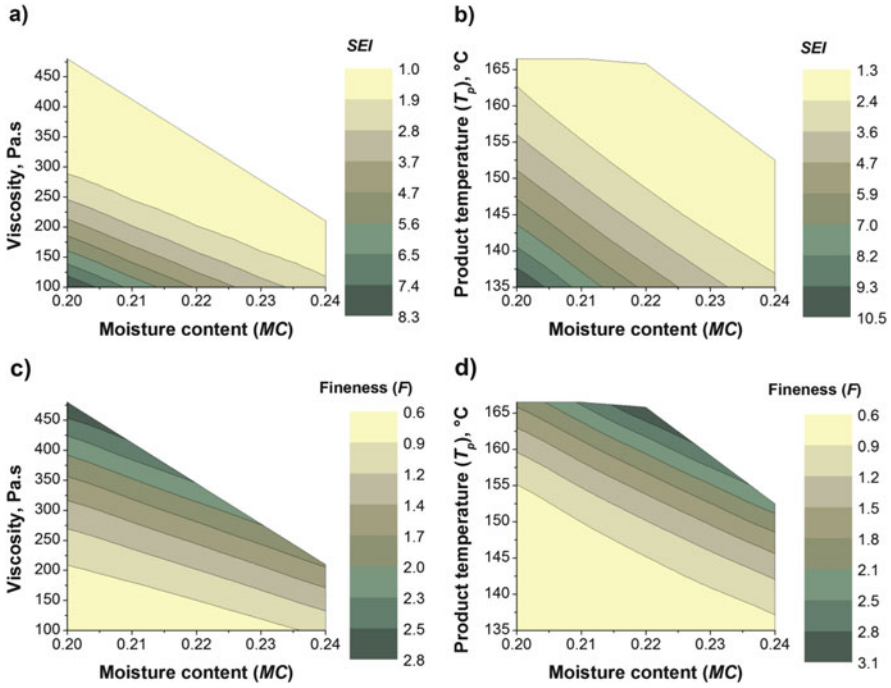

Fig. 6 Simulation of the effect of extrusion variables on expansion (*SEI*) and cellular fineness (F) of wheat flour extruded under conditions used by Robin et al. [30]: contour plots representing the effects of moisture content and (**a**, **c**) melt viscosity, other input variables being constant (T_p 137°C, *SME* 87 kWh/ton), and (**b**, **d**) product temperature at the die exit (T_p), other input variables being held constant (*SME* 87 kWh/ton, Viscosity 100 Pa.s). The variables, such as viscosity and *SME*, at the die exit, were computed using Ludovic® software. The melt storage modulus was approximated using the data of Robin et al. [35]. The fineness (F) was computed from predicted *AF* using relation: $F = 0.91\ AF + 0.53$ ($R^2 = 0.67$). Adapted from Kristiawan et al. [53]

the region of extrusion variables selected, it is possible, in turn, to compute the processing variables leading to this region, using the simulation software of extrusion described in the preceding section. Although this approach may not lead to accurate optimum conditions, it should help to delineate a realistic domain where experimental trials could be successfully achieved for this purpose.

Whereas several mechanisms interact in the case of expansion by extrusion, in *breadmaking*, *bubble growth* may be considered as the main mechanism responsible for the creation of cellular structure [1]. This is because of the production of gas by yeast activity during dough fermentation, which is retained thanks to the extensional properties of the starch-gluten matrix [62]. This mechanism may be described initially by the growth of a single bubble in a viscous medium [58] and adapted to the specific case of wheat flour dough to express the growth rate of the bubble:

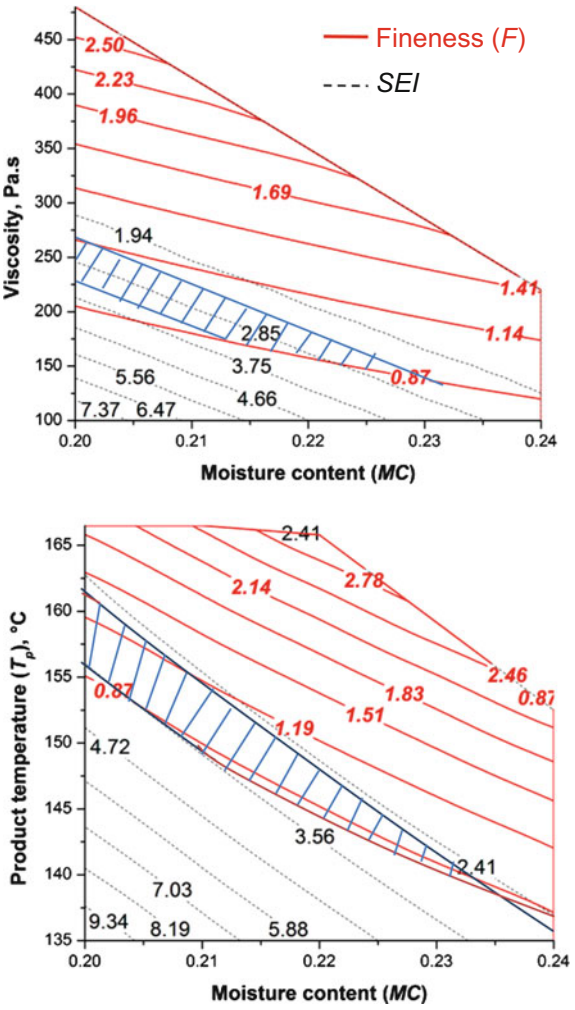

Fig. 7 Examples of finding a compromise between expansion and cellular fineness of wheat flour extruded foam, using an overlaid contour plot technique. The *hatched area* indicates the optimum region for extrusion of wheat flour according to the goals: $SEI = 3$ and fineness $(F) = 1$. The constraints on the response are $2.5 < SEI < 3.5$ and $0.85 < F < 1.25$ and on the extrusion variables: $0.2 < MC < 0.24$, $125 < T_p < 165°C$, $80 < SME < 200$ kWh/ton, $100 < \eta < 500$ Pa. s, and $3 < E' < 11$ MPa

$$\frac{1}{r}\frac{dr}{dt} \approx \frac{P_v}{\eta_E} \tag{14}$$

r being the bubble radius (m), P_v the internal gas pressure of the bubble (Pa), and η_E the bi-extensional viscosity of the matrix (Pa.s), defined by the power law model (Table 1). Equation (3) allows one to check that the strain rate value for bubble growth in the dough is about 10^{-3}/s. Equation (14) is the simplest expression of the mechanism. It should be completed by gas diffusion from dough matrix to bubble, which leads to more complex solutions and involves more uncertainty about the dough properties and bubble number [63–65]. However, these solutions can be validated in a pilot plant for the supervision of the dough fermentation process [66].

Bubble growth in fermenting dough has been studied by X-ray tomography (XRT) which allows the quantifying of the distribution of gas cells width and cell wall thicknesses, their average value *MCS* and *MWT*, and their kinetics [67]. Results showed that, after simple bubble growth, bubbles begin to connect to each other and possibly coalesce, which increases the heterogeneity of cellular structure [68]. In the second stage, after simple bubble growth, (14) is no longer valid and the prediction of the cellular structure requires more sophisticated models based on FEM-3D [69] to take bubble interaction into account. However, this approach requires extensive computing times and there are still uncertainties regarding rheological properties and initial cell numbers. Conversely, a BKM for dough fermenting can be built thanks to the Gompertz model [70] for porosity P kinetics, and an exponential decay for the loss of dough stability, $S(t)$, defined by the ratio of the dough height H to its maximum width L_{max}:

$$P(t) = a \cdot \exp\left(-\exp\left(-\frac{b \cdot e}{a}(t-c)\right)\right) + d \text{ and } S(t) = \frac{H}{L_{max}}(t) = a' \cdot \exp\left(-\frac{t}{b'}\right) + c' \quad (15)$$

t being the proofing time, $e = \exp.(1)$ and parameters a, b, c, d, a', b', c' are fitted to experimental data obtained by simple imaging methods at macroscopic scale [71]. Parameter c is the critical time defining the end of simple bubble growth, inversely correlated to the growth rate predicted from (14). Besides c, an important parameter is the characteristic time, b'. The lower the characteristic time b', the more rapidly the dough spreads and the less stable it is. Extensive spreading or loss of stability is clearly undesirable and can be associated with internal collapse caused by gas cell coalescence [62, 72, 73].

In analogy with the approach described for biphasic media such as emulsions or liquid foams [74], an apparent capillary number is available to integrate the influence of the various levels of organization of fermented dough envisioned by Turbin-Orger et al. [68] as a triphasic medium (gas bubbles /liquid films/starch-gluten matrix):

$$Ca^* = \left(\tau . MWT^2\right)/(\sigma . MCS) \quad (16)$$

where τ is the elongational stress exerted by the gas cell on the starch/gluten matrix, derived from the knowledge of the elongational viscosity, with strain rate $\dot{\varepsilon}$:

$$\tau = K_E.(\dot{\varepsilon})^{m-1} \text{ for a constant strain } \varepsilon_b = 1 \quad (17)$$

The values of the consistency index K_E and the flow behavior index m are reported in Table 1 [37] for the same dough compositions at a strain value $\varepsilon_b = 1$ and the average strain rate value $\dot{\varepsilon} = 2.10^{-4}$/s, in accordance with (14) [68]. They

can be determined by measurements performed with a uniaxial compression test under lubricated conditions [75, 76].

The surface tension σ of dough liquor, taken as a model for liquid films separating bubbles, varies from 35 to 41 mN/m, according to the content of arabino-galactan-protein [77]. The values of the mean cell wall thickness (*MWT)*, taken here as the value of gluten filament thickness, and *MCS*, chosen as the average radius of gas cells, are determined by XRT and the ratio MWT^2/MCS defines the cellular structure. Ca^* has been shown to be linked to the characteristic stability time b' defined in (15), according to the relation

$$b' = a'_0 \,.\, \mathrm{Ln}\, Ca^* + b'_0 \tag{18}$$

with $a'_0 = 3.07$ and $b'_0 = 26$ min as defined by experimental values found by Turbin-Orger et al. [68]. Equations (16)–(18) can be considered as BKM for fermenting dough. Using these equations, it is possible compute the cellular structure ratio for various values of extension stress and stability time (Fig. 8), taking liquid surface tension constant $\sigma = 40$ mN/m. This value should be modified in the case of addition of surface active agents. These curves show that, for the same value of cellular ratio, dough is more stable because it leads to greater stability time for higher τ values. Because cellular structure is mainly acquired during fermentation, and set during baking, they show that it is possible to assess the cellular

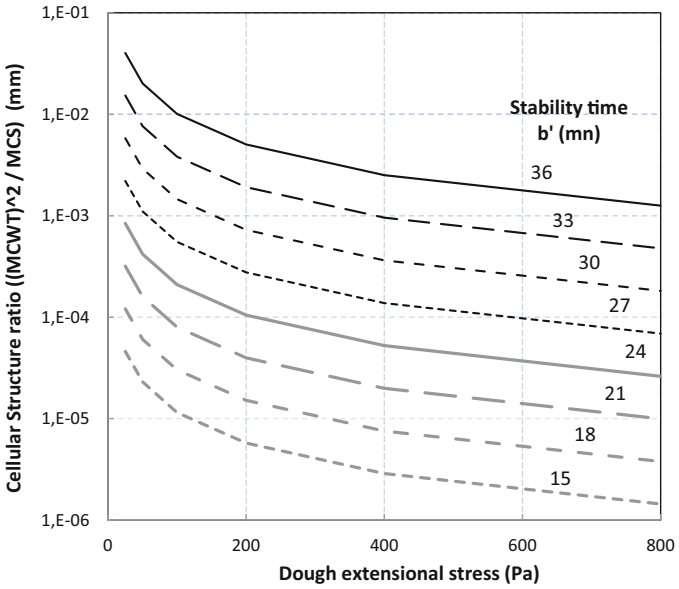

Fig. 8 Variations of fermented dough cellular structure ratio, defined by MWT^2/MCS, mean cell wall thickness of gluten filaments to mean gas cell size, respectively, with dough extensional stress τ and macroscopic stability time b', for a constant value of dough liquor surface tension $\sigma = 40$mN/m. τ is computed for a constant strain =1 and constant strain rate = 2.10–4/s and b' is defined by (15)

structure once dough rheological measurements and macroscopic imaging of fermenting dough follow-ups are performed.

4 Example of the Use of BKMs for Process Integration: From Divided Solid to Cellular Structure

Process integration can be achieved by coupling BKMs. This is achieved for extrusion by coupling the expansion model with simulation software. In the case of breadmaking, BKMs can be integrated to couple the mixing and fermenting operation. By assuming that rheological properties are set after the mixing stage, and not modified during proofing, one may predict, for a specific range of dough composition, the dough porosity and stability during proofing by simply measuring specific energy after mixing, more precisely, specific mixing power P_s and time t_m ($SME \approx P_s.t_m$), and apply the following regression model [78]:

$$\alpha = k_0 \cdot \left(\frac{P_s - \min(P_s)}{\max(P_s) - \min(P_s)} \right)^{k_1} \cdot \left(\frac{t_m - \min(t_m)}{\max(t_m) - \min(t_m)} \right)^{k_2} \tag{19}$$

α being any coefficient of (15). The three parameters k_0, k_1, and k_2 have been determined by fitting the values of the α coefficients to P_s and t_m for a set of mixing conditions previously defined [33]. Subsequently, it is possible to draw the variations of the characteristic times c and b' as functions of P_s and t_m for a given composition of wheat flour dough (Fig. 9).

From these curves it is possible to understand the mixing strategies to obtain dough with desirable porosity and stability, and hence orientate cellular structure using Ca^* rationale, during fermentation. For instance, Fig. 9a clearly shows that intense mixing (high SME) leads to rapid volume increase (low c values) which is typical of industry requirements. These conditions may lead to rapid loss of

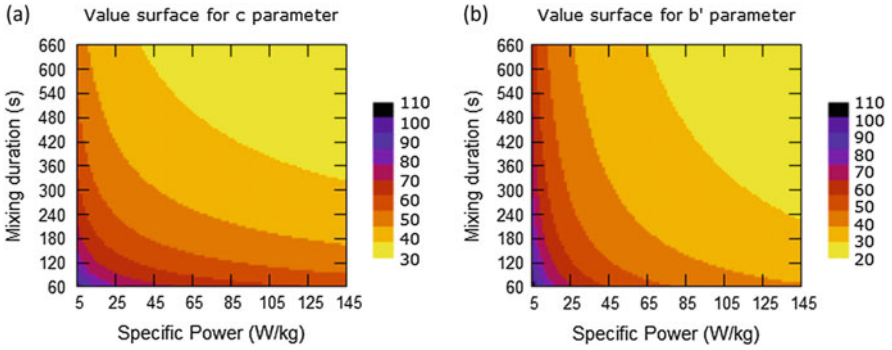

Fig. 9 Contour plots of characteristic times of (**a**) porosity and (**b**) stability from (15) as function of mixing time and specific power, using (19) and experimental data available from Shehzad et al. [33] and Turbin-Orger et al. [37]

stability, but more homogeneous cellular structure, which is solved by fermenting dough in pans. Conversely, mixing at lower *SME* (mild conditions, craft bakery) leads to longer dough development and larger stability time to favor flavor development and structure heterogeneity, characteristic of the traditional "baguette."

5 Conclusion

In this chapter, Basic Knowledge Models for cereals processing, operations have been defined, focusing on the transition to continuous medium and on the creation of cellular structure. By using such models, food engineers can design cereal food products and predict their texture properties. For this purpose, the available technological and scientific knowledge for specific process should be integrated when the use of models based on partial differential equations is still difficult. Subsequently, they should be implemented in computer tools such as a KBS, developed for the modeling of the flour mixing operation, or Ludovic®, software for twin screw extrusion, as exemplified in this chapter. Finally, they could be applied to a wide domain of compositions, provided data on product rheological properties are available.

Such an approach would enable one to cope with the sustainability challenges in the food industry, by contributing to an eco-design of food processes and products. It would also help to design products with improved nutritional properties. For instance, the dietary fiber increase and protein reinforcement in recipes greatly modify the rheological behavior of dough and melts, slightly changing the mechanisms of divided/continuous medium transition and cellular structure creation [79]. Thus the use of integrated models would help one to design products with target nutritional and sensory properties, provided their porosity and cellular structure are precisely characterized. Subsequently, the pathways for reaching these targets could be defined according to the so-called reverse engineering approach.

References

1. Bloksma AH (1990) Dough structure, dough rheology and baking quality. Cereal Foods World 35:237–244
2. Colonna P, Tayeb J, Mercier C (1989) Extrusion-cooking of starch and starchy products. In: Mercier C, Linko P, Harper JM (eds) Extrusion-cooking. AACC, St Paul, pp 247–319
3. Della Valle G, Chiron H, Cicerelli L, Kansou K, Katina K, Ndiaye A, Whitworth M, Poutanen K (2014) Basic knowledge models for the design of bread texture. Trends Food Sci Technol 36:5–14
4. Gibson LJ, Ashby MF (1997) Cellular solids, structure and properties. Cambridge Press University
5. Guessasma S, Chaunier L, Della Valle G, Lourdin D (2011) Mechanical modelling of cereal solid foods. Trends Food Sci Technol 22:142–153

6. Nicolas V, Salagnac P, Glouannec P, Ploteau JP, Jury V, Boillereaux L (2014) Modelling heat and mass transfer in deformable porous media: application to bread baking. J Food Eng 130:23–35
7. Purlis E, Salvadori VO (2009) Bread baking as a moving boundary problem. Part 2: model validation and numerical simulation. J Food Eng 91:434–442
8. Zhang J, Datta AK (2006) Mathematical modeling of bread baking process. J Food Eng 75: 78–89
9. Ganjyal G, Hanna MA, Supprung P, Noomhorm A, Jones D (2006) Modeling selected properties of extruded rice flour and rice starch by neural networks and statistics. Cereal Chem 83: 223–227
10. Grote B, Zense T, Hitzmann B (2014) 2D fluorescence and multivariate data analysis for monitoring of sourdough fermentation process. Food Control 38:8–18
11. Lamrini B, Della Valle G, Trelea IC, Perrot N, Trystram G (2012) A new method for dynamic modelling of bread dough kneading based on artificial neural network. Food Control 26:512–524
12. Datta AK (2016) Toward computer-aided food engineering: mechanistic frameworks for evolution of product, quality and safety during processing. J Food Eng 176:9–27
13. Connelly RK, Kokini JL (2004) The effect of shear thinning and differential viscoelasticity on mixing in a model 2D mixer as determined using FEM with particle tracking. J Non Newtonian Fluid Mech 123:1–17
14. Connelly RK, Kokini JL (2007) Examination of the mixing ability of single and twin screw mixers using 2D finite element method simulation with particle tracking. J Food Eng 79: 956–969
15. Donovan JW (1979) Phase transitions of the starch-water systems. Biopolymers 18:263–275
16. Biliaderis C, Page C, Maurice T, Juliano B (1986) Thermal characterization of rice starches: a polymeric approach to phase transition of granular starch. J Agric Food Chem 34:6–14
17. Cooke D, Gidley MJ (1992) Loss of crystalline and molecular order during starch gelatinization – origin of the enthalpic transition. Carbohydr Res 227:103–112
18. Whittam MA, Noel TR, Ring SG (1990) Melting behaviour of A- and B-type crystalline starch. Int J Biol Macromol 12:359–362
19. Nunez M, Sandoval AJ, Muller A, Della Valle G, Lourdin D (2009) Thermal characterization and phase behavior of a ready-to-eat breakfast cereal formulation and its starchy components. Food Biophys 4:291–303
20. van Soest JJG, Bezzemer RC, De Wit D, Vliegenthart JFG (1995) Influence of glycerol on the melting of potato starch. Ind Crop Prod 5:1–9
21. Vergnes B, Villemaire J-P (1987) Rheological behavior of low moisture molten maize starch. Rheol Acta 26:570–576
22. Vergnes B, Della Valle G, Tayeb J (1993) A specific in-line rheometer for extruded starchy products. Design, validation and application to maize starch. Rheol Acta 32:465–476
23. Horvat M, Ladiges D, Schuchmann HP (2014) Investigation of the nucleation during extrusion cooking of corn starch by a novel nucleation die. Food Bioprocess Technol 7:654–660
24. Xie F, Halley PJ, Averous L (2012) Rheology to understand and optimize processibility, structures and properties of starch polymeric materials. Prog Polym Sci 37:595–623
25. Brugger A, Chaunier L, Della Valle G, Delleman J-P, Kristiawan M (2013) Détermination de comportements visqueux pour la simulation d'extrusion de formulations de céréales petit-déjeuner à l'aide du Rheoplast®. Industrie des Céréales 34/4(184):18–22
26. Vergnes B, Della Valle G, Delamare L (1998) A global computer software for polymer flows in corotating twin screw extruders. Polym Eng Sci 38(11):1781–1792
27. Barron C, Della Valle G, Colonna P, Vergnes B (2002) Energy balance of low hydrated starches transition under shear. J Food Sci 67:1426–1437
28. Berzin F, Tara A, Tighzert L, Vergnes B (2010) Importance of coupling between specific energy and viscosity in the modeling of twin screw extrusion of starchy products. Polym Eng Sci 50(9):1758–1766

29. Della Valle G, Barres C, Plewa J, Tayeb J, Vergnes B (1993) Computer simulation of starchy products' transformation by twin-screw extrusion. J Food Eng 19:1–31
30. Robin F, Engmann J, Pineau N, Chanvrier H, Bovet N, Della Valle G (2010) Extrusion, structure and mechanical properties of complex starchy foams. J Food Eng 98:19–27
31. Meuser F, Van Lengerich B, Reimers H (1984) Extrusion cooking of starches. Starch 36: 194–199
32. Binding DM, Couch MA, Sujata KS, Webster MF (2003) Experimental and numerical simulation of dough mixing in filled geometries. J Food Eng 58:111–123
33. Shehzad A, Chiron H, Della Valle G, Lamrini B, Lourdin D (2012) Rheological and energetical approaches of wheat flour dough mixing. J Food Eng 110:60–70
34. Angioloni A, Dalla Rossa M (2005) Dough thermo-mechanical properties: influence of sodium chloride, mixing time and equipment. J Cereal Sci 41:327–331
35. Robin F, Dattinger S, Boire A, Forny L, Horvat M, Schuchmann HP (2012) Elastic properties of extruded starchy melts containing wheat bran using on-line rheology and dynamic mechanical thermal analysis. J Food Eng 109(3):414–423
36. Babin P, Della Valle G, Dendievel R, Lourdin D, Salvo L (2007) X-Ray tomography study of the cellular structure of extruded starches and its relations with expansion phenomenon and foam mechanical properties. Carbohydr Polym 68:329–340
37. Turbin-Orger A, Shehzad A, Chaunier L, Chiron H, Della Valle G (2016) Elongational properties and proofing behaviour of wheat flour dough. J Food Eng 168:129–136
38. Haraszi R, Larroque OR, Butow BJ, Gale KR, Bekes F (2008) Differential mixing action effects on functional properties and polymeric protein size distribution of wheat dough. J Cereal Sci 47:41–51
39. Peressini D, Peighambardoust SH, Hamer RJ, Sensidoni A, van der Goot AJ (2008) Effect of shear rate on microstructure and rheological properties of sheared wheat doughs. J Cereal Sci 48:426–438
40. Hermannseder B, Haseeb AM, Kugler P, Hitzmann B (2016) Development of a model for the simulation of farinograph measurements. In: Chinesta F, Cueto E (eds) Proceedings of ESAFORM Conference, 27–29 April, Nantes, France. To be published by AIP
41. Ndiaye A, Della Valle G, Roussel P (2009) Qualitative modelling of a multi-step process: the case of French breadmaking. Expert Syst Appl 39:1020–1038
42. Roussel P, Chiron H, Della Valle G, Ndiaye A (2010) Knowledge collection about quality descriptors and state variables of dough and breads for French breadmaking. http://www.cepia.inra.fr/Outils-et-Ressources/Editions/glossaire/%28key%29/2
43. Kansou K, Chiron H, Della Valle G, Ndiaye A, Roussel P (2014) Predicting the quality of wheat flour dough after mixing by modelling expert's know-how. Food Res Int 64:772–782
44. Cheio J (2010) Le pétrissage: mesurer et interpréter pour mieux innover. Ind des céréales 166:14–17
45. Collins B (1982) Breadmaking processes. The master bakers' book of breadmaking. Turret Press, London
46. Della Valle G, Vergnes B, Colonna P, Patria A (1997) Relations between rheological properties of molten starches and their expansion behaviour in extrusion. J Food Eng 31:277–295
47. Moraru CI, Kokini JL (2003) Nucleation and expansion during extrusion and microwave heating of cereal foods. Compr Rev Food Sci Food Saf 2(4):147–165
48. van der Sman RGM, Broeze J (2014) Multiscale analysis of structure development in expanded starch snacks. J Phys Condens Matter 26:1–11
49. Alavi SH, Rizvi SSH, Harriott P (2003) Process dynamics of starch-based microcellular foams produced by supercritical fluid extrusion. I: model development. Food Res Int 36(4):309–319
50. Fan J, Mitchell JR, Blanshard JMV (1994) A computer simulation of the dynamics of bubble growth and shrinkage during extrudate expansion. J Food Eng 23:337–356
51. Schwartzberg HG, Wu JPC, Nussinovitch A, Mugerwa J (1995) Modelling deformation and flow during vapor-induced puffing. J Food Eng 25:329–372

52. Wang L, Ganjyal GM, Jones DD, Weller CL, Hanna MA (2005) Modeling of bubble growth dynamics and nonisothermal expansion in starch-based foams during extrusion. Adv Polym Technol 24:29–45
53. Kristiawan M, Chaunier L, Della Valle G, Ndiaye A, Vergnes B (2016) Modeling of starchy melts expansion by extrusion. Trends Food Sci Technol 48:13–26
54. Della Valle G, Vergnes B, Lourdin D (2007) Viscous properties of thermoplastic starches from different botanical origin. Int Polym Process 22:471–480
55. Nunez M, Della Valle G, Sandoval AJ (2010) Shear and elongational viscosities of a complex starchy formulation for extrusion cooking. Food Res Int 43:2093–2100
56. Padmanabhan M, Macosko C (1997) Extensional viscosity from entrance pressure drop measurements. Rheol Acta 36:143–151
57. Kokini JL, Chang C, Lai L (1992) The role of rheological properties on extrudate expansion. In: Kokini JL, Ho CT, Karwe MV. (eds) Food extrusion science and technology. Marcel Dekker, New York, pp 631–653
58. Amon M, Denson CD (1984) A study of the dynamics of foam growth: analysis of the growth of closely spaced spherical bubbles. Polym Eng Sci 24:1026–1034
59. Alvarez-Martinez L, Kondury KP, Harper JM (1988) A general model for expansion of extruded products. J Food Sci 53:609–615
60. Desrumaux A, Bouvier JM, Burri J (1998) Corn grits particle size and distribution effects on the characteristics of expanded extrudates. J Food Sci 63(5):857–863
61. Robin F, Dubois C, Pineau N, Schuchmann HP, Palzer S (2011) Expansion mechanism of extruded foams supplemented with wheat bran. J Food Eng 107:80–89
62. Van Vliet T, Janssen AM, Bloksma AH, Walstra P (1992) Strain hardening of dough as a requirement for gas retention. J Texture Stud 23:439–460
63. Córdoba A (2010) Quantitative fit of a model for proving of bread dough and determination of dough properties. J Food Eng 96:440–448
64. Shah P, Campbell G, McKee S, Rielly C (1998) Proving of bread dough: modelling the growth of individual bubbles. Food Bioprod Process 76:73–79
65. Stanke M, Zettel V, Schütze S, Hitzmann B (2014) Measurement and mathematical modeling of the relative volume of wheat dough during proofing. J Food Eng 131:58–64
66. Zettel V, Paquet-Durand O, Hecker F, Hitzman B (2016) Image analysis and mathematical modelling for the supervision of the dough fermentation process. In: Chinesta F, Cueto E (eds) Proceedings of ESAFORM Conference, 27–29 April, Nantes, France. To be published by AIP
67. Turbin-Orger A, Boller E, Chaunier L, Chiron H, Della Valle G, Reguerre A-L (2012) Kinetics of bubbles growth in wheat flour dough during proofing studied by computed X-ray microtomography. J Cereal Sci 56:676–683
68. Turbin-Orger A, Babin P, Boller E, Chaunier L, Chiron H, Della Valle G, Dendievel R, Réguerre A-L, Salvo L (2015) Growth and setting of gas bubbles in a viscoelastic matrix imaged by X-ray microtomography: the evolution of cellular structure in fermenting wheat flour dough. Soft Matter 11:3373–3384
69. Bikard J, Coupez T, Della Valle G, Vergnes B (2008) Simulation of bread making process using a direct 3D numerical method at microscale. Part I: analysis of foaming phase during proofing. J Food Eng 85:259–267
70. Trappey CV, Wu HY (2008) An evaluation of the time-varying extended logistic, simple logistic and Gompertz models for forecasting short product lifecycles. Adv Eng Inform 22: 421–430
71. Shehzad A, Chiron H, Della Valle G, Kansou K, Ndiaye A, Reguerre A-L (2010) Porosity and stability of bread dough during proofing determined by video image analysis for different compositions and mixing conditions. Food Res Int 43:1999–2005
72. Gan Z, Ellis PR, Schofield JD (1995) Mini review: gas cell stabilisation and gas retention in wheat bread dough. J Cereal Sci 21:215–230
73. Salt LJ, Wilde PJ, Georget D, Wellner N, Skeggs PK, Mills ENC (2006) Composition and surface properties of dough liquor. J Cereal Sci 43:284–292

74. van der Sman RGM, van der Goot AJ (2008) The science of food structuring. Soft Matter 5: 501–510
75. Chatraei SH, Macosko CW, Winter HH (1981) Lubricated squeezing flow: a new biaxial extensional rheometer. J Rheol 25:433–443
76. Launay B, Michon C (2008) Biaxial extension of wheat flour doughs: lubricated squeezing flows and stress relaxation properties. J Texture Stud 39:496–529
77. Turbin-Orger A, Della Valle G, Doublier JL, Fameau AL, Marze S, Saulnier L (2015b) Foaming and rheological properties of the liquid phase extracted from wheat flour dough. Food Hydrocoll 43:114–124
78. Kansou K, Chiron H, Della Valle G, Ndiaye A, Roussel P, Shehzad A (2013) Modelling wheat flour dough proofing behaviour: effects of mixing conditions on porosity and stability. Food Bioprocess Technol 6:2150–2164
79. Poutanen K, Sozer N, Della Valle G (2014) How can technology help to deliver more of grain in cereal foods for a healthier diet? J Cereal Sci 59:327–336

Adv Biochem Eng Biotechnol (2017) 161: 29–70
DOI: 10.1007/10_2016_52

Published online: 22 November 2016

General Template for the FMEA Applications in Primary Food Processing

Sibel Özilgen and Mustafa Özilgen

Abstract Data on the hazards involved in the primary steps of processing cereals, fruit and vegetables, milk and milk products, meat and meat products, and fats and oils are compiled with a wide-ranging literature survey. After determining the common factors from these data, a general FMEA template is offered, and its use is explained with a case study on pasteurized milk production.

Keywords Basic food groups, Food hazards, Generalized FMEA template, Pasteurization of milk, Primary processing

Contents

S. Özilgen (✉)
Department of Culinary Arts and Gastronomy, Yeditepe University, Istanbul, Turkey
e-mail: sozilgen@yeditepe.edu.tr

M. Özilgen
Department of Food Engineering, Yeditepe University, Istanbul, Turkey
e-mail: mozilgen@yeditepe.edu.tr

1 What Is Primary Processing?

Transformation of inedible raw ingredients into foods for human consumption is achieved through primary, secondary, and tertiary processing. *Primary processing* is the conversion of the inedible raw products into food ingredients. Growing, raising, cultivation, slaughtering, harvesting, storing, processing, packing, and transportation are among the basic stages of primary processing. Agriculture of wheat and production of flour from it is an example of primary processing. The products from primary processing are either send to the market for retail or to the factories as ingredients for secondary or tertiary processes. *Secondary processing* involves the conversion of food ingredients into edible foods. Different types of food ingredients from the primary processes are combined at this stage of processing. Secondary processed foods are prepared either at home or at the industrial level. Bread making at home or in a factory starting with flour, yeast, salt, and other ingredients is an example of secondary processing [1]. Baklava is a traditional sweet pastry made in Turkey. Its ingredients may include wheat flour, eggs, milk, water, semolina, sugar, lemon juice, minced pistachio nuts, and butter. Bringing these ready-to-use ingredients for the baklava making process into a pastry shop or factory is another typical example of secondary food processing [2]. *Tertiary processed* foods are commercially prepared foods such as ready-to-eat pouched, boxed, canned, or frozen meals or TV dinners. Besides industrial manufacturing, hotel kitchens and catering companies, including air travel food service providers are mostly involved with tertiary processing. In a tertiary production process, food may be served by the people providing the service after reconstituting or reheating. Products from primary processes make up the major part of our diet as they are either consumed raw or used as ingredients in secondary and tertiary processes. Failures in primary processing might cause widespread health problems. Globalization of trade and travel may lead to rapid distribution of unsafe or contaminated foods to great numbers of consumers and increase the risk [3, 4]. Chemical and microbial contamination as exemplified in studies by Borgen et al. [5] and Fenlon et al. [6], including pesticides [7, 8], allergens [9], and other biological hazards as exemplified by Bassett and McClure [10], are among the threats challenging primary processing.

2 What Is FMEA?

In a food plant the production line is integrated with quality control, HACCP (Hazard Analysis Critical Control Point), and FMEA (Failure Mode Effect Analysis) practices to assure production of safe food. Quality assurance has become highly efficient with the advanced development of equipment and measurement techniques of quality attributes and statistical techniques including sampling

methods and quality control charts [11]. Safety and high quality are both offered by the food industry to satisfy their consumers [12].

Information provided by Uljas and Ingham [13] about how and to what extent food safety is achieved in apple cider production is highly significant, as it reveals inefficiencies of processes carried by small-scale manufacturers without taking appropriate measures. The fundamental principles of the HACCP help to locate the critical points on the process flow diagram, where the loss of control may have heath-threatening consequences [14–18]. There is a possibility that a risk or threat may escape the HACCP plan, especially when there is no obvious relationship between risk and physical, chemical, and microbiological hazards. FMEA may be applied as an additional systematic preventive procedure to eliminate potential failures, to assess their causes and effects, and to improve the reliability of the products to address customer and government requirements. The FMEA methodology has been successfully employed to assess risk in the production processes of corn curls [19], strudels [20], smoked trout [21], Turkish delight [22], powdered red pepper [23], salmon [24], and dairy products [25]. Although HACCP and FMEA have similarities, they differ significantly in operation: HACCP aims at reducing the risks at the critical points whereas the practitioners applying FMEA methodology divide the manufacturing process into phases and then detect the potential failures of each phase individually. The basic steps in FMEA methodology include (1) drawing a process flow diagram, (2) identifying the potential failure modes, (3) identifying possible effects and causes of each failure mode, (4) assessing the risk level of each failure mode, (5) suggesting corrective actions to reduce and eliminate the potential failures; and (6) re-designing and testing the risk level of the corrected design [20, 23–29]. *Quantitative evaluation* of the risks is the main advantage of FMEA methodology over the other risk analysis methods. The risk levels of the potential failures are identified by calculating a risk priority numbers (RPN) from the frequency of the occurrence of each failure (O), seriousness of the failure to the health of the consumers (S), and the possibility of detecting the failure (D) before consumption. Epidemiological studies, previous observations, and the best expert opinion from the scientific literature regarding similar ingredients or processes that share similar technology for production are considered when estimating the values of S, D, and O [11, 17]. The likelihood of each failure mode is identified (O) on a scale of 1–10. The highest rank indicates the greatest probability of the failure to occur. The possibility for detecting the failure prior to occurring (D) and the seriousness of the failure to the consumer (S) are also rated on a scale of 1–10, where 10 is the least likely chance of detecting the failure and the highest level of the severity of the failure, respectively. Then the risk priority number (RPN) is calculated for each failure by multiplying the values of the variables (O) × (S) × (D). The risk priority numbers higher than 100 are considered as the potential failure modes which require corrective actions. Possible corrective actions are suggested for those potential failure modes, and the RPNs are recalculated to assess the influence of the corrective actions. This chapter offers a systematic approach for quantification of the risk in *primary processing* of five major groups of food as defined by the USDA [30] – cereals, fruit and vegetables, milk and

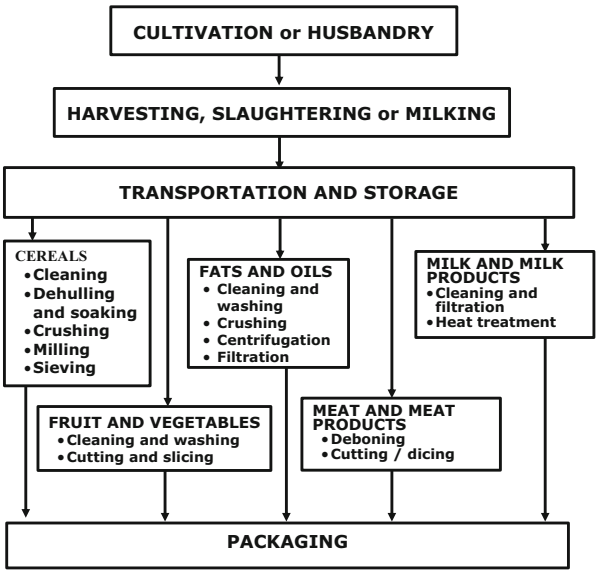

Fig. 1 Schematic description of the common steps for the primary processing of the major food groups

milk products, meat and meat products, fats and oils – to improve their safety and quality. Seeds and nuts are analyzed together using the same procedure as cereals because their primary processes are similar. The most common primary processing steps of each group are shown in Fig. 1.

Table 1 is an FMEA template for the most common steps in the *primary processing* of the major food groups with the potential failure modes, their causes, and suggested corrective actions. For better understanding, a sample FMEA table has been prepared for pasteurized milk production (Fig. 2) by using the real data obtained in a recent study in Turkey (Table 2) [25]. Model Pareto graphs (Fig. 3) have been constructed to identify the higher risk level stages and to assess the improvements in the process after implementing the corrective actions.

3 Potential Biological Failure Modes, Causes, Effects, and Preventive Actions in Primary Food Processing

Food poisoning caused by biological contaminants is a common, usually mild, but sometimes deadly, illness [31, 32]. Pathogens were identified as the basic reason for the 14 million food-borne diseases, 60,000 hospitalizations, and 1,800 deaths annually in the United States [33]. Contamination of fruit and vegetables [34, 35] and meat [36–38] with microorganisms is a common problem in many countries. Some pathogenic microorganisms are particularly important in the food industry because they occur frequently and/or cause the most serious health problems. For example, *Clostridium perfringens* is abundant in the environment and causes severe

Table 1 FMEA template for the common steps of primary processing of cereals and cereal products, fruit and vegetables, milk and milk products, red and poultry meat and their products, and fats and oils

Biological failures and their causes	Before corrective action				Corrective actions	After corrective action				Cereals and cereal products, seeds and nuts	Fruit and vegetables	Milk and milk products	Red and poultry meat and their products	Fats and oils
	O	S	D	RPN		O	S	D	RPN					
Processing stage: cultivation and husbandry														
Contamination with pathogenic microorganisms originating from irrigation water and water used in feeding trough drinking basin					Water must be supplied from the local authority. Sanitary controls of water sources and pipelines must be executed regularly. Microbiological treatment must be applied to water by using chemical agents such as chlorine, ozone, or UV-based systems. The standards of the pipelines and connectors must be ensured. Sewage and fertilizer control is required					+	+	+	+	+
Contamination with pathogenic microorganisms directly or indirectly via people working in the field					Employees and farmers must be properly trained to follow the hygiene and health requirements. Hygiene and sanitation facilities must be provided with hot water and soap to ensure appropriate degree of personal hygiene. Toilets must be placed in appropriate locations. Sick staff should not enter into the field					+	+	+	+	+

(continued)

Table 1 (continued)

Biological failures and their causes	Before corrective action				Corrective actions	After corrective action				Cereals and cereal products, seeds and nuts	Fruit and vegetables	Milk and milk products	Red and poultry meat and their products	Fats and oils
	O	S	D	RPN		O	S	D	RPN					
Contamination with pathogenic microorganisms caused by contaminated soil and misuse of fertilizers					Microbial quality of soil must be controlled. Contamination of soil by surface run-off water from the contaminated areas must be avoided. Manure control is required. Time lapse between the application of manure and planting and harvesting needs to be calculated and applied. To prevent fecal contamination, the fertilizers should not be stored near the growing location					+	+	−	−	+ (oils)
Contamination with pathogenic microorganisms directly or indirectly via wild and/or domestic animals					Wild and/or domestic animals must be separated from the field and water sources. Distress machines or scarecrows can be used to keep undesirable animals away from the field					+	+	+	+	+
Contamination with pathogenic microorganisms from animals with diseases such as mastitis					Periodic veterinary controls on fields are required. Somatic cell count must be done regularly. Parasite analysis must be carried out regularly					−	−	+	+	+ (fats)

Contamination with pathogenic microorganisms caused by inadequate cleaning or improper storage of the equipment and utensils used in the field					Proper maintenance, usage, and sanitation recommendations made by the equipment manufacturers must be followed. Harvesting bins must be cleaned after every use. Proper clean-out-of-place (COP) and clean-in-place (CIP) techniques for proper degree of hygiene and sanitation are recommended. Periodic microbiological (swab) controls must be carried out for verification					+	+	+	+	+
Pathogenic microorganisms from the environment					The field should be regularly cleaned, maintained, and kept free of litter, trash, standing water, or food waste					+	+	+	+	+
Processing stage: milking														
Contamination with pathogenic microorganisms directly or indirectly via people working in the field					Employees and farmers must be properly trained to follow the hygiene and health requirements. Hygiene and sanitation facilities must be provided with hot water and soap to ensure appropriate degree of personal hygiene. Toilets must be placed in appropriate locations. Sick staff should not enter into the field					−	−	+	+	+ (fats)
Microbiological contamination					Adequate facilities for hygienic milking must be provided					−	−	+	−	+ (fats)

(continued)

Table 1 (continued)

Biological failures and their causes	Before corrective action				Corrective actions	After corrective action				Cereals and cereal products, seeds and nuts	Fruit and vegetables	Milk and milk products	Red and poultry meat and their products	Fats and oils
	O	S	D	RPN		O	S	D	RPN					
caused by improper milking conditions														
Contamination with pathogenic microorganisms caused by inadequate cleaning or improper storage of milking equipment, utensils, and storage tanks					Proper practice, maintenance, and sanitation recommendations by the equipment manufacturers must be followed. Appropriate COP and CIP techniques should be implemented. Periodic microbiological (swab) controls must be carried out for verification					−	−	+	−	+ (fats)
Processing stage: harvesting														
Direct or indirect contamination with pathogenic microorganisms by the people working in the field					Employees and farmers must be trained properly to follow the hygiene and health requirements. Facilities must be provided with hot water and soap to ensure appropriate degree of personal hygiene. Toilets must be placed in appropriate locations. Sick staff should not enter into the field					+	+	−	−	+ (oils)
Contamination with pathogenic microorganisms caused by inadequate cleaning or improper storage of the equipment and utensils used in the field					Proper practice, maintenance and sanitation recommendations by the equipment manufacturers must be followed. Periodic microbiological (swab) controls must be carried out for verification					+	+	−	−	+ (oils)

Processing stage: *slaughtering*														
Contamination with pathogens caused by unsanitary conditions of the environment and improper practices					Employees and farmers must be properly trained to follow standard procedures					−	−	−	+	−
Contamination with pathogenic microorganisms caused by inadequate cleaning or improper storage of equipment and utensils					Proper practice, maintenance and sanitation recommendations by the equipment manufacturers must be followed. Periodic microbiological (swab) controls must be carried out for verification					−	−	−	+	−
Microbial growth caused by environmental temperature fluctuation during slaughtering					Staff training is required. Standard food flow directives must be obeyed. Environmental temperature must be controlled regularly					−	−	−	+	−
Processing stage: *storage prior to transportation*														
Microbial growth caused by temperature abuse during storage					Adequate temperature control must be carried out. Thermometers and probes must be calibrated regularly. Food must be kept properly covered					+	+	+	+	−
Microbiological contamination from delivery carts used for transportation of the food from field to storage unit					Proper cleaning and sanitation practices must be applied. Periodic microbiological (swab) controls must be carried out for verification. Carts should not be placed directly on soil					+	+	+	+	+

(continued)

Table 1 (continued)

Biological failures and their causes	Before corrective action				Corrective actions	After corrective action				Cereals and cereal products, seeds and nuts	Fruit and vegetables	Milk and milk products	Red and poultry meat and their products	Fats and oils
	O	S	D	RPN		O	S	D	RPN					
Contamination with pathogens caused by unsanitary conditions of the storage units					Proper cleaning procedure must be implemented. Periodical maintenance and control of the refrigeration system is required. Disinfection with ozone may be used to reduce the contamination risk of the storage units					+	+	+	+	+
Processing stage: transportation														
Contamination with pathogens caused by mishandling					Staff training is required. Standard food flow directives must be obeyed					+	+	+	+	+
Contamination with pathogens caused by unsanitary conditions of transportation vehicles					Proper cleaning procedure must be applied. Periodical maintenance is required. Disinfection technologies such as ozone can be used to reduce contamination risk from the transportation vehicles					+	+	+	+	+
Microbial growth caused by temperature abuse during transportation					Adequate control of time and temperature must be done. Thermometers and probes must be calibrated regularly. Humidity control is recommended					+	+	+	+	+
Processing stage: processing in the plant														
Contamination with pathogens caused by					Water must be supplied from the local authority. Sanitary controls					+	+	–	–	+ (Oil)

contaminated washing water					of the water sources and pipelines must be executed regularly. Water must be treated with chemicals such as chlorine or ozone or with UV light. The standards of the pipelines and connectors must be ensured									
Contamination with pathogenic microorganisms directly or indirectly via people working in the processing unit					Employees and farmers must be trained properly to follow the hygiene and health requirements. Hot water and soap must be provided to ensure appropriate degree of personal hygiene. Toilets must be placed in appropriate locations. Sick staff should not be permitted to be on the field					+	+	+	+	+
High number of pathogenic microorganisms in milk and meat caused by improper handling during receiving					Standard food flow directives must be implemented. Immediate cooling below 5°C is required after receiving. pH and/or acidity controls must be done on every batch of milk					−	−	+	+	+ (fats)
Contamination with pathogens caused by pests and flies					Processing facility must be isolated. Proper cleaning and sanitation procedures must be implemented. Periodical premises maintenance and effective pest control management is required					+	+	+	+	+
Contamination with pathogenic microorganisms originating from unsanitary equipment and tools					Proper practice, maintenance and sanitation recommendations by the equipment manufacturers must be followed. Proper COP and CIP techniques are recommended to achieve a					+	+	+	+	+

(continued)

Table 1 (continued)

Biological failures and their causes	Before corrective action				Corrective actions	After corrective action				Cereals and cereal products, seeds and nuts	Fruit and vegetables	Milk and milk products	Red and poultry meat and their products	Fats and oils
	O	S	D	RPN		O	S	D	RPN					
such as sieves and filters					proper degree of hygiene and sanitation. Periodic microbiological (swab) controls must be carried out for verification									
Microbial growth caused by improper process control, such as time and temperature control					Process control must be computerized. Thermometers and probes must be calibrated regularly					+	+	+	+	+
Microbial growth caused by increased time lapse between processes					Staff training is required. Standard food flow directives must be obeyed					+	+	+	+	+
Microbial contamination caused by unsanitary processing environment					The production unit should be regularly cleaned and maintained. Litter, trash, standing water, or food waste must be regularly removed from the premises					+	+	+	+	+
Processing stage: packaging (when required)														
Microbial growth caused by improper process control					Packaging must be carried out under hygienic conditions immediately after processing					+	+	+	+	+
Contamination from the packaging materials and/or lids					Periodic microbiological (swab) controls must be carried out for verification					+	+	+	+	+

Chemical failures and their causes	Before corrective action				Corrective actions	After corrective action				Cereals and cereal products, seeds and nuts	Fruits and vegetables	Milk and milk products	Meat and meat products (red meat and poultry)	Fats and oils
	O	S	D	RPN		O	S	D	RPN					
Processing stage: cultivation and husbandry														
Contamination caused by heavy metals in irrigation water and water used in feeding troughs and drinking basins					Water must be supplied from the local authority. Periodic analysis must be carried out for verification. The standards of pipelines and connectors must be ensured. Approved maintenance procedure must be followed					+	+	+	+	+
Contamination caused by chemical substances (bromate, cyanide, benzene, etc.) in irrigation water and water used in feeding troughs and drinking basins					Water must be supplied from the local authority. Periodic analysis must be carried out for verification. Approved maintenance procedure must be followed					+	+	+	+	+
Nitrite or nitrate contamination from irrigation water and water used in feeding troughs and drinking basins					Water must be supplied from the local authority. Periodic analysis must be carried out for verification. Approved maintenance procedure must be followed					+	+	+	+	+

(continued)

Table 1 (continued)

Chemical failures and their causes	Before corrective action				Corrective actions	After corrective action				Cereals and cereal products, seeds and nuts	Fruits and vegetables	Milk and milk products	Meat and meat products (red meat and poultry)	Fats and oils
	O	S	D	RPN		O	S	D	RPN					
Environmental chemical contaminants caused by air pollution					Fields must be separated from industrial and residential areas, roadsides, and crowded commercial districts					+	+	+	+	+
Contamination with chemicals caused by contaminated soil and misuse of fertilizers					Chemical quality of soil must be controlled. Contamination of soil by surface water run-off from the contaminated areas must be avoided. Employees and farmers must be properly trained to follow use of fertilizers. Manure control is required					+	+	−	−	+ (oils)
Pesticide residues from contaminated feed and/or water (dioxins, organophosphates, etc.)					Periodic pesticide analysis must be carried out					+	+	+	+	+
Pesticide residues caused by improper pesticide applications					Staff and farmers must be properly trained. Application methods, application rates, days to harvest restrictions and other pest management recommendations must be followed. Periodic pesticide analysis must be carried out					+	+	+	+	+

Veterinary drug residues in milk caused by improper veterinary practices					Misuse of veterinary drugs must be avoided. Veterinary drugs without a license are not supposed to be administered. Health conditions of the animals must be checked regularly by licensed veterinarians					−	−	+	−	+ (fats)
High level of aflatoxin in milk caused by improper agricultural practices and from contaminated feed used on the field					Supplier must be reliable. Total aflatoxin analysis must be carried out for each batch with aflatoxin kits					−	−	+	−	+ (fats)
Contamination with chemicals such as, detergents and sanitizers caused by improper cleaning or sanitation procedures					Proper maintenance, usage, and sanitation recommendations by the equipment manufacturers must be followed. Proper COP and CIP techniques are recommended					+	+	+	+	+
Processing stage: milking														
Contamination with chemicals such as, detergents and sanitizers caused by improper cleaning and/or sanitation procedures					Proper maintenance, usage and sanitation recommendations by the equipment manufacturers must be followed. Proper COP and CIP techniques are recommended for milking equipment and storage tanks					+	+	+	+	+

(continued)

Table 1 (continued)

Chemical failures and their causes	Before corrective action				Corrective actions	After corrective action				Cereals and cereal products, seeds and nuts	Fruits and vegetables	Milk and milk products	Meat and meat products (red meat and poultry)	Fats and oils
	O	S	D	RPN		O	S	D	RPN					
Processing stage: harvesting														
Contamination with chemicals such as, detergents and sanitizers caused by improper cleaning and/or sanitation procedures					Proper usage and sanitation recommendations by the equipment manufacturers must be followed. Proper COP and CIP techniques are recommended for harvesting equipment					+	+	−	−	+ (oils)
Contamination with chemicals such as machine lubricants					Standard maintenance program must be applied. Food grade lubricating oils must be used					+	+	−	−	+ (oils)
Processing stage: slaughtering														
Contamination with chemicals such as detergents and sanitizers, caused by improper cleaning and/or sanitation procedures					Proper usage and sanitation recommendations by the equipment manufacturers must be followed. Proper COP and CIP techniques are recommended for harvesting equipment					−	−	−	+	−

Processing stage: storage prior to transportation														
Mycotoxin contamination caused by improper storage conditions					Time, temperature, and humidity control during storage must be done					+	+	−	−	−
Contamination with chemicals such as detergents and sanitizers caused by improper storage practices					Store chemicals in designated areas away from food, packaging and food contact surfaces. All hazardous substances must be clearly marked					+	+	+	+	+
Contamination with toxic chemicals used for pest control during storage					Staff must be trained on the use and handling of pest control chemicals. Staff should obtain and read instructions for use. Chemicals must be used for their specific purpose only					+	+	+	+	+
Processing stage: transportation														
Microbial contamination caused by improper transportation conditions					Transportation vehicle must be cleaned and sanitized regularly. Time, temperature, and humidity control during transportation must be done					+	+	+	+	+
Processing stage: processing in the plant														
Heavy metal residues from water used for washing the foods					Periodic analysis must be carried out for verification. A suitable filtration system such as reverse osmosis must be used when necessary. Approved maintenance procedures must be followed					+	+	+	+	+

(continued)

Table 1 (continued)

Chemical failures and their causes	Before corrective action				Corrective actions	After corrective action				Cereals and cereal products, seeds and nuts	Fruits and vegetables	Milk and milk products	Meat and meat products (red meat and poultry)	Fats and oils
	O	S	D	RPN		O	S	D	RPN					
Contamination caused by uncontrolled use of intentional food additives and preservatives, for example sulfates, nitrates, and antioxidants, and/or spraying after production					Staff must be trained on proper practices. Periodic preservative analysis must be carried out for verification					+	+	+	+	+
Detergent and/or disinfectant residue from the equipment and utensils caused by inadequate rinsing and improper cleaning procedures					Proper usage and sanitation recommendations by the equipment manufacturers must be followed. Periodic pH and/or electrical conductivity tests must be carried out in the final rinsing water of the process					+	+	+	+	+

Lubricant residues in foods from the machines					Standard maintenance program must be applied. Food grade lubricating oils must be used					+	+	+	+	+
Contamination caused by improper use of pest control chemicals					Staff must be trained on the use and handling of pest control chemicals. Staff should obtain and read instructions for use. Chemicals must be used for their specific purpose only					+	+	+	+	+
Processing stage: packaging (when required)														
Heavy metal residues from the packaging material					Supplier must be reliable. Food grade materials only must be used. Quality control of packaging materials must be done periodically					+	+	+	+	+
Migration of chemicals from the packaging materials					Supplier must be reliable. Food grade materials only must be used. Quality control of packaging materials must be done periodically					+	+	+	+	+
Contamination from the hand sanitizers placed close to the packaging lines					Staff training is required. Hand sanitizers must be placed away from the packaging lines					+	+	+	+	+

(continued)

Table 1 (continued)

Biological failures and their causes	Before corrective actions				Corrective actions	After corrective actions				Cereals and cereal products, seeds and nuts	Fruits and vegetables	Milk and milk products	Red and poultry meat and their products	Fats and oils
	O	S	D	RPN		O	S	D	RPN					
Processing stage: cultivation and husbandry														
Heavy soil contamination in the field.					Harvesting bins, cages, and containers should not be placed on soil					+	+	−	−	+ (oils)
Processing stage: milking														
Insect parts, hair, etc. from the environment					Milking facility must be isolated. Effective pest control management is required					−	−	+	−	+ (fats)
Processing stage: harvesting														
Physical hazards caused by timeworn harvesting equipment and utensils					Standard maintenance program must be applied. Harvest bins must be properly maintained.					+	+	−	−	+ (oils)
Metal, pieces of broken glass, wood from bushes or trees, stones, and other waste left in the field					Field must be monitored frequently, and physical hazards must be removed safely when they appear					+	+	−	−	+ (oils)
Processing stage: *slaughtering*														
Soil, dust and dirt originating from the environment					Processing facility must be isolated. Proper cleaning and sanitation procedures must be applied. Periodical premises maintenance is required. Doors and windows must be securely closed					−	−	−	+	−

Physical hazards caused by timeworn equipment and utensils					Standard maintenance program must be applied					−	−	−	+	−
Processing stage: storage prior to transportation														
Foreign materials originating from the transferring equipment (boxes, cars, etc.)					Proper cleaning procedures must be applied. The sanitary conditions of the equipment must be controlled regularly					+	+	+	+	+
Pests, flies and dust from the environment					Processing facility must be isolated. Proper cleaning and sanitation procedures must be applied. Periodical premises maintenance is required. Doors and windows must be securely closed. Effective pest control management is required					+	+	+	+	+
Processing stage: transportation														
Contamination caused by improper practices during distribution					Staff training is required. The sanitary conditions of trucks must be controlled regularly					+	+	+	+	+
Processing stage: processing in the plant														
Contamination caused by improper practices in processing					Staff training is required. Protective gear such as gloves and arm covers must be provided and used. Jewelry and long nails must be prohibited and strictly controlled					+	+	+	+	+

(continued)

Table 1 (continued)

Biological failures and their causes	Before corrective actions				Corrective actions	After corrective actions				Cereals and cereal products, seeds and nuts	Fruits and vegetables	Milk and milk products	Red and poultry meat and their products	Fats and oils
	O	S	D	RPN		O	S	D	RPN					
Physical contamination from the damaged equipment					Standard maintenance program must be applied. Equipment must be checked regularly for loose or missing pieces					+	+	+	+	+
Pests and flies originating from the environment					Processing facility must be isolated. Proper cleaning and sanitation procedures must be applied. Periodical premises maintenance is required. Effective pest control management is required					+	+	+	+	+
Processing stage: packaging (when required)														
Physical contaminants or small pieces originating from the packaging materials and/or lids					Staff training is required. Quality control of packaging materials and lids must be done periodically					+	+	+	+	+
Pests and flies from the environment					Processing facility must be isolated. Proper cleaning and sanitation procedures must be applied. Periodical premises maintenance is required. Effective pest control management is required					+	+	+	+	+

Contamination caused by improper practices in processing					Staff training is required. Protective gear such as gloves and arm covers must be provided and used. Jewelry and long nails must be prohibited and strictly controlled					+	+	+	+	+

O: Frequency of occurrence for each failure
S: Seriousness of the failure to the consumer
D: Possibility of detecting the failure
RPN: Risk Priority Number = (O) × (S) × (D)
+: common risk in primary processing of the given food group
−: uncommon risk in primary processing of the given food group

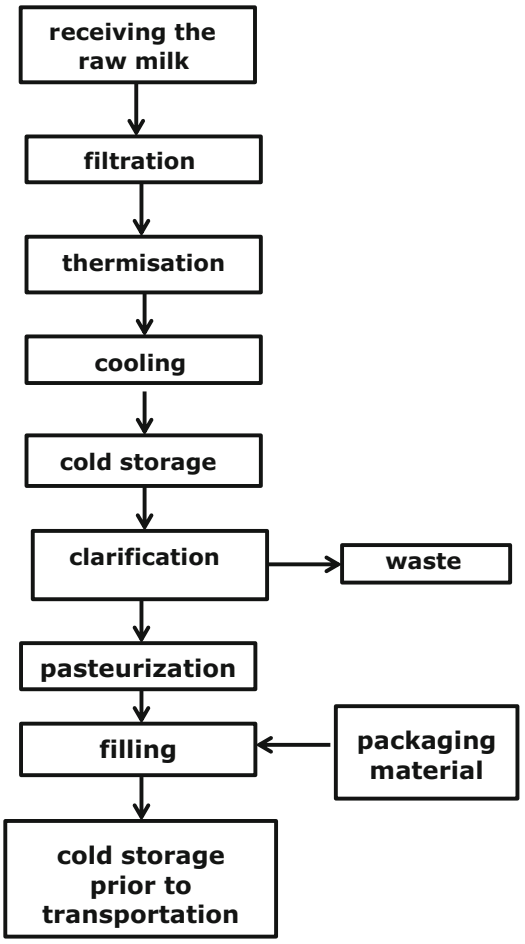

Fig. 2 Stages of pasteurized milk processing

abdominal cramps and diarrhea when ingested. Some strains can cause more severe illnesses and even death. *Clostridium botulinum* toxin causes paralysis and death if not treated immediately and properly. Water diarrhea, abdominal cramps, nausea, and pain are the basic symptoms of poisoning caused by *Bacillus cereus* toxins [33]. Food contaminated with *Salmonella* may cause diarrhea, fever, vomiting, and abdominal cramps 12–72 h after ingestion. In severe cases of diarrhea the consumer may be dangerously dehydrated. In 1998, after excluding unreported cases, 12,330 food poisoning incidences involving *Brucella ssp*, 120 cases involving *Clostridium botulinum*, 30,269 cases involving *Salmonella typhi*, and 1,457 cases involving *Shigella ssp*. were reported in Turkey [29].

At the cultivation or husbandry stage of primary processing (Fig. 1), foods may be contaminated with microorganisms coming from water and soil, wild and domestic animals, untreated manure, sick animals, and cross contamination from inadequately cleaned or improperly stored field equipment (Table 1)

Table 2 FMEA implementation of corrective actions to pasteurized milk production

Common biological failures and their cause	Before corrective actions				Corrective actions	After corrective actions			
	O	S	D	RPN		O	S	D	RPN
Processing stage: receiving of raw milk									
High number of pathogen (*E. coli* O157:H7, *Salmonella spp., Mycobacterium tuberculosis, Shigella dysenteria*, etc.) in milk caused by improper handling	8	10	9	720	Supplier must be reliable. Immediate cooling below 5°C is required after receiving. Cold chain must be kept from farm to receiving. The pH and/or acidity controls must be done for each batch. Periodic pathogen analysis must be done for verification	3	10	3	90
High number of spoilage microorganisms in milk caused by improper handling before and during receiving	9	7	5	315	Supplier must be reliable. Immediate cooling below 5°C is required after receiving. Cold chain must be kept from farm to receiving. The pH and/or acidity controls must be done for each batch	4	7	2	56
Isolation of *Staphylococcus spp. and Streptococcus spp. in* milk which might be the indication of animals with mastitis disease	5	8	5	200	Periodic veterinary controls on fields are required. Somatic cell count must be done regularly	2	8	2	32
Parasites (*Protozoa – Cryptosporidium spp.* etc.) in milk from unhealthy animal sources	3	8	8	192	Supplier must be reliable. Parasite analysis must be carried out regularly. Periodic veterinary controls on fields are required	2	8	5	80
Processing stage: filtration									
Microbiological contamination caused by inadequate cleaning of equipment, utensils or connectors	5	8	6	240	Proper cleaning procedure must be applied. Periodic microbiological (swab) controls must be carried out for verification	2	8	4	64
Microbiological contamination caused by inadequate, for example, manual, cleaning of the equipment	5	8	4	160	Proper cleaning procedure must be applied. Periodic microbiological (swab) controls must be carried out for verification	2	8	2	32

(continued)

Table 2 (continued)

Common biological failures and their cause	Before corrective actions				Corrective actions	After corrective actions			
	O	S	D	RPN		O	S	D	RPN
Microbiological contamination from inappropriate cleaning materials, for example, sponge	6	7	2	84	Not required	–	–	–	–
Microbiological contamination (*E. coli O157:H7, Shigella spp., Salmonella spp.*) attracts pests such as flies	7	9	3	189	The milk receiving facility must be isolated. Effective pest control management is required	2	9	3	54
Processing stage: thermisation									
Microbiological contamination caused by inadequate cleaning of equipment, utensils or connectors	5	8	6	240	Proper cleaning procedure must be applied. Periodic microbiological (swab) controls must be carried out for verification	2	8	4	64
Microbial growth caused by improper process time and/or temperature	6	8	5	240	The process control must be computerized. Thermometers and probes must be calibrated regularly. Approved maintenance procedures must be followed. Staff must be trained about food safety and controlling the system	1	8	1	8
Processing stage: cooling									
Microbiological contamination caused by inadequate cleaning of equipment, utensils or connectors	5	8	6	240	Proper cleaning procedure must be applied. Periodic microbiological (swab) controls must be carried out for verification	2	8	4	64
Microbial growth caused by improper process time and/or temperature	6	8	5	240	The process control must be computerized. Thermometers and probes must be calibrated regularly. Approved maintenance procedure must be followed. Staff must be trained about food safety and controlling the system	1	8	1	8

(continued)

Table 2 (continued)

Common biological failures and their cause	Before corrective actions				Corrective actions	After corrective actions			
	O	S	D	RPN		O	S	D	RPN
Processing stage: transportation for cold storage									
Microbial growth caused by increased time lapse between processes	6	6	3	108	Staff training is required. Standard food flow directives must be obeyed	2	6	2	24
Microbial contamination caused by mishandling	4	8	7	224	Staff training on personal hygiene and washing hands is required. Personal hygiene control must be done regularly	2	8	3	48
Processing stage: cold storage									
Microbiological contamination caused by improper storage conditions	5	8	6	240	Adequate facilities for hygienic storage must be provided. Proper cleaning procedure must be applied. Periodic microbiological (swab) controls must be carried out for verification	2	8	4	64
Microbial growth caused by improper storage temperature	6	7	6	252	A cooler or heat insulated tank must be employed. The inner temperature of the tank must be measured regularly. Thermometers/probes for temperature measurement must be calibrated regularly	2	7	2	28
Processing stage: clarification									
Microbiological contamination caused by inadequate cleaning	3	8	4	96	Not required	–	–	–	–
Processing stage: pasteurization									
Microbial growth caused by temperature fluctuation during the process	6	6	3	108	Staff training is required. Standard food flow directives must be obeyed. Process control is required	2	6	2	24
Processing stage: packaging									
Microbiological contamination caused by inappropriate practices	7	8	7	392	Process control is required. Periodic microbiological (swab) controls must be carried out for verification	2	8	3	48

(continued)

Table 2 (continued)

Common biological failures and their cause	Before corrective actions				Corrective actions	After corrective actions			
	O	S	D	RPN		O	S	D	RPN
Processing stage: cold storage after packaging									
Microbial growth caused by increased time lapse between processes	6	6	3	108	Staff training is required. Standard food flow directives must be obeyed.	2	6	2	24
Common chemical failures and their causes	Before corrective actions				Corrective actions	After corrective actions			
	O	S	D	RPN		O	S	D	RPN
Processing stage: receiving of raw milk									
Veterinary drug residues in milk caused by improper veterinary practices	7	8	7	392	Supplier must be reliable. Antibiotics analysis must be carried out for every batch with antibiotic kits	2	8	2	32
High level of aflatoxin in milk caused by improper agricultural practices and contaminated feed used on the field	5	8	9	360	Supplier must be reliable. Total aflatoxin analysis must be carried out for each batch with aflatoxin kits	2	8	2	32
Chemicals residues in raw milk caused by adulteration of raw milk (alkaline addition)	5	8	7	280	Supplier must be reliable. Alkaline analysis must be carried out for each batch	3	8	3	72
Pesticide residues in milk from contaminated feed and/or water (dioxins, organophosphates, etc.)	3	8	8	192	Supplier must be reliable. Periodic pesticide analysis must be carried out	2	8	5	80
Processing stage: filtration									
Detergent and/or disinfectant residues originating from the filtration equipment and utensils caused by inadequate rinsing	4	7	6	168	Proper cleaning procedure must be applied. Periodic pH and/or electrical conductivity tests must be carried out in the final rinse water of the equipment	2	7	1	14
Processing stage: thermisation									
Detergent and/or disinfectant residue from the thermization equipment and utensils caused by inadequate rinsing (CIP cleaning)	4	7	6	168	Proper cleaning procedure must be applied. Periodic pH and/or electrical conductivity tests must be carried out in final rinsing water of the process	2	7	1	14
Processing stage: cold storage									
Detergent and/or disinfectant residue caused by	4	7	6	168	Proper cleaning procedure must be applied.	2	7	1	14

(continued)

Table 2 (continued)

Common chemical failures and their causes	Before corrective actions				Corrective actions	After corrective actions			
	O	S	D	RPN		O	S	D	RPN
improper storage of chemicals (CIP cleaning)					Periodic pH and/or electrical conductivity tests must be carried out the in final rinsing water of the process. Detergents and sanitizers must be stored in a separate area away from the foods				
Processing stage: clarification									
Detergent and/or disinfectant residue from the clarification equipment and utensils caused by inadequate rinsing	4	7	6	168	Proper cleaning procedure must be applied. Periodic pH and/or electrical conductivity tests must be carried out in final rinsing water of the process	2	7	1	14
Processing stage: pasteurization									
Detergent and/or disinfectant residue from the pasteurization tank caused by inadequate rinsing (CIP cleaning)	4	7	6	168	Proper cleaning procedure must be applied. Periodic pH and/or electrical conductivity tests must be carried out in final rinsing water of the process	2	7	1	14
Processing stage: packaging									
Chemical residues from the packaging material	5	8	8	320	Food grade materials must only be used. Supplier must be reliable. Quality control of packaging materials must be done periodically	2	8	5	80
Common physical failures and their causes	Before corrective actions				Corrective actions	After corrective actions			
	O	S	D	RPN		O	S	D	RPN
Processing stage: receiving									
Physical contaminants in raw milk caused by improper handling and agricultural practices (glass, metal, insect parts, etc.)	5	6	2	60	Not required	–	–	–	–
Processing stage: filtration									
Physical contamination from torn or damaged filtration equipment	4	4	3	48	Not required	–	–	–	–

(continued)

Table 2 (continued)

Common physical failures and their causes	Before corrective actions				Corrective actions	After corrective actions			
	O	S	D	RPN		O	S	D	RPN
Inadequate filtration caused by torn or damaged filtration equipment	6	4	3	72	Not required	–	–	–	–
Processing stage: transportation for cooling									
Contamination caused by improper practices during processing	5	4	6	120	Staff training is required. Protective gear (gloves, arm covers, etc.) must be provided and used. Personal hygiene and practices must be strictly controlled	2	4	5	40
Foreign materials from the environment	6	5	4	120	Proper cleaning procedure must be applied. Environment must be free from waste and pests. The sanitary conditions of the surroundings must be controlled regularly	2	5	3	30
Processing stage: clarification									
Impurities caused by inadequate clarification	5	6	3	90	Not required	–	–	–	–
Processing stage: packaging									
Physical contaminants or small pieces from the packaging materials and/or lids	6	5	6	180	Supplier must be reliable. Staff training is required. Quality control of packaging materials and lids must be done periodically	3	4	3	36

[32, 38–41]. Johnsen et al. [42] identified horizontal transmission and maintenance of *Escherichia coli* O157:H7 on the farm in water, soil, and manure as the cause of the outbreaks. The producers may obtain water from rivers, underground water wells, surface water reservoirs, and municipal water mains. Several preventive actions can be taken to reduce the risk of contamination with pathogenic microorganisms from these sources (Table 1). Uncontrolled sources of water must be avoided. The microbiological quality of wastewater is usually very poor and hence it requires intensive treatment and control prior to use. Animal fecal contamination and run-off are the major risks in agricultural surface water sources. Reservoirs and wells must be properly constructed, isolated, and protected. Chlorination, filtration, ozone treatment, and solar irradiation are also suggested as possible treatments to reduce the number of pathogenic microorganisms in livestock drinking water and irrigation water [43]. Water is used at different stages of primary processing for cooling or washing food, equipment, and utensils. Recycling the wash water may cause microbial contamination [44, 45]. Getting water from the public water system

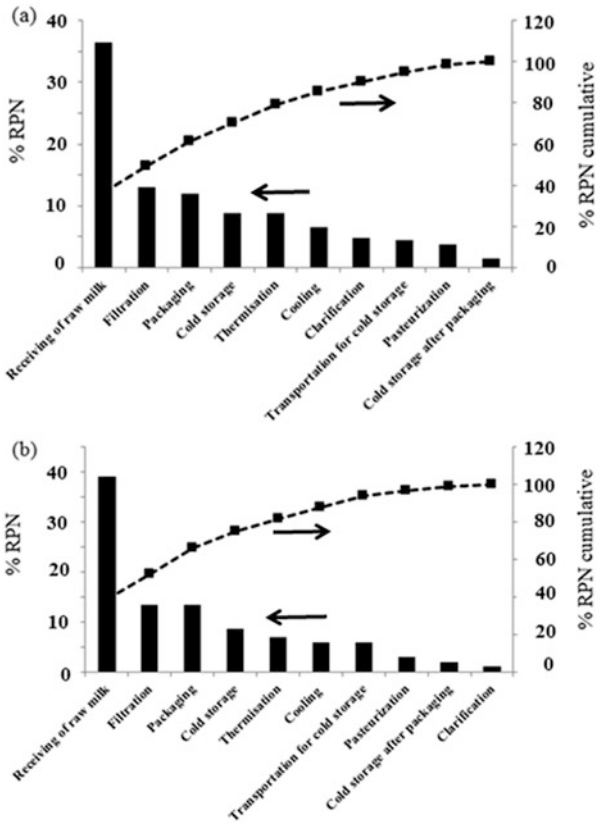

Fig. 3 Pareto diagrams for total risk classification, including chemical, physical, and biological risks, of pasteurized milk processing. (**a**) Prior to corrective actions. (**b**) After corrective actions

and testing its microbial quality regularly may be the most feasible solution to water-borne biological contamination.

Pathogenic microorganisms such as *E. coli O157:H7*, *Salmonella*, and *Campylobacter* in organic fertilizers may be sources of pre-harvest contamination if they are not adequately treated before application [46]. They may directly or indirectly (through the soil and water) introduce microorganisms onto the foods. UV irradiation, pasteurization, drying, alkali digestion, or combinations of these are the main treatment methods used to decrease the pathogenic microorganisms in organic fertilizers. Modification of the animal diet has also been shown to decrease the number of pathogenic microorganisms in organic fertilizers [38]. The type of fertilizer, methods and frequency of application, and the time lapse between fertilizer application and harvesting must be controlled to decrease the risk of contamination [38, 47]. Fertilizers should not be stored near the growing location and run-off must be controlled to avoid soil contamination.

Farms should not be close to areas where land activities may contaminate the products and the soil. Domestic animals and wild animals may carry pathogenic microorganisms to crops and livestock (Table 1). They should therefore be

excluded from fields and water sources. Direct or indirect contamination risk would be high in agricultural areas if they are close to livestock operations. Buffer land between the livestock operation and agricultural production areas helps to reduce the risk. Many animal diseases can pose a risk to consumers via the food chain (Table 1). For example, bovine spongiform encephalopathy, also known as mad cow disease, brucellosis, and bird-flu can cause severe food-borne illness among consumers. Standards of animal management practices during transportation, feeding, housing, and husbandry can help to decrease the risk of spreading food-borne diseases. Proper field sanitation also ensures that consumers are protected from food-borne illnesses. For example, unsanitary milking conditions and unhealthy animals are the main sources of pathogenic microorganisms such as *Staphylococcus ssp*., *Streptococcus ssp*., *Campylobacter spp*., *Listeria monocytogenes*, *E. coli*, *Mycoplasma spp*., *Mycobacterium tuberculosis*, *Cryptosporidium*, *Cyclospora*, and *Toxoplasma* in raw milk [25]. Similarly, *E. coli O157:H17* can cross-contaminate beef carcass during slaughtering if the process is not carried out in approved facilities. Poor management of wastes in the field can significantly increase the risk of food contamination. Fields must be free of litter, trash, animal feces, standing water, and food waste (Table 1) [48].

Equipment coming into direct contact with foods is another primary source of biological contamination. *Clean in place* (CIP) techniques may be used in the cleaning of closed systems such as pipelines, pasteurization equipment, and storage and process tanks (Table 1). Manual cleaning techniques may be used for small utensils and equipment. The CIP technique poses lower biological failure risks compared to manual cleaning, which requires more human involvement. Staff must be educated on implementing the appropriate cleaning, sanitizing, and handling procedures for all equipment and utensils, such as harvest bins, harvesting equipment, pasteurization tanks, filters, utensils, and packaging materials. Equipment and utensils used during primary processing should be maintained in good condition. The proper maintenance recommendations by the manufacturers must be followed. For example, malfunctioning equipment used in the process of removing animals' intestines may cause contamination of personnel and equipment with feces and blood, which may eventually cross-contaminate the food. Timeworn equipment and utensils that cannot be kept in good hygienic conditions must be discarded [25].

Wrong temperature settings or temperature fluctuations during slaughtering, milking, processing, storage, and transportation may contribute to the growth of bacteria (Table 1). Most microorganisms grow fast in high-risk foods at temperatures between 5 and 60°C, and therefore high-risk foods should be kept out of this temperature range. Milk, meat, and fresh produce must be cooled rapidly as soon as possible after milking, slaughtering, and harvesting. Temperatures of the storage units, refrigerators, and freezers need to be checked regularly with an appliance thermometer. Product-specific process design and control are very important to minimize the risk of microbial growth and the growth of spore-forming microorganism in foods. Sanitary conditions, humidity, and temperature of the environment must be optimized, especially during storage and transportation [49–52]. Underprocessing or improper process design may increase the risk of food contamination.

Spore-forming bacteria such as *Clostridium perfringens, Clostridium botulinum*, and *Bacillus cereus* are among the main concerns in different food groups as they produce very harmful toxins when the food is subject to inappropriate conditions. Under-processing may promote growth of vegetative cells from the spores as soon as conditions become favorable. This problem occurs mainly during storage and transportation of canned and vacuumed meat and vegetables [53–55].

Conditions during transportation between the processing stages, such as transportation from the field to the processing unit or from processing unit to the storage area, also have a great effect on the microbial load of final food products (Table 1). Contamination should be controlled through sanitizing the environment, containers employed in transportation, crates, harvesting bins, and cages. Increased time gaps between the stages resulting from improper *manufacturing practices* must be avoided. Standardization of the process flow and education of staff on procedures are highly recommended. Air quality is commonly neglected but it is a very important factor affecting the safety of foods. Precautions have been suggested to control the quality of air at different stages of the process. Positive pressured air ventilation with HEPA (high-efficiency particulate arresting) filters must be installed. Positive pressured air prevents unfiltered air from entering, so preventing airborne microorganisms being brought into facilities. Ventilation systems and filters must be checked for proper operation and maintained. The microbiological quality of the air must be controlled regularly [25].

Packaging is the final operation in primary food processing if the products are not sold un-packaged. Packaging should be carried out under hygienic conditions. Sanitary conditions of the packaging materials, containers, and lids must be controlled regularly to avoid cross-contamination. Insufficient heat application during sealing, malfunctioning of sealing machine, use of unsuitable covers, and operator mistakes must be avoided as they may result in post-process contamination (Table 1).

People are the major source of contamination in the food industry [25]. Although some behavior is persistent and difficult to change, personal hygiene, food safety, proper food handling, and sanitation training of all employees working at different stages of the process decreases the risk of contamination arising from human activities (Table 1) [17, 28]. Hygiene and sanitation facilities with hot water and soap must be provided and staff should be encouraged to use them. Toilets must be placed in appropriate locations. Staff suffering from diseases or illness should not be allowed to enter the food processing area.

4 Potential Chemical Failure Modes, Causes, Effects, and Corrective Actions in Primary Food Processing

Direct or indirect contamination of food by chemical toxicants such as heavy metals [56, 57], biological toxins, pesticides [7, 8], growth hormones, and veterinary drug residues pose the highest risk in the primary processing of food (Table 1). Cases of

heavy metals such as lead, mercury, and cadmium contamination on fruit and vegetables has been reported in many countries around the world [56–60]. Intentional and incidental disposal of sewage sludge and industrial wastes onto agricultural lands, mining, use of polluted water for irrigation, and increased use of nitrogen-containing fertilizers might be the primary pathway for heavy metal accumulation in the soil and the environment. Large amounts of heavy metal contaminants may enter the food chain because some cereals and vegetables have absorbed them from these sources. In China, lead contamination in lettuce and cadmium contamination in broccoli were reported in products cultivated in soil contaminated by electronic waste processing [57]. Meat and milk products may contain heavy metals if animals are reared on contaminated soils or fed with contaminated feed [58, 59, 61–68]. Heavy metals are mostly not biodegradable and therefore can accumulate in the vital organs of humans. They may cause neurological disorders, Alzheimer's and Parkinson's deceases, cancer, and low birth weight in people if consumption exceeds levels given in the Food Codex [65, 69]. Potential sources of heavy metals in foods need to be detected and removed from the process because concentrations of heavy metals are rarely modified by processing once they enter the foods.

Pesticides and herbicides are chemicals used intentionally to protect crops and to increase yield in agriculture (Table 1). Although the use of these chemicals is controlled by legislation, improper agricultural practices, contamination of water and animals feeds, lack of control may lead to contamination of human by with pesticide and herbicide residues (Table 1) [25, 60, 70–79]. Various preparation activities such as peeling and trimming may remove residues from the outer parts, but the remainder of the food may still contain substantial amount of pesticides because some pesticides are absorbed by the food. The concentration of pesticide residues increases in foods after reducing the water content in drying and condensation processes. Processing such as cooking, boiling, steaming, baking, and refining may reduce the amounts of pesticides remaining in foods depending upon the type of pesticide and length of treatment [80]. Prolonged exposure to pesticides, especially at high concentrations, may result in harmful effects on human health such as soft tissue, brain, lung, liver, digestive system and urinary tract cancers, birth defects, and damage to the nervous system [79].

Veterinary drugs used to treat diseases and to improve the health of animals are a potential chemical hazard in food if they are not administered properly (Table 1) [5]. Drug residues excreted by animals may spread in the environment. Contamination of rice by antibiotics originating from the urine of cattle reaching fields via underground water is reported by Hawker et al. [81]. Antibiotics and growth promoters are the most common veterinary drugs. A decrease in the total number of useful bacteria in the human intestine and increased microbial resistance are possible adverse effects of prolonged exposure of humans to antibiotics [82, 83]. Growth promoter residues in food products create human health concerns [82] and consequently the use of substances with hormonal action in animal feed is banned in many countries [84]. Production of biological toxins such as aflatoxin is another potential chemical hazard in cereal grains, milled cereals, nuts, dried fruits,

dried vegetables, and herbs if temperature and humidity are not controlled appropriately during production, processing, transportation, and storage (Table 1) [23, 49, 85]. Biological toxins may also be found in the milk and meat of animals fed with toxin-containing feed [86–88]. Aflatoxin may be detected in oils if they are produced from contaminated seeds, vegetables, or nuts [89, 90].

The FMEA methodology aims to prevent or reduce potential risks at each stage of a process before entering the next stage. Potential sources of contaminants in a process need to be detected and removed because prolonged exposure to these chemicals can have severe effects on human health. Ensuring proper agricultural and industrial practices, inspection and investigation of pipework in buildings, connecting to a public water system, or installing water treatment devices onto the production units are important preventive measures in minimizing heavy metal and pesticide contamination risks (Table 1) [52, 91]. Veterinary drugs must be used as prescribed by veterinarians and regular animal health controls by veterinarians are required. Withdrawal periods for drugs must be followed strictly [92, 93]. The presence of antibiotics and animal hormones in foods must be controlled strictly by official inspection [83, 94]. Farmers need to be educated about basic animal welfare and the proper use of veterinary drugs (Table 1). Food producers must only use food-grade packaging materials (Table 1). Time, temperature, and humidity control during storage and transportation of foods is the major preventive action in controlling the biological toxin production. Regular internal and governmental controls minimize the risk of potential chemical failure modes (Table 1).

Surfaces contacted by the foods, such as *packaging materials*, may be a source of chemical contamination through migration into foods (Table 1) [95, 96]. Perfluorinated organic chemicals, chemicals used for coating wrapping materials of cartons for burgers, fried chicken, etc., are reported to be contaminating foods [97]. The use of newspaper as a packing material for cooked food items is another common source of chemical contamination in some countries [98]. The amount of contaminants diffusing into foods from contact surfaces should not exceed the acceptable limits defined in the codex [99]. Only food grade materials must be used.

5 Potential Physical Failure Modes, Causes, Effects, and Corrective Actions in Primary Food Processing

Poor agricultural and manufacturing practices are the primary reasons for physical contamination in food products (Table 1) [100]. The most common potential physical threats include soil, dirt, dust, stones, bone pieces, jewelry, and metal fragments from worn or chipped utensils and containers. The physical hazards need to be detected and removed from each stage of the process before entering the next stage. Processing facilities must be isolated first. Proper cleaning and sanitation procedure must be applied to keep equipment, tools, and utensils free from physical

contaminants such as mud, metal fasteners, soil, and dirt. Premises maintenance is required periodically. Doors and windows must be securely closed. Effective pest control management should be applied.

6 Case Study: FMEA Analysis for the Pasteurization of Milk

The general list of the precautions needed to achieve food safety by implementing FMEA methodology is given in Table 1. These principles are applied to a special case here. Figure 2 shows that milk is filtered and thermized after its receipt in the factory. Thermization is a method of sterilization with heat. It is similar to pasteurization, reduces the microbial load [101], but carried out at a lower temperature to allow milk to maintain its original taste. Milk is cooled, cold stored, and goes through a clarification process before pasteurization. The pasteurized milk is filled into containers and then cold stored before being sent out to the retail stores. HACCP can be used as a tool for continual monitoring of a milk processing facility and provides a mechanism for ensuring that appropriate corrective actions are taken in the event of any failure [14]. FMEA may be used to improve the safety of a pasteurization process. The columns labeled O, D, S, and RPN are not filled with numbers in Table 1, although, for the given case study, their estimates are filled in the respective columns in Table 2 [25]. The risk of a high number of pathogens in raw milk because of improper handling practices has an RPN number of 720 before the corrective actions. The corrective actions may include purchasing the raw milk from a reliable supplier, cooling it to 5°C immediately on receipt, carrying out pH or acidity controls, and periodical pathogen analysis. The RPN number is reduced 8-fold to 90 after implementing these actions. There are numerous stages where drastic reductions in the RPNs result upon implementing the corrective actions, and these are listed in Table 2. Figure 3 shows how the RPN percentages of the stages and their relative values, for example, the horizontal axis of Fig. 3a, b, change after implementing the corrective actions.

References

1. Değerli B, Nazir S, Sorguven E, Hitzmann B, Özilgen M (2015) Assessment of the energy and exergy efficiencies of *farm to fork* grain cultivation and bread making processes in Turkey and Germany. Energy 93:421–434
2. Özilgen M (2016) Energy utilization and carbon dioxide emission during production of snacks. J Clean Prod 112:2601–2612
3. McMullan R, Edwards PJ, Kelly MJ, Millar BC, Rooney PJ, Moore JE (2007) Food-poisoning and commercial air travel. Travel Med Infect Dis 5:276–286
4. van Veen TWS (2005) International trade and food safety in developing countries. Food Control 16:491–496

5. Borgen K, Simonsen GS, Sundsfjord A, Wasteson Y, Olsvik Ø, Kruse H (2000) Continuing high prevalence of vanA-type vancomycin-resistant enterococci on Norwegian poultry farms three years after avoparcin was banned. J Appl Microbiol 89:478–485
6. Fenlon DR, Wilson J, Donachie W (1996) The incidence and level of *Listeria monocytogenes* contamination of food sources at primary production and initial processing. J Appl Bacteriol 81(6):641–650
7. de Bon H, Huat J, Parrot L, Sinzogan A, Martin T, Malézieux E, Vayssiéres J-F (2014) Pesticide risks from fruit and vegetable pest management by small farmers in sub-Saharan Africa. A review. Agron Sustain Dev 34:723–736
8. Lozoicka B, Jankowska M, Kaczynski P (2012) Pesticide residues in *Brassica* vegetables and exposure assessment of consumers. Food Control 25:561–575
9. Alvarez PA, Boye JI (2012) Food production and processing considerations of allergenic food ingredients: a review. J Allergy 2012:1–14. doi:10.1155/2012/746125
10. Bassett J, McClure P (2008) A risk assessment approach for fresh fruits. J Appl Microbiol 104:925–943
11. Arduzlar-Kagan D, Özilgen S, Özilgen M (2015) Quality assurance in vegetable processing: state of the science in practice in the 2010s. In: Hui YH, Evranuz EO (eds) Handbook of vegetable preservation and processing, 2nd edn. CRC Press, Florida, Chapter 37, pp 853–869
12. Burlingame B, Pineiro M (2007) The essential balance: risks and benefits in food safety and quality. J Food Compos Anal 20:139–146
13. Uljas HE, Ingham SC (2000) Survey of apple growing, harvesting, and cider manufacturing practices in Wisconsin: implications for safety. J Food Saf 20:85–100
14. Cerf O, Donnat E, The Farm HACCP group (2011) Application of hazard analysis – critical control point (HACCP) principles to primary production: what is feasible and desirable? Food Control 22:1839–1843
15. Gramza-Michalowska A, Korczak J (2008) Vegetable products as HACCP system subject in modern gastronomy. ACTA Scientiarum Polonorum Technologia Alimentaria 3:47–53
16. Horchner PM, Brett D, Gormley B, Jenson I, Pointon AM (2006) HACCP-based approach to the derivation of an on-farm food safety program for the Australian red meat industry. Food Control 17(7):497–510
17. Özilgen M (2011) Handbook of food process modeling and statistical quality control. Taylor and Francis, USA
18. Vilar MJ, Rodriguez-Otero JL, Sanjuan ML, Dieguez FJ, Varela M, Yus E (2012) Implementation of HACCP to control the influence of milking equipment and cooling tank on the milk quality. Trends Food Sci Technol 23:4–12
19. Varzakas TH, Arvanitoyannis IS (2007) Application of failure mode and effect analysis (FMEA), cause and effect analysis, and Pareto diagram in conjunction with HACCP to a corn curl manufacturing plant. Crit Rev Food Sci Nutr 47:363–387
20. Arvanitoyannis SI, Varzakas TH (2007) A conjoint study of quantitative and semi-quantitative assessment of failure in a strudel manufacturing plant by means of FMEA and HACCP, cause and effect and Pareto diagram. Int J Food Sci Technol 42:1156–1176
21. Arvanitoyannis SI, Palaiokostas C, Panagiotaki P (2009) A comparative presentation of implementation of ISO 22000 versus HACCP and FMEA in a small size Greek factory producing smoked trout: a case study. Crit Rev Food Sci Nutr 49(2):176–201
22. Özilgen S (2012) Failure mode and effect analysis (FMEA) for confectionery manufacturing in developing countries: Turkish delight production as a case study. Ciência e Tecnologia de Alimentos 32(3):505–514
23. Özilgen S, Bucak S, Özilgen M (2013) Improvement of the safety of the red pepper spice with FMEA and post processing EWMA quality control charts. J Food Sci Technol 50(3):466–476
24. Arvanitoyannis SI, Varzakas TH (2008) Application of ISO 22000, failure mode, and effect analysis (FMEA) for industrial processing of salmon: case study. Crit Rev Food Sci Nutr 48: 411–429

25. Kurt L, Özilgen S (2013) Failure mode and effect analysis for dairy product manufacturing: practical safety improvement action plan with cases from Turkey. Saf Sci 55:195–206
26. Arvanitoyannis SI, Varzakas TH (2007) Application of failure mode and effect analysis (FMEA), cause, and effect analysis and Pareto diagram in conjunction with HACCP to a potato chips manufacturing plant. Int J Food Sci Technol 42:1424–1442
27. Arvanitoyannis SI, Savelides SC (2007) Application of failure mode and effect analysis and cause and effect analysis and Pareto diagram in conjunction with HACCP to a chocolate-producing industry: a case study of tentative GMO detection at pilot plant scale. Int J Food Sci Technol 42:1265–1289
28. Özilgen S (2010) Application of failure mode and effect analysis model to foodservice systems operated by chefs in practice and by chefs from a culinary school in Turkey. Journal für Verbraucherschutz und Lebensmittelsicherheit 5(3–4):333–343
29. Özilgen S (2011) Food safety education makes the difference: food safety perceptions knowledge, attitudes and practices among Turkish university students. J Consum Prot Food Saf 6: 25–34
30. Willet WC, Stampfer MJ (2003) Rebuilding the food pyramid. Sci Am 288(1):64–71
31. Carmo LS, Dias RS, Linardi VR, Sena JM, Santos DA, Faria ME, Pena EC, Jett M, Heneine LG (2002) Food poisoning due to enterotoxigenic strains of *Staphylococcus* present in Minas cheese and raw milk in Brazil. Food Microbiol 19:9–14
32. Lyytikainen O, Autio T, Maijala R, Ruutu P, Honkanen-Buzalski T, Miettinen M, Hatakka M, Mikkola J, Anttila VJ, Johansson T, Rantala L, Aalto T, Korkeala H, Siitonen A (2000) An outbreak of *Listeria monocytogenes* serotype 3a infections from butter in Finland. J Infect Dis 181:1838–1841
33. Le Loir Y, Baron F, Gautier M (2003) *Staphylococcus aureus* and food poisoning. Genet Mol Res 2(1):63–76
34. Coleman E, Delea K, Everstine K, Reimann D, Ripley D (2013) Environmental health specialists network working group. J Food Prot 76:2126–2131
35. Seow J, Agoston R, Phua L, Yuk H-G (2012) Microbiological quality of fresh vegetables and fruits sold in Singapore. Food Control 25:39–44
36. Buncic S, Sofos J (2012) Interventions to control *Salmonella* contamination during poultry, cattle and pig slaughter. Food Res Int 43:641–655
37. Duffy G, Cummins E, Nally P, O'Brien S, Butler F (2006) A review of quantitative microbial risk assessment in the management of *Escherichia coli* O157:H7 on beef. Meat Sci 74:76–88
38. Gil MI, Selma MV, Suslow T, Jacxsens L, Uyttendaele M, Allende A (2015) Pre- and postharvest preventive measures and intervention strategies to control microbial food safety hazards of fresh leafy vegetables. Crit Rev Food Sci Nutr 55:453–468
39. Busani L, Cigliano A, Taioli E, Caliguiuri V, Chiavacci L, Di Bella C, Battisti A, Duranti A, Gianfranceschi M, Nardella MC, Ricci A, Rolesu S, Tamba M, Marabelli R, Caprioli A (2005) Prevalence of *Salmonella enterica* and *Listeria monocytogenes* contamination in foods of animal origin in Italy. J Food Prot 68:1729–1733
40. Habib I, Sampers I, Uyttendaele M, Berkvens D, De Zutte L (2008) Baseline data from a Belgium-wide survey of *Campylobacter species* contamination in chicken meat preparations and considerations for a reliable monitoring program. Appl Environ Microbiol 74:5483–5489
41. Ofor MO, Okorie VC, Ibeawuchi II, Ihejirika GO, Obilo OP, Dialoke SA (2009) Microbial contaminants in fresh tomato wash water and food safety considerations in South-Eastern Nigeria. Life Sci J 6(3):80–82
42. Johnsen G, Wasteson Y, Heir E, Berget OI, Herikstad H (2001) *Escherichia coli* O157:H7 in faeces from cattle, sheep and pigs in the southwest part of Norway during 1998 and 1999. Int J Food Microbiol 65:193–200
43. Uyttendaele M, Jaykus L-A, Amoah P, Chiodini A, Cunliffe D, Jacxsens L, Holvoet K, Korsten L, Lau M, McClure P, Medema G, Sampers I, Pratima Rao Jasti PR (2015) Microbial hazards in irrigation water: standards, norms, and testing to manage use of water in fresh produce primary production. Compr Rev Food Sci Food Saf 14(4):336–356

44. Goverd KA, Beech FW, Hobbs RP, Shannon R (1979) The occurrence and survival of coliforms and *Salmonellas* in apple juice and cider. J Appl Bacteriol 46:521–530
45. Lang MM, Ingham SC, Ingham BH (1999) Verifying apple cider plant sanitation and HACCP programs: choice of indicator bacteria and testing methods. J Food Prot 62:887–893
46. Mawdsley JL, Bardgett RD, Merry RJ, Pain BF, Thedorou MK (1995) Pathogens in livestock waste their potential for movement through soil and environment pollution. Appl Soil Ecol 2:1–15
47. Olaimat AN, Holley RA (2012) Factors influencing the microbial safety of fresh produce: a review. Food Microbiol 32:1–19
48. Brown CG, Longworth JW, Waldron S (2002) Food safety and development of the beef industry in China. Food Policy 27:269–284
49. Bircan C, Barringer SA, Ulken U, Pehlivan R (2008) Aflatoxin levels in dried figs, nuts, and paprika for export from Turkey. Int J Food Sci Technol 43:1492–1498
50. Chulze SN (2010) Strategies to reduce mycotoxin levels in maize during storage: a review. Food Addit Contam Part A Chem Anal Control Expo Risk Assess 27(5):651–657
51. van Egmond HP (2004) Natural toxins: risks regulations and analytical situations in Europe. Anal Bioanal Chem 378:1152–1160
52. WHO (2008) Hazard analysis and critical control point generic models for some traditional foods - a manual for the Eastern Mediterranean region. WHO Library cataloguing in publication data. Available at http://applications.emro.who.int/dsaf/dsa1100.pdf. Accessed 27 July 2015
53. FDA (2009) Evaluation and definition of potentially hazardous foods. http://www.fda.gov/Food/ScienceResearch/ResearchAreas/SafePracticesforFoodProcesses/ucm094141. Accessed 27 July 2010
54. Heinz G, Hautzinger P (2008) Meat processing technology for small to medium scale processors. Available at http://www.fao.org/3/a-ai407e.pdf. Accessed 27 July 2015
55. Peck MW, Stringer SC (2005) The safety of pasteurized in-pack chilled meat products with respect to the foodborne botulism hazard. Meat Sci 70:461–475
56. Bagdatlioglu N, Nergiz C, Ergunol PG (2010) Heavy metal levels in leafy vegetables and some selected fruits. J Consum Prot Food Saf 5:421–428
57. Huang Z, Pan XD, Wu PG, Han JL, Chen Q (2014) Heavy metals in vegetables and the health risk to population in Zhejiang, China. Food Control 36:248–252
58. Sinha S, Pandey K, Gupta AK, Bhatt K (2005) Accumulation of metals in vegetables and crops grown in the area irrigated with river water. Bull Environ Contam Toxicol 74:210–218
59. Sobukola OP, Adeniran OM, Odedairo AA, Kajihausa OE (2010) Heavy metal levels of some fruits and leafy vegetables from selected markets in Lagos, Nigeria. Afr J Food Sci 4(2): 389–393
60. Turkdogan MK, Kilicel F, Kara K, Tuncer I, Uygan I (2003) Heavy metals in soil, vegetables and fruits in the endemic upper gastrointestinal cancer region of Turkey. Environ Toxicol Pharmacol 13(3):175–179
61. Demirezen D, Aksoy A (2006) Heavy metal levels in vegetables in Turkey are within safe limits for Cu, Zn, Ni and exceeded for Cd and Pb. J Food Qual 29:252–265
62. Falandysz J, Bielawski L (2001) Mercury content of wild edible mushrooms collected near the town of Augustow. Pol J Environ Stud 10(1):67–71
63. Khoshgoftarmanesh AH, Aghili F, Sanaeiostovar A (2009) Daily intake of heavy metals and nitrate through greenhouse cucumber and bell pepper consumption and potential health risks for human. Int J Food Sci Nutr 60:199–208
64. Konuspayeva G, Faye B, Loiseau G (2009) The composition of camel milk: a meta-analysis of the literature data. J Food Compos Anal 22:95–101
65. Muhammad F, Awais MM, Akhtar M, Anwar MI (2013) Quantitative structure activity relationship, and risk analysis of some heavy metal residues in the milk of cattle and goat. Iranian J Environ Health Sci Eng 10:4. doi:10.1186/1735-2746-10-4

66. Perello G, Martí-Cid R, Llobet JM, Domingo JL (2008) Effects of various cooking processes on the concentrations of arsenic, cadmium, mercury, and lead in foods. J Agric Food Chem 56(23):11262–11269
67. Skalicka M, Korenekova B, Nad P, Makoova Z (2002) Cadmium levels in poultry meat. Veterinarski Arhiv 72:11–17
68. Simsek O, Gultekin R, Oksuz O, Kurultay S (2000) The effect of environmental pollution on the heavy metal content of raw milk. Nahrung 44(5):360–363
69. Mates JM, Segura JA, Alonso FJ, Marquez J (2010) Roles of dioxins and heavy metals in cancer and neurological diseases using ROS-mediated mechanisms. Free Radic Biol Med 49: 1328–1341
70. Chen C, Qian Y, Chen Q, Tao C, Li C, Li Y (2011) Evaluation of pesticide residues in fruits and vegetables from Xiamen, China. Food Control 22(7):1114–1120
71. Fuentes E, Baez M, Diaz J (2010) Survey of *organophosphorus* pesticide residues in virgin olive oils produced in Chile. Food Addit Contam Part B 3(2):101–107
72. Guler GO, Cakmak YS, Dagli Z, Aktumsek A, Ozparlak H (2010) Organochlorine pesticide residues in wheat from Konya region, Turkey. Food Chem Toxicol 48(5):12–18
73. Kaushik G, Satya S, Naik SN (2009) Food processing tool to pesticide residue dissipation - review. Food Res Int 42:26–40
74. Kurt PB, Ozkoc HB (2004) A survey to determine levels of chlorinated pesticide and PCBs in mussels and seawater from the mid-Black Sea coast of Turkey. Mar Pollut Bull 48: 1076–1083
75. Muthukumar M, Sudhakar Reddy K, Narendra Reddy C, Kondal Reddy K, Gopala Reddy A, Jagdishwar Reddy D, Kondaiah N (2010) Detection of cyclodiene pesticide residues in buffalo meat and effect of cooking on residual level of endosulfan. J Food Sci Technol 4(3):325–329
76. Osman KA, Al-Humaid AI, Rehiayani SM, Al-Redhaiman KN (2011) Estimated daily intake of pesticide residue exposure by vegetables grown in greenhouses in Al-Qassim region, Saudi Arabia. Food Control 6:947–953
77. Sharma HR, Kaushik A, Kaushik CP (2007) Pesticide residues in bovine milk from a predominantly agricultural state of Haryana, India. Environ Monit Assess 129:349–357
78. Sonchieu J, Ngassoum MB, Tchatchueng JB, Srivastava AK, Srivastava LP (2010) Survey of pesticide residues in maize, cowpea and millet from northern Cameroon: part I. Food Addit Contam Part B 3:178–184
79. Younes M, Galal-Gorchev H (2000) Pesticides in drinking water - a case study. Food Chem Toxicol 38:S57–S90
80. Bajwa U, Sandhu KS (2014) Effect of handling and processing on pesticide residues in food - a review. J Food Sci Technol 51(2):201–220
81. Hawker DW, Cropp R, Boonsaner M (2013) Uptake of zwitterionic antibiotics by rice (*Oryza sativa* L.) in contaminated soil. J Hazard Mater 263:458–466
82. Jeong S-H, Kang D, Lim MW, Kang CS, Sung JH (2010) Risk assessment of growth hormones and antimicrobial residues in meat. Toxicol Res 26(4):301–313
83. Toldra F, Reig M (2006) Methods for rapid detection of chemical and veterinary drug residues in animal foods. Trends Food Sci Technol 17:482–489
84. Kuiper HA, Noordam MY, van Dooren-Flipsen MM, Schilt R, Roos AH (1998) Illegal use of beta-adrenergic agonists: European Community. J Anim Sci 76(1):195–207
85. Salem NM, Ahmad R (2010) Mycotoxins in food from Jordan: preliminary survey. Food Control 21:1099–1103
86. Bakirci I (2001) A study on the occurrence of aflatoxin M1 in milk and milk products produced in Van province of Turkey. Food Control 12:47–51
87. Garrido NS, Iha MH, Santos Ortolani MR, Duarte Favaro RM (2003) Occurrence of aflatoxins M1 and M2 in milk commercialized in Ribirao Preto-SP, Brazil. Food Addit Contam 20(1):70–73

88. Martins ML, Martins HM (2000) Aflatoxin M1 in raw and ultrahigh temperature-treated milk commercialized in Portugal. Food Addit Contam 17(10):871–874
89. Basappa SC, Sreenivasamurthy V (1977) State of aflatoxin in groundnut oil. J Food Sci Technol 14:57–60
90. Dwarakanath CT, Sreenivasamurthy V, Parpia HAB (1969) Aflatoxin in Indian peanut oil. J Food Sci Technol (Mysore) 6(2):107–109
91. Rama Subba Rao R, Sarkar DK, Punnaiah KC, Reddy GPV, Ramasubbaiah K (1986) Studies on persistence of fenitrothion and phosalone residues on brinjal. J Food Sci Technol 23(3):177–178
92. FAO (2004) Good practices for the meat industry, section 2. Practices in primary production. Available at ftp://ftp.fao.org/docrep/fao/007/y5454e/y5454e00.pdf. Accessed 27 July 2015
93. FAO (2004) Guide to good dairy farming practice. Available at ftp://ftp.fao.org/docrep/fao/006/y5224e/y5224e00.pdf. Accessed 27 July 2015
94. Lievaart JJ, Noordhuizen JPTM, van Beek E, van der Beek C, van Risp A, Schenkel J, van Veerser J (2005) The hazard analysis critical control points (HACCP) concept as applied to some chemical, physical and microbiological contaminants of milk on dairy farms. A prototype. Vet Q 27(1):21–29
95. Bradley EL, Boughtflower V, Smith TL, Speck DR, Castle L (2005) Survey of the migration of melamine and formaldehyde from melamine food contact articles available on the UK market. Food Addit Contam 22(6):597–606
96. Lund KH, Petersen JH (2006) Migration of formaldehyde and melamine monomers from kitchen- and tableware made of melamine plastic. Food Addit Contam 23(9):948–955
97. Tittlemier SA, Pepper K, Seymour C, Moisey J, Bronson R, Cao X-L, Dabeka RW (2007) Dietary exposure of Canadians to perfluorinated carboxylates and perfluorooctane sulfonate via consumption of meat, fish, fast foods, and food items prepared in their packaging. J Agric Food Chem 55(8):3203–3210
98. Kurunthachalam SK (2013) Possible adverse implications of chemical migration from food pack materials in India. Hydrol Curr Res 4:156. doi:10.4172/2157-7587.1000156
99. Lau O, Wong S (2000) Contamination in foods from packaging material - review. J Chromatogr A 882(1–2):255–270
100. Olsen AR (1998) Regulatory action criteria for filth and other extraneous materials: I. Review of hard or sharp foreign objects as physical hazards in food. Regul Toxicol Pharmacol 28(3): 181–189
101. Samelis J, Lianou A, Kakouri A, Delbes C, Rogelj I, Bogovic-Matijasic B, Montel MC (2009) Changes in the microbial composition of raw milk induced by thermisation treatments applied prior to traditional Greek hard cheese processing. J Food Prot 72(4):783–790

Adv Biochem Eng Biotechnol (2017) 161: 71–92
DOI: 10.1007/10_2016_51

Published online: 14 March 2017

Machine Vision-Based Measurement Systems for Fruit and Vegetable Quality Control in Postharvest

José Blasco, Sandra Munera, Nuria Aleixos, Sergio Cubero, and Enrique Molto

Abstract Individual items of any agricultural commodity are different from each other in terms of colour, shape or size. Furthermore, as they are living thing, they change their quality attributes over time, thereby making the development of accurate automatic inspection machines a challenging task. Machine vision-based systems and new optical technologies make it feasible to create non-destructive control and monitoring tools for quality assessment to ensure adequate accomplishment of food standards. Such systems are much faster than any manual non-destructive examination of fruit and vegetable quality, thus allowing the whole production to be inspected with objective and repeatable criteria. Moreover, current technology makes it possible to inspect the fruit in spectral ranges beyond the sensibility of the human eye, for instance in the ultraviolet and near-infrared regions. Machine vision-based applications require the use of multiple technologies and knowledge, ranging from those related to image acquisition (illumination, cameras, etc.) to the development of algorithms for spectral image analysis. Machine vision-based systems for inspecting fruit and vegetables are targeted towards different purposes, from in-line sorting into commercial categories to the detection of contaminants or the distribution of specific chemical compounds on the product's surface. This chapter summarises the current state of the art in these techniques, starting with systems based on colour images for the inspection of conventional colour, shape or external defects and then goes on to consider recent

J. Blasco, S. Munera, S. Cubero, and E. Molto (✉)
IVIA, Centro de Agroingeniería, Cra. Moncada-Náquera km 5, 46113 Moncada, Spain
e-mail: molto_enr@gva.es

N. Aleixos
Departamento de Ingeniería Gráfica, Universitat Politècnica de València, Camino de Vera s/n, 46022 Valencia, Spain

developments in spectral image analysis for internal quality assessment or contaminant detection.

Keywords Hyperspectral, Image processing, In-line inspection, Postharvest, Quality, Real-time, Spectral imaging

Contents

1 Introduction

Food standards are evolving both to ensure the sustainability of agriculture and to address consumer concerns. The reputation of producers, and consequently their position in the market, is based on the quality of the product, which makes quality controls essential. The market and consumer exigencies, as well as increasing social concerns about good practices, including environmental, economic and social sustainability and traceability, require guarantees of optimal quality from the earliest stages of the crop to postharvest storage and treatments.

Optical devices and sensors have been introduced in the industry as non-destructive techniques for inspecting fruit [1]. Such technological advancements have been used for various purposes, ranging from the automatic sorting of products into categories to the control of processes which are difficult to observe, for instance, because of their long duration [2]. At this point it is important to note that the quality of biological products is not easy to assess, as individuals of the same category may differ greatly from one to another in terms of colour, shape or size. Furthermore, because they are living products, their physiochemical properties evolve over time. Their inherent variability sometimes introduces a certain amount of subjectivity into quality control, thus increasing the difficulty involved in developing automated inspection systems. Addressing these challenges often requires research in advanced and multidisciplinary technologies, and sometimes the use of expensive equipment.

Machine vision inspection is aimed at ensuring the quality of each product and the correct classification (including rejection) of those individual items based on quality standards. Automation is aimed at reducing production, processing and handling costs, but also at delivering the produce to the appropriate markets, thus optimising the overall profit. Furthermore, the excellence of a commodity is often achieved by ensuring correct and regular sizes, suitable colouring, and absence of external damage, optimal organoleptic properties and the absence of harmful residues. However, despite the great amount of research devoted to machine vision-based inspection systems [2, 3], the introduction of this technology in the industry is still relatively scarce because of its relatively high cost, the complexity of the equipment needed and the particular requirements for each implementation.

Current computer-based applications for the inspection of fruit and vegetables are described in the following sections. Most of these systems use visible (VIS) information to inspect the external quality of the produce using conventional techniques. However, recent advances include hyperspectral imaging to assess chemical composition, inspection of the internal quality of the produce or the detection of invisible damage, almost always for the real-time implementation of automated, in-line inspection and quality control systems.

2 Machine Vision Systems Based on Visible Information

The success of computer vision-based systems for the external inspection of fruit or vegetables depends largely on the quality and resolution of the acquired images, which is closely related to the cameras employed and the illumination of the scene. Frequently, such systems measure and compare colours, and for this reason illumination with a good colour rendering index is required. This index is a quantitative measure of the degree to which a test illuminant renders colours similar to their appearance under a reference illuminant [4]. The illumination must be uniform and avoid specular reflection, which produces bright spots that can mask certain blemishes. This is especially important for the estimation of two of the main external properties associated with the quality of the fruit by consumers, namely the colour and the presence of external defects.

2.1 Measurement of Colour

Colour is one of the most important attributes of many agricultural products that can be expressed using several standard colour spaces, the most used in image processing in agriculture being RGB (Red, Green, Blue), HSI (Hue, Saturation, Intensity) and CIELAB. The first is the native colour space of computers and digital devices and the others try to imitate human perception better. Figure 1 show some examples of apples and the distribution of their colour in different colour spaces obtained using the program FoodColorInspector (available at http://www.cofilab.com).

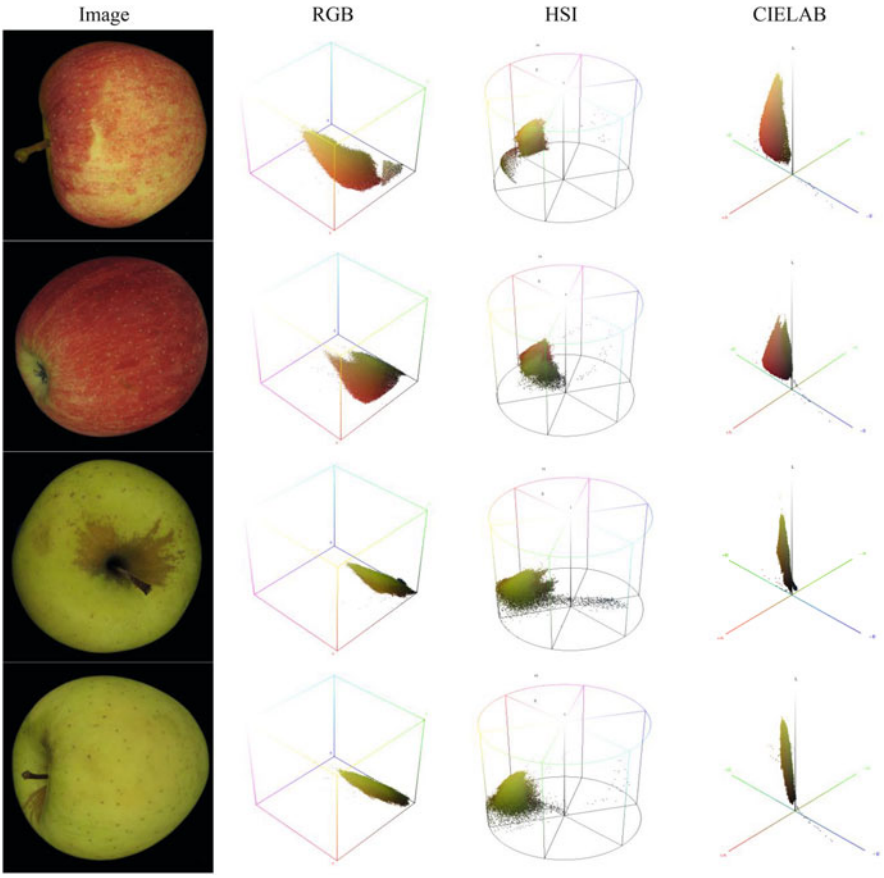

Fig. 1 Apples of Royal Gala and Golden cultivars with different colours and the distribution of the colours in the RGB, HSI and CIELAB colour spaces

As fruit ripens, chlorophyll degrades and new pigments such as anthocyanins or carotenoids start to be synthesised, resulting in the fruit turning from green to a wide variety of colours, mainly ranging from red to blue [5]. Hence, the consumer normally associates colour with the stage of maturity or ripeness of fruit and thus it plays an important role in the purchase decision. For this reason, colour has mainly been studied as an indicator of maturity. However, the presence of discoloration or stains on the skin can make it difficult to measure the average colour of the whole fruit, leading to inaccurate results. For this reason, Mohammadi et al. [6] developed an algorithm to classify persimmon into three maturity stages. In their work, black stains on persimmon were segmented and removed from the analysis. Then they used colour bands such as R and G from the RGB colour space, b^* from the CIELAB colour space, S from the HSI colour space and grey levels and linear (LDA) and quadratic discriminant analysis (QDA) to assess fruit maturity stages with a 90% rate of success. Another approach is reported by Taghadomi-Saberi

et al. [7], who used the CIELAB colour space to study the evolution of the ripening of sweet cherries. The colour coordinates were measured using a chroma meter and a CCD camera-based device that employed an artificial neural network (ANN) classifier. They achieved a coefficient of determination $R^2 = 0.99$ between both measurements. They also observed that L^* and b^* values decreased during the ripening of the cherries, whereas a^* values first increased and then decreased. Baltazar et al. [8] sorted tomatoes using a colorimeter and a firmness sensor. The ratio a^*/b^* and the L^* coordinate of the CIELAB colour space were used to study the changes in colour associated with storage time. El-Bendary et al. [9] used HSV colour coordinates and the first three colour moments (mean, standard deviation and skewness) to sort tomatoes. They employed Principal Components Analysis (PCA) for feature extraction and Support Vector Machines (SVM) and LDA for classification. The performance of the system was evaluated by means of the area under the curve of the receiver-operating characteristic (ROC curve) [10].

The colour of fruit is often expressed using indexes. Guzmán et al. [11] set up a maturity index for olives to determine the optimal harvest time. The index was based on colour segmentation of the olives using the k-nearest neighbour (KNN) algorithm, and calculating the percentage of the area of the olives that belonged to one of four predefined classes (bright-green, greenish-yellow, reddish-brown or black). From these data, olives were assigned a maturity index ranging from 0 to 4. The citrus colour index (CCI) is an industrial standard index to estimate the maturity of oranges and mandarins based on Hunter Lab coordinates. Vidal et al. [12] developed a computer vision system for on-line estimation of this index at a rate of eight fruits per second. The algorithm converted RGB coordinates into Hunter Lab coordinates and calculated the CCI of each fruit individually. Four images from each fruit were acquired as they rotated under the camera, the CCI being assigned an average of the four images.

Apart from colour, other external properties of fruit can be related to maturity and quality. The advantage of image analysis is that it allows several of them to be estimated simultaneously from the same image. For instance, Surya Prabha and Satheesh Kumar [13] developed an image analysis system to assess colour intensity and different geometric features (area, perimeter, major axis length and minor axis length) of bananas.

Furthermore, colour has often been combined with other information for better assessment of ripeness. For example, Vélez-Rivera et al. [14] classified Manila mangoes into four stages of ripeness. They built a PCA-based model that included colour information (CIELAB and HSB colour coordinates), soluble solid contents, total acidity, firmness and a ripening index based on these physical properties.

2.2 *Detection of External Defects*

Most consumers associate fruit and vegetable quality with good appearance, that is colour, shape and total absence of external defects. Deformations and presence of

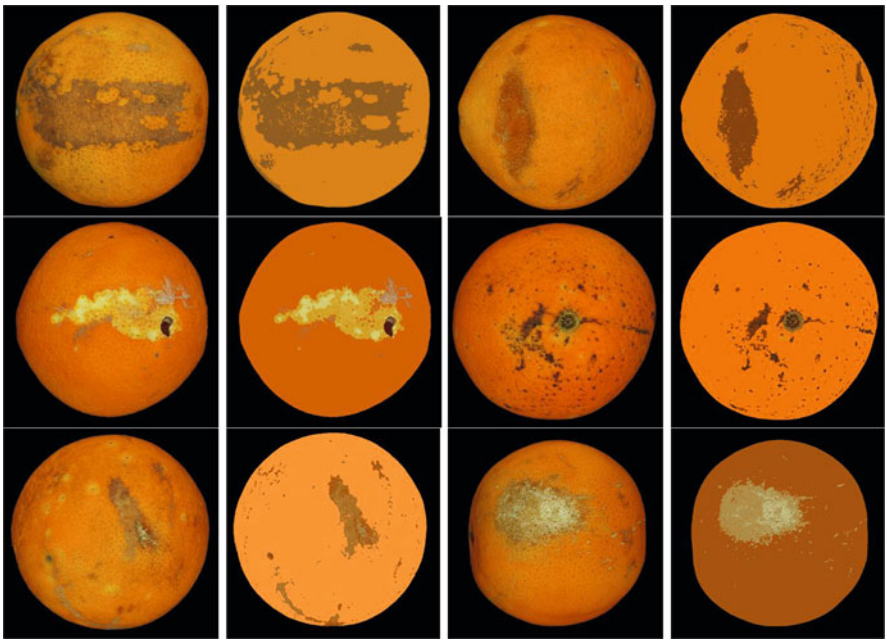

Fig. 2 External defects in *oranges* cv. 'Navel' and the images after a segmentation process

skin damage or diseases are the most influential factors affecting price. However, skin damage and diseases are more difficult to assess or detect than colour, shape or size because of the wide diversity of potential defects that can be found in packing houses [15]. Moreover, particular types of defects may present diverse colourations in the same piece or batch, or even coincide with the colour of the sound skin of other fruit of the same commodity [16]. This can be seen in Fig. 2, which shows images of different types of external defects in oranges cv. 'Navel' and the images after a segmentation process.

Many authors report inspection systems based on colour information alone. Al-Rahbi et al. [17] classified dates into three categories (no-crack, low crack level, high crack level) depending on the extension of the damaged surface found by image analysis. They used the R coordinate of the RGB colour space and the H and V coordinates of the HSV space after selecting the most discriminant ones using LDA. They achieved more than 70% accuracy and more than 80% when the problem was reduced to only two classes (sound and cracked dates).

In some machine vision applications, the calyx or the stem-end can be confused with some skin defects. The colour of the stem/calyx region often differs from the typical colour of the skin of the fruit and it is therefore identified as a defect. For this reason, authors report exploiting other information sources such as morphological or multispectral parameters. Blasco et al. [16] developed a system to detect these elements and 11 different types of defects in oranges developing a region-growing algorithm. A region of the image was considered to be a defect when its colour

diverged from the colour of the largest region of homogenous colour, which was assumed to be the sound skin. The system could detect the defects in 94% of cases, with only 4% of false detections, the stem being distinguished from the defects in 100% of cases. Later, Blasco et al. [18] identified these types of defects, achieving 70% correct identification using colour information alone and 76% on adding multispectral information. These results increased to 86% when morphological information about the regions was included in the decision algorithm [19]. However, correct identification of the stem was achieved in only 66% of cases. Li et al. [20] described a system to discriminate seven types of common defects in oranges with a 99% rate of success by employing colour and morphological information. However, they could not discriminate between these types of defects. Rokunuzzaman and Jayasuriya [21] also used morphological information to differentiate skin defects and calyxes for the automatic inspection of tomatoes at a rate of 180 fruits per minute. They used colour thresholding to detect blossom end rot and a shape factor to discriminate between cracks and calyxes with 87% success. Xu et al. [22] reported a complete machine vision system to grade kiwifruits based on their appearance, including the presence of skin defects. The system was able to grade them by size, shape and defective surface at 1.2 kg/min, with a success rate of 89%, 91% and 94%, respectively.

3 Use of Hyperspectral Imaging for Qualitative Assessment of Fruit and Vegetables

Systems based on the visible spectrum have been described in the previous paragraphs. Such systems have been designed with the intention of emulating the human eye. Nowadays they are relatively low-priced and fast. However, current technology offers the possibility of going far beyond the capabilities of the human eye. For instance, some damage or the presence of contaminant agents can often be observed in particular regions outside the visible spectrum, or their detection may be enhanced at certain specific wavelengths. Initial approaches found in the literature took advantage of the acceptable sensitivity to near-infrared (NIR) of most charge-coupled device (CCD) sensors in many cameras, and combined this information with colour information. The first successful applications were aimed at detecting visible and invisible blemishes [23].

Multispectral systems have been considered to be the first based on non-standard optical devices for simultaneously processing the same scene in different spectral regions. Originally, they consisted of a series of interferometric filters coupled to a wheel placed between a monochrome camera and the scene [24]. These systems had several drawbacks, such as their low acquisition speed and the small number of images that could be acquired. Recent technological progress has allowed faster simultaneous acquisition of images, thereby opening up the possibility of developing new applications in fields such as remote sensing [25] and pest detection

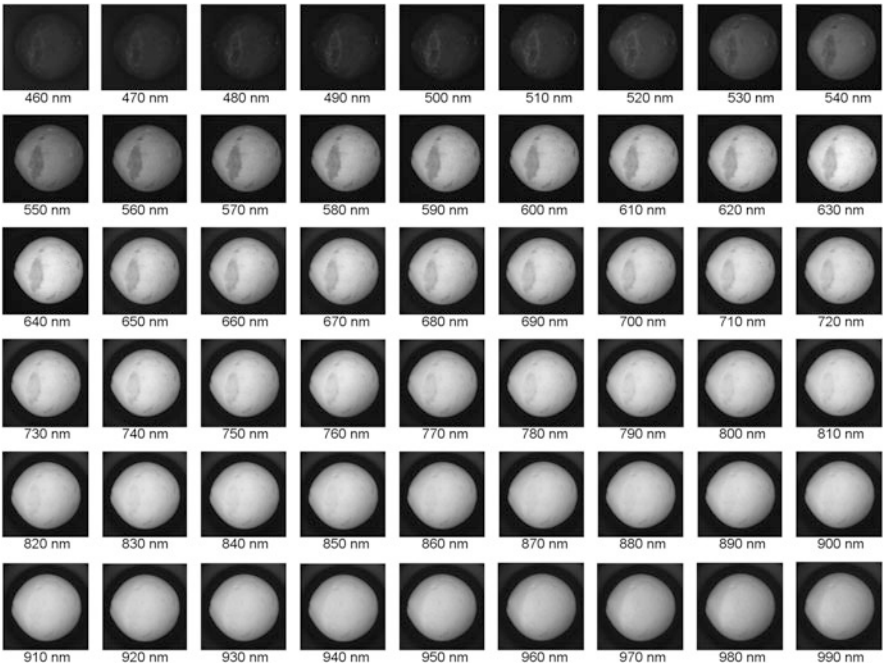

Fig. 3 Hyperspectral image of an *orange* cv. 'Navelate' with an external defect captured in the range 430–1,050 nm

[26, 27] among others. Moreover, the price of the equipment has gradually become more affordable, thus enabling the use of related technologies in many applications to agriculture [28].

Although capturing images in stationary applications can be accomplished by swapping narrow band pass filters in front of the camera lens, a more sophisticated and versatile solution is offered by the use of electronically tuneable filters, capable of acquiring a large number of images at different consecutive wavelengths, thus making it possible to develop new inspection systems based on hyperspectral images [29]. Hyperspectral imaging systems allow spatial and reflectance information to be acquired at the same time, which can be decisive for certain applications [3]. Such systems acquire a huge amount of information, but this is also their major drawback because some of this information is redundant or unnecessary [30, 31]. For this reason, much work using this technology has focused on reducing the amount of redundant information by projecting the high-dimensional data space into a lower-dimensional space and trying to preserve most of the meaningful information [10, 32]. In parallel, spectroscopy has been used to assess certain properties of food and even to detect some pathogens [33, 34]. Figure 3 shows a hyperspectral imaging of an orange with a windscar defect captured in the range 430–1,050 nm with a resolution of 10 nm.

Electronically tuneable filters are devices whose spectral transmission can be electronically controlled by applying a voltage or acoustic signals. Three main technologies are currently available for acquiring hyperspectral images for fruit analysis: image spectrophotometers [35], Acousto-Optical Tunable Filters (AOTF) [36–38] and Liquid Crystal Tunable Filters (LCTF) [39]. AOTF consist of a crystal in which selected wavelengths of light are separated from a broadband source using acoustic waves at specific radio frequencies. Alternative compression and relaxation of the crystal lattice generates density changes that produce refractive index variations which act as a transmission diffraction grating. Unlike a classical diffraction grating, AOTF only diffract one specific wavelength of light, so they act more as a filter than a diffraction grating. LCTF use a stack of successively thicker, polariser birefringent liquid crystal plates which can generate a tuneable retardation of light transmission. Switching speed is limited by the relaxation time of the crystal and is of the order of 50 ms. Spectral resolution of LCTF is typically of the order of several nanometres.

Image spectrophotometers acquire spectral data by scanning the scene line by line, making use of the relative movement of the objects in the scene with respect to the instrument. These sensors usually offer an excellent spectral resolution, but require precise synchronisation of the image acquisition with the movement of the sample or the instrument [40]. This is probably the most extended configuration of AOTF-based systems, offering good tuning times (around 50 ms) and accurate frequency selectivity. However, they have a limited field of view [41]. In general, LCTF-based devices are usually more compact than those based on AOTF and provide a wider field of view. Nonetheless, their major drawback is related to their greater requirements in terms of time needed for tuning [42].

Even if the use of this equipment is expanding, one has still to take into account important requirements for them to work properly, such as adequate spatial and spectral distribution of the lighting, correct focusing of the scene across all the different wavelengths or spectral regions and proper spatial matching of the images, or at least of the objects in the scene, when using changeable filters or when the object of interest is moving during the acquisition. Furthermore, the sensitivity of the different components of the acquisition sensors is not uniform across the spectrum, and this should be taken into account in the design. Suitable calibrations and adjustments are always necessary to keep the results of the image analysis independent of undesired phenomena [43].

Proper lighting is also crucial when acquiring hyperspectral images. Unwanted bright spots must be prevented when providing high-quality, homogenous scene illumination. Light sources have different characteristic spectral emissions. Daylight-type fluorescent tubes rarely go beyond 700 nm and should be discarded in work that uses near-infrared (NIR). Incandescent lamps generate strong NIR emissions but produce directional light which is difficult to diffuse. In addition, it is important to take into account the shape of the object to be analysed to avoid specular reflections. This is particularly important for spherical or quasi spherical shapes. On the other hand, cameras should be sensitive to the specific spectral region used in each application. Standard CCD cameras are almost insensitive to

wavelengths from 900 nm and beyond, which can make it impossible to take full advantage of the possibilities of tuneable filters. Cameras based on InGaAs sensors with a stabilised temperature are sensitive beyond 1,000 nm, thus enabling an optimal use of NIR information. Lenses are also critical and must be properly selected for each particular application. Optical paths through the lens change depending on the frequency of the transmitted light (refraction indexes depend on wavelength). This makes the focus planes vary considerably between bands that are separated by relatively far distances in the spectrum (e.g. between some visible and some infrared bands), resulting in scenes that are focused in some bands being out of focus in others.

3.1 Automatic Assessment of Bio-Chemical Properties of Fruit and Vegetables

Assessment of the ripening stage of many fruits still relies on trained people's experience or on destructive measurements of certain physicochemical properties. These approaches are inefficient and incompatible with large-scale production and trading. Machine vision systems based on hyperspectral imaging offer new tools to assess the concentration of some chemical compounds or properties related to maturity. This is the case of the work reported by Schmilovitch et al. [44], who presented a method for the non-destructive measurement of total soluble solids (TSS), ascorbic acid, chlorophyll and carotenoid contents in three bell pepper cultivars using hyperspectral images obtained using AOTF cameras. By means of partial least squares (PLS) regression models developed throughout the grooving session and specific to each variety, they managed to estimate the distribution of such internal components in whole peppers. Rajkumar et al. [45] analysed hyperspectral images of bananas at different ripening stages, and stored at different temperatures, to develop calibration models for the prediction of some quality parameters (moisture content, TSS and firmness). Munera et al. [46] used hyperspectral images to predict astringency in persimmons and to build the astringency distribution maps.

Hyperspectral image processing can also be used to obtain information about the presence of biochemical substances related to certain damage or physiological disorders of some agricultural produce. For instance, Gaston et al. [47] investigated the potential of visible and near-infrared (VIS/NIR) (445–945 nm) hyperspectral imaging for the prediction of polyphenol oxidase (PPO) enzyme activity, which produces browning on mushroom caps and is the major cause of their quality loss, accounting for a reduction in their market value. Yang et al. [48] studied the anthocyanin contents of the pericarp of lychees, because it is related to postharvest browning. They processed hyperspectral images of fruits in the range 308–1,105 nm by removing differences in light intensity between different areas of the samples, extracting the average spectra from the regions of interest (ROI) and

selecting two sets of optimal wavelengths using successive projection and stepwise regression algorithms. Finally, they built models for mapping the anthocyanin distribution in the samples.

Long-distance transoceanic shipment of fruit requires delivery of high quality, consistent fresh fruit in the country of origin so as to meet the quality standards upon arrival at the destination. Hua et al. [49] investigated the potential of hyperspectral imaging to study how the mechanical properties of blueberries are related to their organoleptic quality, storability, transportability, resistance to mechanical damage and susceptibility to spoilage during postharvest and marketing handling. They tried to link spectral data to mechanical properties obtained from texture profiles and puncture analysis. Similarly, Leiva-Valenzuela et al. [50, 51] acquired reflectance and transmittance hyperspectral images of blueberries in the range 400–1,000 nm to build calibration models to predict TSS and firmness, and to assess the effect of fruit orientation on the durability of the fruit during transportation.

Consumers are willing to pay higher prices for fruit with health-stimulating properties such as bioactive compounds or antioxidant ingredients, for example lycopene and phenolic compounds. Liu et al. [52] reported an application of multispectral imaging for predicting the contents of such compounds in tomatoes, and compared the performance of different prediction models based on PLS, least squares support vector machines (LS-SVM) and back-propagation neural networks (BPNN).

Similarly, anthocyanins are phenolic components of red wine grapes which have a great influence on the quality of wine. Nogales-Bueno et al. [53] developed a non-destructive method, based on hyperspectral images, for the assessment of the important parameters that determine the technological and phenolic maturity of white and red grapes (pH, total acidity, sugar concentration and total phenols). Later, Nogales-Bueno et al. [54] used a similar approach to estimate maturity and sugar content and investigated the possibility of using anthocyanin profiles, colour image analysis and near-infrared hyperspectral imaging tools to distinguish between the varieties Tempranillo, Graciano, Garnacha and Mazuelo. Chen et al. [55] developed a model to estimate the anthocyanin contents of wine grape skins using NIR hyperspectral imaging. They used this information to assess the phenolic maturation stage of grapes after veraison, with the final goal of predicting the best harvest time. Baiano et al. [56] also used hyperspectral imaging to predict the physicochemical indices and sensory characteristics of table grapes. Furthermore, Leiva-Valenzuela et al. [50] studied the potential of VIS/NIR spectroscopy and hyperspectral imaging to estimate the internal or external constituents of potato tubers, which are important to the processing industries.

3.2 Detection of Skin Defects and Diseases

Machine vision systems based on hyperspectral imaging open up the possibility of automatically detecting early stages of fruit damage invisible to the human eye because they can provide information from outside the visible spectrum. For instance, Lü et al. [57] developed a VIS/NIR hyperspectral imaging system covering the spectral region 408–1,117 nm for the automatic detection of bruising caused by excessive mechanical loading and stress of kiwifruits during harvest, transport, handling and storage. Such bruises are very difficult to detect in the first hours after they have been produced. For this purpose they selected particular wavelengths to develop algorithms to differentiate between bruised and sound tissues. Likewise, Baranowski et al. [58] worked on the early detection of bruises in apples, using VIS/NIR and short-wave infrared (SWIR) wavelength ranges. Similarly, Vélez-Rivera et al. [59] reported on the feasibility of an automatic system for early detection of mechanical damage in 'Manila' mangoes using specific spectral bands. Lee et al. [60] investigated an extended range of NIR to detect bruises on pears.

The presence of a few fruits infested by a pest or affected by fungus in a shipment can render the entire consignment unmarketable. Furthermore, many other kinds of skin damage must be detected during postharvest quality control because they can be the starting point of fungal infestations. For instance, tomato cracking is one of the main causes of produce rejection by retailers because it creates a path for the potential entrance of pathogens. Cho et al. [61] investigated the feasibility of an inspection system based on hyperspectral fluorescence and determined optimal wavebands to distinguish between defective areas and sound surfaces to detect cuticle cracks. Analogously, Yu et al. [62] investigated the potential of hyperspectral imaging for crack detection in fresh jujubes. They identified some wavelengths to develop image processing algorithms for locating the cracks, but reported that the best option was to use ratios of bands instead.

Pests themselves are also a major cause of fruit rejection in the market. As an example, the Mediterranean fruit fly causes damage to many different fruits and significant economic losses for growers, processers and exporters, and is impossible to detect using colour information alone [18]. Haffa et al. [63] proposed a system for detecting infested mangoes using greyscale images generated from absorbance levels at particular NIR wavelengths. Another approach was taken by Wang et al. [64] who identified effective wavelengths for maximum discrimination of jujube fruits affected by damage caused by insects. They created a discriminant function to identify the stem-end/calyx-end, the sound cheek and insect damage, and finally a method to distinguish damaged fruits from those free of infestation. This approach has also recently been investigated by Gómez-Sanchis et al. [65, 66] with the aim of detecting decay lesions in citrus fruits.

Physiological disorders and decay are a consequence of postharvest processes which also generate important economic losses. Simko et al. [67] developed several indices to estimate decay and freezing injuries of different cultivars of lettuces,

based on ratios of particular wavelengths obtained from the spectral analysis in the range 380–1,000 nm.

Fruit and vegetable diseases, often caused by bacteria, are also a major source of trouble for fruit and vegetable exporters. For instance, citrus canker is a severe disease of citrus fruit causing enormous socioeconomic loses for those countries affected. Qin et al. [68] used spectral information divergence estimated from NIR images as a method for detecting affected fruit, and Zhao et al. [69] introduced the effect of the harvesting time and its influence on the detection of the damage. Later, Qin et al. [70] exploited particular bands obtained from the PCA technique and used ratios between bands to create a fast detection system. Subsequently, Qin et al. [71] reported a real-time system to detect such canker lesions. A different approach was taken by Wang et al. [72] who compared the spectral reflectance of onions affected by sour skin (a bacterial disease) in the spectral region of 950–1,650 nm and determined optimal bands for identifying infected onions.

3.3 Detection of Pathogens and Contaminants

Foodborne illnesses are also of major concern for consumers and, hence, interest in methods and technologies for detecting contaminated food and preventing the presence of pathogens causing such illnesses has grown significantly, both in the agri-food industries and in regulatory agencies. Hyperspectral imaging offers a vast potential for detecting contaminants and pathogens in food. For instance, Lee et al. [60] determined two significant wavelengths and developed multispectral imaging algorithms to detect faecal contamination on leafy greens (spinach and lettuces) in an automated system for in-line inspection at the processing plants. At the same time, Everard et al. [73] used ultraviolet (UV)-induced fluorescence, violet-induced fluorescence, VIS/NIR reflectance and hyperspectral image processing, in combination with multivariate statistical analysis, for the detection of faecal contamination on spinach leaves.

Tomato hornworm is one of the several types of large caterpillars that attack tomatoes in the United States and whose faecal matter is closely related to the presence of *Escherichia coli* and Salmonella. Yang et al. [74] studied the development of a multispectral imaging algorithm to detect such contamination on the surface of mature red tomatoes. In similar work, Yang et al. [75] developed a simple multispectral algorithm to detect faecal contamination on the surface of apples. *Aspergillus flavus* generates toxins on dates and logically causes food safety concerns which greatly depreciate the value of the product. Teena et al. [76] studied the presence of lesions caused by this fungus using NIR hyperspectral imaging.

4 Specific Problems To Be Solved for Real-Time, Automatic Quality Monitoring

To satisfy market demands, producers must inspect the quality of each piece of fruit or vegetable before shipping. This task is traditionally carried out by workers situated on one or both sides of a conveyor belt. They visually inspect the produce and remove those pieces not meeting the quality standards. Pieces are transported slowly enough to allow the workers to inspect all of them and even manipulate them to ensure the inspection of most of their surface. The quality of the product is not always fully guaranteed because workers have different tolerance criteria and, at the same time, their criteria may vary during the day, as inspection requires concentration and is a tiring, repetitive activity. For all these reasons, this operation is normally time-consuming, subjective and expensive. The alternative is the use of electronic sorters based on machine vision.

In most in-line applications, products travel rapidly under the machine vision system, often carried by a conveyor belt or on top of rollers as shown in Fig. 4. In such cases, the camera has to be able to acquire images at a very high rate when freezing the scene, and computer hardware and software has to be set to cope with very fast image processing. For example, Al-Mallahi et al. [77] developed an automatic machine vision system for sorting potatoes using UV-induced fluorescence capable of discriminating potatoes from undesired material. They processed one image every 94 ms with a success rate of 98%. ElMasry et al. [78] developed an automatic system to sort potatoes by size and shape. Roundness and length features as well as four other parameters calculated from Fourier analysis of the polar signature of the potato boundary were found to be effective in describing potato size and shape. The system achieved a high level of accuracy in estimating the

Fig. 4 Machine for the automatic inspection of fruit in-line using computer vision

shape and size of potatoes travelling at 1 m/s. Nevertheless, real-time inspection encompasses a number of problems which need to be solved. Some are related to the need to avoid blurred images and freezing the movement of the pieces when acquiring the images, whereas others are related to the exact positioning of the piece. Both require very precise synchronisation between the camera shot and the movement of the conveyor. Furthermore, adequate intensity and uniform illumination are always necessary. Other problems to be overcome are associated with processing speed constraints, which require considerable effort in algorithm optimisation and sometimes the use of dedicated hardware. Moreover, the need to inspect the whole surface of the pieces requires the use of specific mechanisms or the use of multiple cameras situated to acquire several points of view.

The electronic shutters of the cameras allow proper synchronisation between the movement of the pieces and the image acquisition and a short exposure time, both required for a correct freezing effect. The fast development of powerful Light Emitting Diodes (LED) has allowed the development of very uniform illumination systems with multiple light sources. Furthermore, it has opened up the possibility of generating accurate light pulses instead of continuously illuminating the scene. Pulsed illumination helps to avoid the blurring effect of the movement of the objects in the images and to save energy, which may be crucial for some applications, especially those related to machines working outdoors. The use of fast shutters and strips of pulsed LEDs was reported by Vidal et al. [12] to take different views of oranges moving at 0.4 m/s on a conveyor. Kohno et al. [79] used this type of illumination on a mobile platform to inspect citrus fruits during harvesting, but they needed 12–20 s to process a single fruit because an NIR spectrometer was also used to estimate the sugar content of fruits. However, Cubero et al. [80] used this type of illumination and settings for real-time inspection of oranges on a citrus harvesting machine. The system was able to work at a rate of eight fruit per second, and captured four images of each fruit to make a decision. They reported a 0.99 coefficient of determination ($R^2 = 0.99$) for size prediction and $R^2 = 0.92$ for colour.

To achieve real-time operation, image segmentation and processing must be carried out extremely quickly. The work of Aleixos et al. [23], who developed a camera capable of acquiring multispectral images (VIS/NIR) from the same scene, is an example of the use of specific hardware and algorithm optimisation to reduce processing time. They used parallel image processing algorithms run on two digital signal processors (DSP) to process 10 citrus fruits per second and sort them by colour, size and presence of defects, using nonlinear discriminant procedures to segment the images and to sort the pieces. However, the processing speed of current hardware allows complex algorithms to be implemented in relatively low-cost devices. Commercial cameras equipped with microprocessors can be used to create smart equipment for in-line processing, as reported by Cubero et al. [80], who achieved real-time colour image processing for citrus sorting by implementing optimised algorithms in a camera with standard computing capability.

Several approaches have been made to solve the problem of inspecting most of the surface of the pieces. Many inspection machines rotate the pieces when a series

of images are captured. Leemans and Destain [81] used a roller conveyor to capture images of apples. They adjusted the rotational speed of the rollers in such a way that a spherical object with a diameter of 72 mm made one complete rotation in exactly four images. Images were acquired at a rate of 11 per second. A hierarchical grading method based on the analysis of 16 external properties including colour, shape, texture and position was used to classify apples. Bennedsen et al. [82] developed a system to capture six different views of each apple as the fruit was transported on a conveyor. Other reported solutions include the use of different cameras to capture different views of the fruit, as depicted by Xiao-bo et al. [83], who employed three colour cameras to inspect rotating apples and classify them into two categories depending on the presence of defects. A cheaper alternative is the use of mirrors instead of cameras, as described by Reese et al. [84], who used parabolic mirrors to show parts of the fruits that were hidden from the camera.

Soft or very small processed fruits are more difficult to handle and hence to inspect, and so may require particular solutions. For instance, Blasco et al. [85] developed a prototype to grade fragile mandarin segments and to separate marketable segments from undesired material such as small pieces of peel, broken segments or segments with seeds. Segments travelled on narrow conveyor belts under two cameras which acquired images every 48 ms. Their vision system was able to process 20 images per second, but mechanical limitations related to the difficulty in handling the segments reduced the operational speed to four images per second. Semitransparent conveyor belts were employed to illuminate the scene from the back, enhance the silhouette of the segments and detect the seeds easily. A similar machine was reported by Blasco et al. [86] for real-time inspection of pomegranate arils using front illumination and opaque blue conveyor belts. In this case, colour parameters were used to detect rotten or immature arils and to grade arils into uniform colour batches, which are more attractive to the consumer.

5 Conclusions

This chapter summarises the current state of the art in computer vision-based fruit and vegetable inspection. The final aim of the technologies described here is the implementation of machines capable of automatically inspecting the quality of these products, removing those not reaching an adequate level of quality and ensuring an objective sorting in categories that make them more attractive for the consumer and optimise their value. To enhance current sorting systems giving high added value to the products, the use of physicochemical and morphological information other than simple visual appearance is becoming more and more relevant.

Machine vision-based systems are always under constant evolution thanks to the development of new types of cameras and imaging devices. UV and NIR acquisition systems are becoming easily available. Hyperspectral systems have demonstrated their ability to capture information invisible to the human eye, such as the presence of internal defects or the measurement of chemical compounds. However,

despite all these technological advancements, a compromise between their increase in performance (image acquisition rate, resolution) and costs must be found in the forthcoming years.

Acknowledgement This work has been partially funded by INIA through research projects RTA2012-00062-C04-01 and RTA2012-00062-C04-03 with the support of European FEDER funds.

References

1. Cubero S, Lee WS, Aleixos N, Albert F, Blasco J (2016) Automated systems based on machine vision for inspecting citrus fruits from the field to postharvest: a review. Food Bioproc Tech 9:1623–1639
2. Cubero S, Aleixos N, Moltó E, Gómez-Sanchis J, Blasco J (2011) Advances in machine vision applications for automatic inspection and quality evaluation of fruits and vegetables. Food Bioproc Tech 4:487–504
3. Lorente D, Aleixos N, Gómez-Sanchis J, Cubero S, García-Navarrete OL, Blasco J (2012) Recent advances and applications of hyperspectral imaging for fruit and vegetable quality assessment. Food Bioproc Tech 5:1121–1142
4. Hunt RWG, Pointer MR (2011) Measuring colour, 4th edn. Wiley, Chichester
5. Sharma RM, Singh RR (2000) Harvesting, postharvest, handling and physiology of fruits and vegetables. In: Verma LR, Joshi VK (eds) Postharvest technology of fruit and vegetables. Indus Publishing Co. New Delhi, pp 94–147
6. Mohammadi V, Kheiralipour K, Ghasemi-Varnamkhasti M (2015) Detecting maturity of persimmon fruit based on image processing technique. Sci Hortic 184:123–128
7. Taghadomi-Saberi S, Omid M, Emam-Djomeh Z, Faraji-Mahyari KH (2015) Determination of cherry color parameters during ripening by artificial neural network assisted image processing technique. J Agric Sci Technol 17:589–600
8. Baltazar A, Aranda JI, González-Aguilar G (2008) Bayesian classification of ripening stages of tomato fruit using acoustic impact and colorimeter sensor data. Comput Electron Agric 60: 113–121
9. El-Bendary N, El Hariri E, Hassanien AE, Badr A (2015) Using machine learning techniques for evaluating tomato ripeness. Expert Syst Appl 42:1892–1905
10. Lorente D, Aleixos N, Gómez-Sanchis J, Cubero S, Blasco J (2013) Selection of optimal wavelength features for decay detection in citrus fruit using the ROC curve and neural networks. Food Bioproc Tech 6(2):530–541
11. Guzmán E, Baeten V, Pierna JAF, García-Mesa JA (2015) Determination of the olive maturity index of intact fruits using image analysis. J Food Sci Technol 52:1462–1470
12. Vidal A, Talens P, Prats-Montalbán JM, Cubero S, Albert F, Blasco J (2013) In-line estimation of the standard colour index of citrus fruits using a computer vision system developed for a mobile platform. Food Bioproc Tech 6(12):3412–3419
13. Surya Prabha D, Satheesh Kumar J (2015) Assessment of banana fruit maturity by image processing technique. J Food Sci Technol 52:1316–1327
14. Vélez-Rivera N, Blasco J, Chanona-Pérez JJ, Calderón-Domínguez G, Perea-Flores MJ, Arzate-Vázquez I, Cubero S, Farrera-Rebollo R (2014) Computer vision system applied to classification of 'Manila' mangoes during ripening process. Food Bioproc Tech 7:1183–1194
15. Li JB, Huang WQ, Zhao CJ (2015) Machine vision technology for detecting the external defects of fruits: a review. Imaging Sci J 63:241–251
16. Blasco J, Aleixos N, Moltó E (2007) Computer vision detection of peel defects in citrus by means of a region oriented segmentation algorithm. J Food Eng 81:535–543

17. Al-Rahbi S, Manickavasagan A, Al-Yahyai R, Khriji L, Alahakoon P (2013) Detecting surface cracks on dates using color imaging technique. Food Sci Technol Res 19:795–804
18. Blasco J, Aleixos N, Gómez J, Moltó E (2007) Citrus sorting by identification of the most common defects using multispectral computer vision. J Food Eng 83:384–393
19. Blasco J, Aleixos N, Gómez-Sanchis J, Moltó E (2009) Recognition and classification of external skin damage in citrus fruits using multispectral data and morphological features. Biosyst Eng 103:137–145
20. Li J, Rao X, Wang F, Wu W, Ying Y (2013) Automatic detection of common surface defects on oranges using combined lighting transform and image ratio methods. Postharvest Biol Technol 82:59–69
21. Rokunuzzaman M, Jayasuriya HPW (2013) Development of a low cost machine vision system for sorting of tomatoes. Agric Eng Int CIGR J 15:173–180
22. Xu L, You Z, Wu S, Zhao H, Wu L (2013) Development and experiment on automatic grading equipment for kiwi INMATEH - agricultural. Engineering 41:55–64
23. Aleixos N, Blasco J, Navarrón F, Moltó E (2002) Multispectral inspection of citrus in real-time using machine vision and digital signal processors. Comput Electron Agric 33:121–137
24. Unay D, Gosselin B, Kleynen O, Leemans V, Destain MF, Debeir O (2011) Automatic grading of bi-colored apples by multispectral machine vision. Comput Electron Agric 75:204–212
25. Lee WS, Alchanatis V, Yang C, Hirafuji M, Moshou D, Li C (2010) Sensing technologies for precision specialty crop production. Comput Electron Agric 74:2–33
26. Pourreza A, Lee WS, Ehsani R, Schueller JK, Raveh E (2015) An optimum method for real-time in-field detection of Huanglongbing disease using a vision sensor. Comput Electron Agric 110:221–232
27. Pourreza A, Lee WS, Etxeberria E, Banerjee A (2015) An evaluation of a vision-based sensor performance in Huanglongbing disease identification. Biosyst Eng 130:13–22
28. Sun D-W (ed) (2010) Hyperspectral imaging for food quality analysis and control. Academic Press, Elsevier Science, London, England
29. Gat N (2000) Imaging spectroscopy using tunable filters: a review. Proc SPIE 4056:50–64
30. Gómez-Sanchis J, Gómez-Chova L, Aleixos N, Camps-Valls G, Montesinos-Herrero C, Moltó E, Blasco J (2008) Hyperspectral system for early detection of rottenness caused by *Penicillium digitatum* in mandarins. J Food Eng 89:80–86
31. Gómez-Sanchis J, Martín-Guerrero JD, Soria-Olivas E, Martínez-Sober M, Magdalena-Benedito R, Blasco J (2012) Detecting rottenness caused by *Penicillium* in citrus fruits using machine learning techniques. Expert Syst Appl 39:780–785
32. Lorente D, Blasco J, Serrano AJ, Soria-Olivas E, Aleixos N, Gómez-Sanchis J (2013) Comparison of ROC feature selection method for the detection of decay in citrus fruit using hyperspectral images. Food Bioproc Tech 6:3613–3619
33. Brandily ML, Monbet V, Bureau B, Boussard-Plédel C, Loréal O, Adam JL, Sire O (2011) Identification of foodborne pathogens within food matrices by IR spectroscopy. Sens Actuators B 160:202–206
34. Nicolaï BM, Beullens K, Bobelyn E, Peirs A, Saeys W, Theron KI, Lammertyn J (2007) Nondestructive measurement of fruit and vegetable quality by means of NIR spectroscopy: a review. Postharvest Biol Technol 46:99–118
35. Zhao J, Ouyang Q, Chen Q, Wang J (2010) Detection of bruise on pear by hyperspectral imaging sensor with different classification algorithms. Sens Lett 8:570–576
36. Bei L, Dennis GI, Miller HM, Spaine TW, Carnahan JW (2004) Acousto-optic tunable filters: fundamentals and applications as applied to chemical analysis techniques. Prog Quantum Electron 28:67–87
37. Jiménez A, Beltrán G, Aguilera MP, Uceda M (2008) A sensor-software based on artificial neural network for the optimization of olive oil elaboration process. Sens Actuators B 129: 985–990
38. Vila-Francés J, Calpe-Maravilla J, Gómez-Chova L, Amorós-López J (2010) Analysis of acousto-optic tunable filter performance for imaging applications. Opt Eng 49:113203–113209

39. Wang W, Li C, Tollner EW, Rains GC, Gitaitis RD (2012) A liquid crystal tunable filter based shortwave infrared spectral imaging system: design and integration. Comput Electron Agric 80:126–134
40. Gowen AA, O'Donnell CP, Cullen PJ, Downey G, Frias JM (2007) Hyperspectral imaging – an emerging process analytical tool for food quality and safety control. Trends Food Sci Technol 18:590–598
41. Vila-Francés J, Calpe-Maravilla J, Gómez-Chova L, Amorós-López J (2011) Design of a configurable multispectral imaging system based on an AOTF. IEEE Trans Ultrason Ferroelectr Freq Control 58:259–262
42. Hecht E (2003) Optics, 4th edn. Addison Wesley, Reading
43. Geladi PLM (2007) Calibration standards and image calibration. In: Grahn HF, Geladi P (eds) Techniques and applications of hyperspectral image analysis. Wiley, Chichester, pp 203–220
44. Schmilovitch Z, Ignat T, Alchanatis V, Gatker J, Ostrovsky V, Felföldi J (2014) Hyperspectral imaging of intact bell peppers. Biosyst Eng 117:83–93
45. Rajkumar P, Wang N, ElMasry G, Raghavan GSV, Gariepy Y (2012) Studies on banana fruit quality and maturity stages using hyperspectral imaging. J Food Eng 108:194–200
46. Munera S, Besada C, Blasco J, Cubero S, Salvador A, Talens P, Aleixos N (2017) Astringency assessment of persimmon by hyperspectral imaging. Postharvest Biol Technol 125:35–4
47. Gaston E, Frías JM, Cullen PJ, O'Donnell CP, Gowen AA (2010) Prediction of polyphenol oxidase activity using visible near-infrared hyperspectral imaging on mushroom (*Agaricus bisporus*) caps. J Agric Food Chem 58:6226–6233
48. Yang YC, Sun DW, Pu H, Wang NN, Zhu Z (2015) Rapid detection of anthocyanin content in lychee pericarp during storage using hyperspectral imaging coupled with model fusion. Postharvest Biol Technol 103:55–65
49. Hua MH, Dong QL, Liu BL, Opara UL, Chen L (2015) Estimating blueberry mechanical properties based on random frog selected hyperspectral data. Postharvest Biol Technol 106: 1–10
50. Leiva-Valenzuela GA, Lu R, Aguilera JM (2013) Prediction of firmness and soluble solids content of blueberries using hyperspectral reflectance imaging. J Food Eng 115:91–98
51. Leiva-Valenzuela GA, Lu R, Aguilera JM (2014) Assessment of internal quality of blueberries using hyperspectral transmittance and reflectance images with whole spectra or selected wavelengths. Innov Food Sci Emerg Technol 24:2–13
52. Liu C, Liu W, Chen W, Yang J, Zheng L (2015) Feasibility in multispectral imaging for predicting the content of bioactive compounds in intact tomato fruit. Food Chem 173:482–488
53. Nogales-Bueno J, Hernández-Hierro JM, Rodríguez-Pulido FJ, Heredia FJ (2014) Determination of technological maturity of grapes and total phenolic compounds of grape skins in red and white cultivars during ripening by near infrared hyperspectral image: a preliminary approach. Food Chem 152:586–591
54. Nogales-Bueno J, Rodríguez-Pulido FJ, Heredia FJ, Hernández-Hierro JM (2015) Comparative study on the use of anthocyanin profile, color image analysis and near-infrared hyperspectral imaging as tools to discriminate between four autochthonous red grape cultivars from La Rioja (Spain). Talanta 131:412–416
55. Chen S, Zhang F, Ning J, Liu X, Zhang Z, Yang S (2015) Predicting the anthocyanin content of wine grapes by NIR hyperspectral imaging. Food Chem 172:788–793
56. Baiano A, Terracone C, Peri G, Romaniello R (2012) Application of hyperspectral imaging for prediction of physico-chemical and sensory characteristics of table grapes. Comput Electron Agric 87:142–151
57. Lü Q, Tang M, Cai J, Zhao J, Vittayapadung S (2011) Vis/NIR hyperspectral imaging for detection of hidden bruises on kiwifruits. Czech J Food Sci 29:595–602
58. Baranowski P, Mazurek W, Pastuszka-Wozniak J (2013) Supervised classification of bruised apples with respect to the time. Postharvest Biol Technol 86:249–258

59. Vélez-Rivera N, Gómez-Sanchis J, Chanona-Pérez J, Carrasco JJ, Millán-Giraldo M, Lorente D, Cubero S, Blasco J (2014) Early detection of mechanical damage in mango using NIR hyperspectral images and machine learning. Biosyst Eng 122:91–98
60. Lee WH, Kim MS, Lee H, Delwiche SR, Bae H, Kim DY, Cho BK (2014) Hyperspectral near-infrared imaging for the detection of physical damages of pear. J Food Eng 130:1–7
61. Cho BK, Kim MS, Baek IS, Kim DY, Lee WH, Kim J, Bae H, Kim YS (2013) Detection of cuticle defects on cherry tomatoes using hyperspectral fluorescence imagery. Postharvest Biol Technol 76:40–49
62. Yu K, Zhao Y, Li X, Shao Y, Zhu F, He Y (2014) Identification of crack features in fresh jujube using Vis/NIR hyperspectral imaging combined with image processing. Comput Electron Agric 103:1–10
63. Haffa RP, Saranwongb S, Thanapase W, Janhiran A, Kasemsumran S, Kawano S (2013) Automatic image analysis and spot classification for detection of fruitfly infestation in hyperspectral images of mangoes. Postharvest Biol Technol 86:23–28
64. Wang J, Nakano K, Ohashi S, Kubota Y, Takizawa K, Sasaki Y (2011) Detection of external insect infestations in jujube fruit using hyperspectral reflectance imaging. Biosyst Eng 108:345–351
65. Gómez-Sanchis J, Blasco J, Soria-Olivas E, Lorente D, Escandell-Montero P, Martínez-Martínez JM, Martínez-Sober M, Aleixos N (2013) Hyperspectral LCTF-based system for classification of decay in mandarins caused by *Penicillium digitatum* and *Penicillium italicum* using the most relevant bands and non-linear classifiers. Postharvest Biol Technol 82:76–86
66. Gómez-Sanchis J, Lorente D, Soria-Olivas E, Aleixos N, Cubero S, Blasco J (2014) Development of a hyperspectral computer vision system based on two liquid crystal tuneable filters for fruit inspection. Application to detect citrus fruits decay. Food Bioproc Tech 7:1047–1056
67. Simko I, Jimenez-Berni JA, Furbank RT (2015) Detection of decay in fresh-cut lettuce using hyperspectral imaging. Postharvest Biol Technol 106:44–52
68. Qin J, Burks TF, Ritenour MA, Gordon Bonn W (2009) Detection of citrus canker using hyperspectral reflectance imaging with spectral information divergence. J Food Eng 93: 183–191
69. Zhao X, Burks TF, Qin J, Ritenour MA (2010) Effect of fruit harvest time on citrus canker detection using hyperspectral reflectance imaging. Sens Instrum Food Qual Saf 4:126–135
70. Qin J, Burks TF, Zhao X, Niphadkar N, Ritenour MA (2011) Multispectral detection of citrus canker using hyperspectral band selection. Trans ASABE 54:2331–2341
71. Qin J, Burks TF, Zhao X, Niphadkar N, Ritenour MA (2012) Development of a two-band spectral imaging system for real-time citrus canker detection. J Food Eng 108:87–93
72. Wang W, Li C, Tollner EW, Gitaitis RD, Rains GC (2012) Shortwave infrared hyperspectral imaging for detecting sour skin (*Burkholderia cepacia*) infected onions. J Food Eng 109:36–48
73. Everard CD, Kim MS, Lee H (2014) A comparison of hyperspectral reflectance and fluorescence imaging techniques for detection of contaminants on spinach leaves. J Food Eng 143: 139–145
74. Yang CC, Kim MS, Millner P, Chao K, Cho B-K, Mo C, Lee H, Chan DE (2014) Assessment of internal quality of blueberries using hyperspectral transmittance and reflectance images with whole spectra or selected wavelengths. Postharvest Biol Technol 93:1–8
75. Yang CC, Kim MS, Kang S, Cho BK, Chao K, Lefcourt AM, Chan DE (2012) Red to far-red multispectral fluorescence image fusion for detection of fecal contamination on apples. J Food Eng 108:312–319
76. Teena MA, Manickavasagan A, Ravikanth L, Jayas DS (2014) Near infrared (NIR) hyperspectral imaging to classify fungal infected date fruits. J Stored Prod Res 59:306–313
77. Al-Mallahi A, Kataoka T, Okamoto H, Shibata Y (2010) Detection of potato tubers using an ultraviolet imaging-based machine vision system. Biosyst Eng 105:257–265
78. ElMasry G, Cubero S, Moltó E, Blasco J (2012) In-line sorting of irregular potatoes by using automated computer-based machine vision system. J Food Eng 112:60–68

79. Kohno Y, Kondo N, Iida M, Kurita M, Shiigi T, Ogawa Y, Kaichi T, Okamoto S (2011) Development of a mobile grading machine for citrus fruit. Eng Agric Environ Food 4:7–11
80. Cubero S, Aleixos N, Albert A, Torregrosa A, Ortiz C, García-Navarrete O, Blasco J (2014) Optimised computer vision system for automatic pre-grading of citrus fruit in the field using a mobile platform. Precis Agric 15:80–94
81. Leemans V, Destain M-F (2004) A real-time grading method of apples based on features extracted from defects. J Food Eng 6:83–89
82. Bennedsen BS, Peterson DL, Tabb A (2005) Identifying defects in images of rotating apples. Comput Electron Agric 48:92–102
83. Xiao-bo Z, Jie-wen Z, Yanxiao L, Holmes M (2010) In-line detection of apple defects using three color cameras system. Comput Electron Agric 70:129–134
84. Reese D, Lefcourt AM, Kim MS, Lo YM (2010) Using parabolic mirrors for complete imaging of apple surfaces. Bioresour Technol 100:4499–4506
85. Blasco J, Aleixos N, Cubero S, Gómez-Sanchis J, Moltó E (2009) Automatic sorting of satsuma (*Citrus unshiu*) segments using computer vision and morphological features. Comput Electron Agric 66:1–8
86. Blasco J, Cubero S, Gómez-Sanchis J, Mira P, Moltó E (2009) Development of a machine for the automatic sorting of pomegranate (*Punica granatum*) arils based on computer vision. J Food Eng 90:27–34

Adv Biochem Eng Biotechnol (2017) 161: 93–120
DOI: 10.1007/10_2017_13

Published online: 27 April 2017

Case Studies in Modelling, Control in Food Processes

J. Glassey, A. Barone, G.A. Montague, and V. Sabou

Abstract This chapter discusses the importance of modelling and control in increasing food process efficiency and ensuring product quality. Various approaches to both modelling and control in food processing are set in the context of the specific challenges in this industrial sector and latest developments in each area are discussed. Three industrial case studies are used to demonstrate the benefits of advanced measurement, modelling and control in food processes. The first case study illustrates the use of knowledge elicitation from expert operators in the process for the manufacture of potato chips (French fries) and the consequent improvements in process control to increase the consistency of the resulting product. The second case study highlights the economic benefits of tighter control of an important process parameter, moisture content, in potato crisp (chips) manufacture. The final case study describes the use of NIR spectroscopy in ensuring effective mixing of dry multicomponent mixtures and pastes. Practical implementation tips and infrastructure requirements are also discussed.

Keywords Bread and confectionery powder mixing, Food process modelling and control, NIR spectroscopy, Potato crisp/chips quality control, Quality control

The online version of this chapter (doi:10.1007/10_2017_13) contains supplementary material, which is available to authorized users.

J. Glassey (✉) and A. Barone
School of Chemical Engineering and Advanced Materials, Newcastle University, Newcastle upon Tyne, UK
e-mail: jarka.glassey@ncl.ac.uk

G.A. Montague and V. Sabou
School of Science and Engineering, University of Teesside, Middlesbrough, UK

Contents

1 Introduction

Food production, quality and the security of supply chains remain critical societal challenges requiring more and more advanced scientific and engineering methods to address the arising issues. The benefits of modelling and control approaches in achieving a better process understanding, higher yields and more consistent product quality have been widely recognised in other industrial activities, such as chemical and biochemical processes [1, 2]. Similar benefits of modelling and control approaches have also been demonstrated in various sectors of the food industry [3–7].

The strict regulatory environment in which the food industry operates also necessitates effective use of modelling and control strategies to ensure food safety, authenticity and quality. For example, Humphrey [8] provides a comprehensive review of the current food safety and regulatory strategies, highlighting in particular the differences between the regulatory schemes in the USA and EU. Dora et al. [4], on the other hand, provide a review of a food quality management system concentrating specifically on the assessment strategies and a feasibility study for small and medium-sized European food enterprises.

Perhaps the most widely recognised and internationally accepted system of effective food safety management is the Hazard Analysis and Critical Control Points (HACCP) approach [9–11]. Glassey [12] discusses the implementation steps of HACCP as well as their interlinkage with the Process Analytical Technologies

(PAT) and the implications of this and other regulatory frameworks upon data management in the food industry.

The major emphasis of this chapter is on advanced modelling and control approaches currently being proposed for use in the food industry sector. Through case studies, the major challenges and approaches are described and the opportunities identified.

1.1 Modelling and Control Challenges in the Food Industry

The fundamental requirements of any control scheme include a reliable measurement of the relevant process variables and the ability to modify identified manipulated variables effectively to maintain the desired process state. These requirements pose specific challenges within the food processing sector, where the ability to obtain representative measurements throughout the processing chain from the raw material though intermediate stages to the final product are frequently affected by a range of external factors. As Hitzmann et al. [13] highlighted in their status report on PAT in the food industry, the properties of raw materials, the complex transformations during the processing chain [14] and the perishable nature of the products all contribute to the increased complexity of the challenge. Ropkins and Beck [15] and Hitzmann et al. [13] argue that traditional end-point food testing does not provide an effective assurance of food safety for a number of reasons. These include [8]:

- The challenge of obtaining a representative sample, requiring substantial sub-sampling of food for analysis
- A limited assurance of safety as only those hazards specifically tested for can be assured
- A range of difficulties associated with traditional testing procedures, such as time and resource demand, destructive nature and the difficulty of interpretation
- Reactive nature of control
- The most significant issue of product safety being assured only at the end-point rather than 'building it into the product through prevention'

1.1.1 Advanced Measurement

Although this chapter deals predominantly with the modelling and control application case studies, it is important to highlight the importance of a representative measurement of the process state as a critical requirement for effective control. A wide range of scientific publications deals with detailed descriptions of traditional and more advanced analytical techniques used to assess the quality and authenticity of raw materials, intermediates and final products in the food processing chain. These range from simple physico-chemical sensors, visual inspection and

image analysis of raw materials and food products (e.g. [16–18]) to more advanced, non-invasive fingerprinting techniques.

For example, Riedl et al. [19] and Nunes [20] review various applications of vibrational spectroscopy and chemometrics to assess authenticity, adulteration and intrinsic quality parameters of food and edible oils and fats, respectively. An extensive review of the benefits of various spectroscopic approaches in this area also provides useful reference material highlighting several modelling and data analysis methods used to interpret the resulting measurements. Similarly, Gutierrez-Capitan et al. [21] provide a review of the electronic tongue approach in monitoring the quality of wines. Electronic tongues (similarly to electronic noses) are devices containing an array of sensors, typically based on ion-selective field effect transistors, providing a 'fingerprint' trace of the analysed food sample (e.g. [18]).

Hitzmann et al. [13] argue the need for optical analytical methods, such as various spectroscopic approaches, for a variety of reasons. These include, for example, oxidative changes of raw materials during storage and processing, as well as the critical importance of the visual impression of the final product and the strict hygiene requirements throughout the production process and storage. In such circumstances, non-invasive sensor systems are particularly useful.

1.1.2 Data Analysis and Modelling Approaches

The increasing use of fingerprinting analytical techniques, such as the optical methods mentioned above, has led to increasing amounts and frequency of data collected during processing, as discussed in Glassey [12]. Multivariate data analysis methods capable of dealing with large, often highly correlated, data sets, reducing their dimensionality and enabling correlations to be built between the measured raw material characteristic, process data and the resulting product quality characteristics have shown their benefits in a number of industries (e.g. [2, 19]). Principal component analysis (PCA) and its variants have been used extensively to identify underlying features in multidimensional data (e.g. [22]). On the other hand, various regression methods, such as locally weighted regression, Partial Least Squares (PLS) and its variants and nonlinear methods including artificial neural networks were effectively used to develop models capable of quantitatively predicting the desired process outputs (e.g. [21, 23]). Whilst this chapter does not intend to provide details on these data analysis methods, they form an essential part of a successful control of any process where process output measurements cannot be directly obtained using analytical techniques. Readers are therefore referred to various sources describing the fundamentals of these methods (e.g. [24, 25]).

1.1.3 Process Control Approaches

The constantly increasing consumer expectations, market competition and strict regulatory environment necessitate the use of increasingly more advanced control approaches in the food industry. Such control approaches could not only contribute to increased product quality consistency and safety; they could also improve the manufacturing process efficiencies through reduced levels of finished product rejections and recalls. These can affect both the economics of the process and the impact upon the public trust and perception of manufacturers.

Several studies have shown the lack of competitiveness of European food industries as compared to North America and Australia [4] and the benefits of using advanced quality management systems and Statistical Process Control (SPC) approaches [26]. A comprehensive review of the use of SPC in the food industry is presented by Lim et al. [5]. They provide a detailed analysis of a number of food sector applications of SPC, with a very helpful time evolution indication for SPC implementation in the food industry, highlighting its increasing integration in the HACCP, ISO 9000:2000 and other quality management frameworks. The reviewed articles highlighted 'reduced process variation, improved food safety control, improved knowledge about the process variation and cost savings' as the most cited benefits [5]. The most cited challenges included 'resistance to change, lack of sufficient statistical knowledge and lack of management support' [5].

The case studies in this chapter indicate how benefits can be obtained even through more established control approaches which often represent less of a challenge in terms of resistance to change or the need for detailed statistical knowledge, yet still lead to tangible quality and cost benefits.

2 Case Study 1: Potato Chips (French Fries) Production

The first case study considers how an existing operating strategy can be ascertained and improvements in the control system derived and justified. The process considered is a French fry line to which lorries transport potatoes from various growers to the factory in loads of 20–30 tonnes. Each load is a single variety and from a single supplier. When they arrive at the factory they are subjected to a number of quality control tests and, if they pass these, they are unloaded into a storage bin. When required for production, the potatoes from the bin are fed via conveyor belt to the production line. First, the potatoes are peeled and then fed to a cutter to produce chips of the required size and characteristics. The size is varied in response to customer requirements. A sophisticated vision analysis system then removes from the line any of the cut potatoes that contain defects. Following this, the cut potatoes are partially cooked in a blancher and then pass into the dryer. The dryer acts to regulate moisture to give the final product its correct texture. Following the dryer, the chips are partially fried. The product is then frozen and packed ready for

distribution to the customer. Quality control tests are carried out on the final packed product to confirm that it meets customers' specifications. The paramount production objective is to manufacture French fries to quality criteria specified by the various customers. To do so requires frequent changes to the processing equipment to make product routinely whose quality falls within the target range.

2.1 Knowledge Elicitation

The first stage in the study involved determining what information existed on process variations and current plant control policy. At the outset it was clear that there was a considerable degree of manual intervention in plant operation. Whilst control loops regulated variables such as blancher, dryer and fryer temperatures, the set points of these controllers were specified by the plant supervisors based upon their process expertise. The first step was to check that these controllers were behaving acceptably. If local loops were not functioning correctly then controller set point specification would be pointless. Observations of loop behaviour confirmed that all local control loops were functioning correctly. Following this, it was necessary to get an appreciation of how and why the operators modified the controller set points to regulate product quality. This information gathering involved a series of knowledge elicitation sessions from the plant technical manager and shift supervisors.

The Knowledge Acquisition Technique (KAT) used was developed by CK Design and has proved to be an efficient knowledge elicitation tool and to result in a complete, correct and consistent knowledge base [27]. The knowledge elicitation proceeds through successive overturning of the states of belief of the expert about the core belief state. The line of questioning is carried out until the expert believes there is no further condition to overturn the belief under the preceding conditions. The knowledge base is structured in the form of exception graphs that capture the expert's decision process. Using the KAT method, working from the core belief that the product quality was under control, exceptions were sought and actions in the event of these exceptions occurring were obtained.

It is usually the case that no one person possesses all the knowledge pertaining to the problem domain. It is therefore necessary in the initial project stages to identify all those that may contribute to the knowledge base. A degree of overlap of knowledge between 'experts' is desirable as inconsistencies can be highlighted. In this project several process supervisors and quality control laboratory staff were interviewed, along with the past and present production manager. A set of several exception graphs from the various experts resulted. The next stage was to combine them into a single exception graph. This requires the project 'owner' to adjudicate if conflicts arise. If the degree of inconsistency between 'expert' views is significant, then little can be gained from the knowledge elicitation other than indicating that the whole process operational strategy requires reconsideration. This was not the

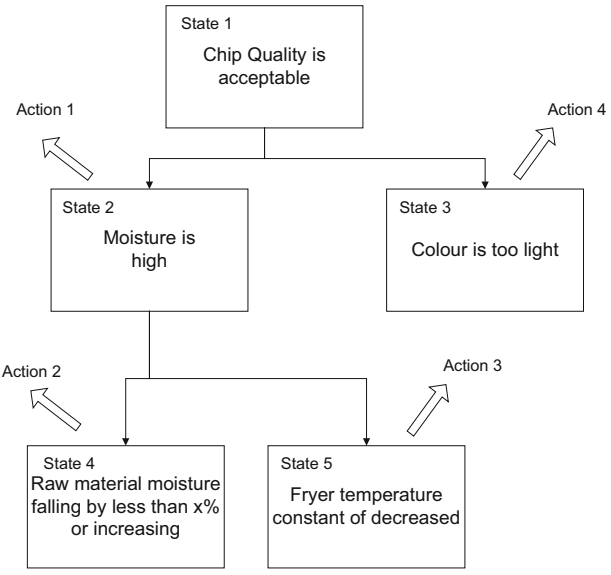

Example from States 1, 2 and 4

Rule 1
Quality is acceptable *unless* moisture is high
Take Action 1 to confirm State 2 is true
If Action 1 confirms this is the case then
If moisture in the raw material is falling by more than x%
take no action (moisture will soon fall)
else
take Action 1

Fig. 1 Example of control strategy information

case in this study, with only minor inconsistencies, primarily in the severity of response operators took in response to process problems. As a result, the current control strategy was determined in the form of an exception graph. The exact details of the current control strategy are confidential as are the precise details of the CK Design technique, but the information shown in Fig. 1 is typical of the rules obtained and level of detail produced.

Here it can be seen that State 1 indicates that the chip quality is acceptable unless State 2 or State 3 is true. To indicate the type of structure and rules that arise, consider the left hand side of the tree and the situation when a measurement is received to indicate that State 2 is true (i.e. the moisture is high). Action 1 associated with State 1 is taken. This confirms that State 1 is in fact true. As moisture is a measured value and subject to error from a variety of sources, this reconfirmation is necessary. If State 1 is still true after reconfirmation then State 4 is considered. If the raw material moisture reduces significantly then it soon results in product moisture reduction so no action is required. Otherwise Action 2 should be taken. In this scenario, Action 2 is likely to involve a reduction in product drying.

2.2 Control Strategy Development

Moisture was identified as particularly important as product is sold by weight and moisture targets set by customers are quite tight. At this stage the managing director of the company not unreasonably asked how much money would be saved by improving moisture control to ascertain whether it was a worthwhile undertaking. Answering such a question requires the use of cost benefit analysis techniques. The fundamental question to answer is how much is a control scheme going to save but this must be answered before it is implemented. To attempt to resolve this 'Catch 22' question, use was made of techniques proposed by Anderson [28] and verified in other industrial sectors (for example [29]). The underlying philosophy is that improved control translates to reduced product variance. By decreasing product quality variance it is still possible to stay within the range of acceptable product but with a mean value of operation which can be changed. In this case, this could lead to the mean value of product moisture increasing but still satisfying the customers' quality control demands. From this situation, a simple financial calculation can be undertaken to reveal what a move in product quality mean is worth. The current operational records provide the information to determine existing variance. The fundamental assumption proposed by Anderson [28] is that, by implementing sophisticated control procedures on a process plant, the variance of the product quality is at least halved. Indeed, in plants where significant manual intervention is currently the norm, this is quite pessimistic. The new product distribution can be estimated and the new mean operating point determined to ensure that quality control still remains within the target range. Clearly, the figures relating to the application are financially sensitive and are unable to be revealed. However, the procedure outlined above was followed and the potential savings indicated were significant and justified the continuation of the study.

Although product moisture is influenced by several operations on the line, the main influence and therefore the control variables are within the dryer. The operation of the dryer is not an insignificant task. Analysis of the existing control policy for moisture control revealed two important issues:

1. The severity of control changes to the same deviation varied from operator to operator
2. The operators acted to correct process deviations using a feedback strategy acting on information from the quality control laboratory

Whilst the first issue could easily be rectified, the second highlighted a fundamental control problem. Feedback control is not a particularly effective means of controlling the process. Delays in the overall loop of 35 min at best are significant. This would occur if a sample was taken from the line immediately a change reached the sampling point. In the worst case, because samples to measure product moisture are only taken every hour then the delay could amount to 95 min. When the line is producing many tonnes of product, this could amount to significant off-specification product. Of equal concern is that, with significant disturbances

coming from raw material variation, a change in product moisture takes at least 55 min to be observed. Corrective action could then be taken but by this time a new load of potatoes are being fed to the line because it takes around 60 min to process a load. Such corrective action would therefore be completely inappropriate. Thus it is clear that this scheme is fundamentally flawed.

In analysing the existing control scheme it is apparent that the problems are a result of process and measurement delays and the sampling rate of the quality variables. Even if the sampling rate could be increased significantly, which given human resource requirements would be difficult, the fundamental problem remains of process delay. Overcoming the problem of delay requires a predictive control philosophy. If the answers to two fundamental questions are obtained then control performance could be considerably improved upon. The two questions are:

1. If a change is made to the dryer, how does the product quality respond? If the product is off-target or a change to the operating target is required, information on how to change the dryer to get the product approximately within range can avoid major reliance on delayed feedback. Although predictive information is never perfect, the predictive action moves the product quality close to the desired value and feedback could provide fine modifications to the operation. This avoids typically well over an hours' worth of production potentially out of specification.
2. If the raw potato quality is known can its effect on product quality be predicted? If so, by how much and when should the dryer be changed to compensate for it? If it can be anticipated how a raw material change influences product quality, corrective action can be taken in a feedforward control sense to nullify any changes in raw material. It is realised that perfect process information is not available but even approximate process information can serve to provide effective feedforward control, with feedback control again providing fine modifications.

The modified control strategy is shown in Fig. 2.

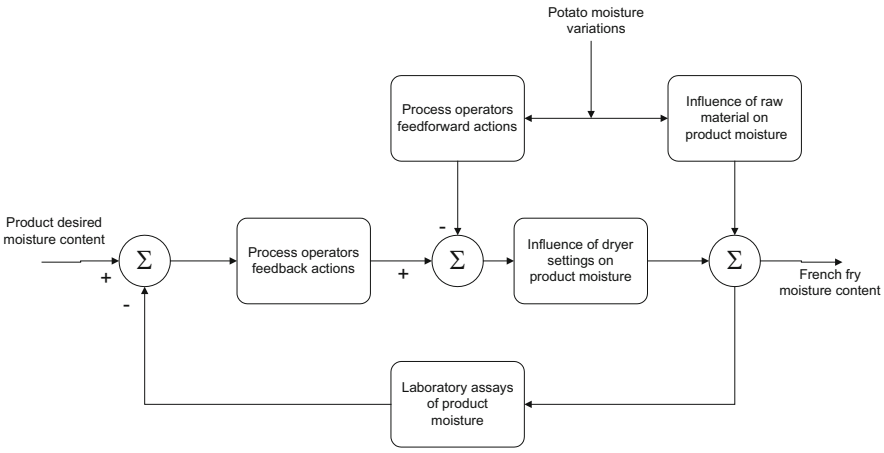

Fig. 2 Modified control strategy for product moisture

Two key control strategy parameters had to be specified for the scheme to function acceptably. First, the feedforward controller gain was determined from analysis of data produced from some simple plant tests. Observations of independent variations of dryer temperature and raw material moisture on product moisture provided the necessary information to determine the feedforward controller gain. Second, inversion of the information on dryer temperature/product moisture provided the predictive information to determine by how much to increase temperature to correct product moisture deviation.

2.3 Control Strategy Implementation

Trials of the new control scheme took place over a number of days of operation. From a practical perspective it is important to note that no new instrumentation was required and few, if any, extra laboratory analyses were undertaken. The essential aspect of the new control philosophy was to use the available information but to respond at appropriate times using knowledge of the likely outcomes of process changes. The initial results were obtained in a series of process tests undertaken by the development team in collaboration with the process operational staff. During such tests, closer attention than normal is obviously paid to the process plant operation. The worry is therefore that, although plant improvements are indicated, in the longer term, when normal day-to-day operation resumes, without a specific focus on the new policy little additional benefit is found. Long-term performance compared with process behaviour prior to the introduction of the scheme is the best way to judge whether this is indeed the case. This information is shown in Fig. 3a. Figure 3a shows the performance of the production line prior to the implementation of the control scheme. Laboratory samples measuring moisture content are shown along with the tight bounds within which it is desirable to operate. It can be seen that deviations outside of the bounds were frequent (56% of the samples fall outside of the bounds). Figure 3b shows the behaviour of the process following the introduction of the control scheme. Much tighter regulation of the moisture content is apparent (10% of the samples fall outside of the bounds). Slight oscillatory behaviour is observed within the bounds of operation. One of the reasons for this is that potato loads are not selected at random to go through the production line. The operators make an effort to put a load of similar moisture content to the previous load through the line, hence introducing the observed perturbations.

In interpreting these figures it must be remembered that the operational bounds are tighter than the customers' requirements but nevertheless, for the reasons discussed previously, it is important to reduce variation as much as possible. Returning to the cost/benefit analysis carried out prior to the implementation, it is interesting to observe that the process variation has been almost exactly halved, which is in line with the prevailing wisdom on improved control benefits.

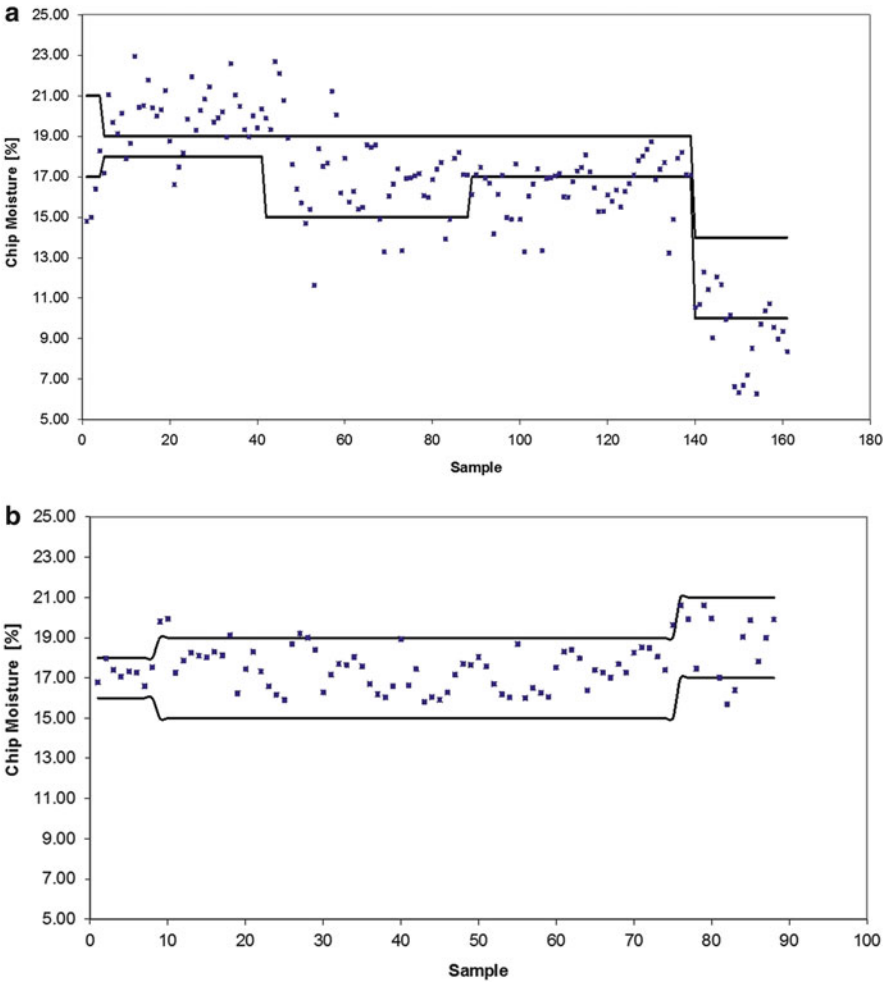

Fig. 3 (**a**) Performance prior to control scheme implementation. (**b**) Performance subsequent to control scheme implementation

In summary, the case study set out to demonstrate that variations in product quality in a food processing line could be reduced by the application of advanced control methods. The KAT knowledge elicitation proved effective at obtaining an initial idea of the control strategy. It highlighted where problems existed but it did not provide a total solution. Once the failings of the current control scheme were identified, cost benefit analysis revealed very clearly that improvements were possible and the likely savings would more than justify the investment. The control strategy itself was fairly straightforward to devise from a theoretical viewpoint, with simple process trials revealing approximate process gains which were sufficient for control design purposes. Implementation on the production line to prove that the methods worked was remarkably trouble free. In the longer term, whilst the

new control strategy is simple to implement, it does rely upon manual changes to be made at roughly the correct time. This is a fundamental problem, as staff in a small company tend to have many calls upon their time and this is seen as one more. However, failing to respond to raw material changes has serious financial consequences on the production line. A general awareness of the scale of the potential loss may be encouragement to adopt the new strategy.

3 Case Study 2: Potato Crisps (Chips) Production

The amount of waste generated by food manufacturing processes presents a high financial cost, making cost reduction one of the priorities for a process analyst. The initial assessment of the process used for this case study indicated that a significant amount of waste was generated by unacceptable levels of moisture in the end product. In terms of moisture levels, the parameters within which the factory operates for 'Product A' are divided into three zones: the Green zone – 1.4–1.8 (product has an optimal moisture level), Amber zone – 1.1–1.3 (the product meets the process parameters but it can be further improved) and Red zone – below 1.1 and above 2.1 (see Fig. 4). When the moisture levels in the end product are situated within the Red zone, the product is rejected from the line and it has to be dealt with as waste. The moisture levels in the end product are measured online by utilising an NDC online NIR gauge that also measures the amount of fat in the end product. On a regular basis, the NDC gauge is giving a moisture reading every 30 s, but for the purposes of this project the NDC gauge was set to give moistures values every 10 s for more data to be captured so as to understand the process dynamics better. After analysing the data generated over a 3-week period, it was estimated that, on

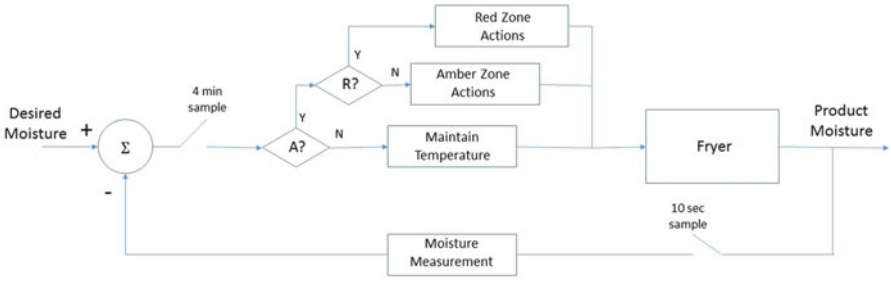

Amber zone	Action
Moisture<1.3	Decrease fryer temperature by 1°C
Moisture>1.9	Increase fryer temperature by 1°C

Red zone	Action
Moisture<1.1	Decrease fryer temperature by 1°C over Amber action
Moisture>2.1	Increase fryer temperature by 1°C over Amber action

Fig. 4 Mechanism of the negative closed loop system utilising the moisture levels in the end product to modify the fryer oil set point temperature to reduce the amount of waste generated by unacceptable levels of moisture in the end product

average, the amount of waste generated on one line by unacceptable levels of moisture in the end product amounts to a weekly cost of approximately €1,250. When the fact there are multiple lines within the factory is considered, this presents a significant opportunity for improvement.

3.1 Developing a Solution

Once the current opportunity was assessed, the next step was to identify possible solutions for reducing the waste and to achieve better process control in terms of moisture levels in the end product. The main mechanism for control of moisture levels in the factory is through the fryer oil temperature. Thus better control over how the fryer was operated was chosen as the main solution for this challenge. A closed loop negative feedback control system that utilises the moisture levels in the end product to modify the set point temperature of the fryer oil to adapt it for the subsequent product stream was developed. The mechanism through which this negative feedback system operates is presented in Fig. 4.

Figure 4 illustrates the modifications to be made to the fryer temperature set point in concordance with the three zones for moisture levels: Green zone, Amber zone and Red zone. The system also requires that, after a change was made on the fryer temperature, 4 min must pass before another change is made. The reason behind this is partly that the time delay of the fryer temperature in this case is around 4 min and also the desire to improve the robustness of the control system in the event of spurious measurements.

The system presented above was designed so that it can be developed as an automatic software solution and installed on the SCADA gauge utilised for controlling the fryers in the factory. Having this negative feedback closed loop system operating in an automated fashion offers many advantages, being more effective and more cost efficient in the long term. Nevertheless, before the software was developed, a series of trials was conducted to identify the efficiency of the system.

3.2 Trials Mimicking the Negative Closed Loop System

Two trials which lasted 12 h each were carried out to assess the efficiency of the negative feedback closed loop system. For the purposes of these two trials, one process operator was assigned to monitor closely the fryer at the control panel on the SCADA gauge and to follow the instructions presented in Fig. 4. By following exactly the system presented in Fig. 4, without being influenced by the effect of the changes on the process, the efficiency of the automatic software was tested. Moisture levels in the end product were measured as usual utilising the online NDC gauge and data was captured and exported every 10 s so that data could be further analysed and compared with previous data.

The results obtained through these two trials were positive, showing lower rejection rates of product based on unacceptable levels of moisture and also less time spent in the Amber zone of moisture content. During the first trial there was no rejected product for poor levels of moisture, although during the second trial 1 min of rejected product was recorded, amounting to around €30. Although only two trials have been carried out to date, the results were positive, giving more confidence for developing and utilising the closed loop system. Currently an automatic software system is being developed and implemented.

4 Case Study 3: Food Mixing Consistency

Consistency of mixing of various dry food mixtures and pastes remains a significant challenge in food processing, despite years of development in this area. To date, the mixing operations are predominantly operated using standard operating procedures with times of mixing specified on the basis of empirically established values to ensure product homogeneity. This may lead to excessive mixing and thus equipment underutilisation or insufficient mixing and product rejection, neither of which are desirable in food manufacturing.

This case study demonstrates how NIR may be used to improve the consistency of mixing processes in food industries. Bread and confectionery powder mixtures aimed at the bakery market were analysed in this study. The main components of these mixtures were flour, sugar, gluten and salt. Four different products were taken into consideration:

1. *Product A*: blend with small particle size distribution and more than one main component
2. *Product B*: blend with small particle size distribution and one main component that accounts for more than 50%
3. *Product C*: blend with small particle size distribution and one main component that counts for more than 90%
4. *Product D*: blend with large particle size distribution and more than one main component

The experiments were performed using two conical screw mixers of nominal capacity of 4,000 L, each equipped with a diffuse reflectance fibre-optic probe connected to a Bruker Matrix-F FT-NIR spectrometer. Figure 5 shows the configuration of the conical screw mixer (Fig. 5a) and how the NIR probe is connected to the blender (Fig. 5b). Spectral data were collected using OPUS software version 7.0 provided by Bruker. Homogeneity studies were performed by analysing spectral data with Matlab version R2014a, and calibration models were built using OPUS software.

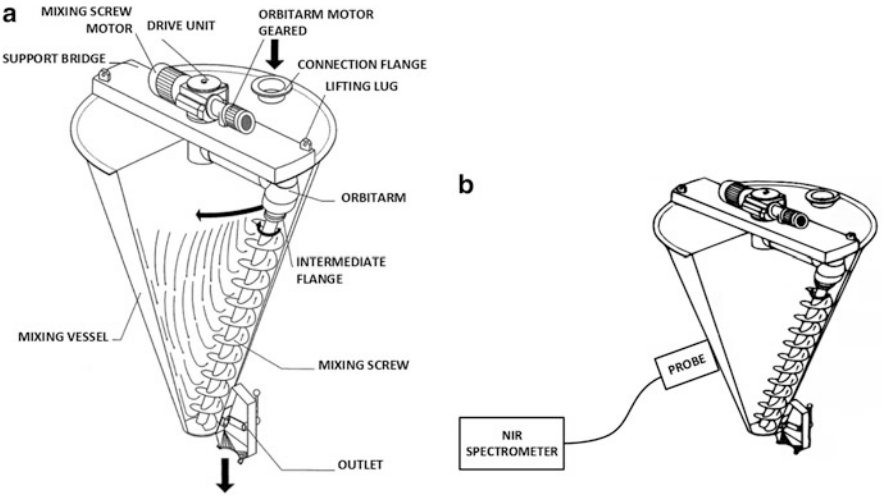

Fig. 5 Conical screw mixer configuration. (**a**) Configuration of the conical screw mixer. (**b**) Connection of the probe to the blender

4.1 Homogeneity Measurement

Spectra were collected continuously during the whole production time from the point of loading the first ingredient until the process was stopped. Dealing with solid samples, data collected were largely influenced by light scattering, and therefore different pretreatments algorithms were used to clean data from scattering. Four types of pretreatment were considered as detailed below.

4.2 Derivatives

Derivatives of spectra are calculated using the Savitzky–Golay algorithm. First and second order derivatives are most common: first order derivatives remove baseline from spectra and second order also eliminate linear trends [30]. Derivatives are very good at enhancing differences between spectra and differentiate the overlapping signature, but they also increase noise.

4.3 Detrending

Detrending subtracts a polynomial fit from the original spectra to correct the baseline [31]. The resulting spectrum is given by

$$X_{Dt} = X - (a_0 + a_1\lambda) \tag{1}$$

4.4 Normalisation

The same weight is given to all the absorbances: each spectrum is in fact normalised to a length of 1 by dividing it by the Euclidian norm [30]:

$$X_{\text{norm}} = \frac{X_{\text{orig}}}{\sqrt{\sum \left(X_{\text{orig}}^2\right)}} \tag{2}$$

4.5 Standard Normal Variate (SNV)

SNV normalises each spectrum to zero mean and unit variance by subtracting the mean of each spectrum and dividing by its standard deviation [30]:

$$X_{\text{SNV}} = \frac{X_{\text{orig}} - X_{\text{mean}}}{\sigma} \tag{3}$$

Deviation from the target spectrum was investigated to establish the mixing time; it was calculated as the Euclidean distance between all the spectra collected and the ideal spectrum referred to the homogeneous blend:

$$d = \sqrt{\sum \left(\text{spectra matrix}_{i,j} - \text{ideal spectrum}\right)^2} \tag{4}$$

In all the experiments the change of spectra over time was observed, eventually converging to the same steady-state spectrum (see example in Fig. 6). Green spectra represent the beginning of the production, when the blend is still under the level of the probe. The characteristic flat shape is because only the air present in the mixer is scanned at this phase. As soon as the probe starts getting covered by the powder mixture, spectra begin to show some peaks. This is represented by the blue spectra. These spectra are shown to change over time, indicating the composition is changing. In fact, during the process, different ingredients are added and blends are continuously mixed, leading to different powders being scanned by the NIR probe. Spectra are seen to start overlapping after a certain time, as illustrated by the red spectra. Because each sample of a given composition and concentration is uniquely identified by a spectrum, the overlap demonstrates that the powder inside the mixer has the same concentration, thus indicating that the blend is homogeneous.

Mixing time is therefore determined by the time it takes for the spectra to start overlapping with each other and a steady-state fully mixed spectrum is reached.

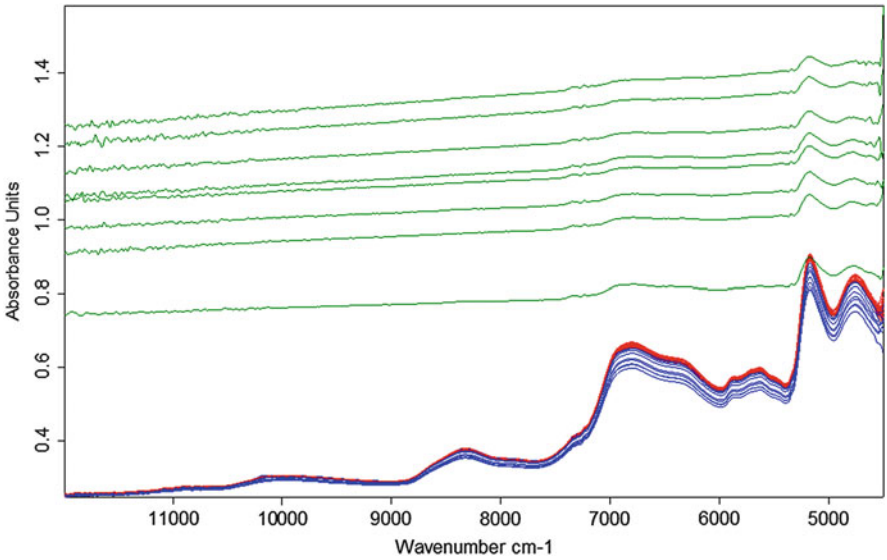

Fig. 6 Example of spectra collected during the production phase. *Green spectra* are recorded when the powder is still under the level of the probe. *Blue spectra* show powder reaching the level of the probe. *Red spectra* represent the homogeneous mixture

The effect of component distribution was evaluated by comparing results obtained for Products A, B and C, and particle size distribution was studied by investigating the different effects on Products A and D. The entire blend run was analysed, employing different combinations of pre-processing techniques. In Fig. 7 the blending profiles of deviation from the target spectrum for all the products are shown using Normalization+SNV+Detrending and Normalization+second derivative. Variations in profiles were observed when using different pretreatments; however, for all the experiments an overall behaviour was observed and plots were generally divided into four parts:

1. *First stationary phase*: the deviation is stable over time and its highest value is recorded. Powder is still under the level of the probe and NIR is scanning only air. Green spectra shown in Fig. 6 represent this phase
2. *Decreasing phase*: deviation suddenly decreases because of the powder approaching the probe level. Referring to Fig. 6, this phase illustrates the passage from green to blue spectra
3. *Oscillations*: deviation changes over time as a consequence of the variation in composition during the production process. Blue spectra shifting over time in Fig. 6 describe the same phenomenon of oscillations
4. *Second stationary phase*: deviation finally approaches zero value and remains stable over time. Red spectra overlapping each other represent the second stationary phase

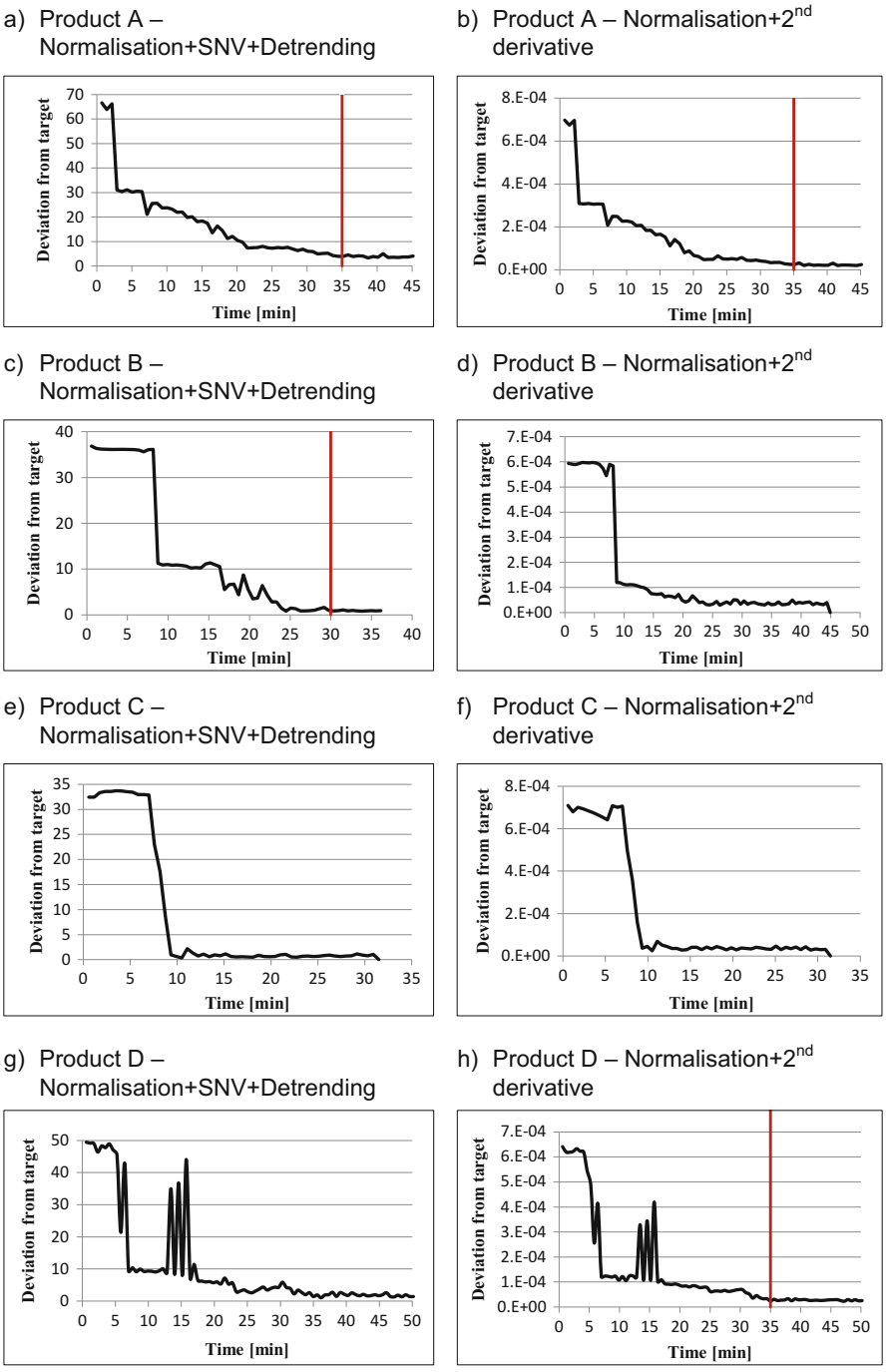

Fig. 7 Comparison of pretreatment combinations for Products A, B, C and D. Data were first pretreated using Normalisation+SNV+Detrending and Normalisation+second derivative. Subsequently, deviation from the target spectrum was calculated. The *red vertical line* represents the

Mixing time is thus identified by the starting point of the second stationary phase, which may change depending on the pretreatment chosen. The value of *d* (deviation from target) which determines the homogeneity starting point is set depending on the product analysed. There is not a general recommended value, but *d* is rather based on experience by analysing previous batches of the same product and establishing the average minimum value when the profile becomes stationary.

Product A mixing time to reach homogeneity was identified with both combinations as shown by the stationary phase achieved at minute 35 in both cases (Fig. 7a, b). The homogeneity of Product B instead could only be identified using Normalisation+SNV+Detrending (Fig. 7c, d) because of the reduced variability of the system. This blend has one main component which counts for more than 50%, whereas Product A has more than one main component. The smaller variation in the component distribution of Product B causes, in turn, a smaller variation in the spectra, which makes it more difficult to detect the changes during production and therefore to understand at which point homogeneity begins. SNV and Detrending, compared to derivatives, accentuate more the spectral differences, so making more evident the homogeneity starting point. Product C homogeneity point could not be identified properly by any of the combinations employed (Fig. 7e, f): the blend in fact appears homogeneous as soon as the powder reached the probe (minute 12), and no variations are shown when different ingredients are added. The main component of Product C is present for more than 90%, so making the quantities of the remaining ingredients very small. Changes in composition are minimised and NIR is unable to detect such small variations. Product D homogeneity could be estimated accurately using Normalisation+derivative, but not by Normalisation +SNV +Detrending (Fig. 7g, h). The large variation in the particle size distribution of Product D is in fact responsible for the increase in variability, and SNV and Detrending accentuate these differences too much, causing oscillations in the second stationary phase too. Derivatives, on the other hand, do not present the issue as they enhance these variations less and are able to show more clearly the homogeneity starting point.

Normalisation+SNV+Detrending gives all the benefits provided by these three techniques: initial scattering is removed, oscillation phase is emphasised and the homogeneity starting point is clearly detectable. This combination can be generally used for products with average or small component distribution, but not for products with a single component concentration higher than 90%. For this kind of material, represented here by Product C, deviation from the target spectrum cannot identify the mixing time required to achieve homogeneity. With regard to the

Fig. 7 (continued) homogeneity starting point. Where the *red line* is missing it was not possible to determine the mixing time. (**a**) Product A – Normalisation+SNV+Detrending; (**b**) Product A – Normalisation+second derivative; (**c**) Product B – Normalisation+SNV+Detrending; (**d**) Product B – Normalisation+second derivative; (**e**) Product C – Normalisation+SNV+Detrending; (**f**) Product C – Normalisation+second derivative; (**g**) Product D – Normalisation+SNV +Detrending; (**h**) Product D – Normalisation+second derivative

particle size distribution, it is preferred to employ Normalisation+derivative as differences would be accentuated too much by SNV-Detrending because of the high variability involved in these products.

4.6 Calibration

Following the homogeneity analyses described in Sect. 4.1, the process was stopped when the mixture was believed to be homogeneous and spectra collected inline were analysed to measure the composition of the blend inside the vessel. To evaluate the concentration of the blend components and to check whether they are within the specifications, calibration models for Near-Infrared probe installed inline were required.

An additional probe of Bruker Matrix-F, the same as installed inline into the two conical screw vessels, was used and it was connected to the spectrometer with fibre optic cable. The probe was placed under a bench in the laboratory in an upside down position so that the sample could be placed on top of the probe and scanned (see Fig. 8). This allowed the making of samples of known composition with a wider range of concentrations, and reducing the time to build a calibration model. Fifty samples of Product D were prepared with varying concentrations of each component and scanned with the spare probe; calibration models were built using a PLS algorithm and data were first pretreated and screened with PCA to eliminate eventual outliers.

Results of cross-validation showed a very good correlation for most of the organic components in the mixture, and gluten is illustrated here as an example. Two factors were checked to measure the quality of predictive capability of the calibration model: Root Mean Square Error of Cross-Validation (RMSECV) and coefficient of determination (R^2). The model for gluten prediction achieved 0.476 for RMSECV and 94.74% for R^2, indicating a very low prediction error and a high correlation. The plot of predicted vs actual values displayed in Fig. 9 shows the

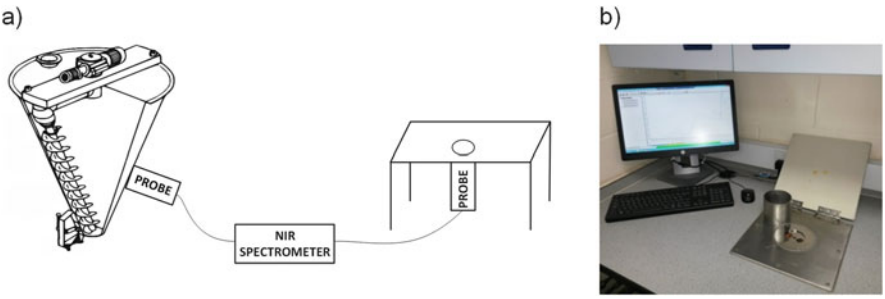

Fig. 8 Additional probe of Bruker Matrix-F installed offline for sample calibration. (**a**) Scheme showing the same NIR spectrometer connected to two Bruker probes, one installed in the conical screw mixer and one installed offline under the bench. (**b**) Top view of the offline probe

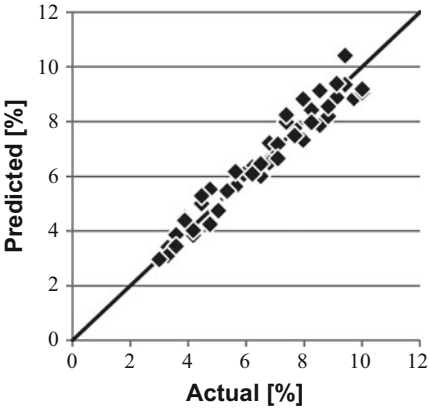

Fig. 9 Cross-validation results obtained for calibration model of gluten using the Matrix-F NIR spectrometer

values lying on the parity line, which indicates that the predictions are very close to the actual values for the whole studied range.

4.7 Tumble Mixer

To evaluate the effectiveness of this methodology independent of the unit operation used, Product E, a bread roll powder mixture mainly composed of flour, salt and sugar, was considered. The blending process of a Matcon tumble blender (see Fig. 10a) of a nominal capacity of 2,000 L was monitored in this experiment. Because in this case the blender itself is always in motion, it would not be possible to apply a traditional NIR probe as seen in Sect. 4.1. The fibre and power cables would rotate together with the mixer, so eventually snapping. Moreover, the considerable size of the probe would not allow it to be applied to the tumble blender, as it would certainly crash against either the floor or the ceiling of the mixer. A MicroNIR PAT (shown in Fig. 10b) was considered for this purpose because of its reduced dimensions and its cable free nature, being Wi-Fi and battery powered.

MicroNIR PAT was applied to the lid of the tumble blender and spectra were collected every time the lid was in the bottom position. Spectral data were collected using the MicroNIR PAT software and then analysed with Matlab version R2014a.

Deviation from the target spectrum, as described in Sect. 4.1, was monitored to establish the starting point at which the spectra overlap.

As with the convective mixer, the change of spectra over time was observed, eventually converging to the same steady-state spectrum. However, in this case the only spectra that can be seen are those varying over time, representing the change of composition (Fig. 11, coloured in blue), and those overlapping each other that exemplify the homogeneity phase (red).

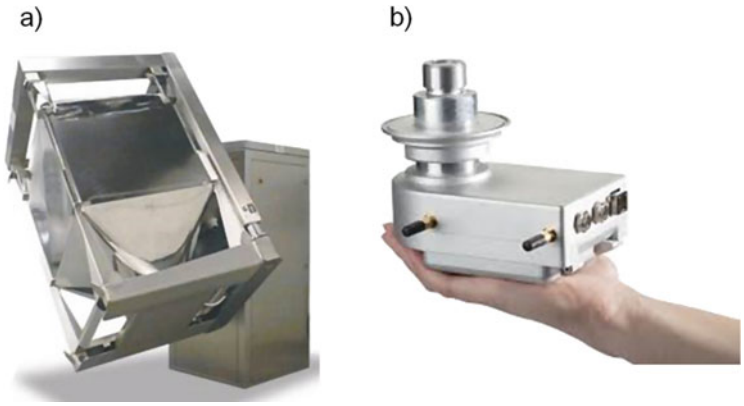

Fig. 10 Matcon tumble blender (**a**) and MicroNIR PAT (**b**)

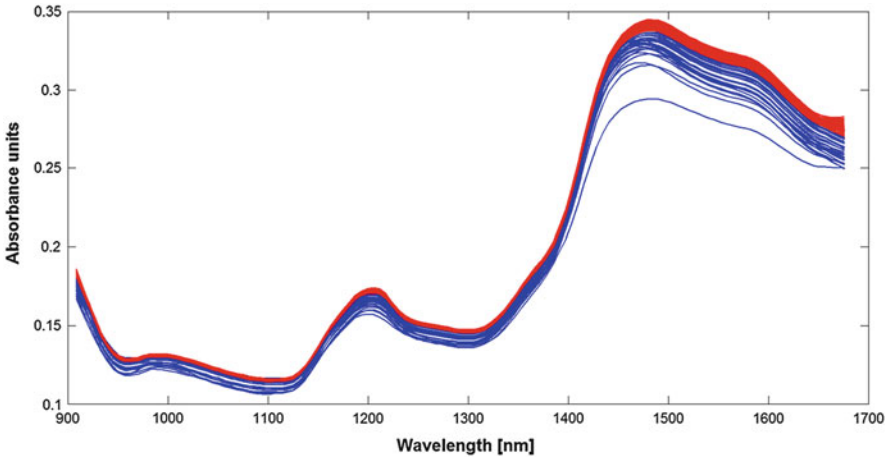

Fig. 11 Spectra collected during production in a tumble mixer. Initial flat spectra are not present as probe was always covered by powder. *Blue* spectra indicate composition changes over time and *red* spectra overlapping each other refer to the homogeneity phase

Blending profile pretreating data with Normalisation+second derivative is shown in Fig. 12. In contrast to the convective mixer, given the initial flat spectra absence, the *first stationary phase* is not observed here. The other phases are evident: the profile starts with the *decreasing phase*, then continues with the *oscillation phase* and ends with the *second stationary phase*.

The homogeneity starting point can be clearly identified using "Deviation from target" and is indicated by a red line in Fig. 12.

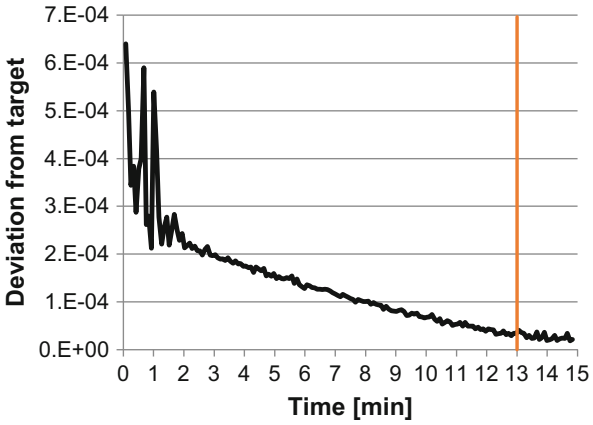

Fig. 12 Blending profiles analysed with "Deviation from target"

4.8 Mixing and Cooking Vessel: Mixing of Pastes

For this part of the case study, paste products, in particular caramel and custard, were analysed. They consist of high density and high viscosity products, produced through high temperature processes. The main ingredients in both products are water and sugar.

NIR spectroscopy was applied to a Giusti mixing and cooking vessel (see Fig. 13), which has a nominal capacity of 2,000 L and is surrounded by a jacket used for cooling and heating. Temperatures vary during the process, from room temperature to a maximum of 120°C.

The spectrometer employed in this case (as in Sect. 4.3) was the MicroNIR PAT. Because of the high temperatures involved in the process, and given the instrument operative temperature range is only 0–40°C, an extended probe was applied to MicroNIR PAT so that the product was not in direct contact with the spectrometer. MicroNIR PAT was applied to the recirculation pipe and not to the vessel itself, because the presence of the jacket surrounding the Giusti mixer does not allow welding the flange. Working with high density and high viscosity materials, it is very likely they stick to the probe surface. To avoid this problem, the spectrometer was placed in the pipe, just above the recirculation pump, so there was enough pressure to remove the product layer and NIR was able to scan the product flowing into the pipe.

The production of caramel was monitored by taking samples every 15 min during the process and analysing them offline to measure different physical properties: colour (light +), refractive index, water activity and moisture. Meanwhile, spectra were collected inline and retrieved at the end of the production process. Four batches were monitored: data from the first three batches were used to build the model and data from the remaining batch were used to test the model and predict the properties. The model was built based on the full spectrum, pretreating data with

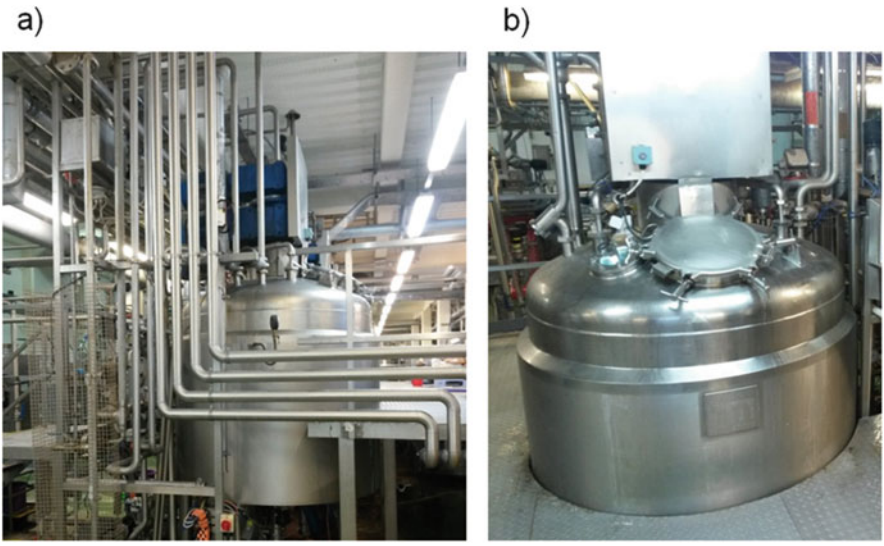

Fig. 13 Giusti mixing and cooking vessel. (**a**) View from the *bottom* of the entire vessel. (**b**) View from the *top* showing the opening where raw materials are added

SNV+first derivative, screening with PCA to check for potential outliers and finally regressing using the PLS algorithm.

The results of the calibration model for caramel for the four physical properties considered – colour, refractive index, moisture and water activity – are shown in Fig. 14.

Figure 14a shows the predicted vs actual values of the model for colour prediction where a high correlation is evident, as values lay along the parity line. This is also supported by the high value of R^2 equal to 82.29% and the low value of RMSE equal to 1.72. Figure 14b shows the results of the calibration model of refractive index for caramel. A very low correlation is evident, with an R^2 equal to 50.79%. Values in the lower calibration range (around 28–29) are actually well-distributed along the parity line, but for higher values of refractive index, points are lying on a horizontal line, which indicates a lack of correlation. RMSE in this case was equal to 1.50. Results of the calibration model of moisture for caramel are reported in Fig. 14c, where the predicted values are very close to the actual values. R^2 was quite high (95.92%) and RMSE was low (0.77), indicating a very high correlation for moisture. Finally, results of water activity are shown in Fig. 14d. A high correlation of predicted vs actual values can be observed, which is confirmed by the value of R^2 equal to 74.37% and of RMSE equal to 0.03.

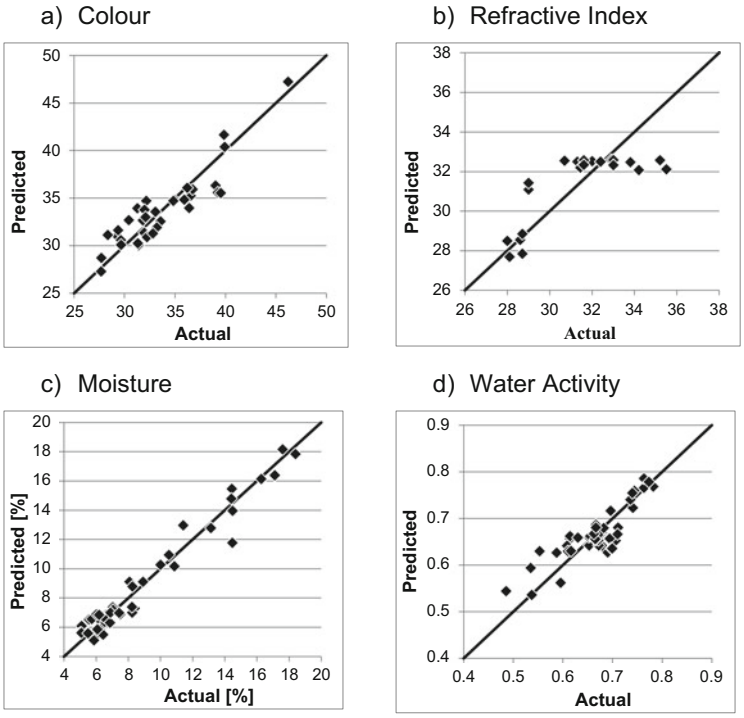

Fig. 14 Inline calibration model results for caramel for different properties: colour (**a**), refractive index (**b**), moisture (**c**), and water activity (**d**)

The models built so far were subsequently tested to assess their potential in predicting physical properties of inline products. Data from the fourth batch were analysed using the models previously built and predicted vs actual values were plotted for the different properties as shown in Fig. 15.

Most of the values of colour are overpredicted (Fig. 15a) whereas refractive index is underestimated (Fig. 15b). Values of moisture (Fig. 15c) and water activity (Fig. 15d) are closer to the parity line, but few outliers are present. Despite the calibration models showing high correlation, the predictions for an unseen batch are not very accurate. However it should be noted that only three batches were used in this study to build the model, so it is not surprising that the model is not sufficiently robust. More data need to be included and more batches have to be monitored to improve the calibration.

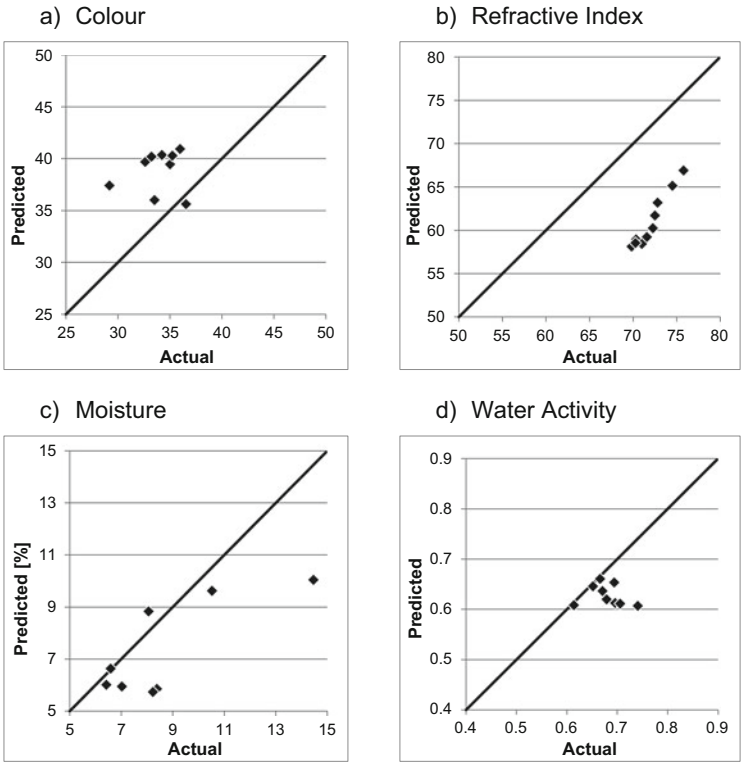

Fig. 15 Validation of the inline calibration models for caramel for colour (**a**), refractive index (**b**), moisture (**c**), and water activity (**d**). Data from the fourth batch were analysed and predicted using the models previously built

5 Conclusions

This chapter discussed the drivers and some methods of food process modelling and control. A range of case studies was used to demonstrate the benefits and the challenges associated with the implementation of established control approaches as well as more advanced monitoring methodologies. Clearly significant benefits can be gained either by reducing waste generation or by increasing product consistency/reducing unit operation time requirements, although care needs to be taken when analysing multivariate spectral data and using this to predict product characteristics.

References

1. Lee JH, Lee JM (2014) Progress and challenges in control of chemical processes. Annu Rev Chem Biomol Eng 5:383–404
2. Tomba E, Facco P, Bezzo F, Barolo M (2013) Latent variable modeling to assist the implementation of quality-by-design paradigms in pharmaceutical development and manufacturing: a review. Int J Pharm 457(1):283–297
3. Al-Mahasneh M, Aljarrah M, Rababah T, Alu'datt M (2016) Application of hybrid neural fuzzy system (ANFIS) in food processing and technology. Food Eng Rev 8(3):351–366
4. Dora M, Kumar M, Van Goubergen D, Molnar A, Gellynck X (2013) Food quality management system: reviewing assessment strategies and a feasibility study for European food small and medium-sized enterprises. Food Control 31(2):607–616
5. Lim SAH, Antony J, Albliwi S (2014) Statistical process control (SPC) in the food industry – a systematic review and future research agenda. Trends Food Sci Technol 37(2):137–151
6. Lim SAH, Antony J, Garze-Reyes JA, Arshed N (2015) Towards a conceptual roadmap for statistical process control implementation in the food industry. Trends Food Sci Tech 44(1): 117–129
7. Montague GA, Glassey J, Willis MJ (2003) French fry quality improvement using advanced control techniques. J Food Eng 57(4):357–365
8. Humphrey J (2012) Food safety, private standards schemes and trade: the implications of the FDA food safety modernization act, IDS working papers No 403, Vol 2012. Available on http://onlinelibrary.wiley.com/doi/10.1111/j.2040-0209.2012.00403.x/pdf. Accessed July 2016
9. CAC (Codex Alimentarius Commision) (2003) General principles on food hygiene, CAC/RCP 1-1969, Revision 4. Available on http://www.fao.org/fao-who-codexalimentarius/standards/list-of-standards/en/. Accessed July 2016
10. CAC (Codex Alimentarius Commision) (2013) Guildelines for the validation of food safety control measures, CAC/GL 69-2008. Available on http://www.fao.org/fao-who-codexalimentarius/standards/list-of-standards/en/. Accessed July 2016
11. Sampersa I, Toyofuku H, Luning PA (2012) Semi-quantitative study to evaluate the performance of a HACCP-based food safety management system in Japanese milk processing plants. Food Control 23(1):227–233
12. Glassey J (2014) Data management systems. In: O'Donnell CP, Cullen PJ, Fagan C (eds) Process analytical technology for the food industry. Springer, New York, pp. 61–71
13. Hitzmann B, Hauselmann R, Niemoeller A, Sangi D, Traenkle J, Glassey J (2015) Process analytical technologies in food industry – challenges and benefits. Biotechnol J 10(8): 1095–1100
14. Ling B, Tang L, Kong F, Mitcham EJ, Wang S (2015) Kinetics of food quality changes suring thermal processing: a review. Food Bioprocess Technol 8(2):343–358
15. Ropkins K, Beck AJ (2000) Evaluation of worldwide approaches to the use of HACCP to control food safety. Trends Food Sci Technol 11:10–21
16. Cubero S, Lee WS, Aleixos N, Albert F, Blasco J (2016) Automated systems based on machine vision for inspecting citrus fruits from the field to postharvest—a review. Bioprocess Technol 9:1623–1639
17. Jekle M, Becker T (2013) Wheat dough microstructure: the relation between visual structure and mechanical behavior. Crit Rev Food Sci Nutr 55(3):369–382
18. Kiani S, Minaei S, Ghasemi-Varnamkhasti M (2016) Fusion of artificial senses as a robust approach to food quality assessment. J Food Eng 171:230–239
19. Riedl J, Esslinger S, Fauhl-Hassek C (2015) Review of validation and reporting of non-targeted fingerprinting approaches for food authentication. Anal Chim Acta 885:17–32
20. Nunes CA (2014) Vibrational spectroscopy and chemometrics to assess authenticity, adulteration and intrinsic quality parameters of edible oils and fats. Food Res Int 60:255–261

21. Gutierrez-Capitan M, Capdevila F, Vila-Planas J, Domingo C, Buettgenbach S, Llobera A, Puig-Pujol A, Jimenez-Jorquera C (2014) Hybrid electronic tongues applied to the quality control of wines. J Sens. Article No: 598317
22. Maldo Paula A, Conti-Silva AC (2014) Texture profile and correlation between sensory and instrumental analyses on extruded snacks. J Food Eng 121:9–14
23. Nache M, Scheier R, Schmidt H, Hitzmann B (2015) Non-invasive lactate- and pH-monitoring in porcine meat using Raman spectroscopy and chemometrics. Chemom Intell Lab Syst 142:197–205
24. Glassey J (2013) Multivariate data analysis for advancing the interpretation of bioprocess measurement and monitoring data. Adv Biochem Eng Biotechnol 132:167–191
25. Wold S, Sjöström M, Eriksson L (2001) PLS-regression: a basic tool of chemometrics. Chemom Intell Lab Syst 58(2):109–130
26. Grigg NP, Walls L (2007) Developing statistical thinking for performance improvement in food industry. Int J Qual Reliab Manage 24:347–369
27. Duke P (1992) KAT: A knowledge acquisition techniques, methodology manual. CK Design Handbook
28. Anderson JS (1996) Control for profit. Trans Inst Meas Control 18(1):3
29. Lant P, Steffens M (1998) Benchmarking for process control: "should I invest in improved process control?". Water Sci Technol 37:49–54
30. Rinnan A, van den Berg F, Engelsen SB (2009) Review of the most common pre-processing techniques for near-infrared spectra. TrAC Trends Anal Chem 28(10):1201–1222
31. Golic M, Walsh KB (2006) Robustness of calibration models based on near infrared spectroscopy for the in-line grading of stonefruit for total soluble solids content. Anal Chim Acta 555(2):286–291

Adv Biochem Eng Biotechnol (2017) 161: 121–152
DOI: 10.1007/10_2017_11

Published online: 20 April 2017

Fluorescence Spectroscopy for the Monitoring of Food Processes

Muhammad Haseeb Ahmad, Amna Sahar, and Bernd Hitzmann

Abstract Different analytical techniques have been used to examine the complexity of food samples. Among them, fluorescence spectroscopy cannot be ignored in developing rapid and non-invasive analytical methodologies. It is one of the most sensitive spectroscopic approaches employed in identification, classification, authentication, quantification, and optimization of different parameters during food handling, processing, and storage and uses different chemometric tools. Chemometrics helps to retrieve useful information from spectral data utilized in the characterization of food samples. This contribution discusses in detail the potential of fluorescence spectroscopy of different foods, such as dairy, meat, fish, eggs, edible oil, cereals, fruit, vegetables, etc., for qualitative and quantitative analysis with different chemometric approaches.

Keywords Chemometrics, Fluorescence spectroscopy, Food analysis, Food applications

M.H. Ahmad
National Institute of Food Science and Technology, Faculty of Food, Nutrition and Home Sciences, University of Agriculture, Faisalabad, Pakistan

Department of Process Analytics and Cereal Science, Institute of Food Science and Biotechnology, University of Hohenheim, Garbenstrasse 23, 70599, Stuttgart, Germany

A. Sahar
National Institute of Food Science and Technology, Faculty of Food, Nutrition and Home Sciences, University of Agriculture, Faisalabad, Pakistan

Department of Food Engineering, Faculty of Agricultural Engineering, University of Agriculture, Faisalabad, Pakistan

B. Hitzmann (✉)
Department of Process Analytics and Cereal Science, Institute of Food Science and Biotechnology, University of Hohenheim, Garbenstrasse 23, 70599, Stuttgart, Germany
e-mail: Bernd.Hitzmann@uni-hohenheim.de

Contents

Abbreviations

ANNs	Artificial neural networks
ATP	Adenosine triphosphate
CCA	Canonical component analysis
CCSWA	Common component specific weight analysis
DDT	Dough development time
EEM	Excitation emission matrix
FADH	Flavin adenine dinucleotide
FDA	Factorial discriminant analysis
FMN	Flavin adenine mononucleotide
GLSW	Generalized least square weighting
HCA	Hierarchical cluster analysis
ICA	Independent component analysis
LDA	Linear discriminant analysis
LWR	Locally weighted regression
NADH	Nicotinamide adenine dinucleotide
N-PLS	Multi-way partial least square regression
PARAFAC	Parallel factor analysis
PCA	Principal component analysis
PCR	Principal component regression
PCs	Principal components
PLS-DA	Partial least square discriminant analysis
PLSR	Partial least square regression
RPD	Ratio of standard deviation to root mean square errors of cross-validation
SFS	Synchronous fluorescence spectroscopy
SIMCA	Soft independent modeling by class analogy

SNV	Standard normal variate
TBA	Thiobarbituric acid
TVC	Total viable count
UHT	Ultra high temperature
UV	Ultra violet

1 Introduction

Application of fluorescence spectroscopy in developing new analytical methodologies in food analysis has drawn the attention and interest of food researcher and industries. This is probably because of increased public interest toward high quality standards in food applications; it has become necessary to acquire qualitative and quantitative information on raw materials and intermediate and final product for optimal processing [1, 2]. Fluorescence is known for its sensitivity and specificity. It is rapid, non-invasive, and cost effective, requiring no sample preparations and producing no pollutants. It is considered to be a promising tool for process monitoring and controlling the important parameters during production to achieve efficiently the required quality of end product and safety standards [3]. It also has a great potential to validate and standardize the different conventional methodologies such as chemical measurements. This contribution therefore reviews the recent application of fluorescence in food analysis, providing an overview of its importance for further research and development for establishing a system with sensor technology on an industrial scale.

2 Fluorescence Spectroscopy

Fluorescence is the process of emission of light with greater wavelength than the light absorbed beforehand by certain molecules (fluorophores) during its excitation from the ground energy state to a higher level. This process can be categorized in three steps and explained by the Jablonski diagram which is presented in Fig. 1. The first step deals with the excitation process caused by absorbed light which transfers the electron in the molecule from the ground state (S_0) to the excited state (S_1) with different vibrational energy levels. The excited state of the molecule is unstable and undergoes some vibrational relaxation and internal conversion to stabilize, resulting in dissipation of energy (step 2). The excited electron returns to its ground state (S_0) by the emission of light with lower energy and larger wavelength (step 3). This emission of light is called fluorescence [2].

Conventionally, there are two types of spectra, namely excitation spectra and emission spectra. Excitation spectra are measured by fixing the emission wavelength whereas emission spectra are recorded as a function of constant excitation wavelength [4]. When emission spectra are taken at a wide range of excitation

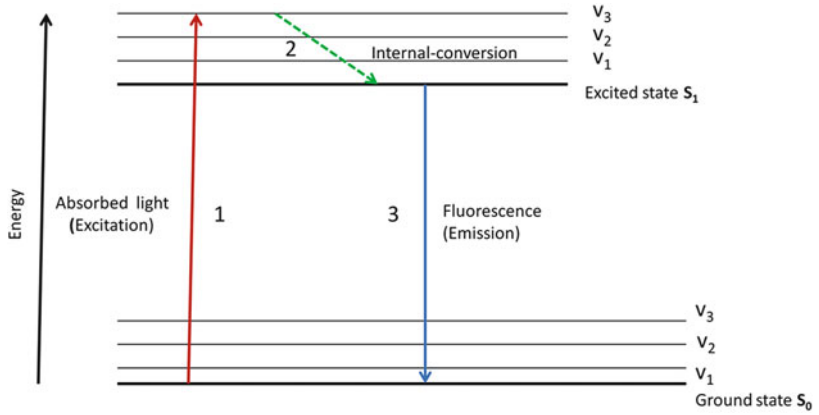

Fig. 1 Process of fluorescence illustrated with the Jablonski diagram comprises three steps – excitation (*1*), internal conversion (*2*), and fluorescence (*3*)

wavelength, it results in excitation-emission matrix (EEM) which has more information about the different fluorophores in the sample matrix. However, there is overlapping of different peaks in this type of spectral data, which can be replaced by synchronous fluorescence spectra (SFS). In SFS, excitation and emission spectra are taken simultaneously by fixing a constant interval (offset) between excitation and emission wavelength [5].

Fluorescence emission caused by the presence of naturally occurring chemicals (fluorophores) present in the sample matrix is sometimes called auto-fluorescence. Food is a complex mixture of different types of fluorophors such as proteins (aromatic amino acid tryptophan, tyrosine, and phenylalanine), cofactors (NADH, FADH, and FMN), vitamins (pyridoxine, vitamin A, tocopherol, and riboflavin), chlorophyll, and porphyrins. Furthermore, during processing and storage, Millard reaction products and oxidation of lipid generate the compounds which induce fluorescence [2]. These fluorophores show the fluorescence in the specific region of spectra which are presented in Fig. 2.

3 Data Analysis

Chemometrics data analysis is being employed that extracts the useful information from spectral data for different applications. There are different chemometric approaches used for qualitative and quantitative analysis which are further categorized into supervised and non-supervised tools as presented in Fig. 3. Non-supervised chemometric tools are also called exploratory analysis, which requires no previous information to analyze the data. Principal component analysis (PCA), hierarchical cluster analysis (HCA), parallel factor analysis (PARAFAC), common component specific weight analysis (CCSWA), and canonical component

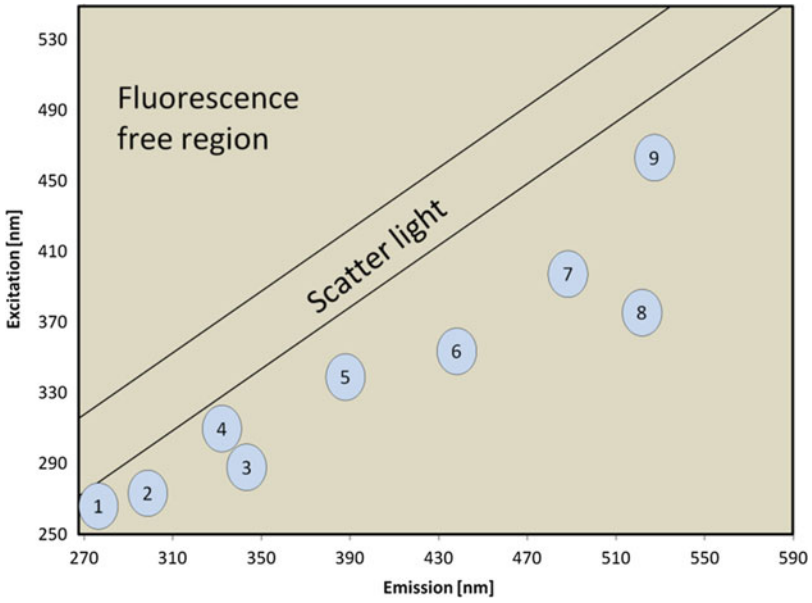

Fig. 2 Contour plot for 2D fluorescence spectrum to show different fluorophors phenylalanine (*1*), tyrosine (*2*), tryptophan (*3*), vitamin E (*4*), pyridoxine and its derivatives (*5* and *7*), NADH (*6*), FMN, FAD, and riboflavin (*8* and *9*)

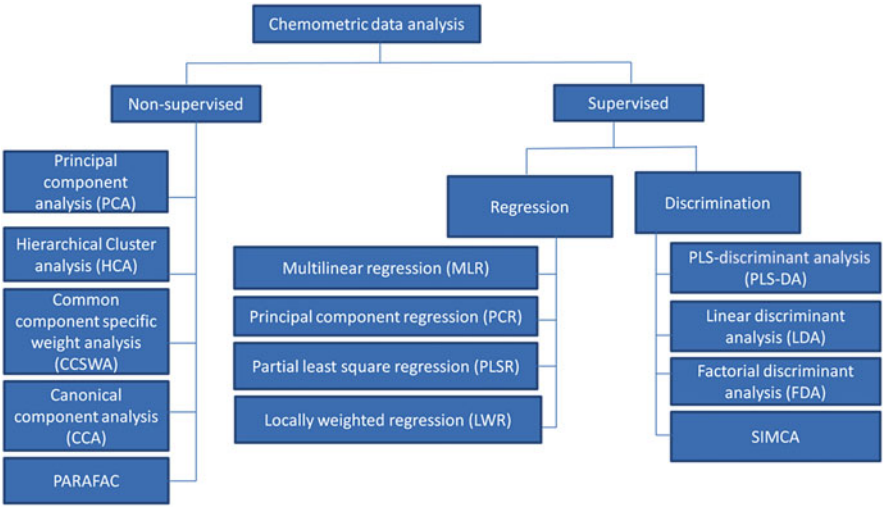

Fig. 3 Overview of chemometric tools for qualitative and quantitative data analysis

Table 1 Reported use of various chemometric analyses for interpretation of fluorescence spectra obtained from different food samples

Food samples	Chemometric tools	References
Dairy products	PCA, FDA, CCSW	[8]
Meat	PCA, PLS, PARAFAC, N-PLS, PLSDA	[5]
Fish	PCA, FDA, PARAFAC	[9]
Eggs	PCA, FDA	[10, 11]
Olive oil	PCA, PARAFAC, LDA, PLSR	[12]
Vegetable oils	LDA	[13]
Honey	PCA, PARAFAC, PLS-DA	[14, 15]
Wines	PCA, FDA	[16]
Beers	PCA, LDA	[17]

analysis (CCA) fall within the category of non-supervised chemometric methods. On the other hand, supervised chemometric tools need prior knowledge of each class to which the spectrum was assigned. Linear discriminant analysis (LDA), factorial discriminate analysis (FDA), and partial least square discriminant analysis (PLS-DA) fall under the umbrella of this category. For quantitative data analysis, multi linear regression (MLR), partial least square (PLS), and principle component regression (PCR) are widely used, whereas locally weighted regression has proved its role in improving the prediction of different parameters [6, 7]. A list of various multi-variant analysis techniques is shown in Table 1. For a complete description of these chemometric methods see [1, 3, 5].

4 Applications of Fluorescence Spectroscopy

Fluorescence spectroscopy has a wide range of applications in food analysis. The major applications include characterization of food products, identification of thermal changes during food processing, detection of food adulteration, monitoring geographical origin of foods, detection of food authenticity, monitoring of chemical and rheological properties of foods, determination of microbial spoilage of foods, and detection of lipid oxidation in foods. Detection capability of fluorescence spectroscopy is based on the presence of various fluorophores in different types of foods. Table 2 gives an overview of the presence of fluorophores in different types of foods.

4.1 Dairy Products

Different fluorescent molecules are present naturally in dairy products, including aromatic amino acids (tryptophan, tyrosine, and phenylalanine), cofactors (NADH,

Table 2 Applications of fluorescence spectroscopy in the food industry for detecting various fluorophores present in foods

Types of foods	Fluorophores	References
Dairy products	Amino acids, nucleic acids, Maillard reaction products, NADH, FADH, oxidation products, retinol, riboflavin	[2]
Meat	Amino acids, nucleic acids, collagen, oxidation products	[18]
Fish	Amino acids, nucleic acids, NADH, oxidation products	[19]
Eggs and egg products	Amino acids, nucleic acids, Maillard reaction products, oxidation products, polyphenols, retinol	[10, 11]
Edible oils	Chlorophylls, ferulic acid, tocopherols	[20]
Cereals	Amino acids, nucleic acids, polyphenols	[21]
Sugar	Amino acids, nucleic acids, Maillard reaction products, NADH	[22]
Fruits and vegetables	Amino acids, nucleic acids, chlorophylls	[23]

Table 3 Classification of dairy products by fluorescence spectroscopy at varied emission and excitation wavelengths

Fluorescent molecules present in dairy products	Emission wavelength (nm) suitable for detection	Excitation wavelength (nm) suitable for detection	References
Tryptophan residues	345	290	[5]
Maillard reaction products	305–450	–	[8, 24]
Riboflavin	525–531	380	[8]
Vitamin A	410	250–350	[24]
Lipid oxidation products	400–640	380	[5]
Lumichrom	310–590	270–550	[5]

FADH, and FMN), vitamins (retinol, riboflavin, and pyridoxine), chlorophyll, and porphyrins, which induce the fluorescence employed by this methodology for classification, monitoring, and optimization of process and storage. This technique has therefore been widely used in the dairy industry for the last few decades [8]. Different ranges of emission and excitation wavelengths are selected for characterization of dairy products as presented in Table 3.

4.1.1 Milk Characterization

The composition of milk is strongly influenced by the feed and the genotype of the lactating animals. Zaïdi et al. [25] therefore explored the potential of fluorescence to differentiate the sheep milk during the 15 weeks of lactation based on the genotypes. Only the spectra recorded in aromatic amino acid and nucleic acid region generated a good identification of the milk samples using PCA. Similarly, Hammami et al. [26] described the suitability of fluorescence to classify sheep milk -corresponding to the feeding system (soybean-rich and scotch bean-rich diets)

using PCA and FDA. The authors found poor discrimination using PCA whereas FDA generated a good classification of the milk based on different feeding systems. A similar approach was used by combining the fluorescence with mid-infrared spectroscopy in further investigations which generated a successful classification of sheep milk quality during the lactation period of 11 weeks [27].

4.1.2 Changes During Thermal Processing of Milk and Its Products

In different processing operations, thermal treatment of the milk is necessary to reduce microbial contamination to increase shelf life. Proper labeling of milk samples according to thermal treatment is an important issue for commercialization of milk in international markets. Ntakatsane et al. [28] described the feasibility of using fluorescence in characterization of thermally treated milk, that is, pasteurized and UHT having different compositions according to origin. Emission spectra were recorded in the region of 400–600 nm for Millard products/riboflavin and 300–400 nm for tryptophan by fixing the excitation wavelength at 360 nm and 290 nm, respectively. PCA differentiated different samples of milk according to composition and origin. Similarly, Hougaard et al. [29] reported the characterization of pasteurized milk at different temperature and time combinations using fluorescence. Multi-way PARAFAC was employed to extract useful information from spectral data using two components that are attributed to protein and vitamin A. Previously, Kulmyrzaev et al. [30] investigated the effect of different processing time (0.5–30 min) and temperature (57–72°C) combinations on the composition of the milk with the help of fluorescence spectroscopy. PCA recognized a clear discrimination of the sample treated at different time and temperature combinations. The high correlations between measured and predicted data for alkaline phosphatase and β-lactoglobulin with fluorescence were one of the interesting findings of this research work. Furthermore, Mungkarndee et al. [31] reported the successful identification and classification of commercially available milk samples such as pasteurized, sterilized, UHT, and recombined milk (UHT processed milk obtained from the combination of fresh milk and dried milk powder) with respect to their thermal processing using LDA out of spectral data. This classification of milk samples with respect to their thermal processing is based on the induction of fluorescence fingerprints generated by different fluorophore and protein interactions.

Heat treatment of milk not only changes the molecular structure by inducing the Millard reaction but also alters the organoleptic and nutritional parameters of dairy products. Diez et al. [32] therefore explored the potential of fluorescence spectroscopy to predict the nutritional parameters of heat treated infant formulas. Fluorescence spectra were recorded in the tryptophan and advance Millard products for intact milk samples at different processing temperatures (70–115°C) and time (2–9.5 min). Vitamin C content and ratio of Millard reaction products to soluble whey proteins showed a prediction error of 12% and 18%, respectively, using PLSR.

Different biochemical changes in milk taking place during storage and processing were investigated by Liu and Metzger [33]. Nonfat dry milk samples were stored for 8 weeks at different temperatures (4, 22, 35, and 50°C) and fluorescence spectra were recorded. Milk samples stored at high temperature (50°C) showed a clear differentiation by using PCA, as the biochemical changes such as the Millard reaction, degradation of riboflavin, and alteration of tryptophan catalyze at this temperature.

4.1.3 Monitoring of Cheese Processing

Cheese manufacturing and ripening is an important step which not only generates desirable physico-chemical, rheological, and organoleptic characteristics, especially the aroma to get a high quality end product but also produces undesirable changes such as oxidation of lipids. Fluorescence was utilized in determining the aforementioned parameters. Karoui et al. [24] investigated the potential of fluorescence for monitoring the oxidation of semi-hard cheese during the ripening period of 60 days. The authors found that the spectra recorded (λ_{ex} = 380 nm and λ_{em} = 400–640 nm) on the surface layer of the cheese showed good discrimination (90%) compared to the inner layer (62%) using FDA. Karoui et al. [34] reported the suitability of fluorescence to predict the rheological parameters of the cheese from days 2 to 60 of the ripening period. The authors found a high correlation ($R^2 > 0.80$) of different rheological parameters such as storage and loss moduli, strain and viscosity from out of spectral data taken in the tryptophan and riboflavin regions using PLSR. Karoui et al. [35] have continued their work for characterization of cheese by predicting the chemical parameters (dry matter, fat, pH, total nitrogen, and water-soluble nitrogen) with the help of fluorescence by taking the spectra in the tryptophan (λ_{ex} = 290 nm and λ_{em} = 305–450 nm), riboflavin (λ_{ex} = 380 nm and λ_{em} = 400–640 nm), and vitamin A (λ_{ex} = 270–350 nm and λ_{em} = 410 nm) regions. The authors found high correlation ($R^2 > 0.85$) for the aforementioned parameters with the fluorescence data using PLSR. Karoui et al. [36] has extended the previous approach to discriminate cheese on the basis of manufacturing process and sampling zone. The spectra recorded in the vitamin A region showed good discrimination with the help of PCA whereas CCSWA was efficiently used to identify cheese according to manufacturing process and sampling zone with spectra in the tryptophan, riboflavin, and vitamin A regions. Kraggerud et al. [37] investigated the spectroscopic methods to predict the sensory characteristics of the cheese during the ripening process. They found that the combination of spectral data improved the prediction performance of sensory parameters compared to single-spectral data. In a recent publication, Kokawa et al. [38] used fluorescence to study the maturation process of cheese up to 329 days of ripening. The results obtained in this study showed high correlation with R^2 of 0.93, 0.79, and 0.90 for maturation time, proteolysis index, and free amino acid, respectively, from spectral data using PLSR modeling. Emission spectra at 345 nm excitation wavelength showed an

increase in the intensity which was caused by the Millard products and lipid oxidation with the passage of the maturation process.

4.1.4 Detection of Adulteration

Fluorescence was employed to detect the adulteration of low quality ingredients in dairy products. Dankowska et al. [39] has investigated the detection of plant oil in cheese using SFS. The authors found the lowest detection limit of 4.4% by taking spectra in the range of 240–700 nm with different offsets (10, 20, . . ., 80 nm). MLR established a high correlation with less than 2% error in predicting the level of adulteration. The classification results described the better performance of successive projection algorithm linear discriminant analysis as compared to PCA-LDA in terms of errors, especially with the offset of 60 nm. A similar approach was made by Ntakatsane et al. [40], who reported the adulteration of milk fat with vegetable oil in the concentration range of 0–40% using two-dimensional and multi-wave fluorescence spectroscopy in combination with gas chromatography. The authors found that adulterated and pure milk fat sample can be classified based on the saturated fatty acid profile, tryptophan, tocopherol, and riboflavin using PCA. The lowest detection limit was found 5% whereas saturated fatty acid has a better prediction performance (R^2 = 0.73–0.92) than the unsaturated fatty acids (R^2 = 0.20–0.65) using PLSR modeling.

4.2 Meat and Meat-Based Products

Meat is one of the perishable food commodities which increase interest in the measurement of quality parameters and their composition to produce an efficient processing and monitoring operation in the industry. Fluorescence spectroscopy is a promising tool to determine the different parameters that are relevant to the quality of the end product and to ensure safe food for consumers.

4.2.1 Chemical and Rheological Parameters

Collagen content not only determines the economic value of meat but also imparts its role in texture and tenderness of meat and meat based products. Egelandsdal et al. [41] used fluorescence spectroscopy for its quantification in beef masseter and latissimus dorsi and pork glutens medius muscles based on the variation in color and quality of connective tissues. Application of PLS regression helped to predict the collagen content in meat in the range of 1.3–4.0% with a prediction error of 0.55% using different pre-processing tools. Redness of the meat showed a high influence on the emission spectra generated by myoglobin variations. Fluorescence

showed a better prediction of collagen in sausage batter as compared to NIR spectroscopy, another interesting finding of this investigation [41].

Different rheological and chemical parameters are important and can be utilized for classification of beef muscles because of their different dry matter, fat, collagen, protein, and cooking loss as reported by Sahar et al. [42]. Excitation wavelengths were fixed at 290, 322, and 382 nm to produce emission spectra in the range of 305–400 nm and 410–700 nm using front-face fluorescence spectroscopy, respectively, for seven beef muscles. ANOVA showed a clear distinction in different types of muscles on the basis of chemical and rheological parameters. However, PLS-DA showed poor validation of 53% and 55% based on cooking loss and protein, respectively, in the range of 305–400 nm, whereas good classification of 75% for fat content in the range of 340–540 nm was observed. Similarly, the above-mentioned approach was further investigated using three different muscles with the application of PLSR and PLS-DA, which show its feasibility in identification and classification of muscles [43]. Furthermore, the fat and fatty acid profile of meat plays a vital role in human nutrition as well as for determination of sensory characteristics. Front face and synchronous fluorescence spectroscopy was applied in estimating the fat and fatty acid profile of beef, which showed correlation with R^2 of 0.66 for saturated fatty acid, whereas mono- and polyunsaturated fatty acid gives the correlation ($R^2 < 0.48$) by using spectral data. Front face fluorescence showed better prediction performance than SFS, which is another notable finding of this investigation [44].

4.2.2 Analysis of Meat Cooking

Cooking of meat is one of the most important processing operation which not only catalyzes the Millard reaction but also alters the molecular structure because of the denaturation of the protein. Sahar et al. [18] reported fluorescence spectroscopy in combination with PARAFAC to investigate the effect of cooking meat. Fluorescence spectra were recorded for meat at 237°C for 1–10 min by fixing the excitation wavelength of 250–550 nm using an offset of 0–160 nm with an interval of 10 nm between excitation and emission wavelength. The best PARAFAC model has used two components which were attributed to Millard reaction products and tryptophan residues generated from the effect of cooking. In a recent application, Sahar et al. [45] reported the same approach using three different temperatures (66, 90, and 237°C) with the same cooking times of 1–10 min. They clearly showed the effect of cooking by separating the meat sample using PCA and PARAFAC. Furthermore, SFS was employed to investigate heterocyclic aromatic amino acids (2-amino-I-methyl-6-phenylimidazo [4,5-*b*]pyridine, 2-amino-3,4,8-trimethylimidazo[4,5-*f*] quinoxaline, etc.) during the cooking of meat using PARAFAC and N-PLS. The best PARAFAC model has two components and N-PLS resulted in a good correlation between heterocyclic aromatic amino acids and spectral data [46]. Undercooked meat products can pose a severe health problem to the consumer. Fluorescence and Raman spectroscopy were therefore used in combination

to determine the endpoint temperature to ensure the proper cooking of ready-to-eat meat products. Fluorescence was applied to determine the changes in aromatic amino acids during the process of cooking, which supported well the results of Raman spectroscopy [47].

4.2.3 Microbial Spoilage and Lipid Oxidation

Microbial spoilage and lipid oxidation of raw and processed meat products have attained special interest as they are considered critical points for health concerns and limiting factors for acceptability of these items. For example, cooking of meat before consumption becomes a source oxidation of protein and fat in meat and meat products, spoiling the quality of the end product. Therefore, Gatellier et al. [48] has reported fluorescence to be a fast and rapid tool to investigate the accumulation of fluorescent pigments generated in cooked meat during storage. The strong correlation of thiobarbituric acid (TBA) reactive substances and protein carbonyls with fluorescence emission demonstrated that the interaction between proteins and aldehyde products of lipid peroxidation is mainly involved in the production of fluorescent pigments in cooked meat. Similarly, lipid oxidation was investigated in chicken breast of different genotypes (a fast-growing line, a medium-growing line, and a slow growing line) with the help of fluorescence spectroscopy using TBA. No change was observed in lipid oxidation for the first 3 days although it increased in certified and labeled genotypes of chicken. Fluorescence and TBA show a correlation with R^2 of 0.73 which determines its feasibility in predicting the lipid oxidation rapidly and non-destructively [49].

Microbial spoilage was investigated in minced meat using a portable spectrofluorometer [50]. In this investigation, total viable counts (TVC), Pseudomonas, lactic acid bacteria, and yeast/mold counts were quantified using PLSR out of fluorescence spectra. The results showed a correlation of $R^2 = 0.5–0.99$ using cross-validation with ratio to standard deviation RPD_{CV} settled in the range of 1.40–8.95, which proved its feasibility for determination of microbial spoilage. Furthermore, Sahar et al. [51] investigated the potential of SFS for determination of microbial load on the chicken fillet during 1–8 days aerobic storage at 5°C and 1–5 days storage at 15°C. Total viable count (TVC), Pseudomonas, Enterobacteriaceae, and *Brochothrix thermosphacta* were estimated from the spectral data, which were taken at the excitation range of 250–550 nm with an offset of 20–180 nm using an interval of 20 nm. The best PARAFAC model showed three and two components for 5 and 15°C respectively whereas PLS-DA resulted in clear classification of TVC during the storage using four factors. N-PLS showed a high correlation of 0.99 with a low error of 0.1–0.2 log cfu/cm^2 for estimation of TVC, Pseudomonas, Enterobacteriaceae, and *B. thermosphacta* out of fluorescence spectra.

Yoshimura et al. [52] reported the estimation of aerobic plate count on the surface of the beef from 0–48 h using fluorescence signature by the application of PLSR. As the result of the metabolic activity of the microbes, peaks were observed in NADH, vitamin A, porphyrin, tryptophan, and flavin regions of the spectra. The

microbial count was predicted with a small prediction error of 0.752 log cfu/cm^2 from the spectral data recorded for both excitation and emission wavelengths in the range of 200–900 nm using PLSR. This approach was extended using fiber optic fluorescence spectroscopy to determine the aerobic plate count on beef surface by increasing the storage time to 3 days at 15°C. However, the prediction error was found to be 0.831 log cfu/cm^2, a bit higher than previous work [53]. Similarly, the surface of pork was used to estimate ATP content and plate count with the help of fluorescence. Spectra were taken in the tryptophan ($\lambda_{ex} = 295$ nm and $\lambda_{em} = 335$ nm) and NADH ($\lambda_{ex} = 335$ nm and $\lambda_{em} = 450$ nm) regions which revealed a change under the influence of microbial activity. The result obtained showed R^2 to be in the range of 0.84–0.87 for ATP and plate count using PLSR [54].

Porphyrin fluorescence is an important indicator to determine the quality of fresh meat during the whole process chain. Fluorescence spectroscopy was used to determine the age of the meat by using protoporphyrins [55]. In this study, fluorescence spectra of Porcine *musculus longissimus dorsi* (*MLD)* were recorded at excitation of 420 nm and an emission range of 550–750 nm during storage in slices over 20 days at 5 and 12°C. PCA was applied showing a clear separation of fluorescence of meat slices at day 5 when stored at 12°C and day 10 stored at 5°C. The reason for the differences in the fluorescence signals were further reported by Durek et al. [56]. The potential of fluorescence spectroscopy for monitoring of microbial contamination using porphyrin fluorescence was investigated. Pork and lamb meat were stored at 5°C for a period of 20 days. Fluorescence spectral data in NADH and porphyrin were used to correlate the microbial contamination. The porphyrin peaks increased after 9 days in pork and 2 days in lamb meat slices. The percent absolute error was found to be 12% and 16% for pork and lamb, respectively.

4.3 Fish and Seafood

Fish and other seafood are susceptible to spoilage rapidly because of high water activity, neutral pH, low content of connective tissues, and the presence of autolytic enzymes that cause the production of unpleasant odor and flavor during storage [9]. Different processing operations such as freezing and refrigerating of the fish are therefore adopted to minimize the process of autolysis and maintain freshness.

4.3.1 Determination of Fish Freshness

Most focused studies of fluorescence application in fish are evaluation of freshness and classification of fish based on species, geographic origin, and processing conditions. However, some applications also elaborate the lipid oxidation and other physico-chemical parameters during storage. Dufour et al. [19] have used fluorescence to distinguish between fresh and aged fish during storage of 1, 5, 8, and

13 days. Spectra were recorded for different species of fish (cod, mackerel, and whiting fillets) in aromatic amino acid + nucleic acid (AAA + NA) ($\lambda_{ex} = 250$ nm, $\lambda_{em} = 280–480$ nm), NADH ($\lambda_{ex} = 336$ nm, $\lambda_{em} = 360–600$ nm), and tryptophan ($\lambda_{ex} = 290$ nm, $\lambda_{em} = 305–400$ nm) regions. Applying PCA to the spectra recorded for AAA + NA allowed good discrimination of fresh and aged fish fillets for different species of fish. Similarly, Karoui et al. [57] expanded this approach to distinguish between fresh and frozen-thawed fish fillets. Slow and fast thawing processes were applied to the frozen fish. Spectra were recorded in the tryptophan and NADH regions with slight modifications. Applying PCA allowed a good separation between fresh and thawed fish samples from spectra taken in the NADH region. Further application of FDA to the five PCs gave 71% and 100% discrimination between fresh and thawed fillets for the tryptophan and NADH spectra, respectively. Hassoun and Karoui [58] have recently confirmed the above-mentioned idea by applying fluorescence to whiting fish fillets under different refrigeration conditions during storage for 12 days. The authors also investigated some parameters such as TBA and pH, which were found to increase during the storage of fish fillets. The reasons for the changes in these parameters are further elaborated with fluorescence by storing the fish under modified atmospheres (50% N_2/50% CO_2 and 80% N_2/20% CO_2) for up to 15 days at 4°C. The best classification was observed with different fish fillets using PCA from fluorescence spectral data. A modified atmosphere allowed the reduction of pH and TBA during storage and the authors recommend this to maintain the quality of fish fillets [59]. Furthermore, Elmasry et al. [60] used EEM for estimating the freshness of horse mackerel (*Trachurus japonicus*) during storage. *K*-value (the ratio of non-phosphorylated ATP metabolites to the total ATP breakdown products) was used as a freshness index. Applying PLSR allowed a good prediction of *K*-value ($R^2 = 0.90$ with RMSECV =10%) from spectral data. Elmasry et al. [61] continued their work and found that excitation at 390 nm is most promising and induces fluorescence of fluorophors responsible for predicting the *K*-value. By fixing this excitation, eight emission wavelengths – 440, 450, 480, 500, 530, 600, 640, and 710 nm – in the normalized EEM spectra were found to be very sensitive in predicting *K*-values in frozen whole fish ($R^2 = 0.85$, RMSECV =12%), whereas seven emission wavelengths – 500, 520, 530, 540, 650, 660, and 670 nm – in the normalized EEM spectra of fillet samples were found to be very important in predicting *K*-values ($R^2 = 0.94$, RMSECV = 7%). Moreover, shelf life stability of cod caviar paste was assessed by using fluorescence under exposure of light with concentration of oxygen in the headspace. Applying PLSR allowed the high correlation for fresh ($R^2 = 0.92$), rancid ($R^2 = 0.94$), and TBA ($R^2 = 0.89$) content from spectral data during storage [62]. On the other hand, SFS was used in determining the pyrene concentration in the gills of carp [63]. Spectra were recorded in the range of 280–450 nm by maintaining the offset of 50 nm. The excitation and emission peaks for pyrene were observed at 334.5 nm and 384.5 nm, respectively. The authors found a high correlation of 0.99 between pyrene and spectral data which is a notable finding of this investigation.

4.3.2 Geographical Classification of Seafood

Application of fluorescence to other seafood is scarce in the literature, although the classification of shrimps based on geographic region was reported by Eaton et al. [64]. Spectra were recorded in excitation (230–600 nm) and emission (240–600 nm) ranges to classify two species of shrimp collected from four different countries (Ecuador, Philippines, Thailand, and the USA). PARAFAC in combination with SIMCA generated a good discrimination (95%) of shrimps corresponding to the country of origin. Hence, fluorescence fingerprints can help to classify shrimps on the basis of their geographic region, which is an interesting finding of this investigation. The emission and excitation wavelengths used for the characterization of meat and fish are presented in Table 4.

4.4 Egg and Egg-Based Products

Freshness of eggs is an important attribute which has a strong impact on the quality of egg-based products as it alters the different physicochemical parameters, including thinning of albumin, increase of water content of yolk, pH value, and weakening of vitelline membrane. All these parameters affect the functional characteristics of the egg albumin and yolk. Karoui et al. [10] therefore performed a series of experiments to explore the potential of fluorescence spectroscopy to determine the freshness of eggs, a non-invasive and non-destructive tool for screening. In the first experiment, fluorescence spectra were recorded directly from the thin and thick albumin in tryptophan ($\lambda_{ex} = 290$ nm and $\lambda_{em} = 305$–430 nm) and Millard

Table 4 Characterization of meat and fish using fluorescence spectroscopy

Fluorophores in meat and fish	Emission wavelength (nm) suitable for detection	Excitation wavelength (nm) suitable for detection	References
Fat (collagen and NADH)	390–475	340	[5]
Bone, cartilage, and connective tissues (collagen and NADH)	455	340	[5]
Meat oxidation products	300–400	290	[65]
Wholesome and unwholesome chicken carcasses differentiation	386–538	380	[5]
Tryptophan residues in fish	305–400	290	[19]
Aromatic amino acids and nucleic acids in fish	280–480	250	[19]
Proteins and NADH	360–600	336	[5]
Differentiation of frozen-thawed and fresh fish (NADH fluorescence spectra)	455 (fresh fish) 379 (frozen-thawed fish)	340	[57]

reaction ($\lambda_{ex} = 360$ nm and $\lambda_{em} = 380–580$ nm) regions during a storage period of 29 days. Applying PCA on the tryptophan spectra for thin albumin allowed a better classification of 69% as compared to the thick egg albumin of 54%. The authors also found a similar trend for the spectra taken in the Millard reaction region of the spectra. However, FDA allowed a much better classification of 91% of thick egg albumin into four groups as a function of storage. In the second part of this work, Karoui et al. [11] used egg yolk in place of egg albumin to determine the freshness of the egg. In this approach, they recorded the spectra in the tryptophan region as described before but spectra in the vitamin A ($\lambda_{ex} = 270–350$ nm and $\lambda_{em} = 410$ nm) region were taken instead of Millard reaction products. Applying FDA allowed a better classification with respect to the spectra taken for vitamin A (91%) as compared to the tryptophan (52%). The authors pooled the spectral data (tryptophan and vitamin A) extracted from the first five PCs into a single matrix and observed an improvement in classification (96%) using the FDA. Karoui et al. [66] continued his investigations and determined the freshness of eggs under modified atmospheric conditions during storage. The authors stored the eggs in daylight at 12.2°C with a relative humidity of 87% and in other treatment 2–4.6% CO_2 was used during a storage period of 29 weeks. Spectra were recorded in AAA + NA ($\lambda_{ex} = 250$ nm; $\lambda_{em} = 280–450$ nm), Millard reaction products, and vitamin A regions for thick albumin and egg yolk. Applying PCA to spectral data taken in the region of vitamin A allowed better classification in terms of storage time and conditions as compared to the other fluorophors which showed poor discriminations. The authors recommended that vitamin A fluorescence can be used as the best tool to discriminate between aged and fresh egg samples. Philippidis et al. [67] recently reported the investigation of amino acids and egg proteins using 2D fluorescence and surface-enhanced Raman spectroscopy. The fluorescence spectra recorded from fresh and aged films indicate the formation of new fluorophores, which revealed alteration and degradation of the proteins taking place during aging.

4.5 Edible Oils

Fluorescence applications in edible oil have not only focused on their classification but also monitored the lipid oxidation which degrades the quality of oils. On the other hand, detection of adulteration of edible oils has gained the interest of food researchers using fluorescence spectroscopy because of the increasing demand for better quality and safety standards. Details about the collection of fluorescence spectra obtained from various fluorophores for characterization of edible oils are described in Table 5.

Table 5 Characterization of edible oils through fluorescence spectroscopy

Fluorescent compounds in edible oils	Emission wavelength (nm) suitable for detection	Excitation wavelength (nm) suitable for detection	References
Chlorophylls in virgin olive oil	681	365	[68]
Vitamin E	445–525	365	[69]
Oxidation products	400–500	365	[69]
Differentiation of edible and lampante virgin olive oil	429–445	–	[69]

4.5.1 Characterization of Edible Oils

Kongbonga et al. [70] have used fluorescence spectroscopy to characterize the different vegetable oils (sweet almond oil, corn oil, sesame oil, high oleic sunflower oil, extra virgin olive oil, argan oil, cotton seed oil, soybean oil, refined palm oil, palmist oil, rape seed oil, walnut oil, pear oil, and grape seed oil). Fluorescence spectra were recorded at excitation and emission wavelengths of 370 nm and 525 nm, respectively, induced by the fluorescence of vitamin E. Applying PCA allowed a clear differentiation of refined and unrefined oils. The authors also reported a better heat stability for high oleic sunflower oil than for extra virgin olive oil. Furthermore, differences in Argan cosmetic and edible oil revealed by the fluorescence spectra were one of the notable findings of this investigation. Similarly, Silva et al. [71] further explored this approach for classification of different vegetable oils (canola, sunflower, corn, and soybean). In this approach, artificial neural networks (ANNs) were applied which allowed the discrimination of different vegetable oils with 72% accuracy. Moreover, palm oil was classified using handheld fluorescence corresponding to the oil quality extracted from ripe, underripe, and overripe fruit [72]. The authors found 90% successful classification in this investigation.

4.5.2 Monitoring of Oxidation Process

Lipid oxidation is one of the notable processes which spoil the quality of oil by producing undesirable changes. This process can be accelerated by different factors including thermal treatment and UV stress, and this was investigated by Poulli et al. [73] using fluorescence techniques in olive oil. The authors found that, because of the accelerated oxidation process when storing samples at high temperatures (80°C for 12 h) and under UV light, there was a large increase in peroxide and anisidine values. These changes showed a linear correlation between fluorescence spectra and parameters of oxidization (peroxide and anisidine value) under UV at different temperatures (20, 40, 60, and 80°C). PCA allowed the discrimination of different samples stored at temperature of 80°C under UV, stress explaining the 95% of

variance by the first two PCs generating five different classes. Similarly, Tena et al. [74] reported the monitoring of the deterioration process of virgin olive oil during thermal processing using fluorescence. Fluorescence spectra were acquired from the oil samples (taken every 2 h from the fryer up to 94 h) of diluted and undiluted samples by fixing the excitation at 350 nm with an emission wavelength of 390–690 nm, whereas HPLC was used to determine the α-tocopherol and different types of phenolic compounds which showed high correlation with $R^2 > 0.90$ from the spectral data. The spectral data was also used to explain the increase in the polar compounds produced by thermoxidation of oil. Diluted samples showed less polar compounds as compared to undiluted heated samples reported by the authors. Furthermore, oxidative stability of baru seed oil (a native Brazilian fruit) was monitored using fluorescence by heating the samples at 110°C for 24 h. The authors reported that the primary compound responsible for oxidation was generated in the first 16 h whereas secondary degrading compound start to be produced after 14 h [75].

4.5.3 Detection of Adulteration in Oils

Olive oil is considered one of the premier oils because of its health benefits and economic value. It is classified according to quality parameters into different grades such as pure, extra virgin, virgin, refined, and olive pomace oil. Adulteration reduces the quality of the olive oil as investigated by [76], who reported the detection of sunflower oil in extra virgin olive oil. Synchronous fluorescence spectra were recorded in the excitation region of 270–720 nm with offset range of 10–120 nm. A contour plot of virgin olive oil showed a clear discrimination with the sunflower oil in the excitation region of 325–385 nm. Applying PLSR reported the quantification of adulteration of sunflower oil with olive oil (0.5–95%) with a detection limit of 3.4% using offset of 80 nm. Poulli et al. [77] continued his investigation to detect the adulteration of other edible oils (olive-pomace, corn, sunflower, soybean, rapeseed, and walnut) with olive oil using the same approach. This time a wavelength interval of 20 nm was found promising to discriminate the different levels of adulteration in the excitation region of 315–400 nm, 315–392 nm, 315–375 nm, 315–365 nm, 315–375 nm, and 315–360 nm for olive-pomace, corn, sunflower, soybean, rapeseed, and walnut oils, respectively. Application of PLSR allowed detection limits of detection of olive-pomace, corn, sunflower, soybean, rapeseed, and walnut oil in virgin olive oil at levels of 2.6, 3.8, 4.3, 4.2, 3.6, and 13.8 wt%, respectively.

Thermal treatment of edible oils accelerates the process of degradation by altering the physico-chemical changes which not only create the off-odor and off-flavor but also produces carcinogenic and other hazardous compounds. Mabood et al. [78] investigated the potential of SFS to discriminate the pure extra virgin olive oil and extra virgin olive oil adulterated with sunflower oil stored at different temperatures (25 and 75°C) with exposure to light and air, which accelerates the process of oxidation. Spectra were recorded in the excitation range of 250–720 nm

with offset of 20, 40, 60, and 80 nm. Applying PLS-DA on difference spectra (75–25°C) reported a good classification between pure and adulterated samples at an adulteration level of 2%. PLSR modeling quantified the level of adulteration of olive oil with sunflower oil with a prediction error of 1.75%. Similarly, Mabood et al. [79] expanded their approach to study the impact of thermal treatment to detect the adulteration of olive oil using the same methodology by storing the oils at two temperatures (25 and 75°C for 8 h). The best PLS-DA models built on difference spectra showed the clear classification of pure and adulterated oil samples. However, quantification of adulteration showed a higher prediction error of 3.2% as compared to the previous work using PLSR. Furthermore, Tao et al. [80] reported the detection of fried oil in edible oil using multiwave fluorescence spectroscopy. The authors found the fluorescence intensity decreases corresponding to the vitamin E level by increasing the concentration of fried oil dosage. Similarly, Xu et al. [81] expanded the idea to detect the vegetable oils in blended oils (peanut, soybean, and sunflower) using cluster analysis and the quasi-Monte Carlo integral method. Spectra were acquired at 250–400 nm (excitation) and 260–750 nm (emission) which showed different peaks for different types of oils induced by the variation in the fatty acid profile for various types of oil. The authors found promising results for detection and quantifications of vegetable oil in blended oil using this approach.

Walnut oil adulteration with sunflower oil was detected using total synchronous spectroscopy [82]. The spectra were recorded in the excitation range of 250–700 nm with a wavelength interval in the region of 10–100 nm. Contour plots of walnut oil showed a clear distinction with sunflower oil at an excitation wavelength of 280 nm. Applying PLSR allowed the limit of detection of 0.3 vol% by using a wavelength interval of 80 nm. Similarly, this approach was expanded by Li et al. [83] by comparing the FTIR with fluorescence spectroscopy to detect the adulteration of walnut oil with soybean oil using SIMCA and PLSR. The authors reported that fluorescence is a more reliable tool in detecting the presence of soybean oil in walnut oil (classification limit less than 5%) than FTIR (classification limit =10%).

4.6 Cereals and Cereal-Based Products

Fluorescence has gained a lot of attention and interest in cereal applications in the last decade because of the increasing use of chemometrics to extract useful information from spectral data using different pre-processing tools.

4.6.1 Determination of Ferulic Acid in Cereal Grains

Ferulic acid is an important fluorophor and therefore the concentration of it has been analyzed in pigmented and non-pigmented cereals using HPLC and

fluorescence [84]. The authors reported the distribution of ferulic acid across the grain, which resulted in variation of fluorescence in the outer as compared to the inner part of grain. Overall correlation ($r = 0.421$ with $p < 0.0001$) was found between ferulic acid concentration and spectral data, which suggested that fluorescence is a promising tool for estimation of ferulic acid in different cereal grains.

4.6.2 Characterization of Wheat Flour

In recent years, Ahmad and coworkers have developed new methods to determine the analytical, rheological, and baking parameters of wheat flours by just taking the spectra signature without any sample preparation using fluorescence [85]. The authors found the best prediction of dough development time (DDT) with a correlation of 0.95 showing error of prediction less than 10% using PLSR. Similarly, the coefficient of determination (R^2) of protein, wet gluten, sedimentation value, water absorption, and volume of bread loaf was found to lie in the range of 0.77–0.95 with a low error of prediction from the spectra of flour. The authors concluded that fluorescence can be used as a rapid method in the cereal industry to replace the laborious and tedious conventional techniques. Similarly, linear and nonlinear chemometrics were applied to predict the nutritional parameters of wheat flours from fluorescence spectral data [6]. The author found a good correlation with R^2 of 0.86–0.89 for fat carbohydrate and moisture. However, application of locally weighted regression (LWR) improved the prediction results of all parameters (fat, carbohydrates, sugars, salt, protein, and saturated fatty acids), showing the correlation with R^2 of 0.88–0.99.

4.6.3 Classification of Cereal Flour and Its Products

Karoui et al. [21] have implemented their preliminary investigations to differentiate cereal products (flours, pasta and semolina obtained from complete kamut, semicomplete kamut, and hard wheat flour) using fluorescence. Spectra were recorded in the tryptophan region by fixing the excitation at 290 nm with emission wavelength of 305–400 nm. Applying PCA not only allowed a good classification between complete kamut and semicomplete kamut and its products made from soft wheat flour but also a similar trend was noticed for pasta prepared from hard wheat flour. However, poor classification was reported in the case of pasta (62%) whereas flours and semolina showed good discrimination of 86% and 87%, respectively. Furthermore, Zeković et al. [86] explored the potential of SFS classification of the different cereal flours (wheat, corn, rye, buckwheat, rice, and barley). The authors found that the contour plots showed a clear discrimination, the rice being especially different from the other types of flour. PCA and cluster analysis showed a clear discrimination using different offset values (2, 7, 10, and 20 nm). The authors concluded that discrimination is possible with low wavelength intervals (< 20 nm).

4.6.4 Determination of Gluten and Starch

Kokawa et al. [87] have performed a series of experiments to determine gluten and starch distribution of dough and bread characteristics using fluorescence imaging techniques. Quantification of the gluten and starch was obtained by extracting the information from fluorescence images in underdeveloped, optimum, and overdeveloped doughs [88]. This approach was further expanded to visualize the gluten starch and butter in pie pastry. Fluorescence images were acquired in the excitation and emission ranges of 270–320 nm and 350–420 nm, respectively, with an interval of 10 nm. The useful information was extracted from the image analysis using the least squares method and clearly visualized the gluten, starch and butter in pie pastry [89].

4.6.5 Monitoring of Kneading Process of Dough

Kneading of the dough is one of the most important operations for getting the desired characteristics to obtain a high quality end product. Ahmad et al. [90] therefore characterized the farinographic kneading process using fluorescence. Applying PCA classified the farinographic curve into four phases (hydration, DDT, dough stability, and softening) out of spectra data using generalized least squares weighting (GLSW) and standard normal variate (SNV). The authors used the same approach to differentiate the different quality of wheat flours (E: elite, A: quality, B: bread, and C: other purposes wheat flour) during the process of kneading. PLSR modeling resulted in the prediction of a middle curve of the farinograph with R^2 of 0.75 out of spectra data, which is one of the notable finding of this investigation. Similarly, Garcia et al. [91] reported the monitoring of the dough process with the help of multiwave fluorescence spectroscopy. The authors found that fluorescence of wheat flour has three peaks which were attributed to protein, ferulic acid, and riboflavin regions of spectra. Addition of ferulic acid resulted in an increase in the intensity of ferulic acid and riboflavin regions and decrease was observed in the protein region of the spectra which may be because of the reabsorption of protein fluorescence by ferulic acid. Application of PCA allowed a clear discrimination of flour with ferulic acid and without it. After the hydration process, there is a decrease in the protein and riboflavin regions of the spectra which was later confirmed by Ahmad et al. [90]. On the other hand, Grote et al. [92] reported the prediction of sour dough parameter (pH and degree of acidity) out of fluorescence spectra using different chemometric tools (PLSR, PCR, and PCA coupled with ANN). The best prediction results were obtained using PLSR as compared to PCR and PCA + ANN. The author reported the prediction error to be in the range of 2.5–5.1% for pH and 6–8.1% in the case of degree of acidity. Using the different temperature and dough yields improved the prediction error by 2%, whereas reduction in error (0.6%) was found caused by the smoothing of noisy spectral data.

4.6.6 Monitoring of Neoformed Contaminants in Cereal Products

Neoformed compounds which are the resultant of Millard reaction products and lipid oxidation during the processing and storage of cereal-based products have also been well-investigated using fluorescence. Rizkallah et al. [93] investigated the potential of fluorescence to monitor the formation of neoformed compounds during the processing of cookies on an industrial scale. Spectral data attained during the process of cookies were decomposed using PARAFAC which were used to identify tryptophan, riboflavin, and other neoformed contaminants (hydroxymethylfurfural, carboxymethyllysine, and acrylamide). The authors found high correlation (R^2 = 0.90–0.98) of these neoformed contaminants with the fluorescence spectra, which is one of the interesting finding of this investigation. Similarly, Botosoa et al. [94] described the role of fluorescence in monitoring lipid oxidation during the process of aging of cakes. The authors stored cakes for up to 20 days and spectra were recorded by fixing the excitation at 325 and 380 nm with emission in the range of 340–490 and 390–680, respectively, and excitation spectra were acquired at excitation of 250–390 nm after emission of 410 nm. Applying PCA allowed a clear classification of cakes according to the aging period. The authors also reported the correlation R^2 = 0.73 of anisidine value with a spectral intensity of 521 nm which assumed that fluorescence can be used for monitoring primary and secondary lipid oxidation products. Botosoa et al. [95] expanded this approach by applying other chemometric models and establishing a correlation of texture with fluorescence to investigate the aging of cakes during storage for 20 days. The author reported that the tryptophan fluorescence (λ_{ex} = 290 nm, λ_{em} = 305–490 nm) has three peaks which were attributed to tryptophan (382 nm) and Millard reaction products (435 nm and 467 nm). Applying PCA allowed a clear differentiation between fresh 1, 6, and 9 days and aged cakes (16 and 20 days). Texture of the cake and tryptophan fluorescence spectral data showed a high correlation with R^2 of 0.99 using canonical correlation analysis, which is an interesting finding of this investigation.

4.7 Fruit and Vegetables

Chlorophyll is an important constituent of fruit and vegetables and serves as an intrinsic fluorophore to induce fluorescence for determination of ripeness and physiological growth of different plant-based products. Kolb et al. [96] reported on chlorophyll fluorescence for analyzing the degree of ripeness of grapes. The authors found a curvilinear trend for glucose, fructose, and total sugars, whereas a linear relationship was established between ratios of fructose/glucose with the spectral data. The authors concluded that sugar accumulation determination during the ripening process of grapes with chlorophyll fluorescence is one of the important finding of this investigation. Similarly, this approach was used by Jiang et al. [97]

with fig fruit to predict the fructose, glucose, and sucrose during ripening. Applying PCA allowed a good discrimination of the fig with respect to the degree of maturity. The authors found a high correlation with R^2 of 0.96, 0.99, and 1.0 for fructose, glucose, and sucrose, respectively, with a low prediction error from spectral data using PLSR modeling. Furthermore, fluorescence coupled with hyperspectral imaging methodology was also used to determine the different quality parameters of apples (fruit skin and flesh color, firmness, soluble solids content, and titratable acidity) by using PCA in combination with ANNs [23]. The spectral images were taken at an excitation wavelength of 408 nm with a blue laser to induce fluorescence with different illumination times (0–5 min). The authors reported a good prediction for apple skin color ($R^2 = 0.94$) whereas other parameters (fruit firmness, skin chroma, and flesh color) showed R^2 of 0.74. Total soluble solid and titratable acidity were predicted using this approach.

Zhu et al. [98] studied the non-enzymatic browning in thermally processed apple juice with the help of fluorescence in combination with different multivariate tools such as PCA, PLSR, and PARAFAC. Spectra were acquired for fruit juices by fixing the excitation at 355 nm and 400 nm in the emission range of 385–600 nm and 430–600 nm, respectively. Applying PCA allowed a good classification (85%) of fresh, heat treated stored apple juices. The authors reported a correlation with R^2 of 0.80 between concentration of 5-hydroxymethylfurfural and spectral data, which suggested the feasibility of this approach for measuring the non-enzymatic browning in fruit. Similarly, Acharid et al. [99] expanded this approach to monitor the neoformed compounds (furosine, carboxymethyllysine, and furan) in carrot-based baby foods. PARAFAC was used to decompose the spectral data which showed an enhanced production of neoformed compounds in thermally processed carrots as compared to fresh and pasteurized carrot puree. The authors reported a high correlation ($R^2 > 0.94$) between neoformed compounds and fluorescence spectra data which concluded that this approach is a practical way to determine the quality of vegetables as well as fruit during storage and processing. Furthermore, Ammari et al. [100] detected the adulteration of orange juice with grapefruit by using 3D fluorescence with the help of free radical scavenging activity and flavonoid content. Applying ICA, allowed a detection limit of 1% of grapefruit in the orange juice, which suggested this approach can be used to prevent fraudulent practices and to attain higher quality and safety standards.

Sensory attributes which increase the acceptability of food products are very important. Fluorescence was therefore used to assess the sensory characteristics of tomato juice [101]. The authors reported two peaks which were found at excitation/emission wavelengths of 290 nm/350 nm and 315 nm/425 nm. Applying PCA resulted in the capturing of a large amount of variance in the first PC which settled at 74% and 75% for aroma and combined flavor and taste of tomato juice, respectively. The authors reported the prediction of the sensory profile of tomato juice (aroma and combined flavor and taste parameters) from fluorescence spectra from the first PC using PLSR with a correlation of 0.8. On the other hand, mangoes were geographically identified using a fluorescence approach [102]. The spectra were taken from the skin and pulp of mangoes obtained from different regions of Japan

(Miyazaki and Okinawa) and China (Taiwan). Application of canonical discrimination analysis for determination of origin showed a misclassification of up to 19% for data collected in 2010 although the spectral data of harvesting season 2010 + 2011 showed a reduced level of misclassification (13%). The authors reported that the selected excitation/emission wavelengths of 260–290 nm/340–360 nm gave a better classification of mangoes corresponding to the origin with spectra taken from the skin than from the pulp.

4.8 Miscellaneous Applications

Fluorescence in combination with chemometrics is widely used in other food applications for classification, authentication, and identification of food products. For instance, Sádecká et al. [103] reported the classification of brandies and wine distillates using fluorescence. Emission spectra were recorded in the region of 360–650 nm by fixing the excitation wavelength at 350 nm whereas SFS spectra were acquired in the range of 200–700 nm with an offset of 90 nm. Application of PCA and HCA allowed clear differentiation between brandies and wines. Moreover, the authors reported that the contour plots of brandies were different from wines as they showed peaks in the excitation/emission range of 390–430 nm/470–520 nm whereas contour plots of wines concentrated in excitation (360–390 nm and 230–250 nm) and emission (450–500 nm and 440–490 nm) regions. Similarly, Airado-Rodríguez and his coworkers [104] investigated fluorescence with PARAFAC to discriminate the wines according to appellation and ripening. Spectra were acquired in excitation (245–345 nm) and emission ranges of (300–500 nm). Applying PARAFAC allowed the decomposition of the spectra into four components which were further used to differentiate the wines corresponding to appellation. The authors reported the discrimination of *Rioja* and *Ribera del Guadiana* samples by plotting the scores of second and third PARAFAC components. The aged and young wine samples were also discriminated by using the same approach. Furthermore, non-enzymatic browning of the wines during storage was analyzed using fluorescence spectroscopy in combination with PARAFAC [105]. The authors reported that the best PARAFAC model has four components in which the first ($\lambda_{ex}/\lambda_{em}$ 280 nm/380 nm) and third factors ($\lambda_{ex}/\lambda_{em}$ 465 nm/530 nm) showed a high correlation with the process of browning.

Monitoring of beer is important to assure its organoleptic properties, nutritional aspects, and safety concerns. Therefore the quality of beer was analyzed during storage using fluorescence spectroscopy [17]. The authors stored fresh beer samples for 3 weeks in darkness and light at different temperatures (4 and 22°C). Recorded spectra showed a decrease in fluorescence intensity in the riboflavin region caused by the exposure to light which resulted in its oxidation. Applying PCA, k nearest neighbor clustering method (kNN) and LDA allowed clear differentiation of samples corresponding to the storage time. Sikorska et al. [106] expanded this approach and develop the calibration model for predicting the riboflavin and aromatic amino

acid in beers using PLSR and N-PLS. The authors found a good correlation ($R^2 > 0.95$) from fluorescence showing the low RMSECV of 14%, 4%, 19%, and 4% for riboflavin, tryptophan, phenylalanine, and tyrosine, respectively.

Phytic acid is an anti-nutrient agent which forms a stable complex and hinders the absorption of different types of nutrients. Cao and colleagues [107] investigated the potential of SFS to determine the phytic acid in different foodstuffs such as bean curd, wheat bran, beans, soybean, corn, and sesame. A stable complex formation by chelating the Cu^{2+} ion with Cu^{II}-2,2′-bipyridine complex that changed to 2-2 bipyridine which induced fluorescence was noted. The limit of detection and quantification for phytic acid was reported to be 0.12 mg/L and 0.18 mg/L, respectively, which is an interesting finding of this contribution. Culinary spices are subjected to adulteration with different dyes which were detected and classified by using SFS [108]. SFS spectra were acquired in the range of 400–690 nm with wavelength intervals of 20–60 nm. Applying PLS-DA classified the adulterated and unadulterated samples with dye in the range of 1–5 mg/L, showing 100% accurate discrimination by using the wavelength interval of 60 nm.

5 Conclusion

Various authors have demonstrated the potential of fluorescence spectroscopy in classification, authentication, and quantification of various parameters in different food applications, which has led to development of sensors based on this spectroscopic method. Research into spectroscopic applications has increased in food analysis over the last few decades but these applications are restricted to the laboratory scale with lower numbers of samples. However, a few applications are being used on the industrial scale, only reducing evaluation costs and time but also replacing conventional methodologies with no sample preparation procedures. Those involved in the industry are still reluctant to utilize these sensor technologies because of the high cost of installation and maintenance. In addition, fluorescence always involves pretreatment and different chemometric tools to extract and retrieve useful information from the spectral data for calibration to quantify the different parameters. This can involve laborious and costly procedures which are limiting factors in the adoption by industry. However, a valuable and cheap tool is the result after development of calibration modeling for estimation of different parameters in the food system. Hence, fluorescence not only has great potential in measurements of food systems, as described in the present contribution, but also can become a valuable tool in other fields (pharmaceutical and biological sciences, etc.) and in chemometric data analysis. This contribution has discussed the potential of fluorescence in food systems, serving as a reliable, non-destructive, and affordable analytical method for monitoring and controlling the whole food production process, leading to high quality standards in the future.

References

1. Christensen J, Nørgaard L, Bro R, Engelsen SB (2006) Multivariate autofluorescence of intact food systems. Chem Rev 106(6):1979–1994
2. Karoui R, Blecker C (2011) Fluorescence spectroscopy measurement for quality assessment of food systems—a review. Food Bioprocess Technol 4(3):364–386
3. Faassen S, Hitzmann B (2015) Fluorescence spectroscopy and chemometric modeling for bioprocess monitoring. Sensors 15(5):10271
4. Lakowicz J (2006) Principles of fluorescence spectroscopy, 3rd edn. Springer, New York
5. SádeCká J, TóThoVá J (2007) Fluorescence spectroscopy and chemometrics in the food classification – a review. Czech J Food Sci 25(4):159–173
6. Ahmad MH, Nache M, Hinrichs J, Hitzmann B (2016) Estimation of the nutritional parameters of various types of wheat flours using fluorescence spectroscopy and chemometrics. Int J Food Sci Technol 51(5):1186–1194
7. Nache M, Scheier R, Schmidt H, Hitzmann B (2015) Non-invasive lactate- and pH-monitoring in porcine meat using Raman spectroscopy and chemometrics. Chemom Intell Lab Syst 142:197–205
8. Andersen CM, Mortensen G (2008) Fluorescence spectroscopy: a rapid tool for analyzing dairy products. J Agric Food Chem 56(3):720–729
9. Hassoun A, Karoui R (2017) Quality evaluation of fish and other seafood by traditional and nondestructive instrumental methods: advantages and limitations. Crit Rev Food Sci Nutr 57 (9):1976–1998
10. Karoui R, Kemps B, Bamelis F, de Ketelaere B, Merten K, Schoonheydt R, Decuypere E, de Baerdemaeker J (2006) Development of a rapid method based on front face fluorescence spectroscopy for the monitoring of egg freshness: 1—evolution of thick and thin egg albumens. Eur Food Res Technol 223(3):303–312
11. Karoui R, Kemps B, Bamelis F, de Ketelaere B, Merten K, Schoonheydt R, Decuypere E, de Baerdemaeker J (2006) Development of a rapid method based on front-face fluorescence spectroscopy for the monitoring of egg freshness: 2—evolution of egg yolk. Eur Food Res Technol 223(2):180–188
12. Guimet F, Ferré J, Boqué R, Rius F (2004) Application of unfold principal component analysis and parallel factor analysis to the exploratory analysis of olive oils by means of excitation–emission matrix fluorescence spectroscopy. Anal Chim Acta 515(1):75–85
13. Sikorska E, Górecki T, Khmelinskii IV, Sikorski M, Kozioł J (2005) Classification of edible oils using synchronous scanning fluorescence spectroscopy. Food Chem 89(2):217–225
14. Lenhardt L, Bro R, Zeković I, Dramićanin T, Dramićanin MD (2015) Fluorescence spectroscopy coupled with PARAFAC and PLS DA for characterization and classification of honey. Food Chem 175:284–291
15. Lenhardt L, Zekovic I, Dramicanin T, Dramicanin MD, Bro R (2014) Determination of the botanical origin of honey by front-face synchronous fluorescence spectroscopy. Appl Spectrosc 68(5):557–563
16. Dufour É, Letort A, Laguet A, Lebecque A, Serra JN (2006) Investigation of variety, typicality and vintage of French and German wines using front-face fluorescence spectroscopy. Anal Chim Acta 563(1-2):292–299
17. Sikorska E, Górecki T, Khmelinskii IV, Sikorski M, de Keukeleire D (2006) Monitoring beer during storage by fluorescence spectroscopy. Food Chem 96(4):632–639
18. Sahar A, Boubellouta T, Portanguen S, Kondjoyan A, Dufour É (2009) Synchronous front-face fluorescence spectroscopy coupled with parallel factors (PARAFAC) analysis to study the effects of cooking time on meat. J Food Sci 74(9):E534–E539
19. Dufour É, Frencia JP, Kane E (2003) Development of a rapid method based on front-face fluorescence spectroscopy for the monitoring of fish freshness. Food Res Int 36(5):415–423
20. Zandomeneghi M, Carbonaro L, Caffarata C (2005) Fluorescence of vegetable oils: olive oils. J Agric Food Chem 53(3):759–766

21. Karoui R, Cartaud G, Dufour E (2006) Front-face fluorescence spectroscopy as a rapid and nondestructive tool for differentiating various cereal products: a preliminary investigation. J Agric Food Chem 54(6):2027–2034
22. Ruoff K, Luginbühl W, Künzli R, Bogdanov S, Bosset JO, von der Ohe K, von der Ohe W, Amadò R (2006) Authentication of the botanical and geographical origin of honey by front-face fluorescence spectroscopy. J Agric Food Chem 54(18):6858–6866
23. Noh HK, Lu R (2007) Hyperspectral laser-induced fluorescence imaging for assessing apple fruit quality. Postharvest Biol Technol 43(2):193–201
24. Karoui R, Dufour É, de Baerdemaeker J (2006) Front face fluorescence spectroscopy coupled with chemometric tools for monitoring the oxidation of semi-hard cheeses throughout ripening. Food Chem 101(3):1305–1314
25. Zaïdi F, Rouissi H, Dridi S, Kammoun M, de Baerdemaeker J, Karoui R (2008) Front-face fluorescence spectroscopy as a rapid and non-destructive tool for differentiating between Sicilo–Sarde and Comisana ewe's milk during lactation period: a preliminary study. Food Bioprocess Technol 1(2):143–151
26. Hammami M, Rouissi H, Salah N, Selmi H, Al-Otaibi M, Blecker C, Karoui R (2010) Fluorescence spectroscopy coupled with factorial discriminant analysis technique to identify sheep milk from different feeding systems. Food Chem 122(4):1344–1350
27. Karoui R, Hammami M, Rouissi H, Blecker C (2011) Mid infrared and fluorescence spectroscopies coupled with factorial discriminant analysis technique to identify sheep milk from different feeding systems. Food Chem 127(2):743–748
28. Ntakatsane MP, Yang XQ, Lin M, Liu XM, Zhou P (2011) Short communication: suitability of fluorescence spectroscopy for characterization of commercial milk of different composition and origin. J Dairy Sci 94(11):5375–5380
29. Hougaard AB, Lawaetz AJ, Ipsen RH (2013) Front face fluorescence spectroscopy and multi-way data analysis for characterization of milk pasteurized using instant infusion. LWT--Food Sci Technol 53(1):331–337
30. Kulmyrzaev AA, Levieux D, Dufour É (2005) Front-face fluorescence spectroscopy allows the characterization of mild heat treatments applied to milk. Relations with the denaturation of milk proteins. J Agric Food Chem 53(3):502–507
31. Mungkarndee R, Techakriengkrai I, Tumcharern G, Sukwattanasinitt M (2016) Fluorescence sensor array for identification of commercial milk samples according to their thermal treatments. Food Chem 197(Part A):198–204
32. Diez R, Ortiz MC, Sarabia L, Birlouez-Aragon I (2008) Potential of front face fluorescence associated to PLS regression to predict nutritional parameters in heat treated infant formula models. Anal Chim Acta 606(2):151–158
33. Liu X, Metzger LE (2007) Application of fluorescence spectroscopy for monitoring changes in nonfat dry milk during storage. J Dairy Sci 90(1):24–37
34. Karoui R, Dufour É (2006) Prediction of the rheology parameters of ripened semi-hard cheeses using fluorescence spectra in the UV and visible ranges recorded at a young stage. Int Dairy J 16(12):1490–1497
35. Karoui R, Mouazen AM, Dufour E, Schoonheydt R, de Baerpemaeker J (2006) Utilisation of front-face fluorescence spectroscopy for the determination of some selected chemical parameters in soft cheeses. Lait 86(2):155–169
36. Karoui R, Dufour E, Schoonheydt R, Baerdemaeker JD (2007) Characterisation of soft cheese by front face fluorescence spectroscopy coupled with chemometric tools: effect of the manufacturing process and sampling zone. Food Chem 100(2):632–642
37. Kraggerud H, Næs T, Abrahamsen RK (2014) Prediction of sensory quality of cheese during ripening from chemical and spectroscopy measurements. Int Dairy J 34(1):6–18
38. Kokawa M, Ikegami S, Chiba A, Koishihara H, Trivittayasil V, Tsuta M, Fujita K, Sugiyama J (2015) Measuring cheese maturation with the fluorescence fingerprint. Food Sci Technol Int 21(4):549–555

39. Dankowska A, Małecka M, Kowalewski W (2015) Detection of plant oil addition to cheese by synchronous fluorescence spectroscopy. Dairy Sci Technol 95(4):413–424
40. Ntakatsane MP, Liu XM, Zhou P (2013) Short communication: rapid detection of milk fat adulteration with vegetable oil by fluorescence spectroscopy. J Dairy Sci 96(4):2130–2136
41. Egelandsdal B, Dingstad G, Tøgersen G, Lundby F, Langsrud Ø (2005) Autofluorescence quantifies collagen in sausage batters with a large variation in myoglobin content. Meat Sci 69(1):35–46
42. Sahar A, Boubellouta T, Lepetit J, Dufour É (2009) Front-face fluorescence spectroscopy as a tool to classify seven bovine muscles according to their chemical and rheological characteristics. Meat Sci 83(4):672–677
43. Sahar A, Dufour É (2015) Classification and characterization of beef muscles using front-face fluorescence spectroscopy. Meat Sci 100:69–72
44. Aït-Kaddour A, Thomas A, Mardon J, Jacquot S, Ferlay A, Gruffat D (2016) Potential of fluorescence spectroscopy to predict fatty acid composition of beef. Meat Sci 113:124–131
45. Sahar A, Rahman UU, Kondjoyan A, Portanguen S, Dufour E (2016) Monitoring of thermal changes in meat by synchronous fluorescence spectroscopy. J Food Eng 168:160–165
46. Sahar A, Portanguen S, Kondjoyan A, Dufour É (2010) Potential of synchronous fluorescence spectroscopy coupled with chemometrics to determine the heterocyclic aromatic amines in grilled meat. Eur Food Res Technol 231(5):803–812
47. Berhe DT, Lawaetz AJ, Engelsen SB, Hviid MS, Lametsch R (2015) Accurate determination of endpoint temperature of cooked meat after storage by Raman spectroscopy and chemometrics. Food Control 52:119–125
48. Gatellier P, Santé-Lhoutellier V, Portanguen S, Kondjoyan A (2009) Use of meat fluorescence emission as a marker of oxidation promoted by cooking. Meat Sci 83(4):651–656
49. Gatellier P, Gomez S, Gigaud V, Berri C, Le Bihan-Duval E, Santé-Lhoutellier V (2007) Use of a fluorescence front face technique for measurement of lipid oxidation during refrigerated storage of chicken meat. Meat Sci 76(3):543–547
50. Aït-Kaddour A, Boubellouta T, Chevallier I (2011) Development of a portable spectrofluorimeter for measuring the microbial spoilage of minced beef. Meat Sci 88(4):675–681
51. Sahar A, Boubellouta T, Dufour É (2011) Synchronous front-face fluorescence spectroscopy as a promising tool for the rapid determination of spoilage bacteria on chicken breast fillet. Food Res Int 44(1):471–480
52. Yoshimura M, Sugiyama J, Tsuta M, Fujita K, Shibata M, Kokawa M, Oshita S, Oto N (2014) Prediction of aerobic plate count on beef surface using fluorescence fingerprint. Food Bioprocess Technol 7(5):1496–1504
53. Mita Mala D, Yoshimura M, Kawasaki S, Tsuta M, Kokawa M, Trivittayasil V, Sugiyama J, Kitamura Y (2016) Fiber optics fluorescence fingerprint measurement for aerobic plate count prediction on sliced beef surface. LWT--Food Sci Technol 68:14–20
54. Oto N, Oshita S, Makino Y, Kawagoe Y, Sugiyama J, Yoshimura M (2013) Non-destructive evaluation of ATP content and plate count on pork meat surface by fluorescence spectroscopy. Meat Sci 93(3):579–585
55. Schneider J, Wulf J, Surowsky B, Schmidt H, Schwägele F, Schlüter O (2008) Fluorimetric detection of protoporphyrins as an indicator for quality monitoring of fresh intact pork meat. Meat Sci 80(4):1320–1325
56. Durek J, Fröhling A, Bolling J, Thomasius R, Durek P, Schlüter OK (2016) Non-destructive mobile monitoring of microbial contaminations on meat surfaces using porphyrin fluorescence intensities. Meat Sci 115:1–8
57. Karoui R, Thomas E, Dufour E (2006) Utilisation of a rapid technique based on front-face fluorescence spectroscopy for differentiating between fresh and frozen–thawed fish fillets. Food Res Int 39(3):349–355
58. Hassoun A, Karoui R (2015) Front-face fluorescence spectroscopy coupled with chemometric tools for monitoring fish freshness stored under different refrigerated conditions. Food Control 54:240–249

59. Hassoun A, Karoui R (2016) Monitoring changes in whiting (*Merlangius merlangus*) fillets stored under modified atmosphere packaging by front face fluorescence spectroscopy and instrumental techniques. Food Chem 200:343–353
60. Elmasry G, Nagai H, Moria K, Nakazawa N, Tsuta M, Sugiyama J, Okazaki E, Nakauchi S (2015) Freshness estimation of intact frozen fish using fluorescence spectroscopy and chemometrics of excitation–emission matrix. Talanta 143:145–156
61. Elmasry G, Nakazawa N, Okazaki E, Nakauchi S (2016) Non-invasive sensing of freshness indices of frozen fish and fillets using pretreated excitation–emission matrices. Sensors Actuators B Chem 228:237–250
62. Airado-Rodríguez D, Skaret J, Wold JP (2010) Assessment of the quality attributes of cod caviar paste by means of front-face fluorescence spectroscopy. J Agric Food Chem 58 (9):5276–5285
63. Liu X, Jing J, Li S, Zhang G, Zou T, Xia X, Huang W (2012) Measurement of pyrene in the gills of exposed fish using synchronous fluorescence spectroscopy. Chemosphere 86 (2):198–201
64. Eaton JK, Alcivar-Warren A, Kenny JE (2012) Multidimensional fluorescence fingerprinting for classification of shrimp by location and species. Environ Sci Technol 46(4):2276–2282
65. Veberg A, Vogt G, Wold JP (2006) Fluorescence in aldehyde model systems related to lipid oxidation. LWT--Food Sci Technol 39(5):562–570
66. Karoui R, Nicolaï B, de Baerdemaeker J (2008) Monitoring the egg freshness during storage under modified atmosphere by fluorescence spectroscopy. Food Bioprocess Technol 1 (4):346–356
67. Philippidis A, Papliaka ZE, Anglos D (2016) Surface enhanced Raman and 2D-fluorescence spectroscopy for the investigation of amino acids and egg proteins. Microchem J 126:230–236
68. Kyriakidis NB, Skarkalis P (2000) Fluorescence spectra measurement of olive oil and other vegetable oils. J AOAC Int 83(6):1435–1439
69. Guimet F, Ferré J, Boqué R (2005) Rapid detection of olive–pomace oil adulteration in extra virgin olive oils from the protected denomination of origin "Siurana" using excitation–emission fluorescence spectroscopy and three-way methods of analysis. Anal Chim Acta 544(1–2):143–152
70. Kongbonga Y, Ghalila H, Onana MB, Majdi Y, Lakhdar Z, Mezlini H, Sevestre-Ghalila S (2011) Characterization of vegetable oils by fluorescence spectroscopy. Food Nutr Sci 02 (07):692–699
71. Silva T, Eduardo C, Filardi VL, Pepe I, Chaves M, Santos CM (2015) Classification of food vegetable oils by fluorimetry and artificial neural networks. Food Control 47:86–91
72. Hazir MHM, Shariff ARM, Amiruddin MD, Ramli AR, Iqbal Saripan M (2012) Oil palm bunch ripeness classification using fluorescence technique. J Food Eng 113(4):534–540
73. Poulli KI, Mousdis GA, Georgiou CA (2009) Monitoring olive oil oxidation under thermal and UV stress through synchronous fluorescence spectroscopy and classical assays. Food Chem 117(3):499–503
74. Tena N, García-González DL, Aparicio R (2009) Evaluation of virgin olive oil thermal deterioration by fluorescence spectroscopy. J Agric Food Chem 57(22):10505–10511
75. Silva VD, Conceição JN, Oliveira IP, Lescano CH, Muzzi RM, Filho OPS, Conceição EC, Casagrande GA, Caires ARL (2015) Oxidative stability of baru (dipteryx alata vogel) oil monitored by fluorescence and absorption spectroscopy. J Spectrosc 2015:6
76. Poulli KI, Mousdis GA, Georgiou CA (2006) Synchronous fluorescence spectroscopy for quantitative determination of virgin olive oil adulteration with sunflower oil. Anal Bioanal Chem 386(5):1571–1575
77. Poulli KI, Mousdis GA, Georgiou CA (2007) Rapid synchronous fluorescence method for virgin olive oil adulteration assessment. Food Chem 105(1):369–375
78. Mabood F, Boqué R, Folcarelli R, Busto O, Al-Harrasi A, Hussain J (2015) Thermal oxidation process accelerates degradation of the olive oil mixed with sunflower oil and

enables its discrimination using synchronous fluorescence spectroscopy and chemometric analysis. Spectrochim Acta, Part A 143:298–303
79. Mabood F, Boqué R, Folcarelli R, Busto O, Jabeen F, Al-Harrasi A, Hussain J (2016) The effect of thermal treatment on the enhancement of detection of adulteration in extra virgin olive oils by synchronous fluorescence spectroscopy and chemometric analysis. Spectrochim Acta, Part A 161:83–87
80. Tao C, Ruan J, Shu S, Han Z (2016) Detection of fried oil in edible oil based on three-dimensional fluorescence spectroscopy. Zhongguo Jiguang 43(1):0115001
81. Xu J, Liu X-F, Wang Y-T (2016) A detection method of vegetable oils in edible blended oil based on three-dimensional fluorescence spectroscopy technique. Food Chem 212:72–77
82. Ge F, Chen C, Liu D, Zhao S (2014) Rapid quantitative determination of walnut oil adulteration with sunflower oil using fluorescence spectroscopy. Food Anal Methods 7 (1):146–150
83. Li B, Wang H, Zhao Q, Ouyang J, Wu Y (2015) Rapid detection of authenticity and adulteration of walnut oil by FTIR and fluorescence spectroscopy: a comparative study. Food Chem 181:25–30
84. Ndolo VU, Beta T, Fulcher RG (2013) Ferulic acid fluorescence intensity profiles and concentration measured by HPLC in pigmented and non-pigmented cereals. Food Res Int 52(1):109–118
85. Ahmad MH, Nache M, Waffenschmidt S, Hitzmann B (2016) A fluorescence spectroscopic approach to predict analytical, rheological and baking parameters of wheat flours using chemometrics. J Food Eng 182:65–71
86. Zeković I, Lenhardt L, Dramićanin T, Dramićanin MD (2012) Classification of intact cereal flours by front-face synchronous fluorescence spectroscopy. Food Anal Methods 5 (5):1205–1213
87. Kokawa M, Fujita K, Sugiyama J, Tsuta M, Shibata M, Araki T, Nabetani H (2011) Visualization of the distribution of multiple constituents in bread dough by use of fluorescence fingerprint imaging. Procedia Food Sci 1:927–934
88. Kokawa M, Fujita K, Sugiyama J, Tsuta M, Shibata M, Araki T, Nabetani H (2012) Quantification of the distributions of gluten, starch and air bubbles in dough at different mixing stages by fluorescence fingerprint imaging. J Cereal Sci 55(1):15–21
89. Kokawa M, Yokoya N, Ashida H, Sugiyama J, Tsuta M, Yoshimura M, Fujita K, Shibata M (2015) Visualization of gluten, starch, and butter in pie pastry by fluorescence fingerprint Imaging. Food Bioprocess Technol 8(2):409–419
90. Ahmad MH, Nache M, Waffenschmidt S, Hitzmann B (2016) Characterization of farinographic kneading process for different types of wheat flours using fluorescence spectroscopy and chemometrics. Food Control 66:44–52
91. Garcia R, Boussard A, Rakotozafy L, Nicolas J, Potus J, Rutledge DN, Cordella CB (2016) 3D-front-face fluorescence spectroscopy and independent components analysis: a new way to monitor bread dough development. Talanta 147:307–314
92. Grote B, Zense T, Hitzmann B (2014) 2D-fluorescence and multivariate data analysis for monitoring of sourdough fermentation process. Food Control 38:8–18
93. Rizkallah J, Morales FJ, Ait-Ameur L, Fogliano V, Hervieu A, Courel M, Birlouez Aragon I (2008) Front face fluorescence spectroscopy and multiway analysis for process control and NFC prediction in industrially processed cookies. Chemom Intell Lab Syst 93(2):99–107
94. Botosoa EP, Chèné C, Karoui R (2013) Use of front face fluorescence for monitoring lipid oxidation during ageing of cakes. Food Chem 141(2):1130–1139
95. Botosoa EP, Chénè C, Karoui R (2013) Monitoring changes in sponge cakes during aging by front face fluorescence spectroscopy and instrumental techniques. J Agric Food Chem 61 (11):2687–2695
96. Kolb CA, Wirth E, Kaiser WM, Meister A, Riederer M, Pfündel EE (2006) Noninvasive evaluation of the degree of ripeness in grape berries (*Vitis vinifera* L. Cv. Bacchus and Silvaner) by chlorophyll fluorescence. J Agric Food Chem 54(2):299–305

97. Jiang L, Shen Z, Zheng H, He W, Deng G, Lu H (2013) Noninvasive evaluation of fructose, glucose, and sucrose contents in fig fruits during development using chlorophyll fluorescence and chemometrics. J Agric Sci Technol 15(2):333–342
98. Zhu D, Ji B, Eum HL, Zude M (2009) Evaluation of the non-enzymatic browning in thermally processed apple juice by front-face fluorescence spectroscopy. Food Chem 113(1):272–279
99. Acharid A, Rizkallah J, Ait-Ameur L, Neugnot B, Seidel K, Särkkä-Tirkkonen M, Kahl J, Birlouez-Aragon I (2012) Potential of front face fluorescence as a monitoring tool of neoformed compounds in industrially processed carrot baby food. LWT--Food Sci Technol 49(2):305–311
100. Ammari F, Redjdal L, Rutledge DN (2015) Detection of orange juice frauds using front-face fluorescence spectroscopy and independent components analysis. Food Chem 168:211–217
101. Trivittayasil V, Tsuta M, Imamura Y, Sato T, Otagiri Y, Obata A, Otomo H, Kokawa M, Sugiyama J, Fujita K, Yoshimura M (2016) Fluorescence fingerprint as an instrumental assessment of the sensory quality of tomato juices. J Sci Food Agric 96(4):1167–1174
102. Nakamura Y, Fujita K, Sugiyama J, Tsuta M, Shibata M, Yoshimura M, Kokawa M, Nabetani H, Araki T (2012) Discrimination of the geographic origin of mangoes using fluorescence fingerprint. Nippon Shokuhin Kagaku Kogaku Kaishi 59(8):387–393
103. Sádecká J, Tóthová J, Májek P (2009) Classification of brandies and wine distillates using front face fluorescence spectroscopy. Food Chem 117(3):491–498
104. Airado-Rodríguez D, Durán-Merás I, Galeano-Díaz T, Wold JP (2011) Front-face fluorescence spectroscopy: a new tool for control in the wine industry. J Food Compos Anal 24 (2):257–264
105. Elcoroaristizabal S, Callejón RM, Amigo JM, Ocaña-González JA, Morales ML, Ubeda C (2016) Fluorescence excitation-emission matrix spectroscopy as a tool for determining quality of sparkling wines. Food Chem 206:284–290
106. Sikorska E, Gliszczyńska-świgło A, Insińska-Rak M, Khmelinskii I, de Keukeleire D, Sikorski M (2008) Simultaneous analysis of riboflavin and aromatic amino acids in beer using fluorescence and multivariate calibration methods. Anal Chim Acta 613(2):207–217
107. Cao S, Dong N, Chen J (2011) Synchronous fluorescence determination of phytic acid in FOODSTUFFS and urine based on replacement reaction. Phytochem Anal 22(2):119–123
108. Di Anibal CV, Rodríguez MS, Albertengo L (2015) Synchronous fluorescence and multivariate classification analysis as a screening tool for determining Sudan I dye in culinary spices. Food Control 56:18–23

Adv Biochem Eng Biotechnol (2017) 161: 153–194
DOI: 10.1007/10_2017_9

Published online: 28 March 2017

How to Decide on Modeling Details: Risk and Benefit Assessment

Mustafa Özilgen

Abstract Mathematical models based on thermodynamic, kinetic, heat, and mass transfer analysis are central to this chapter. Microbial growth, death, enzyme inactivation models, and the modeling of material properties, including those pertinent to conduction and convection heating, mass transfer, such as diffusion and convective mass transfer, and thermodynamic properties, such as specific heat, enthalpy, and Gibbs free energy of formation and specific chemical exergy are also needed in this task. The origins, simplifying assumptions, and uses of model equations are discussed in this chapter, together with their benefits. The simplified forms of these models are sometimes referred to as "*laws*," such as "*the first law of thermodynamics*" or "*Fick's second law*." Starting to modeling a study with such "*laws*" without considering the conditions under which they are valid runs the risk of ending up with erronous conclusions. On the other hand, models started with fundamental concepts and simplified with appropriate considerations may offer explanations for the phenomena which may not be obtained just with measurements or unprocessed experimental data. The discussion presented here is strengthened with case studies and references to the literature.

Keywords 80% to 20% rule, Efficiency, Forcasting, Heat transfer, Mass transfer, Mathematical modeling, Simplifying assumptions, Thermodynamics

Contents

M. Özilgen (✉)
Food Engineering Department, Yeditepe University, 34755 Kayisdagi, Istanbul, Turkey
e-mail: ozilgen.mustafa@gmail.com

1 Modeling

Mathematical modeling is quite a comprehensive subject and may mean different things to different scientists. The ideas presented in this chapter depend on the experience gained in previous books [1–3]. In a typical food production process, material inputs are converted into a set of desired material outputs. In the paper "*energy utilization, carbon dioxide emission, and exergy loss in flavored yogurt production process*" Sorgüven and Özilgen [4] discussed the flavored yogurt production process from the raw materials as described in Figs. 1 and 2. In these figures, material and energy flow are described in detail. It may be possible to extract data regarding the quality, for example, color, aroma, or taste of the inputs and outputs of the process with direct measurements. Mathematical modeling makes it possible to extract more information from this system, which may not be obtained by direct measurements only. Within the context of this study, the inputs are mostly the ingredients and energy, the outputs food. The process units are the equipment, designed to achieve the purpose. A *mathematical model* is an approximate representation of a process in mathematical terms (Fig. 3). A mathematical model is a shorthand description of the processing of data and estimates the values of the outputs (Y_1, Y_2 ... Y_k), when the values of the inputs (X_1, X_2 ... X_n) are entered. The model may help one to understand the details of the relation between

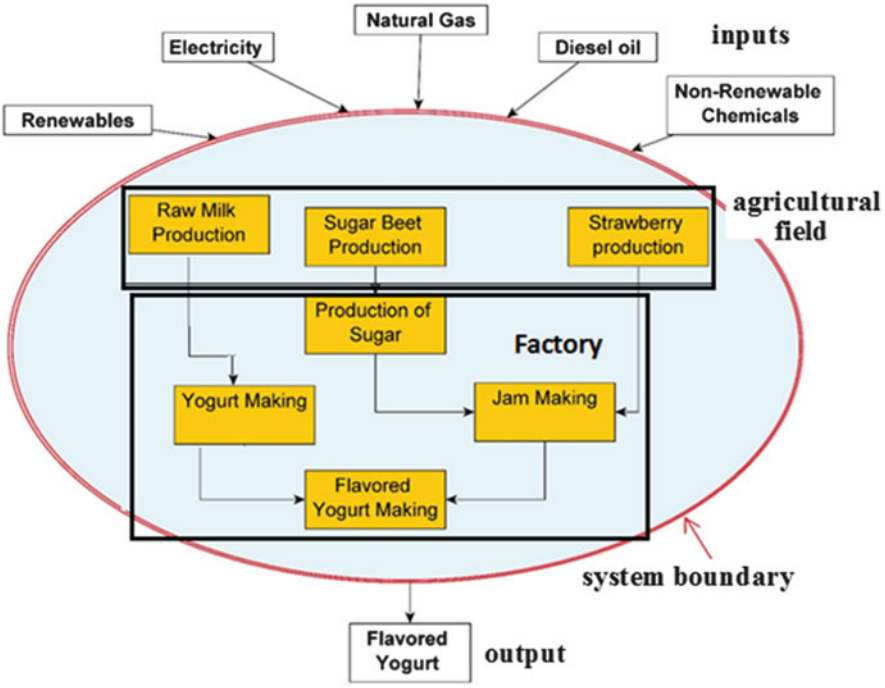

Fig. 1 Flavored yogurt-making process (data adapted from [4])

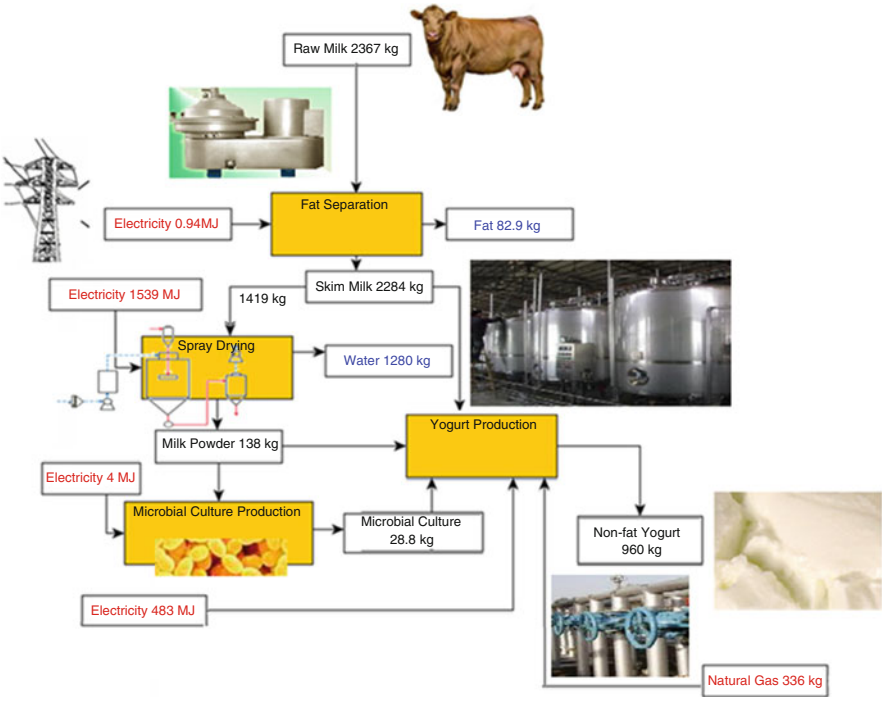

Fig. 2 Mass and energy flow in the flavored yogurt-making process (data adapted from [4])

the inputs and the outputs, which may not be achieved just by plotting the data, and may explain the mechanism of the events. A mathematical model can never be an actual representation of a process, as it would be very difficult, confusing, or impossible to describe the whole system with mathematical formulations. The way that people describe real life in mathematical terms is highly subjective and depends on their previous experience and education. The selection of the parameters for inclusion in the model is highly subjective, and probably the most sensitive point of the model, where invalid decisions may be made. In typical process inputs, $X_1, X_2 \ldots X_n$ may generate the outputs $Y_1, Y_2 \ldots Y_k$, (Fig. 3). A real modeling case study is presented in Fig. 4 where the color of tomatoes changes during a tomato paste production process because of the chemical reactions occurring in the tomatoes. We may use the Barreiro–Milano–Sandoval model [5] to simulate the color change by plugging in the processing conditions and the Hunter Lab (L: lightness; a: redness; b: yellowness when positive, grayness when zero, and blueness when negative) color parameters of the input tomatoes. With a model the cause-and-result relation between the numerical values of the major process inputs ($Z_1, Z_2 \ldots Z_j$) and outputs ($W_1, W_2 \ldots W_h$) may be formulated in mathematical terms after simplification (Fig. 5). Negligible inputs and outputs are not included in the model. The decision about designation of the negligible and non-negligible inputs or outputs involves personal preferences. That is the point where modeling becomes a subjective operation, not an objective work. One of the common difficulties

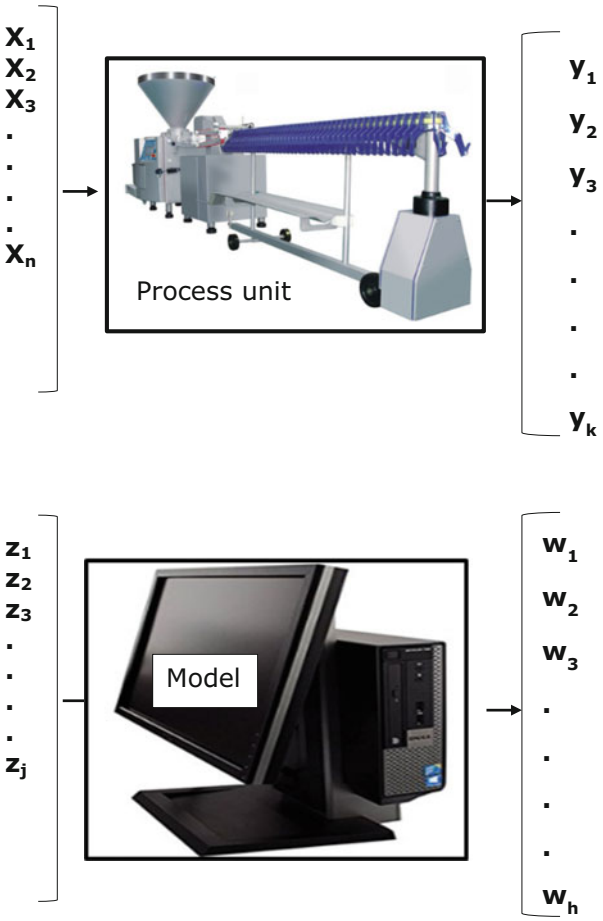

Fig. 3 Comparison of input and output of a process and its model

experienced in modeling is to get lost in the complexity of the process. Referring to "*modeling*" with the word "*kinetics*" in drying studies is an out of standard reference to modeling [6]. Studies which prefer using the phrase "*drying kinetics*" to imply "*modeling*" usually start analysis with "*Fick's second law*", for example, Koukouch et al. [6]. There are also some drying studies in the literature where "*Fick's second law*" was chosen as the starting point of analysis without using the term "*kinetics*" [7]. Gomez de la Cruz et al. [7] referred to the diffusion coefficient they calculated as "*effective diffusivity*" and found it to be related to the sample thickness. There are also some studies in the literature where the term "*kinetics*" refers to the variation of the molecular profile with time without building a mathematical model [8].

The difficulty or complexity level of a mathematical model is a serious decision depending on the aim of the model builder. A model including a lot of detail may be both difficult to build and discouraging to use, and at the same time incur the risk of not including sufficient detail. What is referred to as Fick's second law is actually a

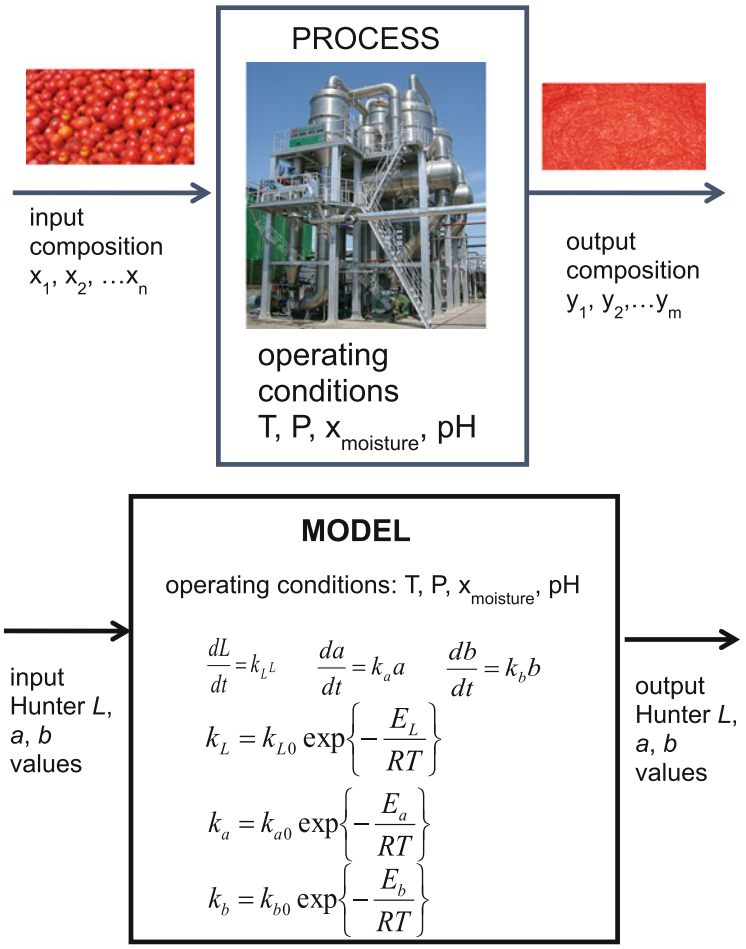

Fig. 4 Schematic description of the color change of the tomatoes during tomato paste production and its simulation with a model

simplified form of the equation of continuity and predicts how diffusion causes the concentration to change with time in a homogeneous media in one dimension:

$$\frac{\partial c_A}{\partial t} = D \frac{\partial^2 c}{\partial x^2}$$

Starting an analysis with "*Fick's second law*" may actually oversimplify the mathematical analysis at the expense of the modeling accuracy. Starting such an analysis after choosing the appropriate terms of the equation of continuity without truncating the significant terms would lead to a more complicated mathematical equation; its solution would probably be more difficult than simply plotting the data but could yield a material-dependent diffusivity, which would not be referred to as

"*apparent*" and not be a function of thickness. One of the best working guides in process modeling is the *80% to 20% rule*, which states "*you get 80% of the benefit with the first 20% of the model complexity*" [9]. It is a loosely defined rule and, in addition to its application within different contexts [10, 11], it is also used in mathematical modeling [2, 3]. It is described as a rule of thumb, that is, a useful principle having wide application but not intended to be accurate or reliable in every situation.

Mathematical models for microbial growth, survival, and inactivation are essential elements in food process modeling [12]. To be useful in a real case, predictive

Rectangular coordinate system

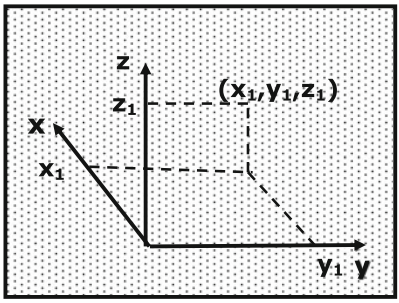

Equation of continuity	Equation of energy
$\frac{\partial c_A}{\partial t}+\left(\frac{\partial N_{Ax}}{\partial x}+\frac{\partial N_{Ay}}{\partial y}+\frac{\partial N_{Az}}{\partial z}\right)=R_A$	$\frac{\partial T}{\partial t}+v_x\frac{\partial T}{\partial x}+v_y\frac{\partial T}{\partial y}+v_z\frac{\partial T}{\partial z}=\frac{\psi_G^{\bullet}}{\rho c}+\frac{\partial}{\partial x}\left(\alpha\frac{\partial T}{\partial x}\right)+\frac{\partial}{\partial y}\left(\alpha\frac{\partial T}{\partial y}\right)+\frac{\partial}{\partial z}\left(\alpha\frac{\partial T}{\partial z}\right)$

Cylindrical coordinate system

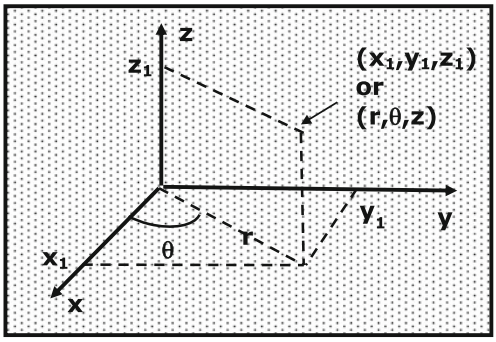

Equation of continuity

$$\frac{\partial c_A}{\partial t}+\left(\frac{1}{r}\frac{\partial\left(rN_{Ar}\right)}{\partial r}+\frac{1}{r}\frac{\partial N_{A\theta}}{\partial\theta}+\frac{\partial N_{Az}}{\partial z}\right)=R_A$$

where $N_{AZ}=x_A\left(N_A+N_B\right)-D_{AB}\frac{dc_A}{dz}$

Fig. 5 Coordinate systems employed with transport phenomena models

Equation of energy

$$\frac{\partial T}{\partial t}+v_r\frac{\partial T}{\partial r}+\frac{v_\theta}{r}\frac{\partial T}{\partial \theta}+v_z\frac{\partial T}{\partial z}=\frac{\dot{\psi}_G}{\rho c}+\frac{1}{r}\frac{\partial}{\partial r}\left(r\alpha\frac{\partial T}{\partial r}\right)+\frac{1}{r^2}\frac{\partial}{\partial \theta}\left(\alpha\frac{\partial T}{\partial \theta}\right)+\frac{\partial}{\partial z}\left(\alpha\frac{\partial T}{\partial z}\right)$$

Spherical coordinate system

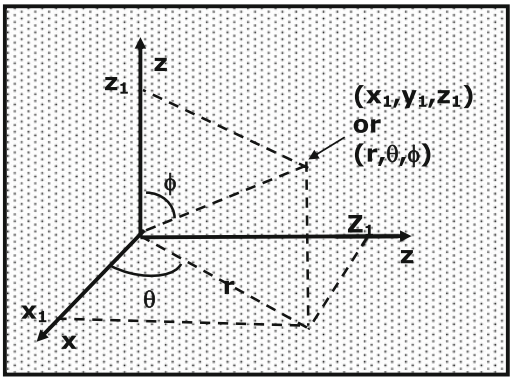

Equation of continuity

$$\frac{\partial c_A}{\partial t}+\left(\frac{1}{r^2}\frac{\partial\left(r^2 N_{Ar}\right)}{\partial r}+\frac{1}{r\sin\theta}\frac{\partial N_{A\theta}\sin\theta}{\partial\theta}+\frac{1}{r\sin\theta}\frac{\partial N_{A\phi}}{\partial\phi}\right)=R_A$$

Equation of energy

$$\frac{\partial T}{\partial t}+v_r\frac{\partial T}{\partial r}+\frac{v_\theta}{r}\frac{\partial T}{\partial \theta}+\frac{v_\phi}{r\sin\theta}\frac{\partial T}{\partial \phi}=\frac{\dot{\psi}_G}{\rho c}+\frac{1}{r^2}\frac{\partial}{\partial r}\left(r^2\alpha\frac{\partial T}{\partial r}\right)+\frac{1}{r^2\sin\theta}\frac{\partial}{\partial\theta}\left(\alpha\sin\theta\frac{\partial T}{\partial\theta}\right)+\frac{1}{r^2\sin^2\theta}\frac{\partial}{\partial\phi}\left(\alpha\frac{\partial T}{\partial\phi}\right)$$

Fig. 5 (continued)

microbial or enzyme inactivation models must be used together with material properties of the food and simulation of heat and mass transfer to the food by employing the transport phenomena models and a predictive microbial model [13]. The material properties may be regarded as the physical properties, such as specific heat or the conduction heat transfer coefficient and the thermodynamic properties of the food. Modeling of each of these properties is explained as a separate issue in this chapter.

2 Transport Phenomena Models

Bird et al. [14] in their monumental book present the derivation of the governing equations of momentum, heat, and mass transfer models (Fig. 5) starting with the shell balances. Özilgen [2] adapted these equations by referring to Bird et al. [14]

without going into the shell balances. It has been almost seven decades since the first edition of the book written by Bird et al. [14]. Information presented therein is regarded as very fundamental knowledge by many chemical engineers, but time has swept away the details, at least for some people, and made it necessary to write this chapter.

The first step of building a mathematical model is definition of the system. The answer to the question "What is going to be predicted by the model by what input data?" should be given when defining the system. Controlling factors of the system should be identified and the data should show the effects of the individual controlling factors. The system may be simplified after neglecting the effects of the marginal inputs, and outputs. The form of the mathematical model may be suggested by an empirical, analog, or phenomenological approach. Availability of information in the literature about the system, skills, and education of the modeler and the purpose of modeling usually determine the form of the model suggested. Comparison of the mathematical model, that is, solution of the equations with the experimental data is the final stage of modeling. The model is validated if it agrees with the data. If such an agreement should not be obtained, all the steps of modeling, starting with the definition of the system, are repeated until a satisfactory representation is reached (Fig. 6).

In Fig. 5, the energy equation is given for the spherical coordinate system as $\frac{\partial T}{\partial t}+v_r\frac{\partial T}{\partial r}+\frac{v_\theta}{r}\frac{\partial T}{\partial \theta}+\frac{v_\varphi}{r\sin\theta}\frac{\partial T}{\partial \varphi}=\frac{\psi_G^{\cdot}}{\rho c}+\frac{1}{r^2}\frac{\partial}{\partial r}\left(r^2\alpha\frac{\partial T}{\partial r}\right)+\frac{1}{r^2\sin\theta}\frac{\partial}{\partial \theta}\left(\alpha\sin\theta\frac{\partial T}{\partial \theta}\right)+\frac{1}{r^2\sin^2\theta}\frac{\partial}{\partial \varphi}\left(\alpha\frac{\partial T}{\partial \varphi}\right)$ This equation originates from shell energy balance [14] where each term has a special meaning, where the term $\frac{\partial T}{\partial t}$ represents the time rate of temperature change at a single point, and where the terms $v_r\frac{\partial T}{\partial r}$, $\frac{v_\theta}{r}\frac{\partial T}{\partial \theta}$, and $\frac{v_\varphi}{r\sin\theta}\frac{\partial T}{\partial \varphi}$ represent the temperature change along the radial direction produced by the flow in the r, θ, and ϕ directions with velocity v in these directions. The term $\frac{\psi_G^{\cdot}}{\rho c}$ represents the heat generation and the terms $\frac{1}{r^2}\frac{\partial}{\partial r}\left(r^2\alpha\frac{\partial T}{\partial r}\right)$, $\frac{1}{r^2\sin\theta}\frac{\partial}{\partial \theta}\left(\alpha\sin\theta\frac{\partial T}{\partial \theta}\right)$, and $\frac{1}{r^2\sin^2\theta}\frac{\partial}{\partial \varphi}\left(\alpha\frac{\partial T}{\partial \varphi}\right)$ represent the conduction heat transfer rates along the radial, θ, and ϕ directions. Here α is the thermal diffusivity of the food and defined in terms of the density ρ, specific heat c_p, and thermal conductivity k of the food as $\alpha=\rho c_p/k$.

Case study 1. Özilgen and Özilgen [15], when developing a model for pasteurization with microwaves in a tubular flow reactor, started with the energy equation as given in Fig. 5 for the cylindrical coordinate systems:

$$\frac{\partial T}{\partial t}+v_r\frac{\partial T}{\partial r}+\frac{v_\theta}{r}\frac{\partial T}{\partial \theta}+v_z\frac{\partial T}{\partial z}=\frac{\psi_G^{\cdot}}{\rho c}+\frac{1}{r}\frac{\partial}{\partial r}\left(r\alpha\frac{\partial T}{\partial r}\right)+\frac{1}{r^2}\frac{\partial}{\partial \theta}\left(\alpha\frac{\partial T}{\partial \theta}\right)+\frac{\partial}{\partial z}\left(\alpha\frac{\partial T}{\partial z}\right)$$

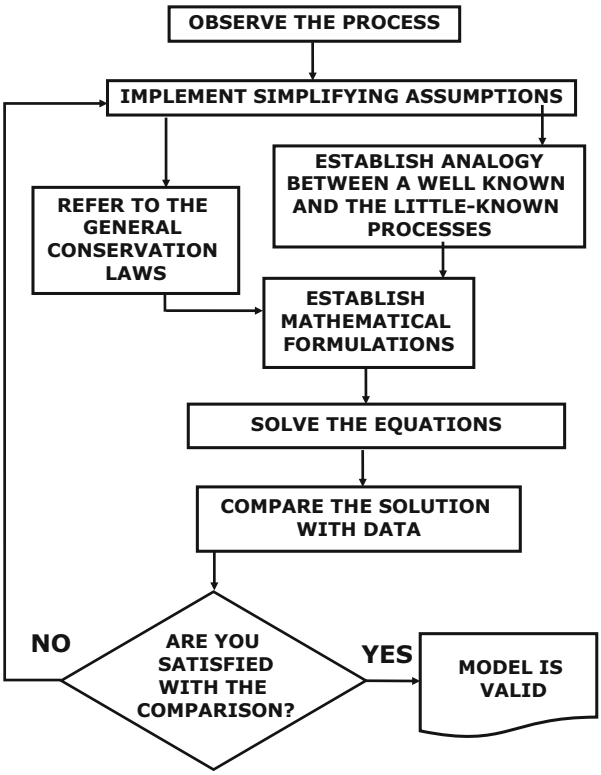

Fig. 6 Schematic description of the events leading to making a decision about the success of the model

In such a flow system, the term representing heat transfer with conduction is substantially smaller than heat transfer caused by flow in:

$$v_r \frac{\partial T}{\partial r} \gg \frac{1}{r} \frac{\partial}{\partial r} \left(r\alpha \frac{\partial T}{\partial r} \right)$$

$$\frac{v_\theta}{r} \frac{\partial T}{\partial \theta} \gg \frac{1}{r^2} \frac{\partial}{\partial \theta} \left(\alpha \frac{\partial T}{\partial \theta} \right)$$

$$v_z \frac{\partial T}{\partial z} \gg \frac{\partial}{\partial z} \left(\alpha \frac{\partial T}{\partial z} \right)$$

The authors, by referring to the 80% to 20% rule, therefore neglected the conduction terms when proceeding with modeling. They knew that they were losing some valuable information here and the apparent convection rates would include those attributable to conduction. On the other hand, the researchers also knew that the molecular mechanism of conduction heat transfer is based on delivering heat from the hotter to the colder molecules with vibration and, in a flow system, heat transfer with conduction would occur at a few orders of magnitudes less than to convection. When indicating such a preference, the authors also knew that their

data were not precise enough to calculate all of these factors separately. When the data are not precise enough, trying to get information at such a significant level would actually mean attempting to model the experimental error. The energy equation gets simpler when $\frac{\partial T}{\partial t} = 0$, for example, under steady-state conditions and when there is no flow in the r and θ directions, for example, $v_r = v_\theta = 0$. Then the final form of the energy equation is

$$v_z \frac{\partial T}{\partial z} = \frac{1}{r} \frac{\partial}{\partial r} \left(r\alpha \frac{\partial T}{\partial r} \right)$$

Case study 2. Özilgen [2], when developing a model for deep fat frying a slab of beef (length $z = 10$ cm, radius $r = 0.8$ cm) started with the equation of energy at the cylindrical coordinates:

$$\frac{\partial T}{\partial t} + v_r \frac{\partial T}{\partial r} + \frac{{v_\theta}^\theta}{r} \frac{\partial T}{\partial \theta} + v_z \frac{\partial T}{\partial z} = \frac{\psi_G^{\bullet}}{\rho c} + \frac{1}{r} \frac{\partial}{\partial r} \left(r\alpha \frac{\partial T}{\partial r} \right) + \frac{1}{r^2} \frac{\partial}{\partial \theta} \left(\alpha \frac{\partial T}{\partial \theta} \right) + \frac{\partial}{\partial z} \left(\alpha \frac{\partial T}{\partial z} \right)$$

The process conditions imply $v_\theta = v_r = v_z = 0$ and $\psi_G^{\bullet} = 0$. The sausage is a thin symmetric cylinder and therefore there is no change produced by θ and conduction through the longer dimension may be neglected. So $\frac{1}{r^2} \frac{\partial}{\partial \theta} \left(\alpha \frac{\partial T}{\partial \theta} \right) = 0$, $\frac{\partial}{\partial z} \left(\alpha \frac{\partial T}{\partial z} \right) = 0$, and the equation becomes

$$\frac{\partial T}{\partial t} = \frac{1}{r} \frac{\partial}{\partial r} \left(r\alpha \frac{\partial T}{\partial r} \right)$$

As α is constant it may be rearranged as

$$\frac{1}{\alpha} \frac{\partial T}{\partial t} - \frac{1}{r} \frac{\partial}{\partial r} \left(r \frac{\partial T}{\partial r} \right) = 0$$

In the same book [2], when modeling drying of rice (radius 1.13 mm, length 6.5 mm) when mass transfer in longitudinal direction was not neglected, the model equation to be solved was

$$\frac{\partial c}{\partial t} = D \left[\frac{1}{r} \frac{\partial}{\partial r} \left(r \frac{\partial c}{\partial r} \right) + \frac{\partial}{\partial z} \left(\frac{\partial c}{\partial z} \right) \right]$$

A good mathematical model should be general (apply a wide variety of situations), realistic (based on correct assumptions), precise (its estimates should be finite numbers, or definite mathematical entities), accurate (its estimates should be correct or very near to correct), and there should be no trend in the deviations of the

model from the experimental data. A good model should be robust (relatively immune to errors in the input data) and fruitful (its conclusions are useful or points the way to other good models).

The 20% to 80% rule employed in mathematical modeling [2] is similar in nature to the diminishing returns hypothesis of economics. This hypothesis states the expected decrease in the incremental output of a production process, as the amount of a single input of production increases continuously while all the others are kept constant [16]. There is evidence that this hypothesis has some applications in nature. Niklas and Cobb [17], when studying the relation between the total leaf area and mass, argued that increases in total leaf area fails to keep pace with increases in total leaf mass across plants differing in size using data from 46 plants with diameters ranging from 0.125 to 0.485 m across 25 woody dicot species.

Choosing an appropriate coordinate system (Fig. 5) with an appropriate origin may facilitate the modeling process substantially. A cylindrical coordinate system with the z axis located on the center line of the cylinder is preferred when the equation of continuity is used to describe the drying behavior of a cylindrical rice grain; a spherical coordinate system with the origin located at the center of the tuber is preferred when the equation of energy is used to evaluate the temperature profiles along a spherical potato.

3 Thermodynamic Modeling

The entire theme of the science of thermodynamics is based on modeling. We may refer to Table 1 for the equations employed in thermodynamic analysis. In a closed system no mass passes through the system boundaries, and the first law may be expressed as

$$\sum_i \dot{Q}_i - \dot{W} = \frac{d\left[m\left(u + e_p + {}^p e_k\right)\right]_{\text{system}}}{dt}$$

When the kinetic and potential energy changes in the system are negligibly small in comparison with the change of the internal energy, we may obtain the following expression:

$$\Delta u = q + w$$

where $\Delta \underline{u}$ is the change in the internal energy per unit mass of the contents of the system between the end and the beginning of the process; similarly, q and w refer to the heat transferred to the closed system and the work done by the unit mass of the contents of this closed system, respectively. In thermodynamic studies, which are often carried out by scientists unfamiliar with mathematical modeling, it is customary to refer to $\Delta u = q + w$ as the first law of thermodynamics. Daniels and

Table 1 Governing equations of mass, energy, entropy, and exergy

Mass balance $\sum_{\text{in}} \dot{m}_{\text{in}} - \sum_{\text{out}} \dot{m}_{\text{out}} = \frac{dm_{\text{system}}}{dt}$
Energy balance (first law of thermodynamics)
$\sum_{\text{in}} \left[\dot{m}\left(h + e_p + e_k\right)\right]_{\text{in}} - \sum_{\text{out}} \left[\dot{m}\left(h + e_p + e_k\right)\right]_{\text{out}} + \sum_i \dot{Q}_i - \dot{W} = \frac{d\left[m\left(u + e_p + {}^p e_k\right)\right]_{\text{system}}}{dt}$
Entropy balance (second law of thermodynamics)
$\sum_{\text{in}} [\dot{m}s]_{\text{in}} - \sum_{\text{out}} [\dot{m}s]_{\text{out}} + \sum_i \frac{\dot{Q}_i}{T_{b,i}} + \dot{S}_{\text{gen}} = \frac{d[m\ s]_{\text{system}}}{dt}$
Exergy balance (second law of thermodynamics)
$\sum_{\text{in}} [\dot{m}ex]_{\text{in}} - \sum_{\text{out}} [\dot{m}ex]_{\text{out}} + \sum_i \left(1 - \frac{T_0}{T_{b,i}}\right)\dot{Q}_i - W - \dot{E}x_{\text{destr}} = \frac{d[m\ ex]_{\text{system}}}{dt}$

where u, h, e_p, and e_k are the internal energy, enthalpy, potential energy, and kinetic energy, respectively; subscripts "in" and "out" refer to the "input" and "output," "system" refers to the contents within the system boundaries, $\dot{m}$, $\dot{Q}_i$, and $\dot{W}$ are the mass, heat flow, and work performance rates, respectively; s is entropy, ex is exergy; $\dot{S}_{\text{gen}}$ and $\dot{E}x_{\text{destr}}$ are the entropy generation and the exergy destruction rates, respectively

Alberty [18], when presenting this equation in their book "*Physical Chemistry*," indicated very clearly that this equation is valid for "*closed systems*." Unfortunately, this expression is used without considering that it is valid for a closed system only as the starting point of a very large number of studies in the literature.

Entropy generation refers to the extent of the irreversibilities (losses) in a process. For an actual process, it is always positive. For an ideal system that undergoes a totally reversible process, entropy generation is zero. However, entropy generation can never be negative when we consider an entire system. There are numerous studies in the literature in which, when the researchers do not start with the open system thermodynamic equations as listed in Table 1, an attempt is made to use the closed system equations to model an open system. In a closed system, entropy change refers to the difference between the final and initial entropies of a system. When we use the entropy balance equation of Table 1 to describe the entropy balance around an open system (Fig. 7), $\sum_{\text{in}} [\dot{m}s]_{\text{in}}$ describes the entropy input to a system, $\sum_{\text{out}} [\dot{m}s]_{\text{out}}$ the entropy output from the system, $\sum_i \frac{\dot{Q}_i}{T_{b,i}}$ the entropy generation produced by the heat exchange between the system and its environment, $\dot{S}_{\text{gen}}$ the entropy generation from any source other than heat transfer, and $\frac{d[m\ s]_{\text{system}}}{dt}$ the entropy accumulation rate in the system.

Entropy of a system may:

- Remain constant (if the system undergoes a steady-state process)
- Increase (if the system gets "disordered")
- Decrease (if the system achieves a higher ordered state)

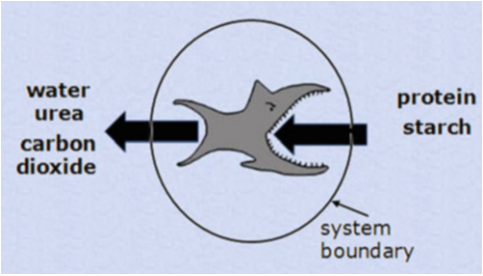

Fig. 7 Schematic description of the entropy balance around a living body

Mass, energy, and exergy balances establish the basis for thermodynamic modeling (Table 1) [1]. Figure 7 describes a nutrient uptake process, where the nutrients such as proteins, starch, and others have highly ordered, low-specific-entropy, structures and the food waste consists of smaller, for example, high-specific-entropy, molecules. After remembering that specific entropy implies entropy per mass, we may conclude that the waste has higher entropy than the inputs. The living creatures such as the fish in Fig. 7 maintain highly ordered structures [1, 19, 20]. According to the "*behavioral homeostasis theory*," in the case of external changes an organism rapidly rearranges itself to cope with new stimuli and minimizes unnecessary energy expenditure [21]. Neglecting the fact that the fish described in Fig. 7 represents an open system can definitely lead to a wrong conclusion. Unfortunately there are numerous studies in the literature ignoring this fact.

After the Arab–Israeli wars of the 1970s, oil prices quadrupled between October 1973 and January 1974 [22]. The perception of energy changed after this price hike and energy sources are starting to be regarded as valuable commodities, research for their conservation having increased dramatically. In the 1990s, reducing the greenhouse gas emissions from food consumption was recognized as an important issue [23]. In the following decades, reports were prepared [24, 25] on work to reduce the impact of food production on the environment. A major fraction of these emissions is related to energy utilization. Between 1970 and 2010, the world-average annual energy utilization for food production increased from 10,008 to 11,850 kJ/person [26]. Within this context, studies were carried out to calculate the energy utilization in the farm-to-fork food production chains, including production of hamburgers [27], bread [28], and meat [29]. The results of these studies make it possible to determine the most energy inefficient and greatest carbon dioxide emitting steps of food production. In a comprehensive review, Rodriguez-Gonzales et al. [30] examined the energy requirements of alternative food-processing technologies, including high-pressure processing, membrane filtration, pulsed electric fields, and ultraviolet radiation, to determine the less-energy-efficient technologies and suggest their replacement with more-energy-efficient ones. The first law of thermodynamics states that energy is conserved; that is, energy can neither be created nor destroyed. However, energy can be transferred from one system to another via heat, work, or mass transfer. The first law does not differentiate between the different modes of energy transfer.

The second law makes this differentiation by defining "entropy," which is a measure for randomness and increases because of losses involved in the processes. It provides insight on the irreversibilities, helps to quantify the energy losses, and proposes measures for minimization of the loss. The exergy balance equation can be derived by multiplying the entropy balance equation with T_0 and subtracting it from the energy balance equation. In the modeling studies aiming at increasing the energy efficiency of the processes, the models were based on the first law of thermodynamics until the 1980s. The basic concept that the models are based on shifted after this date and they were then based on the second law of thermodynamics.

Based on the second law, exergy (also called availability) is defined as the useful work potential above the dead state (Fig. 8). There are some attempts to define internationally recognized reference points for exergy calculations [31]. Exergy of a system is the maximum work that this system can produce if it is brought to thermal, mechanical, and chemical equilibrium with its surroundings via reversible processes. In other words, exergy is the maximum energy content that can be extracted from a system without violating the laws of thermodynamics [32]. The term exergy comes from the Greek words "*ex, from*" and "*ergon, work*" [33]. There are numerous modeling studies in the literature based on exergy analysis. Özilgen and Sorgüven [34] used energy- and exergy-based models for determination of their use and carbon dioxide emission in vegetable oil production; Sorgüven and Özilgen [4] performed a similar modeling study for the flavored yogurt production process. Çatak et al. [35] suggested referring to lifespan entropy generation by the masseter muscle during chewing as an indicator of life expectancy. After noting that the people living in different regions of Turkey have different food habits, Kuddusi [36] calculated the lifetime entropy generation per unit mass of a person and found substantial differences in their life expectancy. Rodriguez-Illera et al. [37] employed a similar

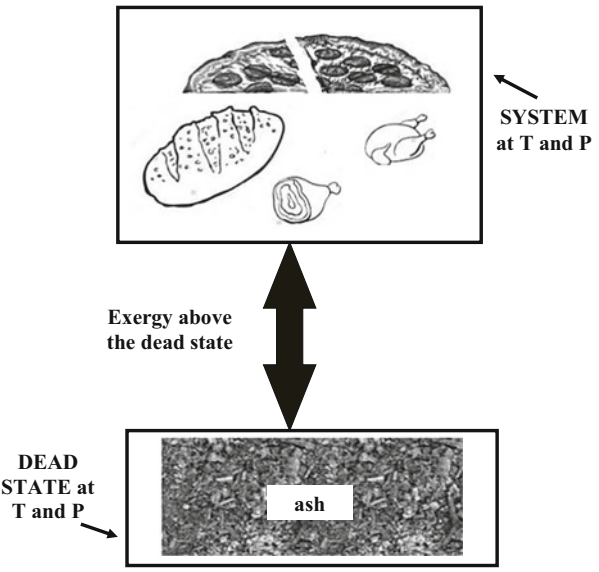

Fig. 8 Schematic description of the exergy of model foods with respect to the common reference "*dead state*"

methodology to determine the exergy efficiency from staple food ingredients to body metabolism by focusing on carbohydrates.

Drying is among the higher amounts of energy utilizing food processing operations because of the energy requirement for the phase change of water. There is a very large number of exergy modeling studies in the literature which analyze drying [38–42]. Icier et al. [43] carried out exergy efficiency studies by using tray, fluidized bed, and heat pump dryers during the processing of broccoli florets and found that the fluidized bed dryer had the highest exergy efficiency (90.86%). Aghbashlo et al. [44] studied the exergy efficiency of the fish oil microencapsulation process by spray drying and reported that the process exergy efficiency was between 1.64% and 14.43%. Tea processing consists of numerous drying stages. Individual stages of the tea production have been the subject of thermodynamic analysis, including withering [45] and drying [46–48]. Erbay and Koca [39] studied the performance of a pilot scale spray dryer during white cheese powder production. Saygi et al. [40] evaluated the performance of a spray drying process of a fruit puree by means of energy and exergy analyses. Experimental exergy analysis is a time-consuming and costly process. With the use of mass, momentum, energy, entropy, and exergy balance equations, the times and costs can be reduced with determination of the most efficient conditions [38]. Nasiri et al. [49] carried out a detailed exergy analysis of an industrial scale ultrafiltered (UF) cheese production plant and Lokadan et al. [50] carried out similar studies with an industrial scale yogurt production plant in order to provide comprehensive insights into the performance of the whole plant and its main subcomponents, including the steam generator, above-zero refrigeration system, pasteurization line, and UF cheese production line.

4 Kinetic Modeling

There are basic differences between the reactions occurring in chemical reactors and food systems. In food systems, numerous chemicals are present in the same location. Therefore, chain reactions are common. In such a system, numerous products and reactants may react [51, 52]. Factors such as light and packaging [52, 53] and the presence of natural antioxidants [53] are among the factors complicating this scheme. It is a very difficult task to present a mathematical model based on the real mechanism in such a sophisticated system. The vast majority of the kinetic models employed for such systems are either apparent or analogy models. Deterioration of foods is usually simulated in analogy with first- or zero-order irreversible monatomic reactions [54]:

$$\frac{dc_A}{dt} = -kc_A$$

or

$$\frac{dc_A}{dt} = -k$$

This does not mean that the reactions taking place are very simple reactions but rather shows that complex systems can be simulated with an apparently simple mathematical models. A first-order apparent reaction may imply that the variation of the other chemicals either has no influence or is relatively negligible in comparison with the chemical of interest. A zero-order apparent reaction implies that the variation is not related to chemical reactions but rather related to other factors, such as mass transfer.

Temperature dependence of reaction rate constants is generally expressed with the Arrhenius expression:

$$k = k_0 \exp\left\{-\frac{E_a}{RT}\right\}$$

The Arrhenius equation is empirical in nature. Eyring and coworkers [18, 55] offered a theoretical explanation for its parameters:

$$E_a = \Delta H^* + RT$$
$$k_0 = 2.72\left(\frac{RT}{N_A h}\right)\exp\left\{\frac{\Delta S^*}{R}\right\}$$

where h is the Planck's constant, N_A is Avagadro's number, and ΔS^* is the activation entropy. Parameter k_0 is related to E_a:

$$\ln k_0 = \alpha E_a + \beta$$

and the activation entropy ΔS^* is related to the activation enthalpy ΔH^* through the kinetic compensation relations:

$$\Delta S^* = \delta \Delta H^* + \phi$$

implying that any change in parameter ln k_0 would be compensated by the change in E_a and any change in ΔS^* would be compensated by a change in ΔH^*. Although parameters k_0, E_a, ΔS^*, and ΔH^* change with the experimental conditions, parameters α, β, δ, and ϕ are constants. Because of the kinetic compensation, parameters E_a, ΔS^*, ΔH^*, and ϕ are not actually independent of each other and when one of them changes with the experimental conditions the others are affected by it. The possible relation between these constants is explained in detail by Özilgen and Özilgen [56].

Predictive microbial models may be used to describe the behavior of microorganisms under different physical and chemical conditions, such as temperature, pH, and water activity. A comprehensive review of these models allows the prediction of microbial safety or shelf life of the products and facilitates development of the

HACCP programs [57]. Microbial kinetics are mostly based on the analogy between the microbial processes and the chemical- or enzyme-catalyzed reactions.

Specific growth rate μ is a constant in the exponential growth phase, which implies that the growth rate is proportional to the viable microbial population, where all the members have equal potential for growth. The specific growth rate may be regarded as the frequency of producing new microorganisms by those already present. When microbial proliferation occurs in a substrate-limited medium, specific growth rate may be related to the substrate concentration by the Monod equation:

$$\mu = \frac{\mu_{\max} c_S}{c_S + K}$$

where c_S is the substrate, for example, carbon source, concentration K is a constant, and μ is the specific growth rate of the microorganism. There are numerous variations of the Monod equation available in the literature [58]. The most common empirical modifications of the Monod equation including substrate and product inhibition are

$$\mu = \frac{\mu_{\max} c_S}{c_S + K + \frac{c_s^2}{K_s}}$$

and

$$\mu = \frac{\mu_{\max} c_S}{c_S + K} \frac{K_p}{K_p + c_p}$$

where K_s and K_p are constants and c_p is the product concentration.

The logistic model is frequently used to simulate microbial growth when a microbial population inhibits its own growth via depletion of a limited nutrient, product accumulation, or unidentified reasons:

$$\frac{dx}{dt} = \mu\, x\left(1 - \frac{x}{x_{\max}}\right)$$

where μ is initial specific growth rate and $x_{\max}$ is the maximum attainable value of x. The logistic equation is an empirical model and it simulates the data when the microbial growth curve follows a sigmoidal path to attain the stationary phase. It is mostly based only on experimental observations. When $x \ll x_{\max}$, the term in parenthesis is almost one and is neglected, and then the equation simulates the exponential growth. When x is comparable with $x_{\max}$, the term in parenthesis becomes important and simulates the inhibitory effect of overcrowding on microbial growth. When $x = x_{\max}$, the term in parenthesis becomes zero, and then the equation predicts no growth, that is, the stationary phase as described with the logistic equation and may be integrated as

$$x = \frac{x_0 e^{\mu t}}{1 - \frac{x_0}{x_{\max}}(1 - e^{\mu t})}$$

The exponential growth model may be modified after substituting

$$\mu = \mu_0 + \mu_1 x - \mu_2 x^2$$

to simulate the Allee effect, which represents a population with maximum specific growth rate at intermediate microbial concentrations when μ_0, μ_1, and μ_2 are positive constants [59].

When parameter μ is a function of time such that

$$\frac{d\mu}{dt} = -\alpha\mu$$

we obtain the Gompertz model, which may also be used to simulate the sigmoidal behavior of the microbial growth curve (α = constant). The Gompertz model is usually expressed in three equivalent versions [59]:

$$\frac{dx}{dt} = \mu\, x, \frac{d\mu}{dt} = -\alpha\, \mu$$

$$\frac{dx}{dt} = (\lambda e^{-\alpha\, t})x$$

and

$$\frac{dx}{dt} = (\kappa \ln x)x$$

where λ and κ are constants.

Primary metabolites are produced by the microorganism for its own metabolic activity. Secondary metabolites are usually produced against the external factors, that is, production of antibiotics starts in the stationary phase to prevent consumption of the limited nutrients by the other microbial species. The yeast *Saccharomyces cerevisiae* may be regarded as a product itself when produced as an additive to achieve leavening in the bakery industry. Sugars are consumed in the energy metabolism. Some microorganisms may not convert them into carbon dioxide but follow a shorter path and excrete the metabolic end products as ethanol or lactic acid. Product formation models relate the product formation rate to fermentation variables, that is, growth rate, biomass, substrate concentration, etc. The Luedeking and Piret [60] model is among the most popular product formation models of food processing interest:

$$\frac{dc_{\mathrm{Pr}}}{dt} = \alpha x + \beta \frac{dx}{dt}$$

where c_{Pr} is product concentration and α and β are constants. The microbial product referred to here is not necessarily a useful product, such as lactic acid [60], xanthan gum [61], or amino acids [62], but may be a detrimental product for the microorganisms, such as an exotoxin [63]. The term αx represents the product formation rate by the microorganisms regardless of their growth; $\beta \frac{dx}{dt}$ represents the additional product formation rate during growth in proportion with the growth rate. This is an empirical equation because it simply relates the experimental observations, mostly without much theoretical basis. When growth-associated product formation rates are much greater than the non-growth-associated product formation rates the Luedeking and Piret equation may be written as

$$\frac{dc_{\mathrm{Pr}}}{dt} = \beta \frac{dx}{dt}$$

When non-growth associated product formation rates are much greater than the growth-associated product formation rates, the Luedeking and Piret model becomes

$$\frac{dc_{\mathrm{Pr}}}{dt} = \alpha x$$

Structured and age distribution models relate cellular structure or age distribution to growth and product formation rates, but need more information for application, are generally difficult to use, and are not widely employed in food research. They are therefore not considered here, but an interested reader may refer to Bailey and Ollis [64] for a detailed discussion.

Microbial death kinetics has a significant importance in food processing as it is one of the major phenomena occurring during pasteurization and sterilization processes. Microbial death is generally described in analogy with a unimolecular, irreversible, first-order rate expression:

$$x \text{ (live microorganism)} \xrightarrow{k_d} x_d \text{ (dead microorganism)}$$

$$\frac{dx}{dt} = -k_d x$$

or

$$\frac{d(\log x)}{dt} = -\frac{1}{D_T}$$

where

$$D_T = \frac{\ln(10)}{k_d}$$

The D_T value is defined as the heating time at constant temperature T to reduce the microbial population by one log cycle, or 10% of its initial value. The z value is defined as the temperature difference required to change the D_T value by a factor of ten, or one log cycle:

$$\frac{d(\log D_T)}{dT} = -\frac{1}{z}$$

This equation may be rearranged and integrated as

$$D_T = D_{T_{\text{ref}}} 10^{(T_{\text{ref}} - T)/z}$$

The z value is related to the activation energy of the Arrhenius expression:

$$z = \frac{\ln(10) RTT_{\text{ref}}}{E_a}$$

A comprehensive list of the thermal death parameters D_T and z are provided by FDA [65]. During thermal processing of foods, microbial death and inactivation of the enzymes are always accompanied with loss of nutrients because of thermal degradation, as they share the same medium. Although death of the microorganisms and destruction of the enzymes and toxins are desired, loss of the nutrients is not. In most processes, spores, vegetative cells, and enzymes are destroyed whereas it is desirable that color, flavor, and vitamins survive. Among the constituents to be destroyed, enzymes usually have the highest D_{121} values, and therefore enzyme inactivation is almost the most difficult task to achieve in thermal processing.

5 Modeling of the Material Properties

There are modeling studies in the literature for estimating the physical properties of the foods.

Cornejo et al. [66] presented a method for the estimation of thermal conductivity $k(T)$ and apparent volumetric specific heat $c(T)$ in the freezing temperature range starting at $-40°C$. There are also other correlations estimating the thermal conductivity as parallel or series or another combination of the thermal conductivity of each constituent [67]):

$$k_{\text{eff}} = \sum_{i=1}^{n} v_i k_i \qquad \text{(parallel model)}$$

$$\frac{1}{k_{\text{eff}}} = \sum_{i=1}^{n} \frac{v_i}{k_i} \qquad \text{(series model)}$$

where, k_i = thermal conductivity of the ith component (W/m K) and v_i = volume fraction of the ith component. The Hill–Leitman–Sunderland model simulates heat transfer through a network in a continuous phase with simultaneous parallel and series conduction:

$$k_{\text{eff}} = \left(2\phi - \phi^2\right)k_d + \left(1 - 4\phi + 3\phi^2\right)k_c + \frac{8\left(\phi - \phi^2\right)k_c k_d}{\phi k_c + (4 - \phi)k_d}$$

where $\varphi = 2 - \sqrt{4 - 2v_d}$
k_{eff} = effective thermal conductivity (W/m K)
k_c = thermal conductivity of the continuous phase (W/m K)
k_d = thermal conductivity of the dispersed phase (W/m K)
v_d = volume fraction of the dispersed phase

A comprehensive review of biomaterial thermal property measurements in the cryogenic regime and their use for prediction of equilibrium and non-equilibrium freezing applications in cryobiology is presented by Choi and Bischo [68].

Most foods and biological solutions contain suspended solids. Atkinson and Mavituna [69] recommend using the following equations to predict viscosity of the microbial suspensions:

$$\mu_m = \mu_1 \left\{ \frac{1 + 0.5\phi_s}{(1 - \phi_s)^4} \right\} \qquad \text{Kunitz equation, used when } \phi_s < 0.4$$

$$\mu_m = \mu_1 \left\{ \frac{1.56\phi_s}{0.52 - \phi_s} \right\} \qquad \text{Mori and Ototake equation, used when } \phi_s < 0.1$$

$\mu_m = \mu_l + (1 + 2.5\phi_s)$ Einstein equation, used at low volume fractions
ϕ_s = fraction of the suspended solids
μ_l = viscosity of the liquid phase
μ_s = viscosity of the solid suspension

Magerramov et al. [70] suggested the use of the following equation for estimating the fruit juice viscosities:

$$\eta = A\left(C_t - a\frac{\rho_{\text{Hg0}}}{\rho_{\text{Hg}}}\right)\left(\rho_{\text{Hg}} - \rho\right)\tau - B_t\frac{\rho}{\tau}$$

where the viscometer constants are $A = \frac{\pi\, g\, r_0^4\, H_0}{8 V_{10} l_0}$, $B_t = \frac{m V_{10}}{8\pi\, l_0}(1 + 2\alpha\Delta T)$, $C_t = \left(1 + \frac{h_0 + 3\alpha\ \Delta T\ L_0}{H_0}\right)$, and $a = \left(\frac{h_0}{H_0}\right)$ where V_{10} is the measuring volume, ρ_{Hg} is the density of mercury at the experimental conditions (at experimental T and P), ρ is the density of the liquid under study at the experimental conditions, ρ_{Hg0} is the density of mercury at room temperature, H_0 is the average mercury level drop, L_0 is the average height of the column at the flowing process, h_0 is the height of the column in the lower vessel at the initial position, $\alpha = 4.31 \times 10^{-6}$/K is the linear expansion coefficient of the capillary material, r_0 is the capillary radius, l_0 is the length of capillary, ΔT is the temperature difference between experimental temperature and room temperature, and $m = 1.12$ is a constant introduced to take account of the shape of the capillary ends (correction factor). To calculate the dynamic viscosity from measured quantities, the values of density of the juice under study at the experimental conditions $\rho(P, T)$ are needed.

Vagenas and Karathanos's [71] diffusivity models which relate the effective diffusivity to those in each phase of the porous solids are similar in nature to the thermal conductivity equations:

$$D_{\mathrm{eff}} = (1 - \varepsilon)D_s + \varepsilon D_g \qquad \text{(parallel model)}$$

$$\frac{1}{D_{\mathrm{eff}}} = \frac{(1 - \varepsilon)}{D_s} + \frac{\varepsilon}{D_g} \qquad \text{(series model)}$$

$$\frac{1}{D_{\mathrm{eff}}} = \frac{(1 - f)}{(1 - \varepsilon)D_s + \varepsilon D_g} + f\left[\frac{1 - \varepsilon}{D_s} + \frac{\varepsilon}{D_g}\right] \qquad \text{(mixed model)}$$

where D = diffusivity in the solid, D_{eff} = effective diffusivity, D_g = diffusion in the gas phase, f = constant, and ε = porosity.

When the factors affecting a physical phenomenon are known but the governing equations are too complicated to solve, the relation between these physical factors may be expressed by establishing an empirical expression embracing the dimensionless numbers of the affecting factors. It should be noted that such equations are reliable within the range of the experimental data on which they are based. Convective heat transfer coefficients are usually expressed as a function of the dimensionless numbers:

$$\mathrm{Nu}_D = 0.135(\mathrm{GrPr})^{0.323} + 0.391 \times 10^{-3}$$

This expression is valid for heat transfer to canned Newtonian liquids in a Steritort [72] in the range $24 \leq \mathrm{Nu}_D \leq 272$, $0.4 \leq \mathrm{Re}_D \leq 458$, $2.8 \leq \mathrm{Pr} \leq 476$, $2.0 \times 10^4 \leq \mathrm{Gr} \leq 2.9 \times 10^9$, and $1.13 \leq \mathrm{L/D} \leq 1.37$

where

$\mathrm{Gr} = gD^3\rho^2\beta\Delta T/\mu^2$ = Grashof number based on can diameter (dimensionless)

$\mathrm{Nu}_D = hD/k$ = Nusselt number (based on can diameter, dimensionless)
$\mathrm{Pr} = c\mu/k$ = Prandl number (dimensionless)
$\mathrm{Re}_D = D^2N\rho/\mu$ = Reynolds number (based on can diameter, dimensionless)
D = can diameter (m)
g = gravitational acceleration (m/s^2)
h = convective heat transfer coefficient (W/m^2 K)
k = thermal conductivity (W/m K)
N = revolutions per second
β = coefficient of volumetric expansion (1/K)
μ = viscosity (Pa s)
ρ = density (kg/m^3)

Reynolds number is the ratio of inertial forces to viscous forces within a fluid which is subject to relative internal movement caused by different fluid velocities. Grashof number is the ratio of the buoyant to viscous forces used in heat transfer, when natural convection is involved in the process. Prandtl number is defined as the ratio of momentum diffusivity to thermal diffusivity and the Nusselt number is the ratio of the convective to conductive heat transfer rates across a heat transfer boundary. A comprehensive review of the use of dimensionless numbers in transport phenomena models has been provided by Ruzicka [73].

Özilgen and Sorgüven [1] provided a chapter on the estimation of the thermodynamic properties in their book "*Biothermodynamics, principles and examples*." The same practice is also valid for the estimation of the thermodynamic properties of foods. Food and biological materials are so sophisticated that their thermodynamic properties are not usually available in books. In such cases the detailed chemical formulas of such chemicals may be used to list the groups contributing to their structure, and then the thermodynamic properties of these contributing methods are added up to estimate those of the entire structure. The molecular groups are not chosen randomly. For example, data of radical groups cannot be calculated separately but are taken as a whole. Benson [74], Shieh and Fan [75], Szargut et al. [76], Domalski and Hearing [77], Marrero and Gani [78], and Gharagheizi et al. [79] are among the researchers who made substantial contributions to the development of this method. Kopp's rule may be regarded as one of the pioneering studies of the group contribution methods for the estimation of the specific heat of solids and liquids. Kopp's rule states that specific heat of a solid compound equals the sum of the heat capacities of its constituting atoms as

$$c_p = \sum_{i=1}^{n} n_i c_{p,i}$$

In this equation, c_p of each molecule is determined experimentally and the number of each atom, n_i, in a molecule is set according to the molecular structure. The equation above stated is written for large data sets that include as many molecules as possible. Later, the values of $c_{p,i}$ are determined via regression analysis to minimize the sum of the square error between the measured values of

c_p and their numerical estimates [80]. Enthalpy, Gibbs free energy of formation, and standard chemical exergy are among the thermodynamic properties which may be estimated with the group contribution method.

6 Use of MATLAB in Modeling

A real modeling case study is presented in Fig. 4 where the color of tomatoes changes during tomato paste production process because of the chemical reactions occurring in the tomatoes. We may use the Barreiro–Milano–Sandoval model [5] to simulate the color change by plugging in the processing conditions and the Hunter Lab color parameters (L: lightness; a: redness; b: yellowness when positive, grayness when zero, and blueness when negative) of the input tomatoes. If we have a MATLAB code to solve the model equations it should take only a few seconds to estimate the color of the paste. If the operator does not like the estimated color, he may change the processing conditions until an acceptable estimate is obtained.

MATLAB is a high-level scripting computer language which can be used very easily and efficiently in food process calculations. A scripting language executes the tasks one by one in the same way as a human operator. Every command is executed independently in the given order as when asking people to do something such as:

- Solve the given equation with the given initial conditions for the given time span
- Plot the data with the given legends specifications, plot the model with the given line specifications, and use the requested labels within the given scale

In such a string, the code solves the given equation first and then plots the model as the second step of the task. The code written by the user of MATLAB is the interface provided by the software manufacturer, for example, MATLAB. The interface communicates with the software (path 2). The computations are actually carried out by the software. The details of the computational method are usually explained in detail by the manufacturer. The model equation is obtained as explained in Fig. 9. When we use the software to solve an equation, such as ode45, we create an m-function in the interface, which converts the equation into computer code and communicates the software (path 2). The input data is added to the syntax (path 1), so ode45 communicates it to the software too (path 2). After solving the model equation, the results are sent to the interface by following path 3. The code which is employed in the interface may plot or print out the results (path 4). We frequently repeat the sentence "*comparison of the experimental data and the model is shown in Fig. . ..*" This sentence actually means that two of the boxes given in Fig. 3 are compared. Experimental data are presented, usually with symbols, and represent the process; the mathematical model is obtained through the pertinent steps in the other box and is presented as solid, dashed, or dotted lines. Özilgen [2]

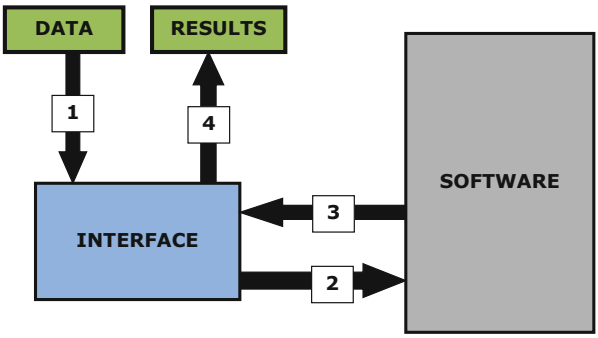

Fig. 9 Schematic description of implication of a mathematical model with MATLAB

and Özilgen and Sorgüven [1] presented fully solved examples of modeling with MATLAB. The following case studies may help to reiterate this subject.

Case study 3. Kinetics of inactivation of the peroxidase isoenzymes during blanching of potato tuber

Peroxidase is usually present in fruit and vegetables as a combination of various isoenzymes with different heat stabilities. During blanching of a spherical potato tuber the controlling equation of the temperature profile is [81]

$$\frac{T - T_1}{T_0 - T_1} = \frac{R}{r}\left(\frac{2}{\pi}\right) \int_{n=0}^{\infty} \left\{ \left\{ \frac{(-1)^{n+1}}{n} e^{-(\pi n)2} \left(\frac{\alpha t}{R^2}\right) \sin\left(\frac{\pi\, nr}{R}\right) \right\} \right.$$

Inactivation kinetics of the enzyme may be described with separate first-order reactions for heat stable and heat labile fractions [81]:

$$\frac{dc_{E1}}{dt} = -k_1 c_{E1}$$

and

$$\frac{dc_{E2}}{dt} = -k_2 c_{E2}$$

Total enzyme activity is

$$c_E = c_{E1} + c_{E2}.$$

Temperature effects on the inactivation rate constants k_1 and k_2 were described with the Arrhenius expression:

$$k_1 = k_{10} \exp\left\{-\frac{E_{a1}}{R_g T}\right\}$$

and

$$k_2 = k_{20} \exp\left\{-\frac{E_{a2}}{R_g T}\right\}$$

The MATLAB code of case study 3 describes the variation of temperature and enzyme activity as a function of time (Fig. 10):

MATLAB CODE CASE STUDY 3

Command Window

```
clear all
close all

% enter the constants of the model
        T1 = [65 70 75]; % blanching water temperature
        k = ['k -', 'k :', 'k.- ']; % color and line characteristics
        T0 = 15; % initial temperature of the potato
        T(1) = T0;
        Rg = 8.3e-3; % gas constant (kJ/mol K)
        alpha = (1.93e-7)*60; % thermal diffusivity (m2/min)
        k0 = 3e14; % pre-exponential constant
        Ea1 = 101.2; % activation energy (kJ/mol)
        Ea2 = 83.6; % activation energy (kJ/mol)
        E1(1) = 0.027; E2(1) = 0.028-E1(1); E(1) = E1(1)+E2(1);

% enter the radius of the potato and the radial distance where the calculations will be done
```

```
        r = 0.5e-2; % distance from the center (m)
        R = 4.1e-2; % radius of the potato (m)

% enter the beginning of the time vector
time(1) = 0;

% determine the temperature profile from the model
      for n=0:100
        s(n+9)=sin(pi*n*r/R);
       end
     Csin = sum(s)*(r/R);

for i=1:length(T1)
       for t=10:10:70
              for n=0:100
                 s(n+9)=(Csin)*exp(-((pi*n)^2)*alpha*t/(R^2))*sin(n*pi*r/R);
               end
          T(t/10+1)=(R/(r))*(sum(s))*(T0-T1(i))+T1(i);
          time(t/10+1)=t;
          ss(t/10+1)=sum(s);
          k1(t/10+1) = k0*exp(-Ea1/(Rg*(T(t/10+1)+273)));
          k2(t/10+1) = k0*exp(-Ea2/(Rg*(T(t/10+1)+273)));
          E1(t/10+1) = E1(1)*exp(-k1(t/10+1)*t);
          E2(t/10+1) = E2(1)*exp(-k2(t/10+1)*t);
          E(t/10+1) = E1(t/10+1) + E2(t/10+1);
       end

            figure(1) % start a new figure
            % plot the temperature profiles as determined by the model
            plot(time,T,k((3*i-2):(3*i)), 'LineWidth',2); hold on
            % define the figure labels
            ylabel('Temperature (C)');
            xlabel('Time (min)');
           % enter the legend and grid requirements
           legend('65 oC','70 oC','75 oC',3,'Location','Best')
           grid on

         % plot the enzyme inactivation model
            figure(2)
            plot(time,E,k((3*i-2):(3*i)),'LineWidth',2); hold on % enzyme inactivation
            ylabel('E (Eu)');
            xlabel('Time (min)');
            legend('65 oC','70 oC','75 oC',3,'Location','Best')
           grid on
end
```

Case study 4. Continuous processing of liquid foods containing particles

In the holding tube of the aseptic processing equipment, when heat transfer from the liquid to the particles may be neglected, the temperature of the liquid (T_L) approaches the ambient temperature (T_a) exponentially:

$$\frac{T_L - T_a}{T_{L0} - T_a} = \exp\left\{-\frac{U_{\text{tube}} A_{\text{tube}}}{\rho_L c_L V_{\text{tube}}}\right\}$$

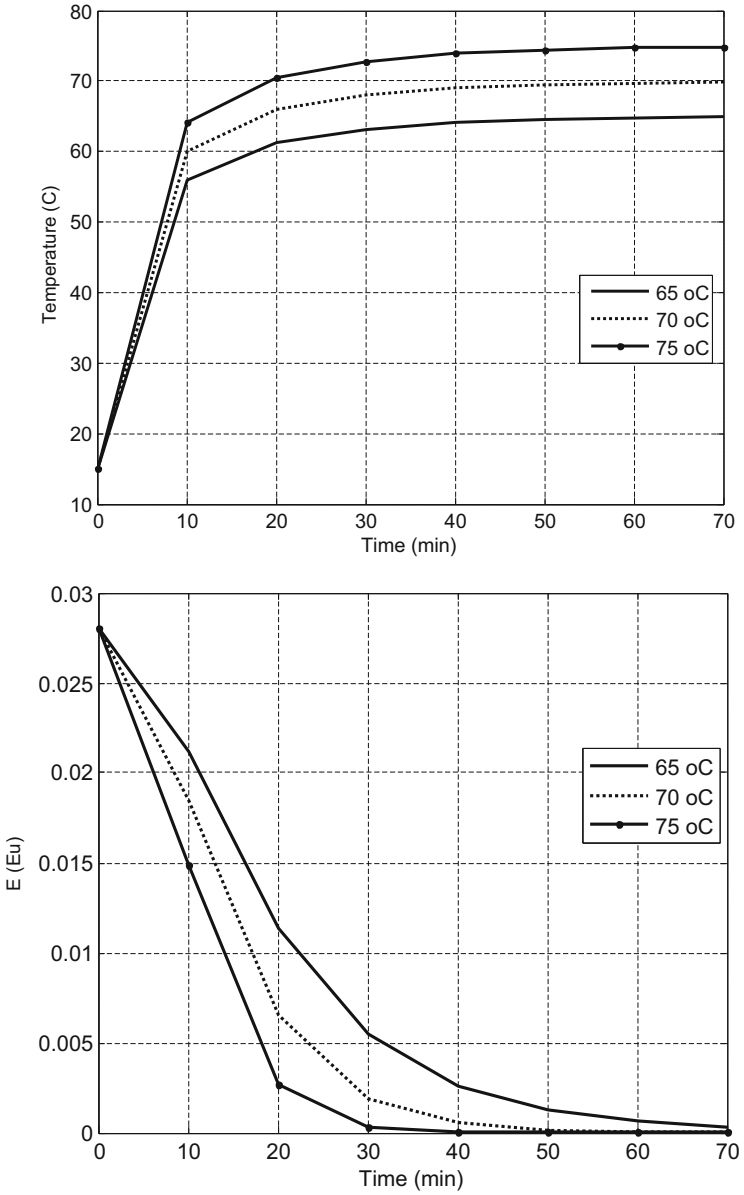

Fig. 10 Temperature and enzyme activity profiles at $r = 0.5$ cm distance from the center during thermal processing of whole potatoes. Constants of the model are adapted from [81]

where T_{L0} is the initial temperature of the liquid at the entrance of the tube, A_{tube}, U_{tube}, and V_{tube} are the heat transfer area, total heat transfer coefficient, and the volume of the tube, respectively, parameter ρ_L is the density, and c_L is the specific heat of the liquid. The governing equation of heat transfer into the particle with conduction is obtained after simplification of the energy equation [82]:

$$\rho_p c_p \frac{\partial T}{\partial t} = k_p \frac{\partial^2 T}{\partial r^2} + k_p \frac{\beta - 1}{\rho} \frac{\partial T}{\partial r}$$

where β is a geometric factor ($\beta = 1$ for infinite slab, $\beta = 2$ for infinite cylinder, $\beta = 3$ for sphere), r is the distance in the heat transfer direction, k_p, ρ_p, and c_p are thermal conductivity, density, and specific heat of the particles, respectively. The initial and the boundary conditions of this equation are

$$\text{Initial condition} \quad T = T_{p0} \quad \text{at } 0 < r < r_p \ \text{ when } t = 0$$

$$\text{Boundary condition} \quad \frac{dT}{dr} = 0 \quad \text{at } r = 0 \ \text{ when } t > 0$$

$$\text{Boundary condition} \quad -k_p \frac{dT}{dr} = h_{Lp}[T_L(t) - T] \quad \text{at } r = r_p \ \text{ when } t > 0$$

where r_p is the radius of the particle and h_{Lp} is the convective heat transfer coefficient from liquid to particle. With a spherical particle ($\beta = 3$), applying the L'Hopital rule at $r = 0$ on the second term of the energy equation gives

$$\text{Boundary condition} \quad \rho_p c_p \frac{\partial T}{\partial t} = 3k_p \frac{\partial^2 T}{\partial r^2} \quad \text{at } r = 0 \text{ when } t > 0$$

The thermal process time required to reduce the initial microbial load x_0 to a final safe final concentration x at a constant temperature T_{ref} is

$$F_{\text{required}} = D_{T_{\text{ref}}} \log(x_0/x)$$

where $\log(x_0/x)$ is the number of the log cycles of microbial reduction required for a safe product and $D_{T_{\text{ref}}}$ is the heating time at T_{ref} for one log cycle of reduction. Parameter $D_{T_{\text{ref}}}$ may be used to compute D_T at any temperature T as

$$D_T = D_{T_{\text{ref}}} 10^{(T - T_{\text{ref}})/z}$$

Thermal processing received under variable temperature $T(t)$ may be calculated as

$$F_{\text{process}} = \int_0^t 10^{(T - T_{\text{ref}})/z_{\text{microorganisms}}} dt$$

and the weighted average F value of a particle is

$$F_{\text{process}} = \int_0^\infty F_i(t) E(t) dt$$

where $E(t)$ is the residence time distribution function. The energy equation is the only equation to be solved to evaluate the time temperature history at the critical

point of the particle to calculate the average $F_{process}$ of the food. The MATLAB code of case study 4 computes the time-temperature profile of the fluid and the particles (at the surface and the center) and the F values of particle (on the surface and center) (Fig. 11). The results are presented in Fig. 12.

MATLAB CODE CASE STUDY 4

Command Window

```
clear all
close all
format compact

% define E(t) as a Gaussian distribution function
deltaE=0.5; % notice that sum(E)=1.0
mu=200; % population mean residence time in the holding tube
sigma=10; % variance of the holding times in the holding tube

% Enter the model constants as adapted from Yang et al. (1992)
kp = 0.556; % W/m2 C
Cpp = 3.27e3; % specific heat of the particles (J/kg C)
Pp = 1040; % particle density (kg/m3)
Ta = 27; % C (air temperature)
Tfi = 135; % initial temperature of the fluid in the holding tube (C)
Uhd = 10; % convection heat transfer coefficient (W/m2 C)
D = 0.0508; % diameter of the holding tube (m)
Pf = 930.8; % fluid density (kg/m3)
Cpf = 4.266e3; % specific heat of the fluid (J/kg C)
Tref = 121.1; % reference temperature (C)
z = 10; % z value

% compute the minimum and the maximum residence times
RTmin=mu-3*sigma; % the minimum residence time
RTmax=mu+3*sigma; % the maximum residence time
RTincrement=(RTmax-RTmin)/61
RT=[RTmin:RTincrement:RTmax]

% compute the expected fraction of the residence times
for j=1:1:length(RT)
E(j)=(1/(sigma*sqrt(2*pi)))*exp(-(1/2).*((RT(j)-mu)/sigma)^2);
end
 % check the sum of the fractions of the residence times (notice sum(E) must be 1)
Esum=sum(E)


n = 22; % n=1 and n=22 refers to fluid, n=2 and n=21 refers to surface, n=12 refers to center
```

```
dr = 0.001; % m
dt = 1; % s

% finite difference solution
T(:,1) = ones(1,(n+1)) * 100; % construct a matrix of 1s only, to replace 1s with the model values later
T(1,1) = Tfi; T((n+1),1) = T(1,1);
% enter the beginning of the time vector
time(1) = 0;

% calculate the model values
for t = 1:mu
   T(1,(t+1)) = Ta - (Ta - Tfi) * exp(- Uhd * 4 * t / (Pf * Cpf * D));
   T((n+1),(t+1)) = T(1,(t+1));
   for i = 2:n
      T(i,(t+1)) = ((3 * kp / (Pp * Cpp)) * dt / (dr^2)) * (T((i+1),t) - 2*(T(i,t)) + T((i-1),t)) + T(i,t);
      F(i,(t+1)) = 10^((T(i,(t+1)) - Tref) / z) * (t / 60); % minutes
   end
   % convert the time in seconds for plotting
   time(t+1) = t;
end

% plot the model
 plot(time, T(1,:), 'k-.','LineWidth', 2.0); hold on % T fluid
[AX,H1,H2] = plotyy(time, T(2,:), time, F(2,:)); hold on % T particle surface and F surface
[AX,H3,H4] = plotyy(time, T(12,:), time, F(12,:)); hold on % T particle center and F particle center

% enter the required line parameters
set(H1, 'LineStyle', '-', 'LineWidth', 1.5, 'Color', 'Black');
set(H2, 'LineStyle', '-', 'LineWidth', 1.5, 'Color', 'Black');
set(H3, 'LineStyle', ':', 'LineWidth', 2.0, 'Color', 'Black');
set(H4, 'LineStyle', '-.', 'LineWidth', 1.5, 'Color', 'Black');

% enter the label requirements
ylabel('Temperature \circ C')
set(get(AX(2),'ylabel'), 'string', 'F (min)')

% enter the limits of the axis in the plot
ylim(AX(2), [0 40])
ylim(AX(1), [80 140])

% enter the legend requirements
legend('T fluid','T particle surface','T particle center','Location','West')
legend(H2,'F particle surface','F particle center','Location','East')
legend(H4,'F particle center','Location','SouthEast')
```

```
% compute the minimum and the maximum processing received by the particle

for t = 1:RTmin
   T(1,(t+1)) = Ta - (Ta - Tfi) * exp(- Uhd * 4 * t / (Pf * Cpf * D));
   T((n+1),(t+1)) = T(1,(t+1));
   for i = 2:n
      T(i,(t+1)) = ((3 * kp / (Pp * Cpp)) * dt / (dr^2)) * (T((i+1),t) - 2*(T(i,t)) + T((i-1),t)) + T(i,t);
      F(i,(t+1)) = 10^((T(i,(t+1)) - Tref) / z) * (t / 60); % minutes
   end
end

fprintf('\nminimum processing received by the particle surface is %.2g min',F(2,RTmin))
fprintf('\nminimum processing received by the particle center is %.2g min \n',F(12,RTmin))

for t = 1:RTmax
   T(1,(t+1)) = Ta - (Ta - Tfi) * exp(- Uhd * 4 * t / (Pf * Cpf * D));
   T((n+1),(t+1)) = T(1,(t+1));
   for i = 2:n
      T(i,(t+1)) = ((3 * kp / (Pp * Cpp)) * dt / (dr^2)) * (T((i+1),t) - 2*(T(i,t)) + T((i-1),t)) + T(i,t);
      F(i,(t+1)) = 10^((T(i,(t+1)) - Tref) / z) * (t / 60); % minutes
   end
end

fprintf('\nmaximum processing received by the particle surface is %.2g min',F(2,RTmax))
fprintf('\nmaximum processing received by the particle center is %.2g min \n',F(12,RTmax))

% compute the average processing received by the particle on the surface and at the center
for j=1:1:length(RT)

% compute the residence time distribution function
E(j)=(1/(sigma*sqrt(2*pi)))*exp(-(1/2).*((RT(j)-mu)/sigma)^2);

for t = 1:RT(j)
   T(1,(t+1)) = Ta - (Ta - Tfi) * exp(- Uhd * 4 * t / (Pf * Cpf * D));
   T((n+1),(t+1)) = T(1,(t+1));
   for i = 2:n
      T(i,(t+1)) = ((3 * kp / (Pp * Cpp)) * dt / (dr^2)) * (T((i+1),t) - 2*(T(i,t)) + T((i-1),t)) + T(i,t);
      F(i,(t+1)) = 10^((T(i,(t+1)) - Tref) / z) * (t / 60); % minutes
   end
end

% compute the F values
FincrementSurface(j)=F(2,(t+1));
FincrementCenter(j)=F(12,(t+1));

end
```

```
FsurfaceAverage=sum(FincrementSurface.*E);
FcenterAverage=sum(FincrementCenter.*E);

% print the computed F values
fprintf('\naverage processing received by the particle surface is %.2g min',FsurfaceAverage)
fprintf('\naverage processing received by the particle center is %.2g min \n',FcenterAverage)
```

When we run the code the following lines and **Fig. 11** will appear in the screen.

```
Esum =
   1.0143

minimum processing received by the particle surface is 25 min
minimum processing received by the particle center is 7.5 min

maximum processing received by the particle surface is 29 min
maximum processing received by the particle center is 19 min

average processing received by the particle surface is 28 min
average processing received by the particle center is 13 min
```

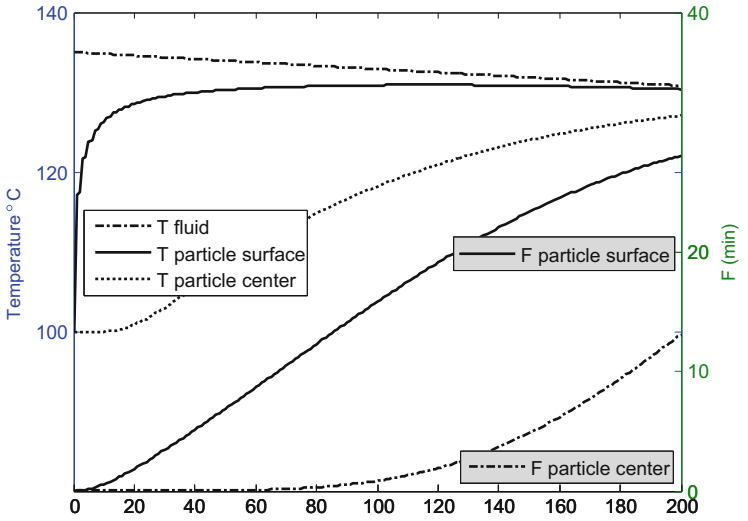

Fig. 11 Variation of the temperature and processing received at different locations with time, when there is no residence time distribution (residence time = population mean residence time)

Case study 5. Predictive quality modeling by using microbial lag time

Predictive microbial models provide rapid, inexpensive, and reliable estimates of shelf life. A food may be regarded as safe as long as the microorganisms remain inactive after processing. Although various other definitions are available, the time required for the initial microbial load to increase twofold may be referred to as the lag time. Predictive microbial modeling is usually a two-step process. First kinetic models are developed to have a full description of the process; then these models,

together with their predetermined constants, are used to predict the microbial quality of the food. An extended logistic equation may be used to simulate microbial growth [84]:

$$\frac{dx}{dt} = \mu_0[T(t) - T_{\min}]^2 \left(\frac{q(t)}{1+q(t)}\right) x \left(1 - \frac{x}{x_{\max}}\right)$$

where μ_0 = constant, $T(t)$ = temperature at time t, and $T_{\min}$ = minimum temperature required for microbial growth. Most of the intracellular chemical reactions follow Michaelis–Menten kinetics. The empirical term $q(t)/1 + q(t)$ may describe the rate-determining step involved in the healing of cellular damage or adaptation to a new growth medium. It is not possible to associate $q(t)$ with a specific metabolite because the rate-determining reactions are usually case specific and may change with time, even in the same case. The temperature dependence term $T(t) - T_{\min} = 0$ when $T(t) < T_{\min}$. The MATLAB code of case study 5 gives prediction of the shelf life of ice cream contaminated with *Listeria monocytogenes*:

MATLAB CODE CASE STUDY 5

Command window

```
clear all
close all

% enter the temperature data
Temperature=[7 4 0 -3 5 2 3 4 5 -1 -2 -3  -4 6 7 2 3 3 5 5 7 4  -4  6 7]; % average daily
storage temperatures

% construct the storage time data vector
n=length(Temperature);
Time=[0:1:n-1]; % storage time

% enter the parameters of the microbial growth kinetics model
mu0=4e-4; % 1/min
Tmin=-2.1; % oC
x0=1; % cfu/g
xMax=1e9; % cfu/g
deltaTime=60*24; % min

% plot the temperature versus time data
plot(Time,Temperature,'k:','LineWidth',2); hold on
ylabel('STORAGE TEMPERATURE (oC)');
xlabel('STORAGE TIME (days)');

% microbial growth model
counter=1;
xk=1; % ice cream is assumed to be contaminated with 1 cfu/g at the beginning of storage
```

```
for i=1:1:n; % calculate the growth based on the extended logistic equation
time(i)=(i-1)*24; % storage time (hours)
timeDays(i)=time(i)/24; % convert the time in h into number of the days in storage
N=timeDays(i);
  TTmin=((Temperature(i)-Tmin))^2;
     if Temperature(i)<=Tmin
       TTmin=0;
     end
         % the term describing the healing of the cellular damage
         q(i)=16e-3+3e-4*(Temperature(i)-4);
          x(i)=xk+mu0*TTmin*(q(i)/(1+q(i)))*xk*(1-(xk/xMax))*deltaTime;
            if x(i)>=80
              if counter==1;
                 % print the number of days in storge
                  fprintf('\nshelf life of ice cream is %.2f days in storage',N)
                 counter=2;
              end
            end
         xk=x(i);
    end
figure; % plot the microbial concentration versus time
plot(timeDays,x,'k-','LineWidth',2); hold on; ylabel('x (cfu/g)'); xlabel('STORAGE TIME
(days)');
legend('MICROBIAL GROWTH CURVE', 'Location','North')
```

When we run the code the following line and **Fig. 12** will appear in the screen:

```
shelf life of ice cream is 19.00 days in storage
```

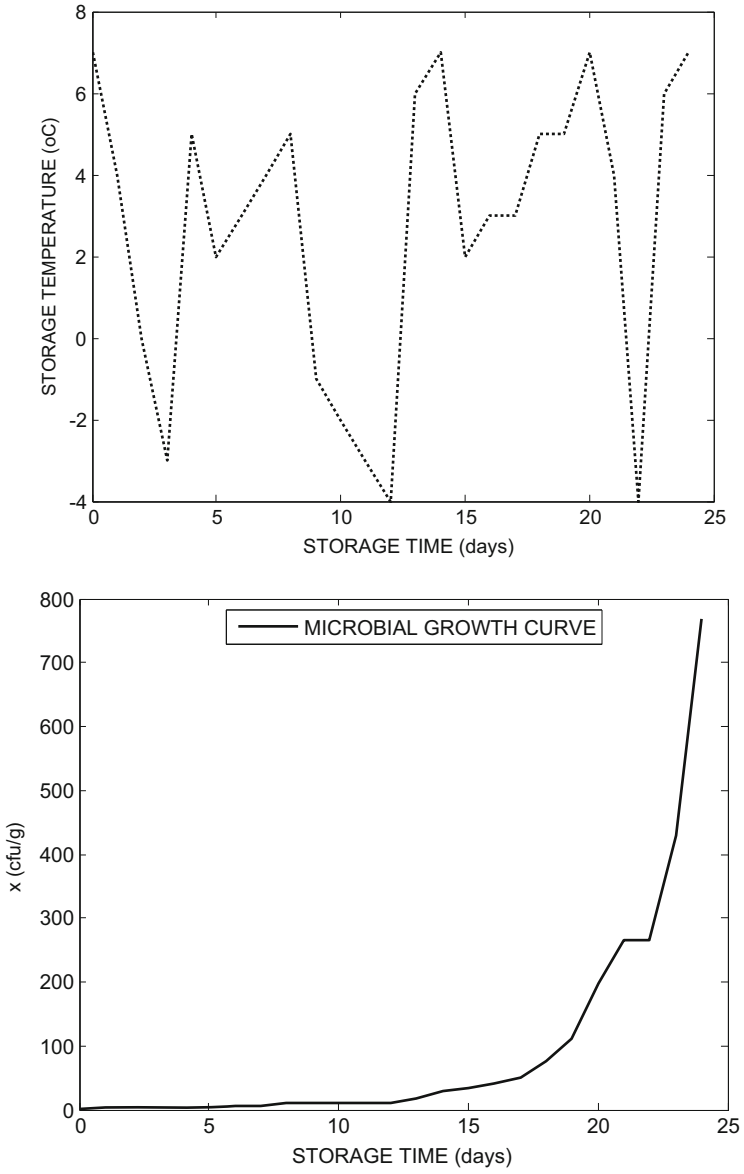

Fig. 12 Storage temperature fluctuations of the ice cream and predicted microbial population of ice cream contaminated with $x_0 = 1$ cfu/g of *Listeria monocytogenes* at $t = 0$ and then subjected to temperature fluctuations in storage. It was assumed that $x_0 = 1$ cfu/g was sufficient to start deterioration and ice cream was inedible when $x = 80$ cfu/g. Model parameters were adapted from Gougouli et al. [83]

7 Overview

Mathematical models based on thermodynamic, kinetic, heat, and mass transfer analysis have been central to this chapter along the same principles as described by Özilgen [2] and Özilgen and Sorgüven [1]. Microbial growth, death, and enzyme inactivation models and the modeling of the material properties, including those pertinent to conduction and convection heating, mass transfer, such as diffusion and convective mass transfer, the thermodynamic properties, such as specific heat, enthalpy, and Gibbs free energy of formation, and specific chemical exergy are the additional models needed in this task. The origins, simplifying assumptions, and uses of the model equations are discussed in this chapter together with their benefits. The simplified forms of these models are sometimes referred to as "*laws*," such as "*the first law of thermodynamics*" or "*Fick's second law*." Starting to model study with such "*laws*" without considering the conditions under which they are valid runs the risk of ending up with erronous conclusions. On the other hand, models started with the fundamental concepts and simplified with appropriate considerations may offer explanations to the phenomena which may not be obtained just with measurements or unprocessed experimental data. The discussion presented here is strengthened with case studies and references to the literature.

References

1. Özilgen M, Sorgüven E (2016) Biothermodynamics. Taylor & Francis, Boca Raton
2. Özilgen M (2011) Handbook of food process modeling and statistical quality control. Taylor and Francis, Boca Raton
3. Özilgen M (1998) Food process modeling and control, chemical engineering applications. Gordon and Breach, Amsterdam
4. Sorgüven E, Özilgen M (2012) Energy utilization, carbon dioxide emission, and exergy loss in flavored yogurt production process. Energy 40:214–225
5. Barreiro JA, Milano M, Sandoval AJ (1997) Kinetics of color change of double concentrated tomato paste during thermal treatment. J Food Eng 33:359–371
6. Koukouch A, Idlimam A, Asbik M, Brahim Sarh B, Izrar B, Bostyn S, Bah A, Omar Ansari O, Zegaoui O, Amine A (2017) Experimental determination of the effective moisture diffusivity and activation energy during convective solar drying of olive pomace waste. Renew Energy 101:565–574
7. Gomez de la Cruz FJ, Palomar-Carnicero JM, Casanova-Pelaez PJ, Cruz-Peragon F (2015) Experimental determination of effective diffusivity during the drying of clean olive stone: dependence of temperature, moisture, moisture content and thickness. Fuel Process Technol 137:320–326
8. Caldeira I, Santos R, Ricardo-da-Silva JM, Anjos O, Mira H, Belchior AP, Canas S (2016) Kinetics of odorant compounds in wine brandies aged in different systems. Food Chem 211:937–946
9. Glasscock DA, Hale JC (1994) Process simulation: the art and science of modeling. Chem Eng 101(11):82–89
10. Bender PS (1981) Mathematical modeling of the 20/80 rule: theory and practice. J Bus Logistics 2:139–157

11. Furman ME (1997) Reverse the 80–20 rule. Manag Rev 86(1):18–21
12. Marks BP (2008) Status of microbial modeling in food process models. Compr Rev Food Sci Food Safety 7:137–143
13. Lebert I, Lebert A (2006) Quantitative prediction of microbial behaviour during food processing using an integrated modeling approach: a review. Int J Refrig 29:968–984
14. Bird RB, Steward WE, Lightfoot EN (1960) Transport phenomena. Wiley, New York
15. Özilgen S, Özilgen M (1991) A model for pasteurization with microwaves in a tubular flow reactor. Enzyme Microb Technol 13:419–423
16. Case KE, Fair RC, Oster SE (2009) Principles of microeconomics, 9th edn. Pearson Prentice Hall, Upper Saddle River
17. Niklas KJ, Cobb ED (2008) Evidence for "diminishing returns" from the scaling of stem diameter and specific leaf area. Am J Bot 95:549–557.
18. Daniels F, Alberty RA (1975) Physical chemistry, 4th edn. Wiley, New York
19. Balmer RT (1982) Entropy and aging in biological systems. Chem Eng Commun 17:171–181
20. Schrödinger E (1944) What is life? The physical aspects of a living cell. Cambridge University Press, Cambridge
21. Einstein EM, Eisenstein DL, Sarma JSM, Knapp H, Smith JC (2012) Some new speculative ideas about the "behavioral homeostasis theory" as to how the simple learned behaviors of habituation and sensitization improve organism survival throughout phylogeny. Commun Integr Biol 5(3):233–239
22. Park S-H (1992) Falling oil prices and exchange rate fluctuation. In: Shojai S, Katz BS (eds) The oil market in the 1980s. Praeger, New York
23. Carlsson-Kanyama A (1998) Climate change and dietary choices - how can emissions of greenhouse gases from food consumption be reduced. Food Policy 23:277–293
24. CIAA (2007) Managing the environmental stability in the European food & drink industries. Confederation of the Food and Drink Industries of the EU, Brussels. Available at http://www.fooddrinkeurope.eu/documents/brochures/brochure_CIAA_envi.pdf. Accessed 22 Feb 2015
25. Foster C, Green K, Bleda M, Dewick P, Evans B, Flynn A, Mylan J (2006) Environmental impacts of food production and consumption: a report to Department of Environment, Food and Rural Affairs. Manchester Business School. Defra, London. Available at http://www.ifr.ac.uk/waste/Reports/DEFRA-Environmental%20Impacts%20of%20Food%20Production%20%20Consumption.pdf. Accessed 5 Jan 2017
26. Smith P et al (2014) Agriculture, Forestry and Other Land Use (AFOLU). In: Edenhofer et al (ed) Climate change 2014: mitigation of climate change. Contribution of working group III to the fifth assessment report of the intergovernmental panel on climate change. Cambridge University Press, Cambridge. Available at https://www.ipcc.ch/pdf/assessment-report/ar5/wg3/ipcc_wg3_ar5_chapter11.pdf. Accessed 25 July 2016
27. Carlsson-Kanyama A, Faist M (2008) Energy use in the food sector: a data survey. Available at http://mmm.comuv.com/wordpress/wp-content/uploads/2010/06/Energy-use-in-the-food-sector-Carlsson-Kanyama-and-Fiest.pdf. Accessed 9 Aug 2013
28. Değerli B, Nazir S, Sorgüven E, Hitzmann B, Özilgen M (2015) Assessment of energy and exergy efficiencies of *farm to fork* grain cultivation and bread making processes in Turkey and Germany. Energy 93:421–434
29. Opio C, Gerber P, Mottet A, Falcucci A, Tempio G, MacLeod M, Vellinga T, Henderson B, Steinfeld H (2013) Greenhouse gas emissions from ruminant supply chains – a global life cycle assessment. Food and Agriculture Organization of the United Nations (FAO), Rome
30. Rodriguez-Gonzales O, Buckow R, Koutchma T, Balasubramaniam VM (2015) Energy requirements for alternative processing technologies – principles, assumptions, and evaluation of efficiency. Compr Rev Food Sci Food Safety 14:536–554
31. Szargut J, Valero A, Stanek W, Valero A (2005) Towards an international reference environment of chemical exergy. Elsevier Science, Oxford. Available at http://www.exergoecology.com/papers/towards_int_re.pdf. Accessed 5 Dec 2016

32. Sorgüven E, Özilgen M (2010) Thermodynamic assessment of algal biodiesel utilization. Renew Energy 35:1956–1966
33. Dinçer I, Çengel Y (2001) Energy, entropy and exergy concepts and their roles in thermal engineering. Entropy 3:116–149
34. Özilgen M, Sorgüven E (2011) Energy and exergy utilization and carbon dioxide emission in vegetable oil production. Energy 36:5954–5967
35. Çatak J, Develi AÇ, Sorgüven E, Özilgen M, Inal HS (2015) Lifespan entropy generated by the masseter muscles during chewing: an indicator of the life expectancy? IJEX 18:46–66
36. Kuddusi L (2015) Thermodynamics and life span estimation. Energy 80:227–238
37. Rodriguez-Illera M, Nikiforidis CV, van der Goot AZ, Boom RM (2017) Exergy efficiency from staple food ingredients to body metabolism: the case of carbohydrates. J Clean Prod 142:4101–4113
38. Aghbashlo M, Mobli H, Rafiee S, Madadlou A (2013) A review on exergy analysis of drying processes and systems. Renew Sust Energ Rev 22:1–22
39. Erbay Z, Koca N (2014) Exergoeconomic performance assessment of a pilot-scale spray dryer using the specific exergy costing method. J Biosyst Eng 122:127–138
40. Saygi G, Erbay Z, Koca N, Pazır F (2015) Energy and exergy analyses of spray drying of a fruit puree (Cornelian Cherry puree). IJEX 16:315–336
41. Sivakumar R, Saravanan R, Perumal AE, Iniyan S (2016) Fluidized bed drying of some agro products – a review. Renew Sust Energ Rev 61:280–301
42. Khanali M, Aghbashlo M, Rafiee S, Jafari A (2013) Exergetic performance assessment of plug flow fluidised bed drying process of rough rice. IJEX 13:387–408
43. Icier F, Colak N, Erbay Z, Kuzgunkaya EH, Hepbasli A (2010) A comparative study on exergetic performance assessment for drying of broccoli florets in three different drying systems. Dry Technol 28:193–204
44. Aghbashlo M, Mobli H, Rafiee S, Madadlou A (2012) Energy and exergy analyses of the spray drying process of fish oil microencapsulation. Biosyt Eng 111:229–241
45. Saraç BE (2015) Exergy analysis in the withering process for Turkish black tea production. IJEX 18:323–339
46. Özahi E, Demir H (2013) A model for the thermodynamic analysis in a batch type fluidized bed dryer. Energy 59:617–624
47. Sinha A, Gupta R, Pandey KM, Dey SK (2015) Exergy analysis of coal fired tea drying furnace. IJEX 17:54–73
48. Souraki BA, Ghanadzadeh H, Imami N, Tabarsa M (2014) Thermodynamic modeling of convective drying of green tea. In: 8th International Chemical Engineering Congress and Exhibition, Kish, 2014
49. Nasiri F, Aghbashlo M, Rafiee S (2016) Exergy analysis of an industrial scale ultrafiltrated (UF) cheese production plant: a detailed survey. Heat Mass Transfer 53:407. doi:10.1007/s00231-016-1824-3
50. Lokadan MJ, Aghbashlo M, Mohtasebi SS (2015) Comprehensive exergy analysis of an industrial-scale yogurt production plant. Energy 93:1832–1851
51. Arena S, Renzone G, D'Ambrosio C, Salzano AM, Scaloni A (2017) Dairy products and the Maillard reaction: a promising future for extensive food characterization by integrated proteomics studies. Food Chem 219:477–489
52. Gorji DG, Smyth HE, Sharma M, Fitzgerald M (2016) Lipid oxidation in mayonnaise and the role of natural antioxidants: a review. Trends Food Sci Technol 56:88–102
53. Mattioli S, Dal Bosco A, Szendrö Z, Cullere M, Gerencser Z, Castellini MC, Zotte AD (2016) The effect of dietary Digestarom® herbal supplementation on rabbit meat fatty acid profile, lipid oxidation and antioxidant content. Meat Sci 121:238–242
54. Labuza TP (1980) Enthalpy/entropy compensation in food reactions. Food Technol 34 (2):67–77
55. Glasstone S, Laidler KJ, Eyring H (1941) The theory of rate processes: the kinetics of chemical reactions, viscosity, diffusion and electrochemical phenomena. McGraw-Hill, New York

56. Özilgen S, Özilgen M (1992) Enthalpy – entropy and frequency factor – activation energy compensation relations for death of *Escherichia coli* with microwaves in a tubular flow reactor. Acta Aliment Hung 21:195–203
57. Whiting RC, Buchanan RL (1994) Microbial modeling. Food Technol 48(6):113–120
58. Mulchandani A, Luong JHT (1989) Microbial growth kinetics revisited. Enzyme Microb Technol 11:66–72
59. Edelstein-Keshet L (1988) Mathematical models in biology. Random House, New York
60. Luedeking R, Piret EL (1959) A kinetic study of lactic acid fermentation. Batch process at controlled pH. Biotechnol Bioeng 1:393–412
61. Weiss RM, Ollis DF (1980) Extracellular microbial polysaccharides. I. Substrate, biomass, and product kinetic equations for batch xanthan gum fermentation. Biotechnol Bioeng 4:859–870
62. Özilgen M (1988) Kinetics of amino acid production by over-producer mutant microorganisms. Enzyme Microb Technol 10:110–114
63. Tokatli K, Özilgen M (1991) Kinetic model of microbial exotoxin production. Lebensm Wiss Technol 24:274–277
64. Bailey EJ, Ollis DF (1986) Biochemical engineering fundamentals, 2nd edn. McGraw-Hill, New York
65. FDA (2014) Kinetics of microbial inactivation for alternative food processing technologies – overarching principles: kinetics and pathogens of concern for all technologies. Available at http://www.fda.gov/Food/FoodScienceResearch/SafePracticesforFoodProcesses/ucm100198.htm. Accessed 10 Jan 2017
66. Cornejo I, Cornejo G, Ramirez C, Almonacid S, Simpson R (2016) Inverse method for the simultaneous estimation of the thermophysical properties of foods at freezing temperatures. J Food Eng 191:37–47
67. Miles CA, van Beek G, Veerkamp CH (1983) Calculation of thermophysical properties of foods. In: Jowitt R, Escher F, Hallstrom B, Th Meffert HF, Spiess WEL, Vos G (eds) Physical properties of foods. Applied Science Publishers, London
68. Choi J, Bischo JC (2011) Review of biomaterial thermal property measurements in the cryogenic regime and their use for prediction of equilibrium and non-equilibrium freezing applications in cryobiology. Cryobiology 60(1):52–70
69. Atkinson B, Mavituna F (1991) Biochemical engineering and biotechnology handbook, 2nd edn. McMillan Pub. Ltd, New York
70. Magerramov MA, Abdulagatov AI, Azizov ND, Abdulagatov IM (2007) Effect of temperature, concentration, and pressure on the viscosity of pomegranate and pear juice concentrates. J Food Eng 80:476–489
71. Vagenas GK, Karathanos VT (1991) Prediction of moisture diffusivity in granular materials, with special applications to foods. Biotechnol Progr 7:419–426
72. Rao MA, Cooley HJ, Anantheswaran RC, Ennis RW (1985) Convective heat transfer to canned liquid foods in steritort. J Food Sci 50:150–154
73. Ruzicka MC (2008) On dimensionless numbers. Chem Eng Res Des 86:835–868
74. Benson SW (1965) Bond energies. J Chem Educ 42:502–518
75. Shieh JA, Fan LT (1982) Estimation of energy (enthalpy) and exergy (availability) contents in structurally complicated materials. Energy Source 6:1–46
76. Szargut J, Morris DR, Steward FR (1988) Exergy analysis of thermal, chemical, and metallurgical processes. Hemisphere Publishing, New York
77. Domalski ES, Hearing ED (1993) Estimation of the thermodynamic properties of C-H-N-O-S-halogen compounds at 298.15 K. J Phys Chem Ref Data 22(4):805–1159
78. Marrero J, Gani R (2001) Group-contribution based estimation of pure component properties. Fluid Phase Equilibr 183–184:183–208
79. Gharagheizi F, Ilani-Kashkouli P, Mohammadi AH (2014) A group contribution method for determination of the standard molar chemical exergy of organic compounds. Energy 70:288–297

80. Hurst JE, Harrison BK (1992) Estimation of liquid and solid heat capacities using a modified Kopp's rule. Chem Eng Commun 112:21–30
81. Sarikaya A, Özilgen M (1991) Kinetics of peroxidase inactivation during thermal processing of whole potatoes. Lebensm Wiss Technol 24:159–163
82. Yang BB, Nunes RV, Swartzel KR (1992) Lethality distribution in the holding section of an aseptic processing system. J Food Sci 57:1258–1265
83. Gougouli MAS, Angelidis AS, Koutsoumanis K (2007) A study on the kinetic behavior of Listeria monocytogenes in icecream stored under static and dynamic chilling and freezing conditions. J Dairy Sci 91:523–530
84. Alavi SH, Puri VM, Knabel SJ, Mohtar RH, Whiting RC (1999) Development and validation of a dynamic growth model for Listeria monocytogenes in fluid whole milk. J Food Protect 62:170–176
85. Hill JE, Leitman JD, Sunderland JE (1967) Thermal conductivity of various meats. Food Technol 21(8):91–96

Index